4159
7456

[redacted]

CONFIDENTIAL

019093 R
AIC TEST

WT-748

Copy No. 158 A

L-1460-79

Operation UPSHOT-KNOTHOLE

NEVADA PROVING GROUNDS

March - June 1953

Project 5.1

ATOMIC WEAPON EFFECTS ON AD TYPE AIRCRAFT IN FLIGHT (U)

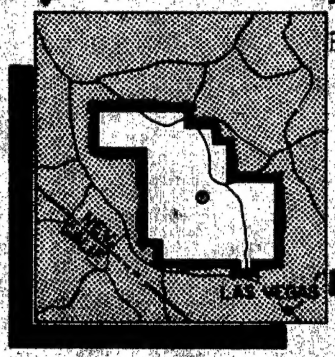

HEADQUARTERS FIELD COMMAND, ARMED FORCES SPECIAL WEAPONS PROJECT
SANDIA BASE, ALBUQUERQUE, NEW MEXICO

[redacted]

1 Mar 2001
[redacted] D
W/ENCLS.

[redacted]

Atch #12

[redacted]

Defense Threat Reduction Agency
8725 John J Kingman Road MS 6201
Ft Belvoir, VA 22060-6201

TDANP/TRC

March 2, 2001

MEMORANDUM TO THE DEFENSE TECHNICAL INFORMATION CENTER
ATTN: OCQ

SUBJECT: DOCUMENT UPDATES

The Defense Threat Reduction Agency Security Office has performed a classification/distribution statement review of the following documents. The documents should be changed to read as follows:

WT-1628, AD-357954, OPERATION HARDTACK, PROJECT 3.4, LOADING AND RESPONSE OF SURFACE-SHIP HULL STRUCTURES FROM UNDERWATER BURSTS, UNCLASSIFIED, DISTRIUBTION STATEMENT A.

WT-1301, AD-341065, OPERATION REDWING, PROJECT 1.1, GROUND SURFACE AIR BLAST PRESSURE VERSUS DISTANCE, UNCLASSIFIED, DISTRIBUTION STATEMENT A.

WT-748, OPERATION UPSHOT KNOTHOLE, PROJECT 5.1, ATOMIC WEAPON EFFECTS ON AD TYPE AIRCRAFT IN FLIGHT. UNCLASSIFIED, DISTRIBUTION STATEMENT A. FORWARD TO YOU FOR YOUR COLLECTION

WT-9001-SAN, GENERAL REPORT ON WEAPONS TESTS, UNCLASSIFIED, DISTRIBUTION STATEMENT A. FORWARD TO YOU FOR YOUR COLLECTION.

POR-2260-SAN, OPERATION SUN BEAM, SHOTS LITTLE FELLER 1 AND 2, PROJECT 1.1, AIRBLAST PHENOMENA FROM SMALL YIELD DEVICES, SANITIZED VERSION. UNCLASSIFIED, DISTRIBUTION STATEMENT A. FORWARD TO YOU FOR YOUR COLLECTION.

If you have any questions, please call me at 703-325-1034.

Ardith Jarrett

ARDITH JARRETT
Chief, Technical Resource Center

[redacted]

WT-748

This document consists of 198 pages
No. 158 of 260 copies, Series A

OPERATION UPSHOT-KNOTHOLE

Project 5.1

ATOMIC WEAPON EFFECTS ON AD TYPE AIRCRAFT IN FLIGHT

REPORT TO THE TEST DIRECTOR

by

Leo Rogin
Alden C. DuPont
Christian G. Weeber

March 1954

[redacted]

Naval Air Material Center
Philadelphia 12, Pennsylvania

[redacted]

[redacted]

ABSTRACT

This report presents measured, observed and calculated data associated with atomic weapon effects upon the structure of Model AD aircraft in the vicinity of an atomic explosion. Data covering weapons effects and airplane structural response to these effects are presented for aircraft in level flight attitude, tail toward the blast in a vertical plane containing the burst point. This orientation represents an escape position of an AD type aircraft following delivery of an atomic weapon.

During Operation UPSHOT-KNOTHOLE, this project participated in a total of five shots. One or the other of two Navy Model AD aircraft converted to drone configuration was flown in Shots 1, 2, 7, 8, and 9. The slant ranges at burst time involved in these shots varied from 14,400 ft for the AD-2 piloted flight of Shot 1 to 6200 ft for the AD-2 pilotless flight of Shot 7. In Shot 7, the actual yield exceeded the planned yield by greater than 30 per cent. The drone aircraft was positioned for near critical weapon effects and the higher thermal radiation severely weakened all the blue painted skin on the underside of the wing. Both the port and starboard outboard wing panels were torn off at the time of shock arrival as a result of the weakened skin and combined overpressure and gust effects. A considerable amount of valuable information on thermal damage to aircraft in flight was obtained from these panels which were recovered after the test. Neither panel incurred any significant additional damage due to the free fall and subsequent ground impact. Visual analysis of the structural failures indicated that the aircraft might have survived had the bottom skin of the wing been bare aluminum or painted heat resistant white instead of standard blue.

In addition to the above flight tests, aluminum alloy panels of various thicknesses and paint finishes were exposed at three different stations on the ground during Shot 9 to obtain supplemental information on the effects of thermal radiation. Effective thermal absorptivity coefficients obtained ranged in value from 0.12 to 0.16. The results of these tests are reported in Appendix B.

Measured overpressures were in agreement with the theoretical values. Measured thermal radiation was seen to be appreciably greater than predicted as a direct result of ground reflectivity. Thermal calculations using $\beta = 0.55$, (albedo) provided good correlation with test measurements. Peak aircraft accelerations as

measured were approximately double the calculated values; however, the measured wing and tail loads were in close agreement with the loads calculated using rigid body relationships. Aircraft elasticity effects, even on this comparatively rigid airplane, were readily seen. No direct correlation between measured and calculated aircraft skin temperature rise has been established, although the effects of heat received, skin thickness, and surface finish, are indicated. The arbitrary assumption of turbulent or laminar airflow, and corresponding cooling rates, resulted in agreement with the rates as measured during time histories of skin temperature rise. Results of metallurgical studies on aircraft skin specimens, begun in an attempt to determine skin temperature rise in Shot 7, indicated effects normally associated with temperatures far in excess of those recorded. This is believed to be due to microscopic thermal concentrations in the grain structure of the material brought about by the instantaneous application of the thermal pulse. The effects are so localized that no serious structural consequences, exceeding those indicated by the thermal data presented in this report, are expected. Appendix A presents these metallurgical results. Appendix B presents data on ground panels which may prove useful in further analysis of the temperature problem.

The use of the data presented in this report for the purpose of improving analytical methods for predicting the effect of atomic weapons on Naval aircraft is recommended. Recommendations for future tests include thermal radiation measurements in flight to further evaluate ground reflectivity and measurement of time histories of aircraft skin temperature rise in flight, followed by metallographic study of the structure.

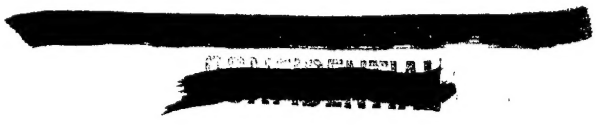

FOREWORD

This report is one of the reports presenting the results of the 78 projects participating in the Military Effects Tests Program of Operation UPSHOT-KNOTHOLE, which included 11 test detonations. For readers interested in other pertinent test information, reference is made to WT-782, Summary Report of the Technical Director, Military Effects Program. This summary report includes the following information of possible general interest.

a. An over-all description of each detonation, including yield, height of burst, ground zero location, time of detonation, ambient atmospheric conditions at detonation, etc., for the 11 shots.

b. Compilation and correlation of all project results on the basic measurements of blast and shock, thermal radiation, and nuclear radiation.

c. Compilation and correlation of the various project results on weapons effects.

d. A summary of each project, including objectives and results.

e. A complete listing of all reports covering the Military Effects Test Program.

ACKNOWLEDGMENTS

The test program reported herein was successfully accomplished only through the combined efforts of many individuals, both military and civilian, representing many different agencies. Although individual acknowledgments cannot be made here, the following is a list of the organizations who contributed to the success of this program:

Bureau of Aeronautics of the Navy

Directorate of Weapons Effects Tests,
Armed Forces Special Weapons Projects

Douglas Aircraft Company, El Segundo Division

Electronics Associates. Long Branch, N. J.

Massachusetts Institute of Technology, Dept.
of Aeronautical Engineering

Naval Air Development Squadron Five

Naval Materials Laboratory

Naval Ordnance Test Station

Naval Radiological Defense Laboratory

Signal Corps Engineering Laboratory

Special Weapons Center of the Air Force

Wright Air Development Center

[redacted]

[redacted]

CONTENTS

[redacted]

ILLUSTRATIONS

[redacted]

[redacted]

[redacted]

TABLES

[redacted]

CHAPTER 1

INTRODUCTION

1.1 OBJECTIVE

1.1.1 Purpose of Project

Project 5.1 was established for the specific purpose of obtaining flight test data and information which can be used in defining those regions in space which are unsafe for Model AD type naval aircraft following the delivery of an atomic air burst weapon. Much of the flight test information gathered, however, was to be generally applicable to the study of weapon effects on aircraft in the vicinity of an atomic weapon explosion.

1.1.2 Need for Project

To date, most of the information available for defining unsafe regions has been either static ground test data or of a theoretical nature, based to some extent on limited flight data obtained at comparatively low levels of weapons effects. To reach optimum effectiveness in atomic weapon delivery it is essential that the gaps in these data be filled.

Specifically it is anticipated that the data obtained by this project will be used as follows:

a. To experimentally verify or redefine the structurally safe regions for a Model AD airplane flying in the vicinity of an atomic explosion.

b. To improve methods for analytically determining the effects of atomic weapons on naval aircraft structures.

1.1.3 Report Objective

The objective of this report is to present the measured, observed, and calculated data associated with atomic weapon effects upon the structure of Model AD aircraft in flight in the vicinity of an atomic explosion. Five separate sets of data,

[redacted]

corresponding to Shots 1, 2, 7, 8, and 9, Operation UPSHOT-KNOTHOLE are presented. Direct correlation between certain items of data is presented as observed; however, no attempt has been made to include in this report all the theoretical studies necessary to correlate the data presented.

1.2 EXPERIMENT DESIGN

1.2.1 Background

Reference (1) presents procedures for determining the regions in space which are unsafe for naval aircraft following the explosion of an air burst atomic weapon. In order to investigate these regions and their specific application to AD aircraft, two standard blue AD type aircraft, a Model AD-2, Bureau Number 122363, and a Model XBT2D-1, Bureau Number 09103, were converted to drone aircraft and instrumented for the measurement of atomic weapon effects. (See Fig. 1.1.)

1.2.2 Instrumentation

The specific items measured were as follows:

a. Burst time; by modified photoelectric cell (blue box).

b. Thermal radiation: by the Naval Radiological Defense Laboratory calorimeters and by thermal cloths, both mounted on underside of wing; 0 to 30 cal/cm^2.

c. Aircraft skin maximum temperatures; by temperature sensitive papers on reverse side of panels with various surface finishes;+129 to +579°F. See Fig. 1.2, locations 1-16.

d. Aircraft skin and spar temperatures; BN and PN resistance temperature gages; -100 to +400°F and -100 to +250°F, respectively. See Fig. 1.2, locations 17 and 18.

e. Free stream overpressure; by the National Advisory Committee for Aeronautics' pressure pickup on wing tip boom; 0 to 4 psi range, 1000 cps maximum frequency on starboard, 80 cps on port side.

f. Aircraft normal accelerations at center of gravity and tail by Statham accelerometers; 0 to 10g, 70 cps (also 10 cps Giannini accelerometer at center of gravity through AN/UKR-5 telemeter).

g. Wing bending; by SR-4 strain gage bridges at one inboard station on starboard side and several stations on port side; to limit load, 80 cps.

h. Wing shear at one inboard station on port side.

i. Wing torsion at one inboard station on the port side.

j. Horizontal stabilizer bending at one inboard station on port and/or starboard side.

k. Horizontal stabilizer shear at one inboard station on port and/or starboard side.

l. Aircraft altitude; by modified SCR-584 radar,

Electronics Associates plot board and telemetering of Giannini pressure pickups.

m. Aircraft horizontal range relative to burst; by radar plot.

n. Aircraft velocity by radar and by telemetering of Giannini pressure pickup.

o. Aircraft pitch and roll attitude by telemetering of Giannini pitch and roll gyro.

p. Gamma radiation; by Signal Corps Engineering Laboratories photographic films; 0-50 Roentgens. See Fig. 1.2, locations A-G.

Fig. 1.1 Model AD Type Drone Aircraft (AD-2)

[redacted]

TEMPERATURE PLATES			
LOC.	DESCRIPTION	LOC.	DESCRIPTION
1	0.032 HEAT RES. WHITE	11	0.051 BLUE
2	0.040 ALUMINIZED	12	0.051 BLACK
3	0.064 BLUE	13	0.032 BLUE
4	0.064 ALUMINIZED	14	0.032 STD. WHITE
5	0.040 HEAT RES. WHITE	15	0.010 BLUE
6	0.032 BLUE	16	PORT FLAP
7	0.040 ALUMINIZED	17	STBD FLAP
8	0.051 BLUE	18	0.051 BLUE S.G.
9	0.051 BLACK	19	0.040 BLUE S.G.
10	0.040 ALUMINIZED	20	

GAMMA BOXES	
LOC.	DESCRIPTION
A	INSIDE WING FOLD
B	INSIDE WING FOLD
C	INSIDE LOWER FUSELAGE
D	COCKPIT BEHIND HEADREST
E	COCKPIT ON FLOOR
F	COCKPIT ON FLOOR
G	OUTSIDE BELOW WING

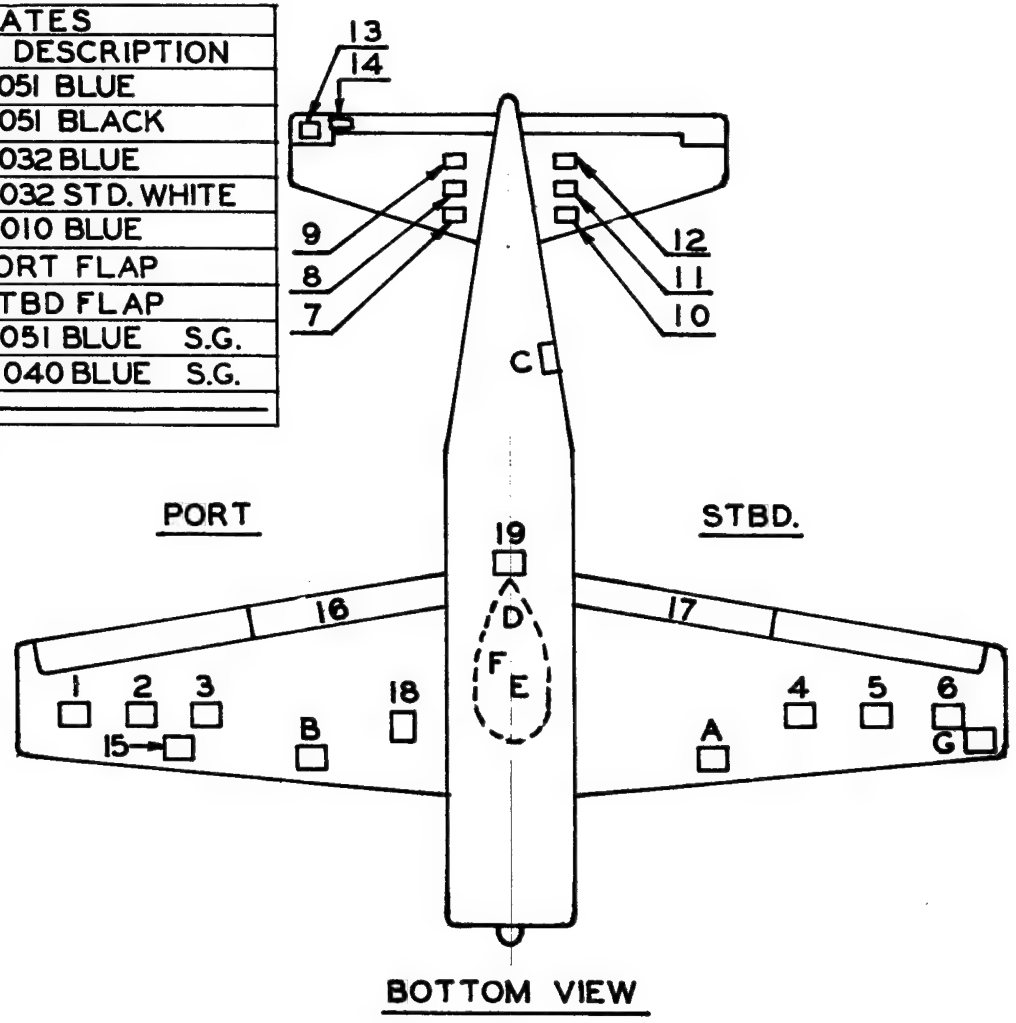

Fig. 1.2 Bottom View of AD Drone showing Temperature and Gamma Measurement Locations.

The information provided by the above instrumentation is both general with respect to atomic weapons radiation and blast characteristics and specific with respect to aircraft structural response to these inputs. The complete load measuring installation is described in refs (2) and (3). The modified SCR-584 radar used is described in ref (4). Reference (5) describes the airborne instrumentation and gives sensitivities for all records.

1.2.3 Analytical Methods

Aircraft test positions were established following the general procedures described in ref (6).

1.2.3.1 Aircraft Attitude and Orientation

The aircraft was to be in level flight attitude, tail toward the blast in a vertical plane containing the burst point, simulating an escape position of an AD type aircraft following delivery of an atomic weapon. This was accomplished in all tests.

1.2.3.2 Thermal Effects

Thermal effects were considered applicable at t_o. The expression for temperature rise in the aircraft skin exposed to radiation from the burst was assumed to be:

$$\Delta T = \frac{\mu_e Q \ SIN \ \theta}{0.833 t} \qquad (1.1)$$

In positioning the aircraft for critical thermal effects an equivalent absorbtivity, μ_e, of 0.3 was taken for standard blue painted aircraft skin, considering the minimum skin gage of 0.016 in. Ground reflectivity calculations are based on the methods of ref (9) using the relationship:

$$I_R \times 10^3 = \frac{\beta \times 2h_2^2}{11.68 h_1^4} \left\{ \frac{1 + \frac{1}{2[(\Delta h/h_1)+1]^2}}{[(\Delta h/h_1)^2 + 2(\Delta h/h_1)]^2} - \frac{3\pi}{4[(\Delta h/h_1)^2 + 2(\Delta h/h_1)]^{5/2}} \right\} \qquad (1.2)$$

This equation is valid for the case where $h_2 > h_1$ and as such is suitable for all shots. (See Figs. 3.3 and 3.4) Multiplying I_R by the thermal yield in calories (1 KT thermal yield = 10^{12} calories) gives the reflected radiation in calories per centimeter^2. In accordance with ref (20), a thermal yield = $.44W^{0.94}$ was used.

1.2.3.3 Gamma Radiation

Gamma radiation was considered to have no structural significance. Since the aircraft used in the manned flights were to receive no appreciable amount, gamma radiation was not considered as a positioning criteria; however, it was calculated and measured. The following is the method presented in ref (10) for determining gamma radiation at a given aircraft position: Find reduced range by multiplying R_A by σ. Using this reduced range and the angular position of the aircraft with respect to the burst (e.g., 12 o'clock, aircraft directly over burst; 3 o'clock, aircraft at burst level) find the reduced dosage, D/σ^2 for a 1 KT weapon. (See Fig. 3.18.) Multiplying by the factor $\sigma^2 Y$ gives the expected dosage. Since the emission of gamma radiation is time dependent, Fig. 13, ref (8), the aircraft motion is considered by using a method similar to that given in ref (6) to obtain total nuclear radiation received on a moving aircraft.

1.2.3.4 Overpressure

Time of shock arrival (Fig. 3.20) must be known in order to establish the aircraft position at shock arrival for a given test condition. The free-stream overpressures for the test conditions were based on the data of ref (10), free air or surface burst depending on the triple point trajectory, corrected for both height of burst other than sea level and for aircraft test altitude. The relationships used to correct overpressure and slant range for burst height are:

$$R_H = R_{SL}\left(P_{SL}/P_H\right)^{1/3} \tag{1.3}$$

$$\Delta P_H = \Delta P_{SL}\left(P_{SL}/P_H\right) \tag{1.4}$$

For aircraft at test altitudes other than burst altitude the relationships for overpressure and slant range are:

$$R_A = R_H/\lambda \tag{1.5}$$

$$\Delta P_A = \Delta P_H\, \lambda\left(P_A/P_H\right)^{1/2}\left(T_H/T_A\right)^{1/4} \tag{1.6}$$

The slant range at a given overpressure for any yield is obtained from the known range and yield by

$$R_1 = R_2\left(Y_1/Y_2\right)^{1/3} \tag{1.7}$$

Overpressure at the test position can now be predicted. (See Fig. 3.22.)

1.2.3.5 Gust Effects

With a given overpressure there is a corresponding pressure ratio at each test altitude. Density ratios and gust velocities corresponding to the pressure ratios can be predicted. (Figs. 3.23 and 3.24.) Reference (11) is a source for these data. The effect of gust velocity on aircraft is determined in terms of allowable aircraft load factors. The following equation, given in ref (6) is used to predict the incremental load factor experienced by the airplane.

$$\Delta g = \frac{SC_{L\alpha}}{2W} \rho_A \left[0.3+0.7 \frac{P_1}{P_A}\right] U_1 \, w \sin\theta \tag{1.8}$$

where:

$$U_1 = \sqrt{(U_A - w\cos\theta)^2 + (w \sin\theta)^2} \tag{1.9}$$

ρ_1/ρ_A can be substituted directly for the expression $\left[0.3+0.7 \, P_1/P_A\right]$ in equation 1.8 if a ρ_1/ρ_A vs P_1/P_A curve is available. For the aircraft used, $SC_{L\alpha}$ for the wing is taken as 1840. Wing and tail loads are assumed to be directly proportional to the calculated load factor. Structural dynamic response was not considered in the analysis. The general expression for the calculated load is

$$\Delta L = \Delta g \left[K_1 W + K_2\right] \tag{1.10}$$

For the wing, the aerodynamic constant K_1, and inertia constant K_2, are both based on the normal spanwise load distribution identical to that for the positive high angle of attack, forward c.g. condition presented in ref (12), assuming a linear lift curve. The horizontal stabilizer load coefficients were obtained using a value of

$$\left(SC_{L\alpha}\right)_{\text{HOR. STAB.}} / \left(SC_{L\alpha}\right)_{\text{WING}} = 0.206$$

and a normal load distribution proportional to the horizontal stabilizer chord, based on information from ref (13). These constants are presented in Table 1.1. Steady state pullouts performed as a flight check of the load measuring installation result in measured wing loads in direct agreement with loads calculated using this table.

TABLE 1.1 - Calculated Wing and Horizontal Stabilizer Load Constants

Station	Load	K_1	$K_2 \times 10^{-3}$
W.S. 57	Shear	0.436	-1.529
N.S. 57	Bending	37.90	-98.60
W.S. 107	Bending	22.08	-44.30
W.S. 162	Bending	9.77	-17.88
S.S. 21	Shear	0.0799	-0.1255
S.S. 21	Bending	3.515	-10.24

1.2.4 Operational Procedures

Two Navy Model AD aircraft, single place, single engine attack bombers were converted to drones using the Naval Air Experimental Station Type I Remote Control Equipment. One participated in Shot 1, the other in Shot 9 as manned aircraft in preparation for drone operation. Lower range data were obtained in this manner.

For NOLO (no live occupant) operations, the drone take-off was under the control of a pilot at a ground station located beside the runway. Once airborne, the drone was turned over to a pilot flying a Navy Model F8F "mother" control plane. Upon arrival at the test site, control was turned over to a pilot at the radar plotting board. Using data from the radar plot and from telemetering direct reading meters, the pilot guided the drone to its predetermined position relative to the burst at time zero. Following the test, the "mother" aircraft again took control and the drone was returned to the base where the pilot at the runway station controlled the drone landing. An operational tolerance of $\pm$ 1 sec of time in positioning was allowed at time zero.

CHAPTER 2

RESULTS AND OBSERVATIONS

2.1 RESULTS

Records of thermal and blast effects were obtained for all shots with the exception of Shot 7 where the drone was destroyed at shock arrival, resulting in the loss of the blast data. Figure 3.2 presents the time histories of measured thermal radiation. Figure 3.7 presents time histories of measured skin temperature rise. Figures 3.25 through 3.31 are reproductions of time histories of measured blast effects. Table 2.2 presents a summary of primary data for all shots. Numerical data, observations and photographs for each shot are presented in Section 2.2 below.

2.2 DATA AND OBSERVATIONS

2.2.1 Shot 1

2.2.1.1 General Data

Date of Test: 17 March 1953

Test Aircraft: Model AD-2 Drone; Manned Flight

Type of Test: 300' Tower (T-3) Ground elevation 4025 MSL

Weapon Yield: 15 KT planned; 16.2 KT Radiochemical

2.2.1.2 Test Conditions

Altitude of Test Aircraft: 17,200' MSL; 12,900' above burst

Temperature at Test Altitude: -0.4°F

Pressure at Test Altitude:	7.7 psi
True Airspeed:	359 fps
Slant Range from Burst:	t_o, 14,400'; t_s, 16,800'
Time of Shock Arrival:	14.4 sec
Aircraft Gross Weight (Shock Arrival):	13,550 lb
Aircraft Angular Position:	t_o, 63°; t_s, 50°30' from horizontal; (θ)

2.2.1.3 Effects Data - Shot 1

(1) From Weapon

Thermal Radiation (cal/cm^2)

Port Wing Calorimeter: 2.7: (2.9, filter correction, 8%)
Normal to Horizontal Plane: 3.2

Gamma Radiation (r)

Less than 0.1 inside the aircraft

Thermal In Cockpit (cal/cm^2)

Less than 1.0, from temp. cloth and paper

Free-stream Overpressure (psi)

Starboard wing pressure pickup: 0.3

(2) On Test Aircraft

Incremental Normal Acceleration (g's)

Center of Gravity Accelerometer: 2.1
Tail Accelerometer: 2.0
Center of Gravity, Calculated: 0.97

Aircraft Attitude Change (deg)

Pitch Gyro: 2.3 Nose Down
Roll Gyro: 1.4 Right Wing Up

Incremental Structural Loads Above 1g Level Flight - Shot 1

		Measured Load	% of Design Limit Load
Starboard Wing Bending	(Sta. 57)	512×10^3 in. lb.	10.6
Port Wing Bending	(Sta. 57)	525×10^3 in. lb.	10.9
Port Wing Bending	(Sta. 107)	308×10^3 in. lb.	12.7
Port Wing Bending	(Sta. 162)	112×10^3 in. lb.	9.3
Port Wing Shear	(Sta. 57)	4.63×10^3 lb.	11.6
Port Wing Torsion	(Sta. 57)	-6.5×10^3 in. lb.	0.7
Port Stabilizer Bending	(Sta. 21)	44.3×10^3 in. lb.	16.7
Port Stabilizer Shear	(Sta. 21)	1.22×10^3 lb.	15.2

Temperature Rise in Aircraft Skin, °F
(Temperature Gages)

Color	Skin Thickness	Temperature Rise
Standard Blue	0.051	57
Standard Blue	0.040	97

2.2.1.4 Oscillograph Data

See Figure 3.31

2.2.1.5 Observations

No visible damage

2.2.2 Shot 2

2.2.2.1 General Data

Date of Test: 24 March 1953

Test Aircraft: Model AD-2 Drone; No live occupant (NOLO) flight.

Type of Test: 300' Tower (T-4), Ground elevation 4308' MSL.

Weapon Yield: 40 KT Planned, 24.5 Radiochemical

2.2.2.2 Test Conditions

Altitude of Test Aircraft:	10,800' MSL; 6200' above burst.
Temperature at Test Altitude:	33°F
Pressure at Test Altitude:	9.90 psi
True Airspeed:	477 fps
Slant Range from Burst:	t_o 8100', t_s 10,900'
Time for Shock Arrival:	8.0 sec
Aircraft Gross Weight (Shock Arrival):	13,360 lb.
Aircraft Angular Position:	t_o, 50°; t_s, 34° from horizontal; (θ)

2.2.2.3 Effects Data

(1) From Weapon

Thermal Radiation (cal/cm^2)

Port Wing Calorimeter:	11.5; (12.4, filter correction, 8%)
Tail Calorimeter:	9.8; (10.6, filter correction, 8%)
Port Wing Thermal Indicator Cloth:	9.5
Tail Thermal Indicator Cloth:	11.0
Normal to Horizontal Plane:	12.8

[redacted]

Gamma Radiation - Shot 2

Location	Dosage (r)	Shielding Material	Shielding Thickness, in.
Inside Cockpit:			
Behind Headrest	4.2	Aluminum	0.174
		Rubber and cloth	0.75
		Gasoline	74.8
On floor, forward	4.2	Aluminum	0.683
On floor, port	2.5	Aluminum	0.464
		Rubber and cloth	0.75
		Gasoline	35.6
Inside Wing Fold:			
Port	6.0	Aluminum	1.55
Starboard	6.0	Aluminum	1.55
Inside Rear Fuselage:			
Starboard	8.8	Aluminum	0.040

Free Stream Overpressure (psi)

Starboard Wing Pressure Pickup: 1.0

(2) On Test Aircraft

Incremental Normal Acceleration (g's)

Center of Gravity Accelerometer: 3.8
Tail Accelerometer: 3.6
Center of Gravity, Calculated: 2.14

Aircraft Attitude Change (deg)

Pitch Gyro: 2.5 Nose down
Roll Gyro: 0

Incremental Structural Loads Above 1 g Level Flight - Shot 2

	Measured Load	% of Design Limit Load
Starboard Wing Bending (Sta. 57)	947×10^3 in. lb.	19.7
Port Wing Bending (Sta. 57)	829×10^3 in. lb.	17.2
Port Wing Bending (Sta. 107)	559×10^3 in. lb.	22.9
Port Wing Bending (Sta. 162)	328×10^3 in. lb.	27.3
Port Wing Shear (Sta. 57)	9.00×10^3 lb.	22.5
Port Wing Torsion (Sta. 57)	29.0×10^3 in. lb.	2.1
Port Stabilizer Bending (Sta. 21)	72.5×10^3 in. lb.	26.7
Port Stabilizer Shear (Sta. 21)	1.86×10^3 lb.	23.2

Temperature Rise in Aircraft Skin, °F - Shot 2

Color	Skin Thickness	Temperature Rise
Standard Blue	0.064	>171 <190
Standard Blue	0.051	>171 <190
Standard Blue	0.051	156
Standard Blue	0.051	*187
Standard Blue	0.040	*225
Standard Blue	0.032	250
Black	0.051	>171 <190
Black	0.051	>171 <190
Aluminized Lacquer	0.064	138
Aluminized Lacquer	0.040	156

[redacted]

Aluminized Lacquer	0.040	> 144	< 156
Aluminized Lacquer	0.040	138	
Heat Resistant White	0.040	138	
Heat Resistant White	0.032	> 144	< 156

* Temperature gage measurements. All other are temperature sensitive paper measurements.

2.2.2.4 Oscillograph Data

See Figs. 3.29 and 3.30. Values used for the approximately 0.1 sec interruption of strain gage amplifier operation were estimated, based on damping ratios established using strain gage records from Shots 1, 8 and 9.

2.2.2.5 Observations

All standard blue paint on 0.016 alclad aircraft skin on the under side of the control surfaces was scorched except in the immediate vicinity of the rivets (see Figs. 2.1, 2.2 and 2.3). All standard blue on 0.020 skin was scorched except where in contact with heavier structural members (see Fig. 2.4). None of the standard blue paint on .025 skin was scorched with the exception of the curved portion aft of the rear shear web which was directly facing the burst point (see Figs. 2.4 and 2.5), and the hinged aft edge of the outboard wing panel which was exposed to direct radiation from the underside as well as indirect radiation received through the aperture between this panel and the aileron (see Fig. 2.6). Slight irregular scorch on blue paint marks were noted on the underside of the outboard wing panel on skin up to and including 0.032 (see Fig. 2.7).

The rubberized fabric aerodynamic seals between the elevator and horizontal stabilizer were destroyed (see Fig. 2.8). The aileron seals were not directly exposed to thermal radiation and these remained intact. The fabric lightening hole covers on the horizontal stabilizer rear spar were burned through where direct thermal radiation was received (see Fig. 2.9). The airplane in this test had covered wheel wells so the tires were not exposed. There was no thermal damage to the tires.

2.2.3 Shot 7

2.2.3.1 General Data

Date of Test: 25 April 1953

Test Aircraft: Model AD-2 Drone; NOLO Flight, Aircraft Destroyed.

[redacted]

Type of Test: 300' Tower (T-1), Ground Elevation 4238' MSL

Weapon Yield: 33 KT Planned, 43.4 KT Radiochemical

2.2.3.2 Test Conditions

Altitude of Test Aircraft: 10,450' MSL; 5900' above burst

Temperature at Test Altitude: 43°F

Pressure at Test Altitude: 10.08 psi

True Airspeed: 417 fps

Slant Range from Burst: t_o, 6,200'; t_s, 6700'

Time for Shock Arrival: 3.75 sec

Aircraft Gross Weight (Shock Arrival): 13,400 lb.

Aircraft Angular Position: t_o 73°; t_s 60°30' from horizontal; (θ)

2.2.3.3 Effects Data

(1) From Weapon

Thermal Radiation, (cal/cm^2)

Port Wing Calorimeter: 19.4; (20.9, filter correction, 8%)
32 to 35 (corrected for 1/2 to 3/4 fireball miss)

Normal to Horizontal Plane: 54.6

Free Stream Overpressure (psi) - Shot 7

2.7 estimated.
Based on Project 5.1 flight test data and observation, as given in this report.

(2) On Test Aircraft

Incremental Normal Acceleration (g's)

Center of Gravity Acceleration: 16, estimated.
Based on calculated 8.25 g, Project 5.1 flight

[redacted]

test data and observation, and assuming that thermal damage had no effect on acceleration.

Aircraft Attitude Change (deg)

Pitch Gyro: 65 Nose Down
Roll Gyro: 85 Right Wing Down

Incremental Structural Loads Above 1 g Level Flight

		Estimated Load	% of Design Limit Load
Starboard Wing Bending	(Sta. 57)	3.38×10^6 in. lb.	70
Port Wing Bending	(Sta. 57)	3.38×10^6 in. lb.	70
Port Wing Bending	(Sta.107)	2.08×10^6 in. lb.	85
Port Wing Bending	(Sta.162)	0.93×10^6 in. lb.	80
Port Wing Shear	(Sta. 57)	35.6×10^3 lb.	90
Port Wing Torsion	(Sta. 21)	50×10^3 in. lb.	5
Port Stabilizer Bending	(Sta. 21)	304×10^3 in. lb.	110
Port Stabilizer Shear	(Sta. 21)	7.79×10^3 lb.	100

Based on Project 5.1 data and observation, as given in this report.

Temperature Rise in Aircraft Skin (°F)

Color	Skin Thickness	Temperature Rise
Standard Blue	0.064	500
Standard Blue	0.016	1200

Temperature Rise in Aircraft Skin (°F) - Shot 7

Color	Skin Thickness	Temperature Rise
Aluminized Lacquer	0.064	400
Aluminized Lacquer	0.040	450*
Bare Aluminum	0.066	300
Bare Aluminum	0.016	800

Heat Resistant White	0.064	200
Heat Resistant White	0.016	600

* Temperature sensitive paper measurement. All others estimated, based on Project 5.1 flight test data and observation, as given in this report.

2.2.3.4 Oscillographic Data

All pertinent oscillographic data for the period after shock arrival was unintelligible. The time history of thermal radiation measured from burst time to time of shock arrival is included in Fig. 3.2.

2.2.3.5 Observations

In this test the actual yield exceeded the planned yield by greater than 30 per cent. Since the aircraft was positioned for near critical weapon effects based on the planned yield, the resulting thermal radiation severely damaged or weakened all the blue painted skin on the underside of the wing. The thermal damage to the aircraft skin is presented in Table 2.1.

TABLE 2.1 Thermal Damage to Aircraft Skin - Shot 7

Surface Finish	Effects	Figure No.
	0.016 Skin Thickness	
Standard Blue	Panels missing except for small circular pieces around each rivet	2.10; 2.11
Standard White	Panels missing except for edges	2.12; 2.19
Aluminized Lacquer	Panels missing except for edges	2.13; 2.14
Heat Resistant White	Panels remained intact	2.15
Bare Aluminum	Pieces missing; panel broken along center line	2.15
	0.025 Skin Thickness	
Standard Blue	Panel missing except for edges	2.10; 2.13
Standard White	Pieces missing; panel broken along center line	2.12
Aluminized Lacquer	Panel broken along center line	2.13

TABLE 2.1 - Continued

Surface Finish	Effects	Figure No.
Aluminized Lacquer	Pieces missing; panel broken along center line	2.14
Heat Resistant White	Panels remained intact	2.15
Bare Aluminum	Panels remained intact	2.15
	0.032 Skin Thickness	
Standard Blue	Panel missing except for edges. NOTE: White lettering gave added protection.	2.16
Heat Resistant White	Panel remainted intact	2.17
	0.040 Skin Thickness	
Standard Blue	Pieces missing; panel broken along center line, except on narrow panels. NOTE: White lettering gave added protection.	2.18; 2.14; 2.16
Aluminized Lacquer	Panel remained intact	2.18
	0.051 Skin Thickness (AL-3-SO)	
Standard Blue	Skin apparently unaffected; paint scorched	2.16

The blue 0.025 skin on the hinged aft edge of the outboard wing panel in some places suffered the same damage as 0.016 skin on other parts of the wing. This panel was exposed to direct radiation from the underside as well as indirect radiation received through the aperture between this panel and the aileron (see Fig. 2.14). This is seen to be consistent with the damage experienced in Shot 2, as shown in Fig. 2.6.

The fabric lightening hole covers destroyed in Shot 2 were replaced with fabric covers coated with aluminized lacquer. These covers were slightly scorched but not burned through (see Fig. 2.19). Aileron seals remained intact (see Fig. 2.11). The top side of the wing gave no indication of thermal damage other than softening of standard blue paint on 0.016 skin on the aileron (see Fig. 2.20) where the under side skin was completely destroyed.

No effects directly attributed to overpressure were noted.

The above information was obtained from the wing outboard panels and sections of the elevator and horizontal stabilizer which were torn off at shock arrival and received only minor additional damage due to the fall. Evidence indicates that the wing failure resulted when the thermally weakened skin was further damaged by shock effects, thereby reducing the over-all strength of the wing. The sections of the empennage were torn off when struck by the wing panels.

2.2.4 Shot 8

2.2.4.1 General Data

Date of Test:	19 May 1953
Test Aircraft:	Model XBT2D-1 Drone, NOLO Flight
Type of Test:	300' Tower (T-3a), Ground elevation 4025' MSL
Weapon Yield:	37 KT Planned; 27 KT Radiochemical

2.2.4.2 Test Conditions

Altitude of Test Aircraft:	11,200' MSL; 6,900' above burst
Temperature at Test Altitude:	39°F
Pressure at Test Altitude:	9.8 psi
True Airspeed	386 fps
Slant Range from Burst:	t_o, 7200'; t_s, 8100'
Time for Shock Arrival	5.6 sec
Aircraft Gross Weight (Shock Arrival):	12,800 lb.
Aircraft Angular Position:	t_o, 73°; t_s, 58° from horizontal; (θ)

2.2.4.3 Effects Data - Shot 8

(1) From Weapon

Thermal Radiation (cal/cm^2)

Port Wing Calorimeter: 17.8; (19.2, filter correction, 8%
Starboard Wing Calorimeter: 24.9; (26.9, filter correction, 8%
Port Wing Thermal Indicator Cloth: 17
Starboard Wing Thermal Indicator Cloth: 27
Normal to Horizontal Plane: 25.4

Gamma Radiation

Location	Dosage (r)	Shielding Material	Thickness
Inside Cockpit	28	Aluminum	0.25 to 0.75 in.
		Rubber and cloth	0 to 0.75 in.
		Gasoline	5 to 15 in.
Inside Wing Fold, Port	38	Aluminum	0.051
Starboard	38	Aluminum	0.051
Inside Rear Fuselage	46	Aluminum	0.040
Underside of Starboard Wing	52.5	No shielding	

(2) On Test Aircraft

Free Stream Overpressure (psi)

Port Wing Pressure Pickup: 1.8

Incremental Normal Acceleration (g's)

Center of Gravity Accelerometer: 8.6
Tail Accelerometer: 8.5
Center of Gravity Calculated: 4.52

Aircraft Attitude Change (deg)

Pitch Gyro: 8.1 nose down
Roll Gyro: 4 right wing up

Incremental Structural Loads (Above 1 g Level Flight) - Shot 8

		Measured Load	% of Design Limit Load
Starboard Wing Bending	(Sta. 57)	$1{,}970 \times 10^3$ in.lb.	41
Port Wing Bending	(Sta. 57)	$1{,}950 \times 10^3$ in.lb.	40.5
Port Wing Bending	(Sta. 162)	546×10^3 in.lb.	45.5
Port Wing Shear	(Sta. 57)	15.97×10^3 lb.	40.0
Port Wing Torsion	(Sta. 57)	35.00×10^3 in.lb.	2.5
Starboard Stabilizer Bending	(Sta. 21)	154.5×10^3 in.lb.	56.9
Port Stabilizer Bending	(Sta. 21)	139.6×10^3 in.lb.	51.4
Starboard Stabilizer Shear	(Sta. 21)	3.71×10^3 lb.	46.4
Port Stabilizer Shear	(Sta. 21)	3.54×10^3 lb.	43.6

Temperature Rise in Aircraft Skin, °F

Color	Skin Thickness	Material	Temperature Rise
Standard Blue	0.064	24ST	225
Standard Blue	0.064	75ST	>250 <288
Standard Blue	0.051	24ST	>250 <351
Standard Blue	0.051	24ST	>250 <288
Standard Blue	0.051	24ST	>250 <351
Standard Blue	0.051	---	250
Standard Blue	0.040	24ST	>322 <442
Standard Blue	0.040	24ST	>288 <442
Standard Blue	0.032	24ST	>351 <442

[redacted]

Color	Skin Thickness	Material	Temperature Rise
Standard Blue	0.032	52SH34	>322 <442
Standard Blue	0.025	--	>401 <482
Standard Blue	0.020	24S0	>482 <579
Standard Blue	0.020	24S0	>401 <462
Standard Blue	0.016	24ST	>442 <579
Standard Blue	0.016	24ST	>351 <442
Black	0.051	24ST	351
Black	0.051	24ST	>250 <351
Aluminized Lacquer	0.064	75ST	>174 <190
Aluminized Lacquer	0.040	75ST	225
Aluminized Lacquer	0.040	24ST	>225 <250
Aluminized Lacquer	0.040	24ST	250
Aluminized Lacquer	0.025	--	>351 <442
Aluminized Lacquer	0.020	--	>351 <442
Aluminized Lacquer	0.016	24ST	>401 <482
Standard White	0.040	24ST	>174 <225
Standard White	0.020	24S0	250
Standard White	0.016	24ST	>225 <250
Heat Resistant White	0.040	75ST	225
Heat Resistant White	0.040	24ST	156
Heat Resistant White	0.032	24ST	225
Heat Resistant White	0.032	52SH34	>156 <174
Heat Resistant White	0.032	52SH34	>156 <190

Color	Skin Thickness	Material	Temperature Rise
Heat Resistant White	0.025	---	>156 <190
Heat Resistant White	0.020	24S0	>171 <190
Heat Resistant White	0.020	24S0	>190 <225
Heat Resistant White	0.016	24ST	>171 <225
Heat Resistant White	0.016	24S0	>190 <225
Bare Aluminum	0.040	24ST	225
Bare Aluminum	0.040	24ST	190
Bare Aluminum	0.040	24ST	>225 <250
Bare Aluminum	0.032	52SH34	>225 <291
Bare Aluminum	0.025	---	250
Bare Aluminum	0.020	24S0	>288 <322
Bare Aluminum	0.016	24ST	>250 <351
Bare Aluminum	0.016	24ST	>250 <351

2.2.4.4 Oscillographic Data

Figures 5.25 and 3.26 contain direct reproductions of the oscillograph traces at time of shock arrival. These traces were separated as shown to eliminate the overlap of traces brought about by the high level of the measured effects data.

2.2.4.5 Observations

In this test the complete underside of the aircraft was stripped down to bare aluminum with exception of panels on the aileron and elevator (see Figs. 2.21, 2.22, 2.23, 2.29 and 2.30). In addition, thermal panels consisting of 0.016 to 0.064 alclad aircraft skin with different paint finishes were installed on the underside of both flaps (Figs. 2.24, 2.25, 2.26. 2.27) as well as on several locations on the wing.

No thermal damage was visible on any unpainted aircraft surface. The 0.016 blue painted control surface tips had the paint completely burned off and the surface itself was badly warped. Due to the fact that all flap specimens were hand painted under field conditions, direct visual comparison with specimens prepared by standard procedures was not readily obtainable; however, the surface damage in all cases appeared consistent with the temperature

rise data given under "Results." These temperatures can be taken as indicative of the thermal damage to the surface finish.

The fabric lightening hole covers destroyed in Shot 2 were replaced with heat resistant white covers. These remained intact.

The airplane in this test had uncovered wheel wells. The tires, exposed to direct thermal radiation, were covered with heat resistant white paint. They experienced no thermal damage.

2.2.5 Shot 9

2.2.5.1 General Data

Date of Test:	8 May 1953
Test Aircraft:	Model XBT2D-1 Drone, Manned Flight
Type of Test:	Air Drop, Height of Burst 2432' above ground, Ground Elevation 3708' MSL
Weapon Yield:	31 KT Planned, 26.0 KT Radiochemical

2.2.5.2 Test Conditions

Altitude of Test Aircraft:	21,900' MSL; 16,400' above burst
Temperature at Test Altitude:	-17°F
Pressure at Test Altitude:	6.26 psi
True Airspeed:	420 fps
Slant Range from Burst:	t_o, 16,400'; t_s, 18,000' at first shock; 18,700' at third shock.
Time for Shock Arrival:	15.5 sec first shock; 19.8 sec third shock.

Aircraft Gross Weight (Shock Arrival): 13,150 lb.

Aircraft Angular Position:	t_o, 85°; t_s, 64° at first shock, 60° at third shock; (θ)

2.2.5.3 Effects Data

(1) From Weapon

Thermal Radiation (cal/cm^2)

Port Wing Calorimeter: 1.9; (2.0, filter correction,

8%) 2.8 to 3.3 (corrected for 1/2 to 3/4 fireball miss)
Normal to Horizontal Plane: 3.6

Free-Stream Overpressure (psi)

Starboard Pressure Pick-up: 0.5 first shock
Starboard Pressure Pick-up: 0.1 third shock

(2) On Test Aircraft

Incremental Normal Acceleration (g's)

Center of Gravity Accelerometer: 2.3 First Shock, 1.0 Third Shock.
Tail Accelerometer: 2.6 First Shock, 1.1 Third Shock.
Center of Gravity Calculated: 1.42 First Shock, 0.43 Second Shock.

Aircraft Attitude Change (deg)

Pitch Gyro: 3.2° First Shock, 2.4° Third Shock, Nose Down.
Roll Gyro: 3° First Shock, 3.7° Third Shock, Right Wing Up.

Incremental Structural Loads above 1 g Level Flight

Item and Location	Measured Load		% of Design Limit Load	
	First Shock	Third Shock	First Shock	Third Shock
Starboard Wing Bending (Sta. 57)	584 x 10^3 in.lb.	243 x 10^3 in.lb.	12.1	5.1
Port Wing Bending (Sta. 57)	524 x 10^3 in.lb.	230 x 10^3 in.lb.	11.8	4.8
Port Wing Bending (Sta.162)	147 x 10^3 in.lb.	64 x 10^3 in.lb.	12.3	5.3
Port Wing Shear (Sta. 57)	4.14 x 10^3 lb.	2.7 x 10^3 lb.	10.3	6.7
Port Wing Torsion (Sta. 57)	18 x 10^3 in.lb.	-5.5 x 10^3 in.lb.	1.3	0.4
Starboard Stabilizer Bending (Sta. 21)	43.2 x 10^3 in.lb.	18.4 x 10^3 in.lb.	15.9	6.8

[redacted]

Item and Location	Measured Load		% of Design Limit Load	
	First Shock	Third Shock	First Shock	Third Shock
Port Stabilizer Bending (Sta. 21)	35.7×10^3 in.lb.	15.5×10^3 in.lb.	13.1	5.7
Star Stabilizer Shear (Sta. 21)	1.76×10^3 lb.	600 lb.	22.0	7.5
Port Stabilizer Shear (Sta. 21)	1.11×10^3	360 lb.	13.9	4.5

Temperature Rise in Aircraft Skin (°F)

Color	Skin Thickness	Temperature Rise
Blue	0.012	185 *

*Results of three identical readings.

2.2.5.4 Oscillographic Data

Figures 3.32 and 3.33 present the oscillographic data associated with the first and third shocks. The second shock, which occurred 0.5 seconds before the third shock, was so small that no accurate effects readings could be made.

2.2.5.5 Observations

No visible effects damage.

TABLE 2.2 Summary of Primary Data for All Shots

Test Conditions	Shot 1	Shot 2	Shot 7	Shot 8	Shot 9
		(1	9 5	3)	
Date of Test	17 Mar	24 Mar	25 Apr	19 May	8 May
Test Aircraft	AD-2 Manned	AD-2 NOLO	AD-2 NOLO	XBT2D-1 NOLO	XBT2D-1 Manned
Test Area	T-3 Yucca	T-4 Yucca	T-1 Yucca	T-3a Yucca	Frenchman Flat
Ht. of Burst (ft MSL)	4325	4608	4538	4325	5510
Ground Elevation (ft MSL)	4025	4308	4238	4025	3078

[redacted]

TABLE 2.2 (Continued)

Test Conditions	Shot 1	Shot 2	Shot 7	Shot 8	Shot 9
Planned Yield (KT) (Radchem)	15	40	33	37	31
Actual Yield (KT)	16.2	24.5	43.4	27.0	26.0
Aircraft Altitude (ft MSL)	17,200	10,800	10,450	11,200	21,900
Aircraft Ht above Burst (ft)	12,900	6200	5900	6900	16,400
Temp. at Test Altitude (°F)	-04	33	43	39	-17
Pressure at Test Alt.(psi)	7.7	9.9	10.1	9.8	6.3
Wind Velocity at Test Alt. (deg and fps)	270; 67	160; 27	265; 17	210; 25	250; 88
True Airspeed (fps)	359	477	417	386	420
Aircraft True Course (deg)	290	270	283	277	
Slant Range at t_o (ft)	14,400	8100	6200	7200	16,400
Slant Range at t_s (ft)	16,800	10,900	6700	8100	18,000(a) 18,700(c)

TABLE 2.2 (Continued)

Test Conditions	Shot 1	Shot 2	Shot 7	Shot 8	Shot 9
Aircraft Weight at t_s (lb)	13,550	13,360	13,400	12,800	13,150
Position Relative to Burst at t_o (deg)	63	50	73	73	85
Position Relative to Burst at t_s (deg)	50.5	34	60.5	58	64(a) 60(c)

[redacted]

TABLE 2.2 (Continued)

Test Results						
Thermal Radiation* (cal/cm^2)	3.2	12.8	54.6	25.4	3.7	
					First Shock	Third Shock
Time of Shock Arrival (sec)	14.4	8.0	3.75	5.6	15.5	19.8
Overpressure (psi)	0.3	1.0	2.7	1.8	0.5	0.1
c.g. Acceleration (Δg) Meas.	2.1	3.8	16(est)	8.6	2.3	1.0
Tail Acceleration (Δg) Meas.	2.0	3.6	16(est)	8.5	2.6	1.1
Incremental Wing Loads (% of Design Limit Load)						
Inboard Bending	11	18	70	40	12	5
Inboard Shear	12	22	90	40	10	7
Incremental Tail Loads (% of Design Limit Load)						
Bending	17	27	110	51	13	6
Shear	15	23	100	45	15	5

* Normal to horizontal plane.

Fig. 2.1 AD-2, Starboard Aileron Showing Scorched Blue Paint on 0.016 Skin - Shot 2

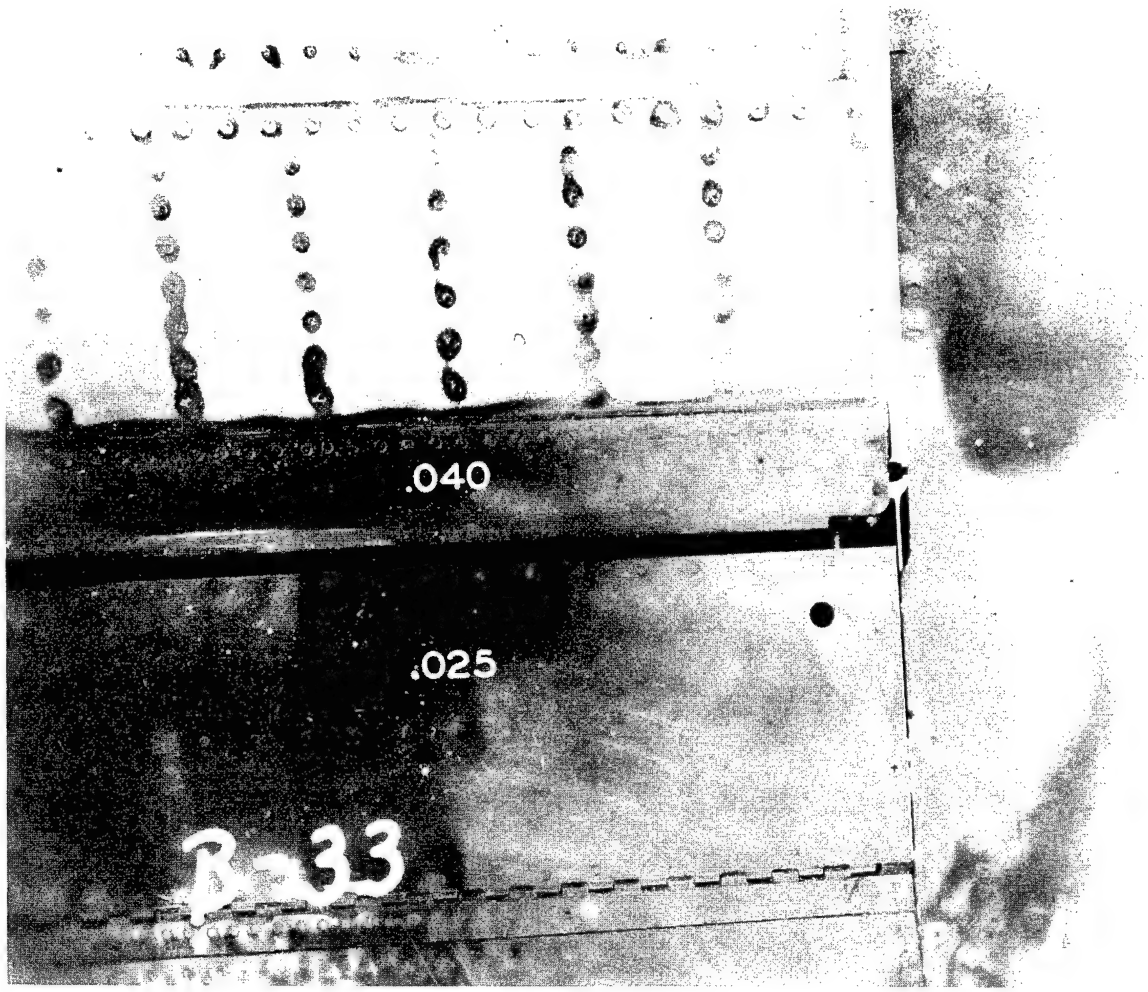

Fig. 2.2 AD-2, Starboard Aileron and Wing Tip Showing Scorched Blue Paint on 0.016 Skin - Shot 2

Fig. 2.3 AD-2, Port Elevator and Horizontal Stabilizer Showing Scorched Blue Paint on 0.016 Skin - Shot 2

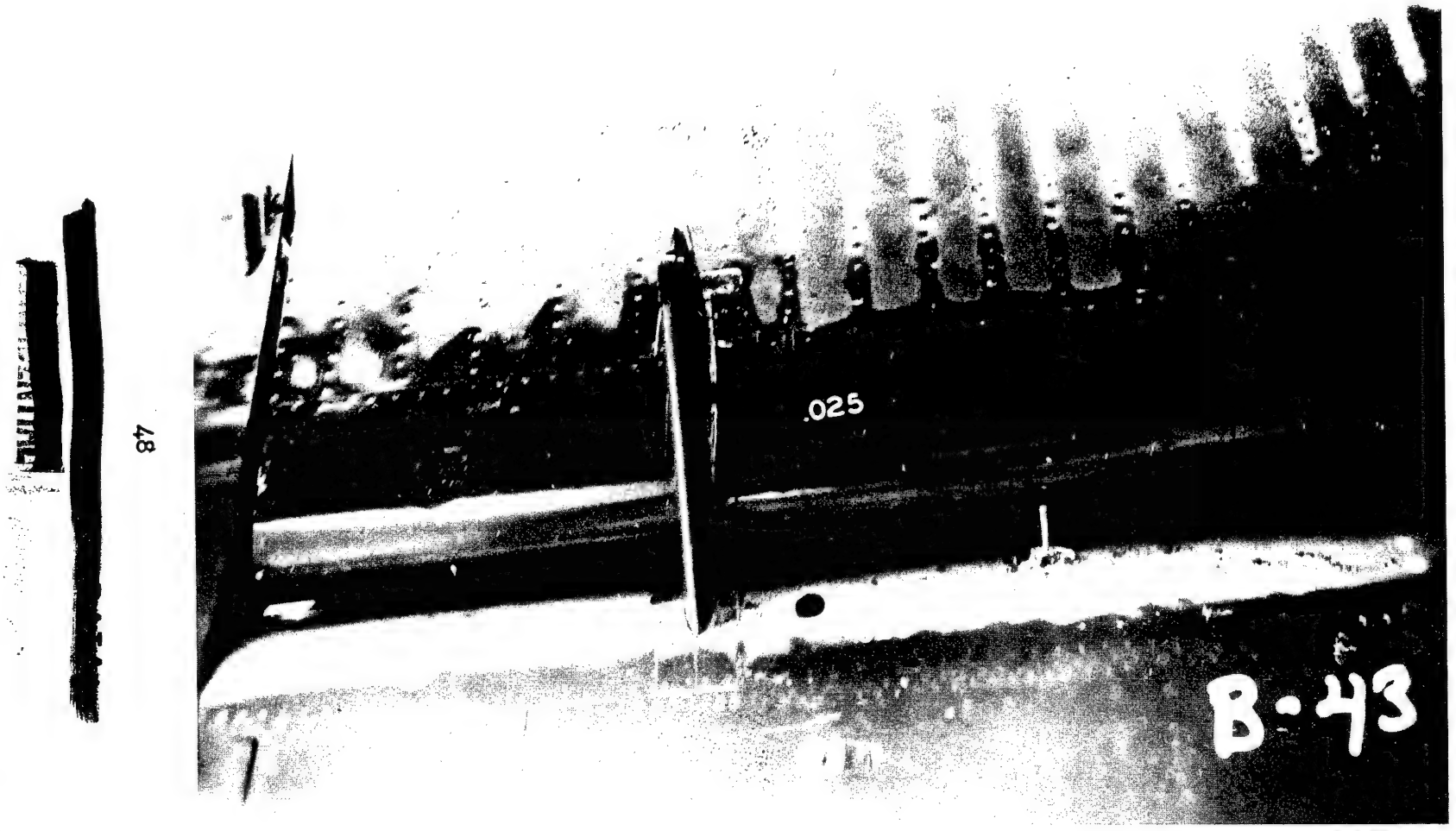

Fig. 2.4 AD-2, Port Wing Flap Showing Scorched Blue Paint on 0.020 Skin, and on 0.025 Skin Forming Curved Portion Aft of Rear Shear Web Facing the Burst - Shot 2

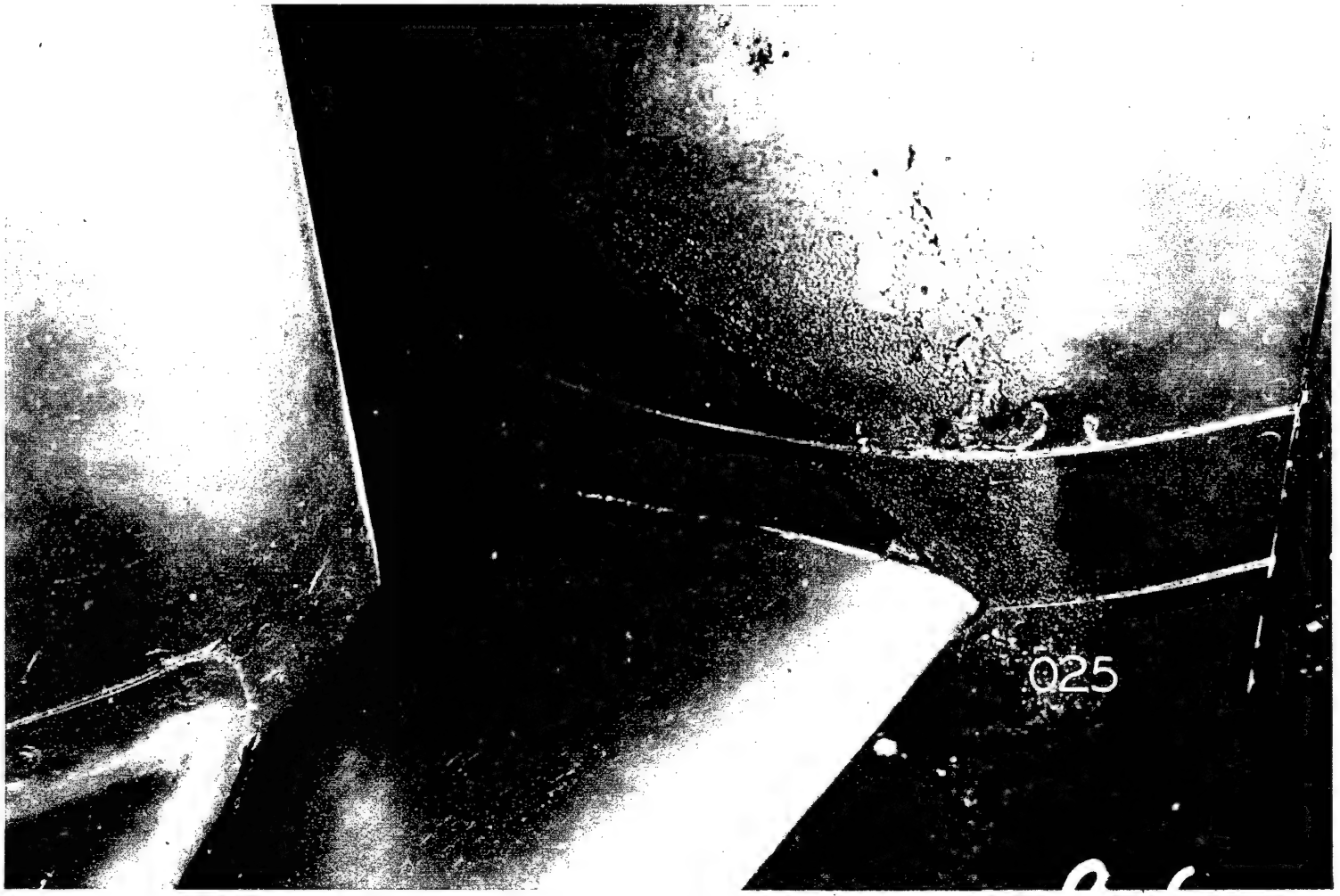

Fig. 2.5 AD-2, Port Wing Flap Showing Scorched Blue Paint on 0.025 Skin Forming Curved Portion Aft of Rear Shear Web Facing the Burst - Shot 2

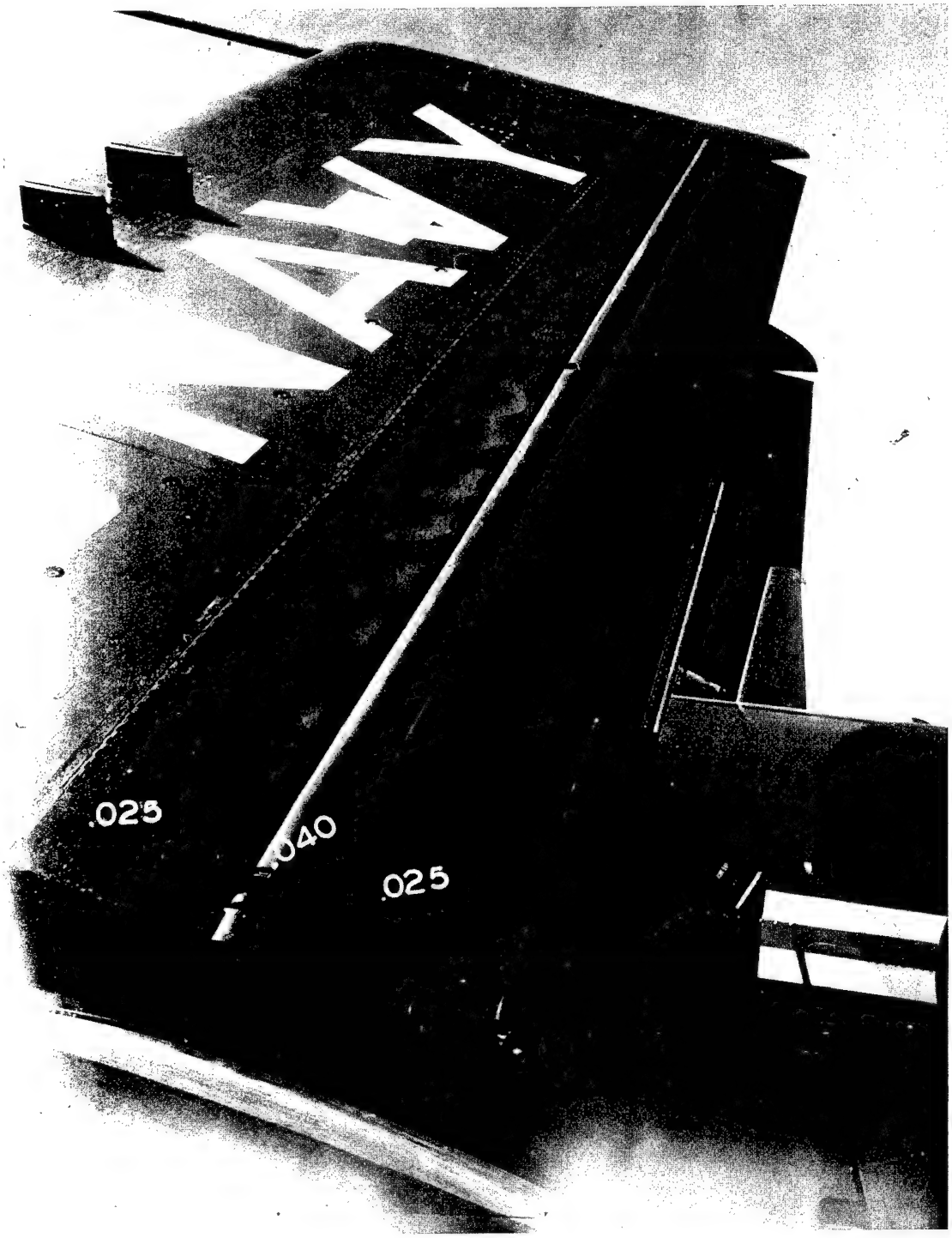

Fig. 2.6 AD-2, Port Wing Showing Scorched Blue Paint on 0.025 Skin on Hinged Aft Edges of Wing Panel - Shot 2

Fig. 2.7 AD-2, Port Wing Panel and Tip Showing Scorched Blue Paint on 0.032 Skin - Shot 2

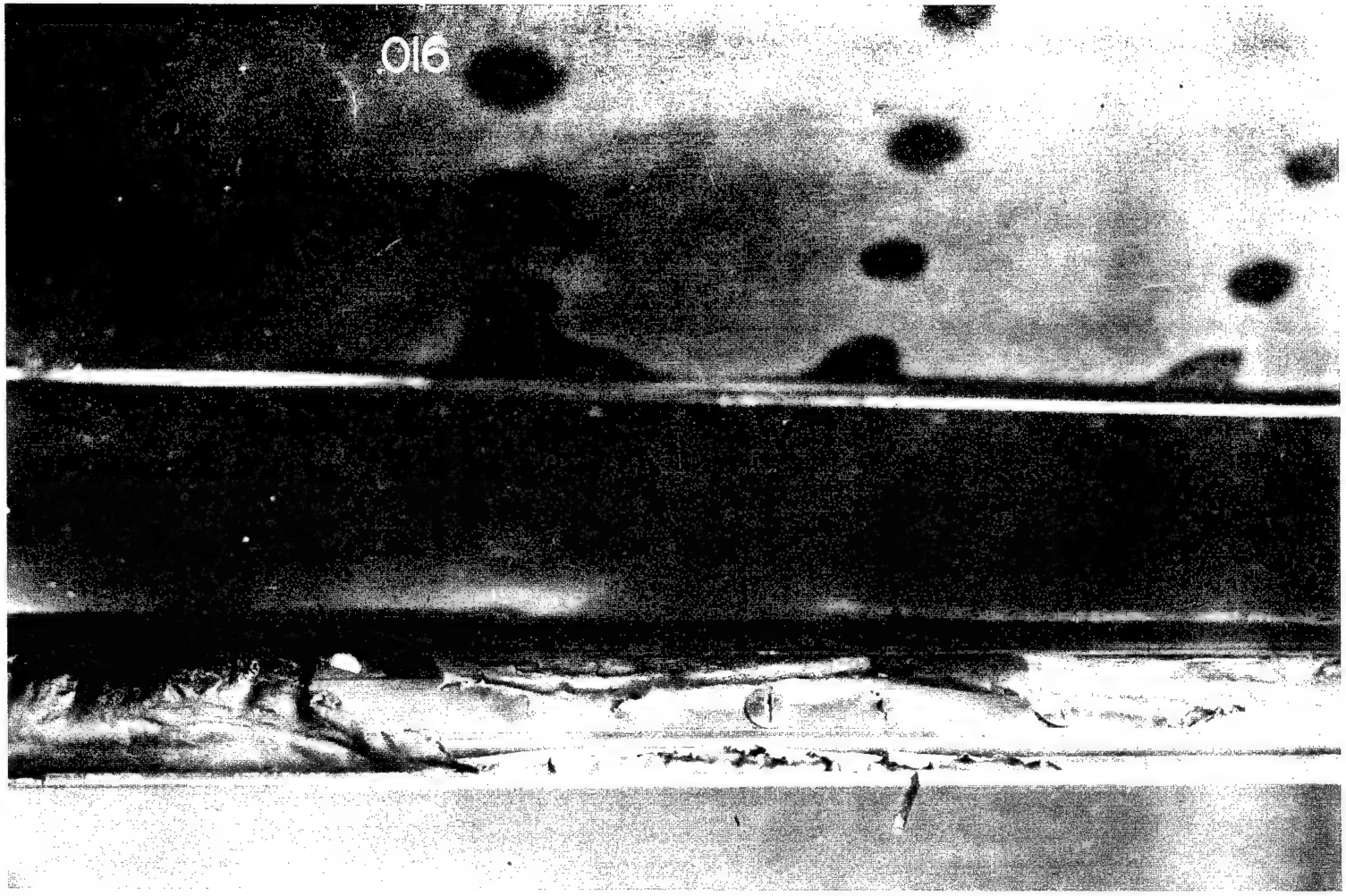

Fig. 2.8 AD-2, Aperture between Elevator and Horizontal Stabilizer Showing Destroyed Rubberized Fabric Aerodynamic Seal - Shot 2

Fig. 2.9 AD-2, Aft of Rear Spar of Horizontal Stabilizer Showing Burned Fabric Lightening Hole Covers - Shot 2

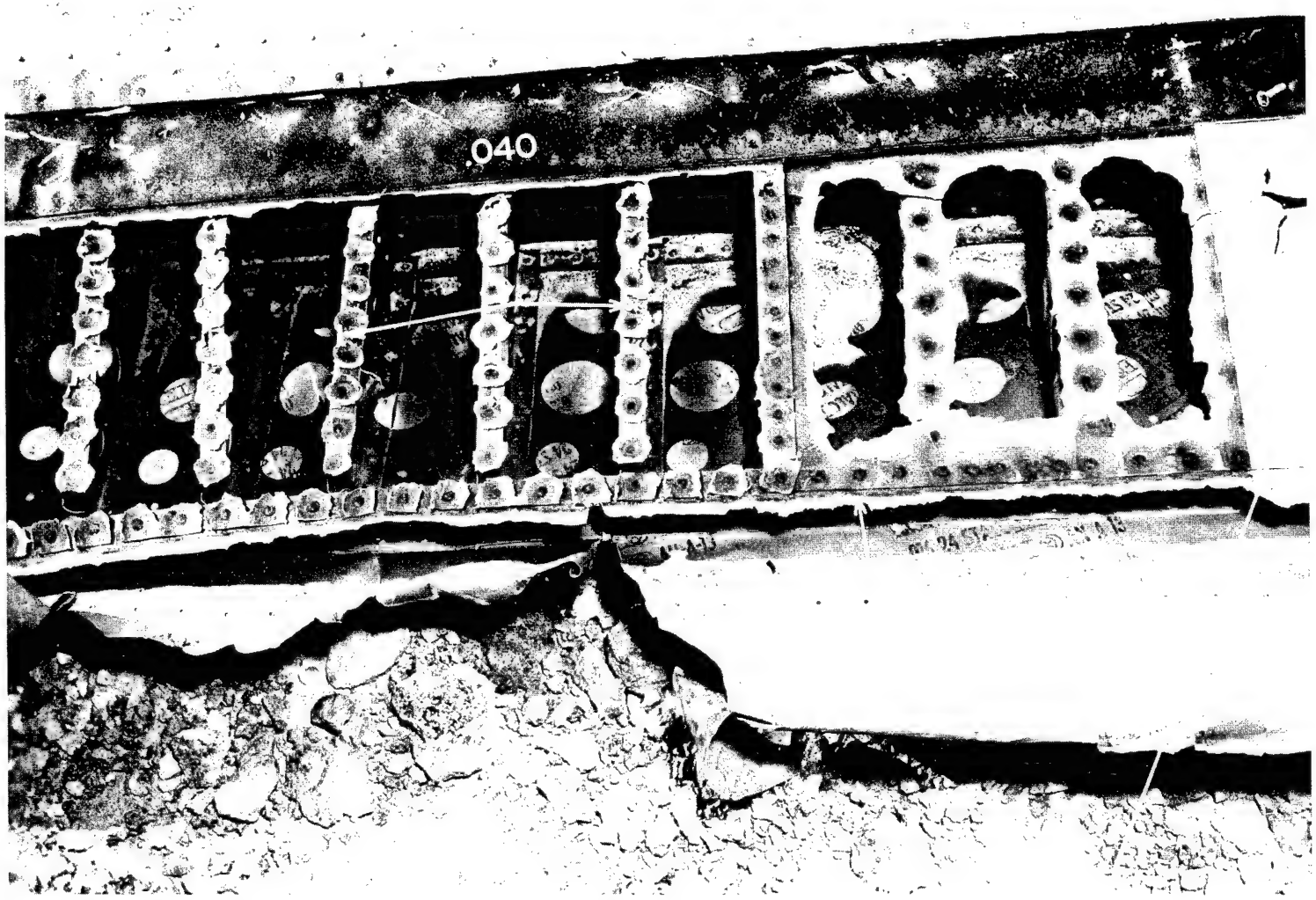

Fig. 2.10 AD-2. Center of Starboard Aileron Showing Burned Out 0.016 and 0.025 Panels - Shot 7

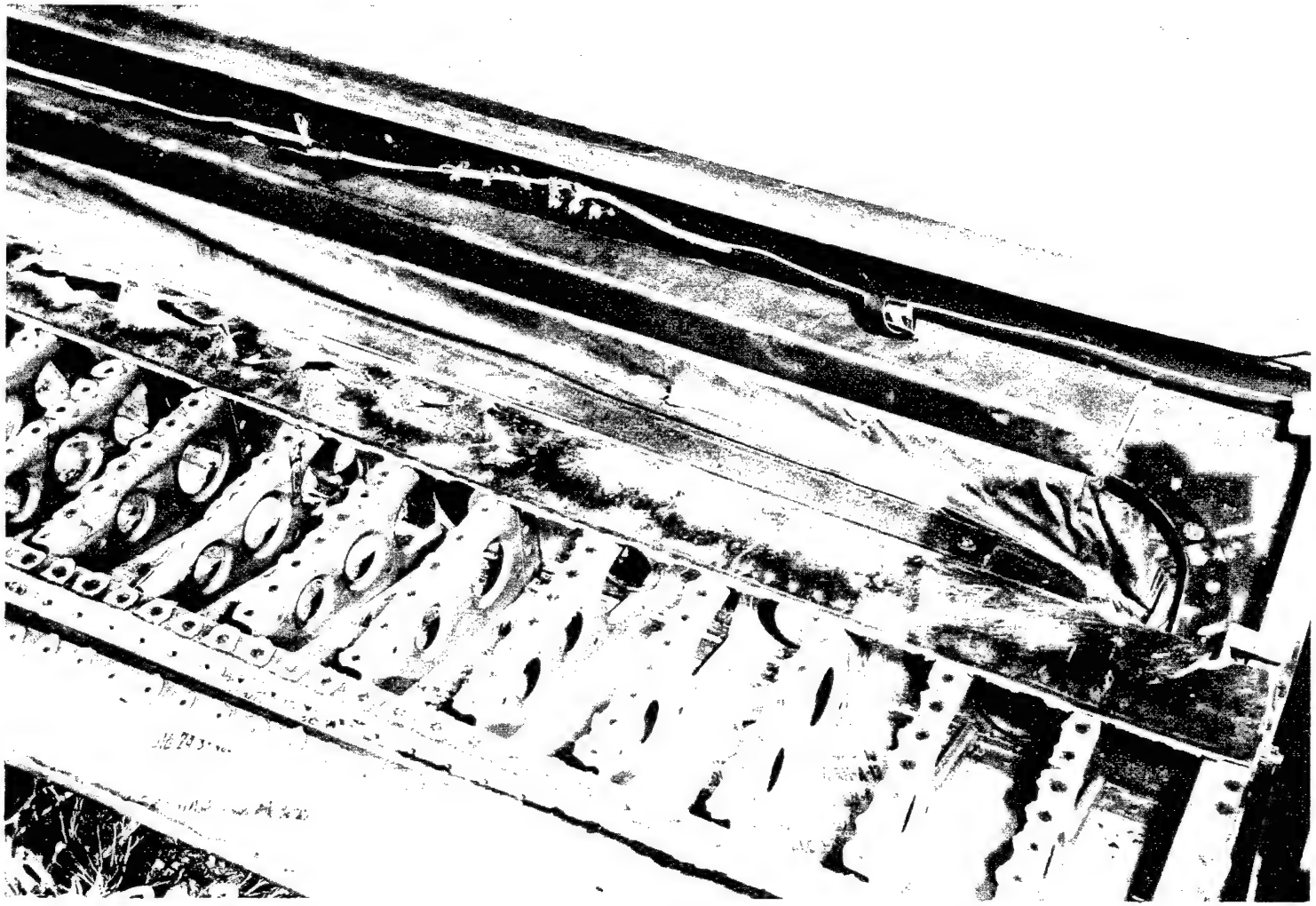

Fig. 2.11 AD-2, Port Aileron Showing Aileron Seal Intact - Shot 7

Fig. 2.12 AD-2, Port Aileron - Showing Relative Damage to Various Combinations of Surface Finish and Skin Thickness - Shot 7

Fig. 2.13 AD-2, Starboard Aileron - Showing Thermal Damage to Aluminized Lacquered 0.025 Skin Compared with Standard Blue Painted 0.025 Skin - Shot 7

Fig. 2.14 AD-2, Port Aileron - Showing Thermal Damage to Aluminized Lacquered 0.025 Skin Compared with Standard Blue Painted 0.025 Skin - Shot 7

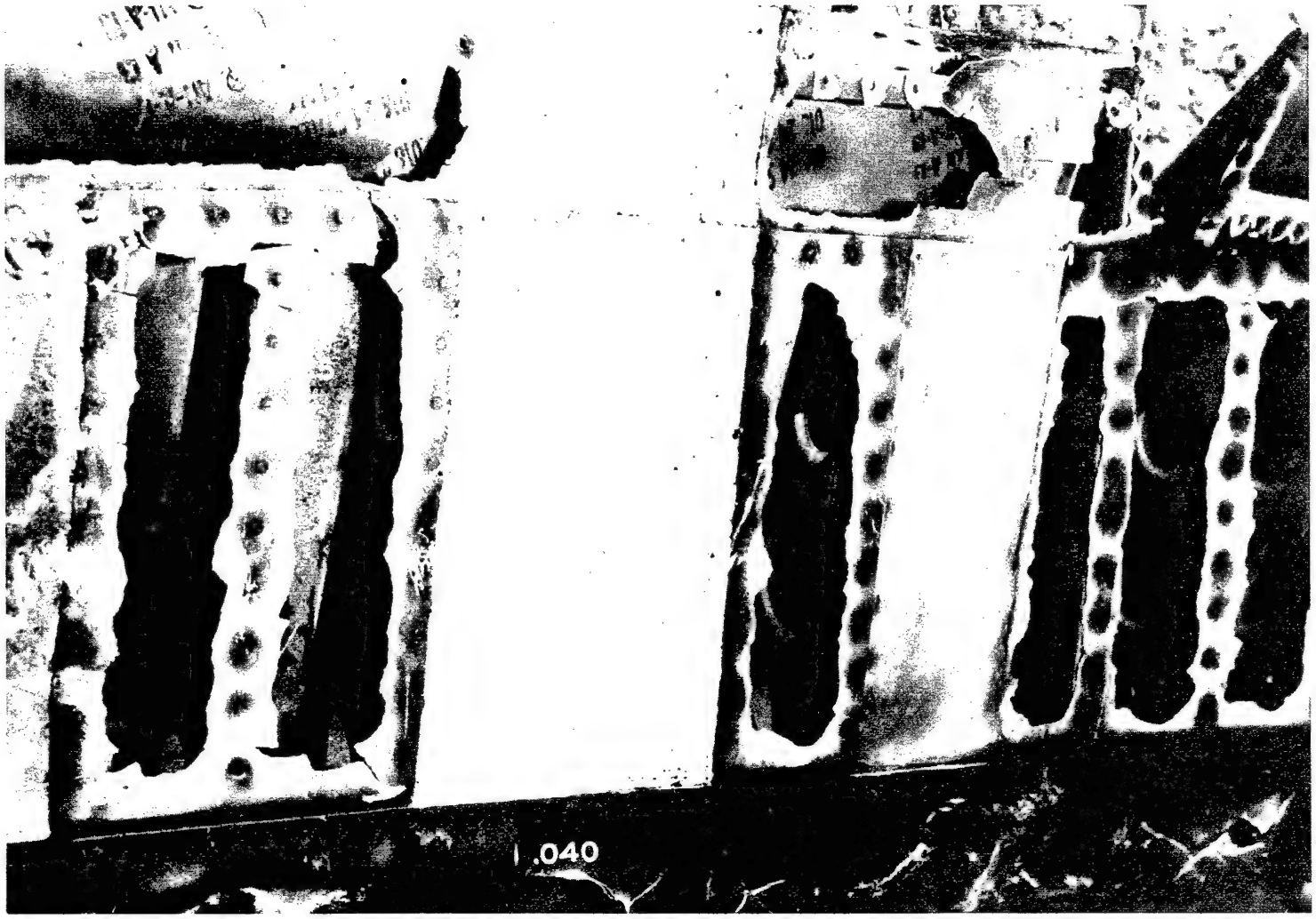

Fig. 2.15 AD-2, Port Aileron - Showing Relative Damage to Various Combinations of Surface Finish and Skin Thickness - Shot 7

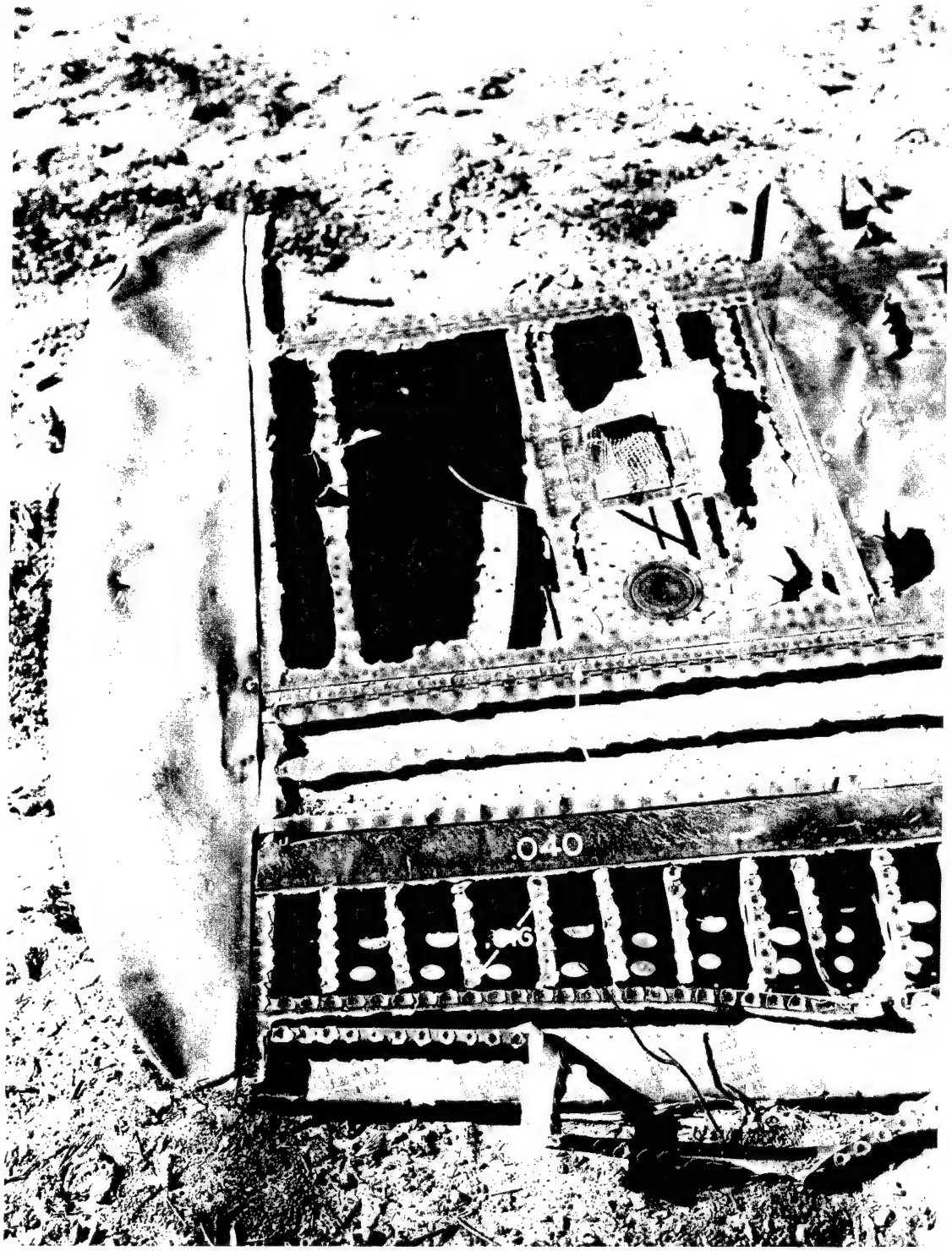

Fig. 2.16 AD-2, Outboard Port Wing Panel and Wing Tip Showing Wing Tip Intact. Note how white star protected 0.032 skin. - Shot 7

[redacted]

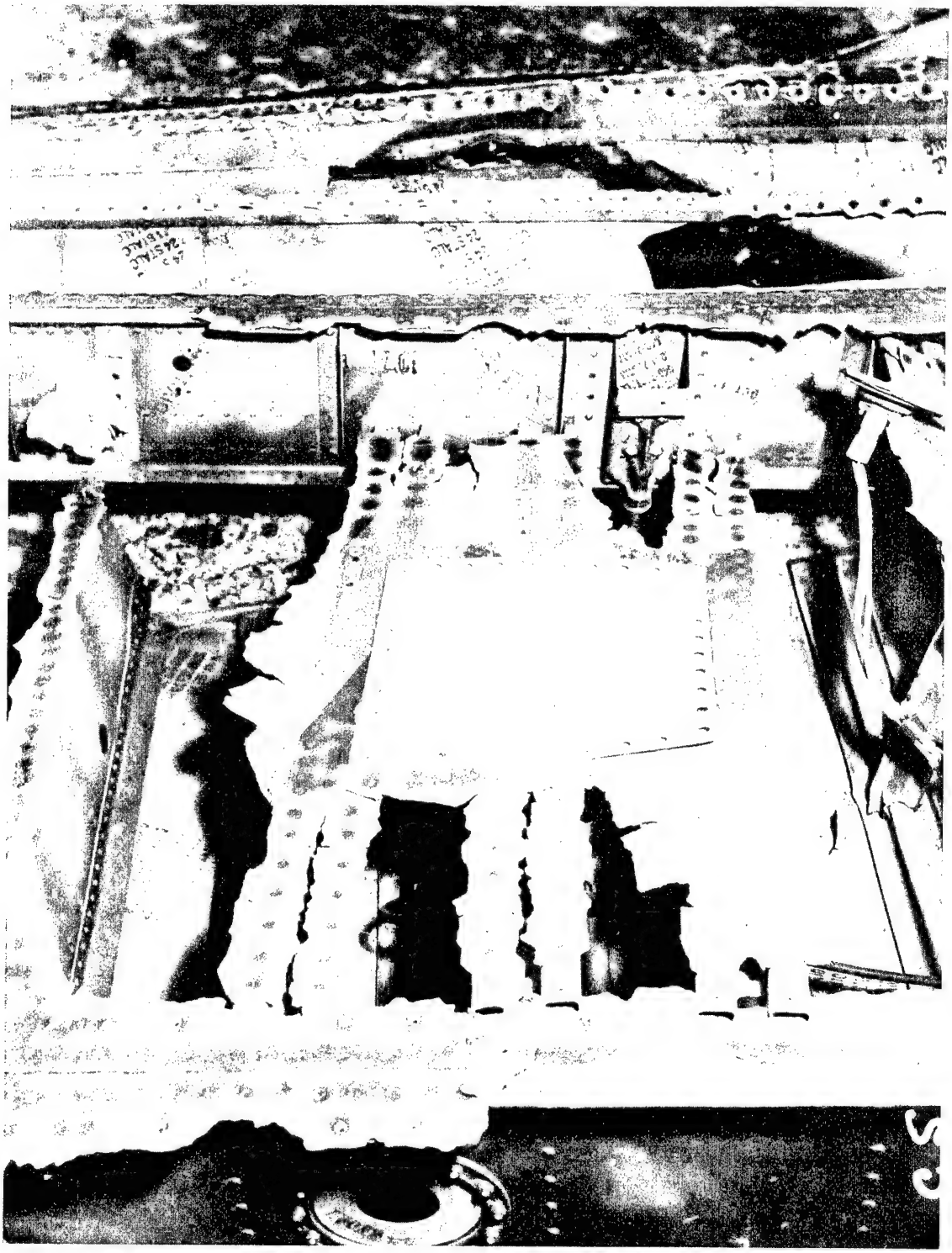

Fig. 2.17 AD-2, Outboard Port Wing Panel Showing Heat Resistant White Painted 0.032 Plate - Shot 7

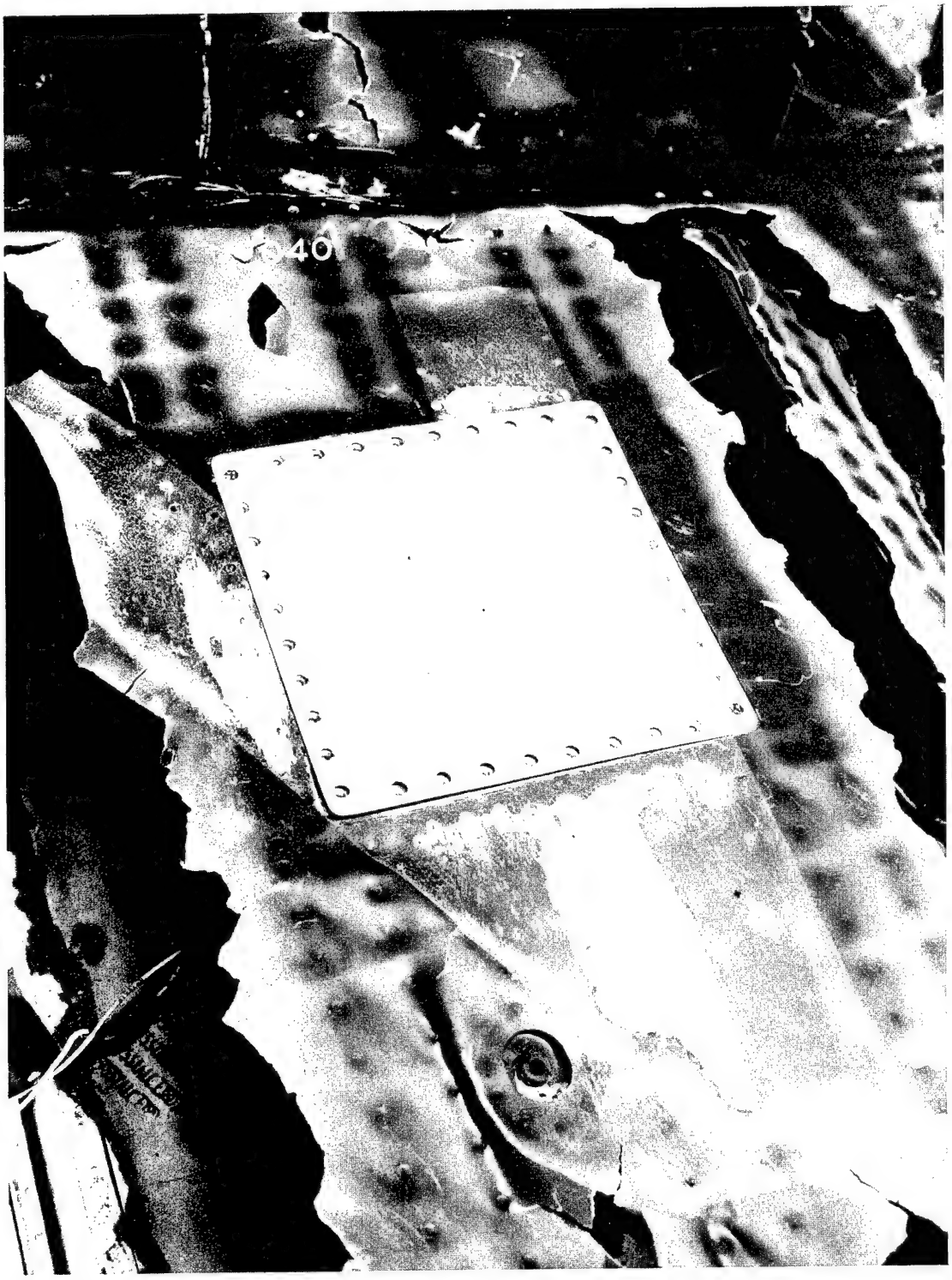

Fig. 2.18 AD-2, Outboard Port Wing Panel Showing Aluminized Lacquered 0.040 Plate - Shot 7

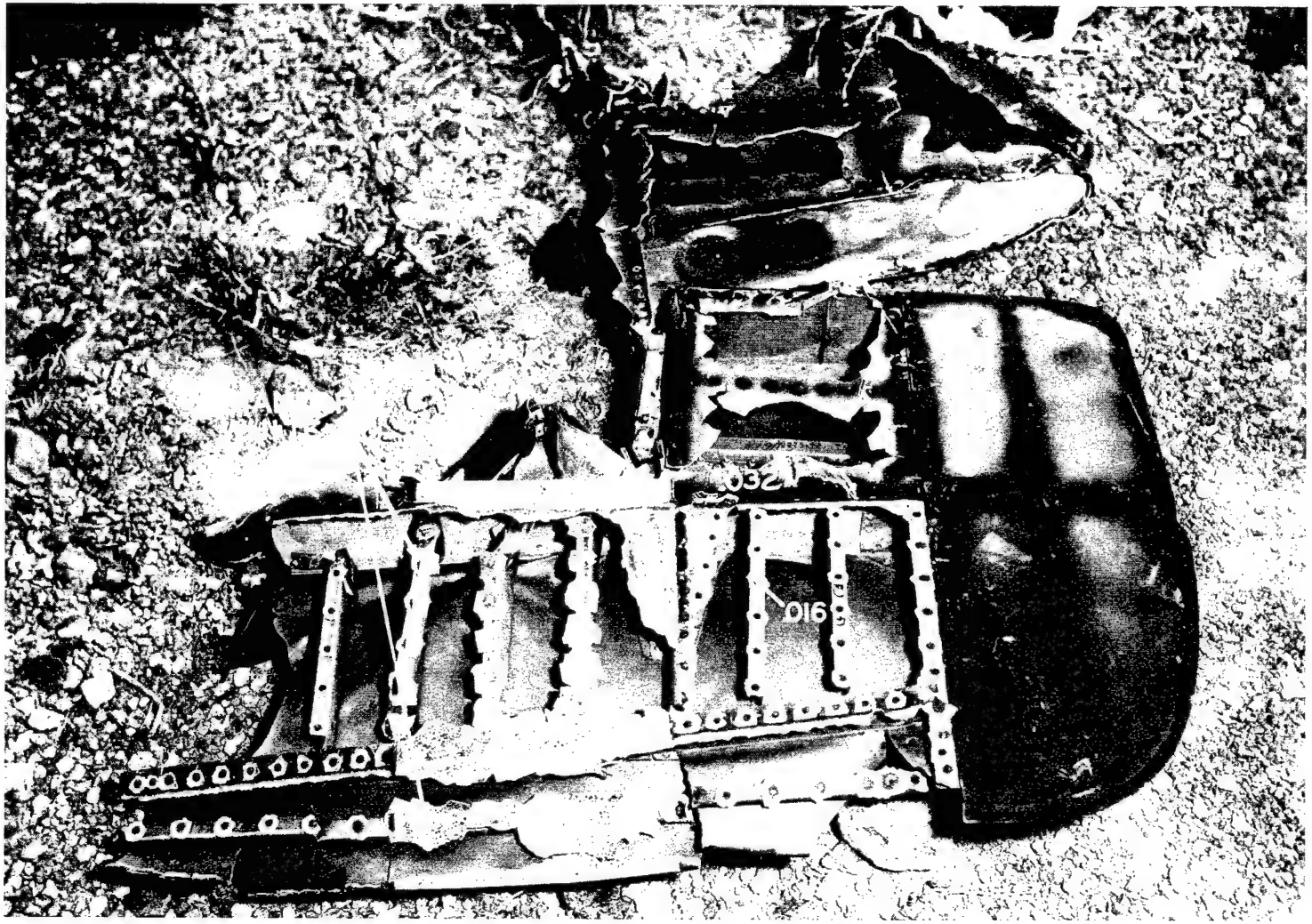

Fig. 2.19 AD-2, Tip of Elevator and Horizontal Stabilizer Showing Fabric-Lightening Hole Covers and Elevator Tip Intact - Shot 7

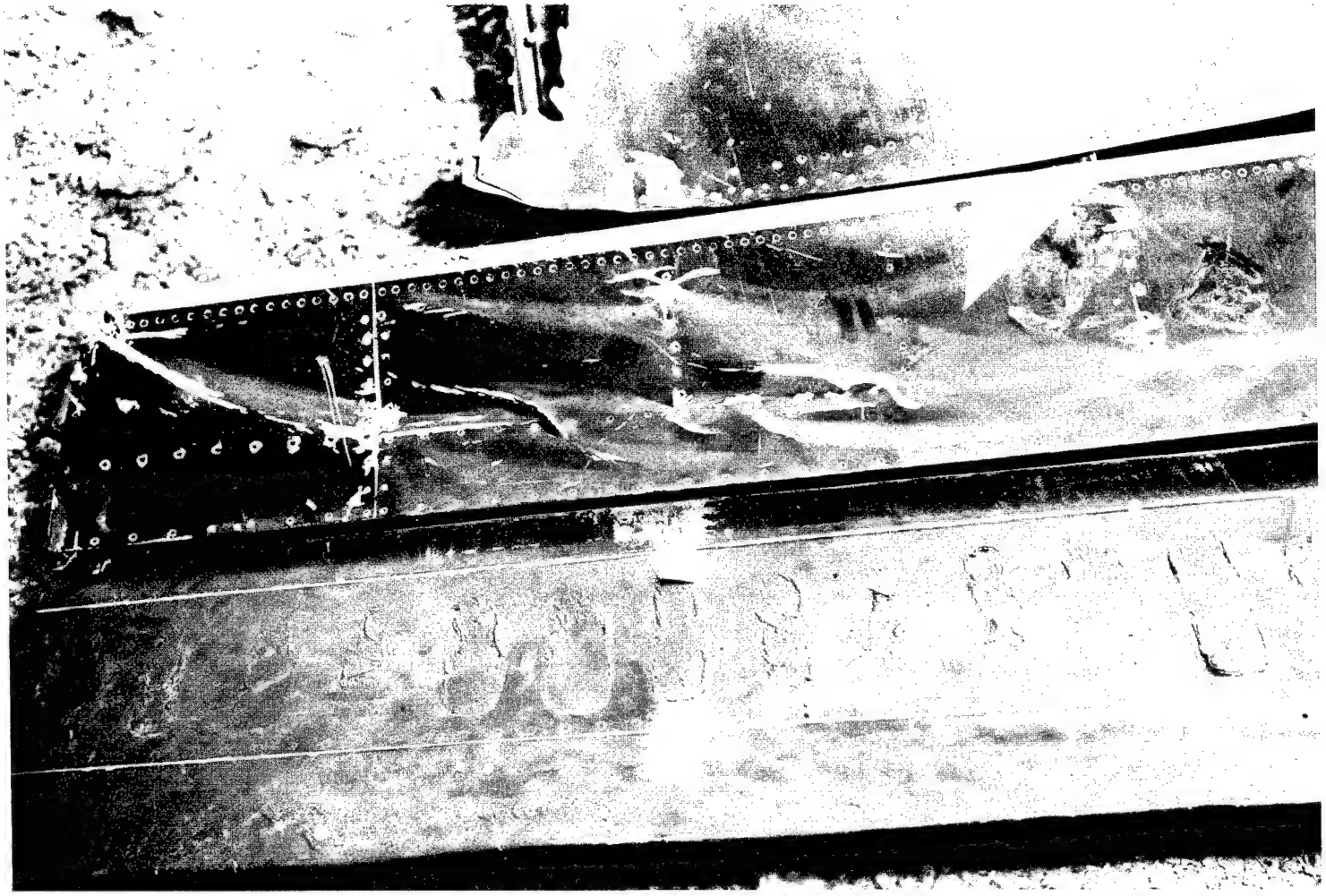

Fig. 2.20 AD-2, Topside of Port Wing Panel Showing Scorched Blue Paint on 0.016 Skin - Shot 7

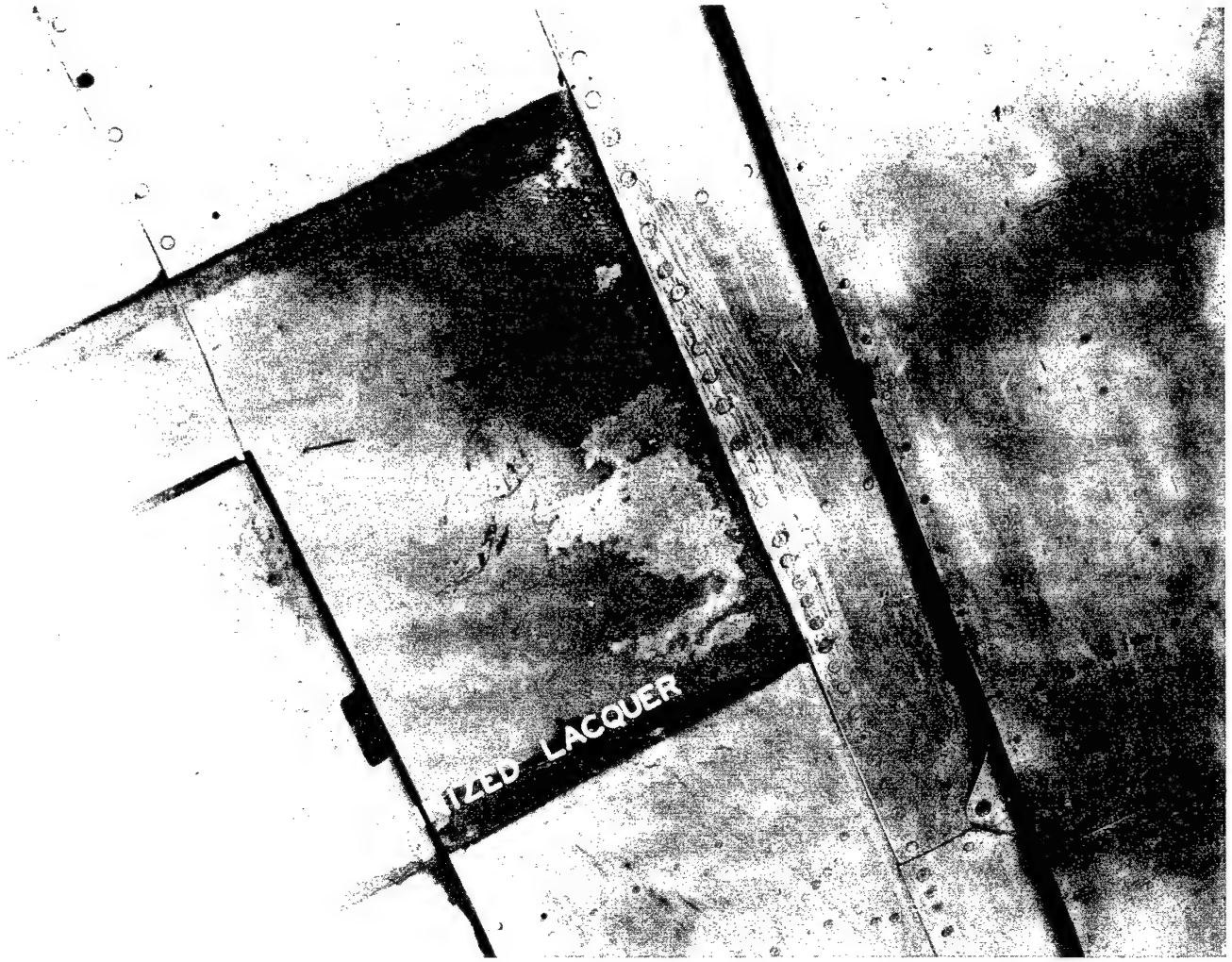

Fig. 2.21 XBT2D-1, Starboard Aileron Showing Scorched Aluminized Lacquer on 0.016 and 0.025 Skin - Shot 8

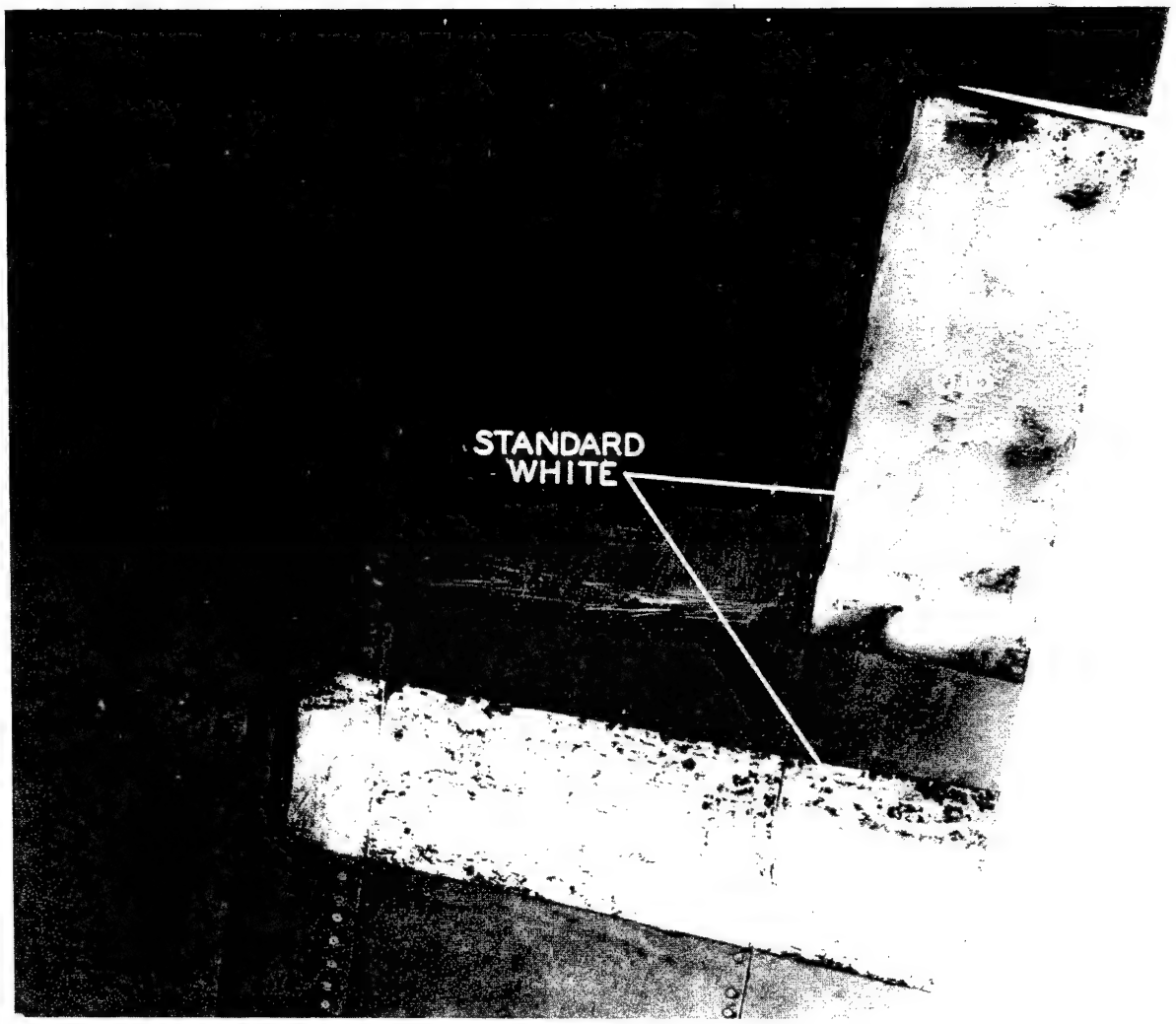

Fig. 2.22 XBT2D-1, Port Aileron Showing Scorched Standard White Paint on 0.016, 0.025 and 0.040 Skin - Shot 8

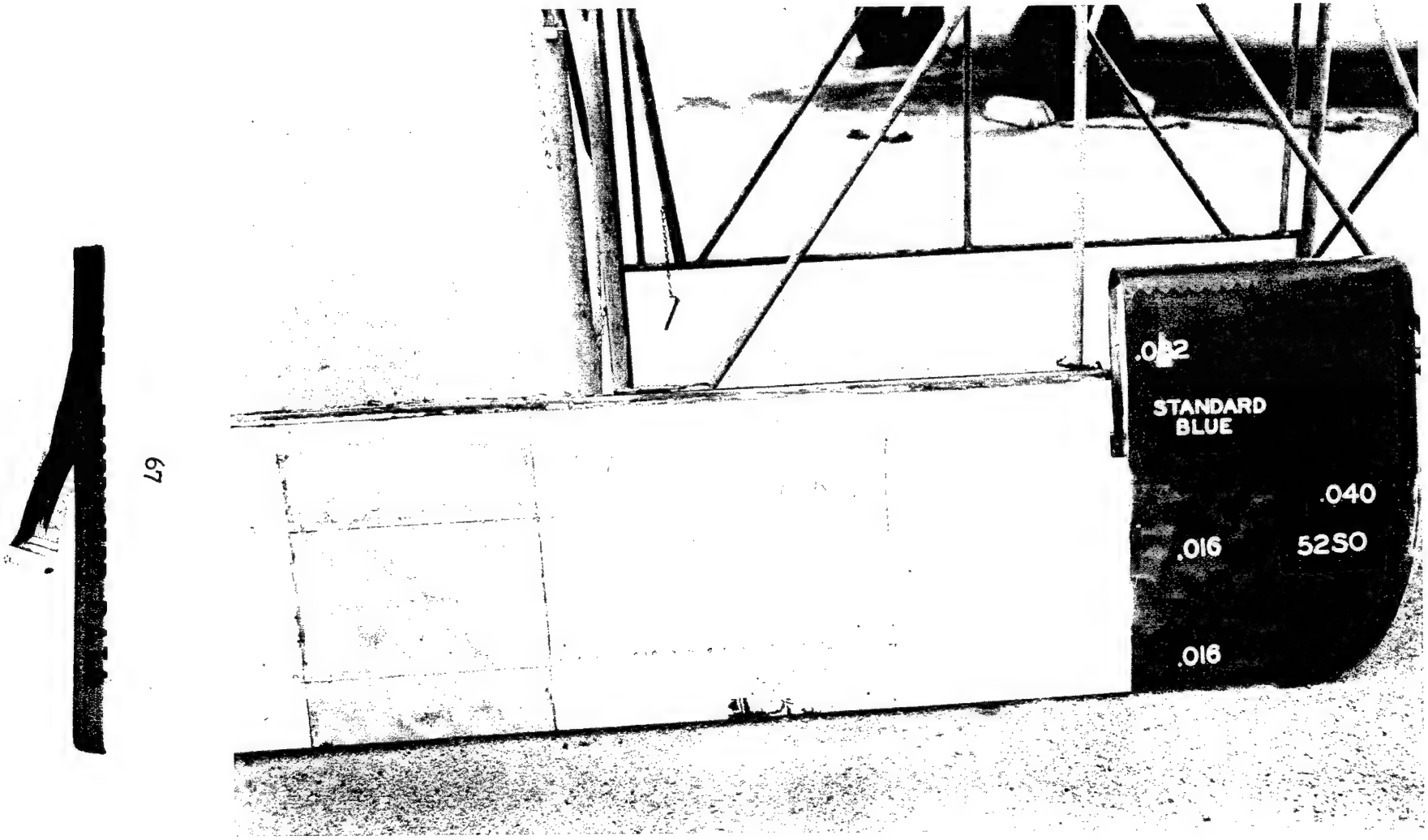

Fig. 2.23 XBT2D-1, Port Elevator Showing Scorched Painted Surfaces. Note skin ripples on 0.016 standard blue painted and aluminized lacquered surfaces. - Shot 8

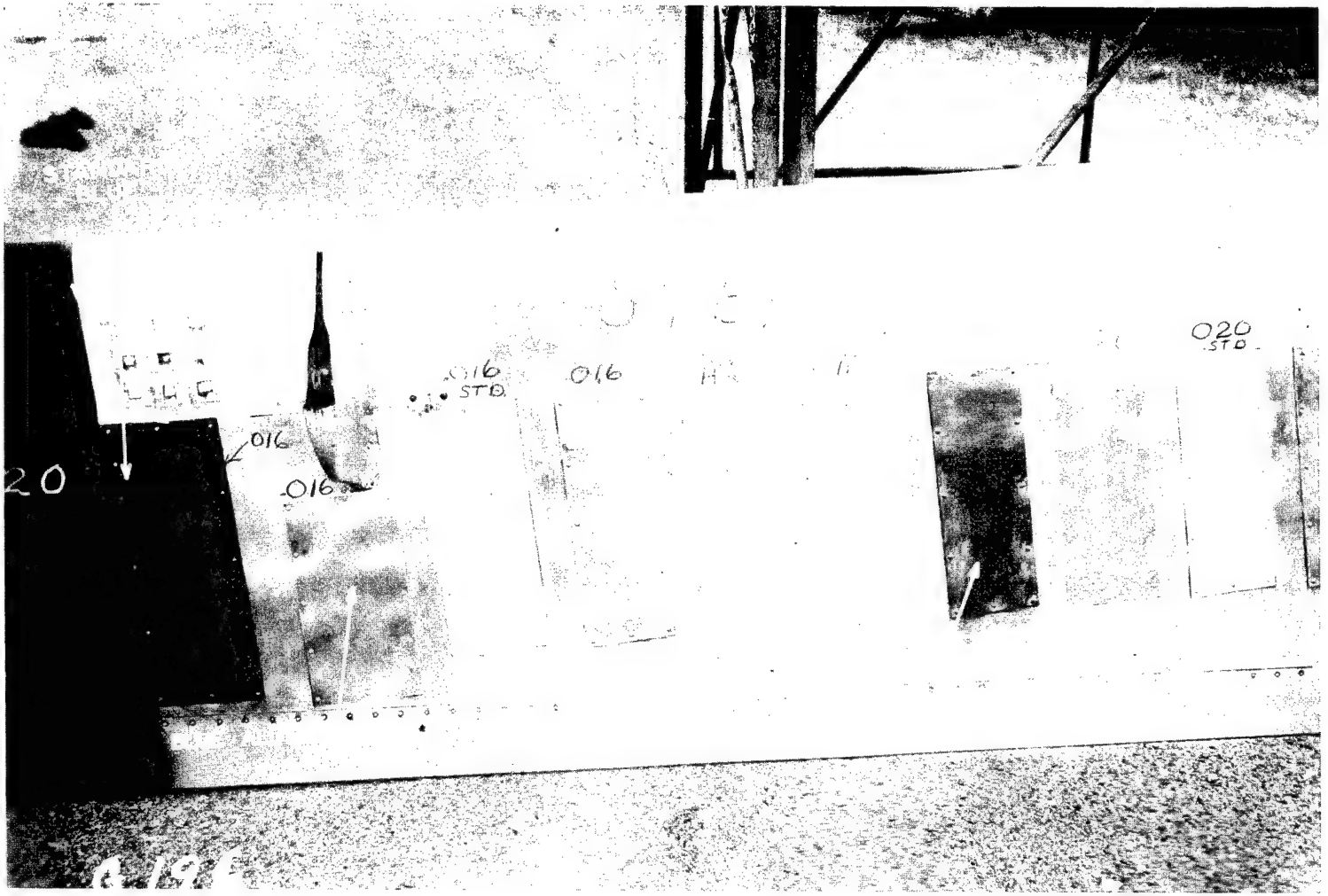

Fig. 2.24 XBT2D-1, Starboard Wing Flap with Thermal Test Panels Installed, Outboard Portion - Shot 8

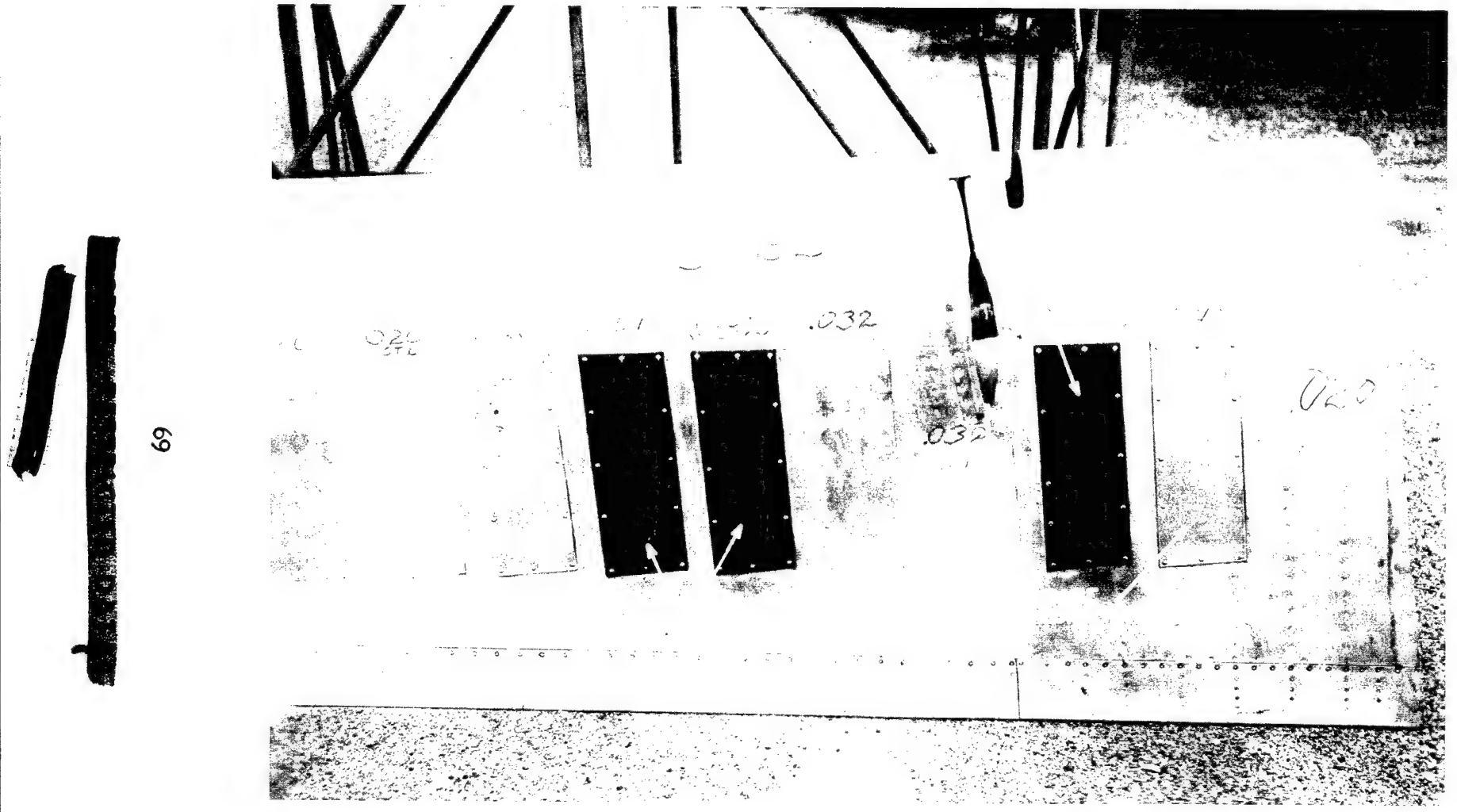

Fig. 2.25 XBT2D-1, Starboard Wing Flap with Thermal Test Panels Installed, Inboard Portion - Shot 8

Fig. 2.26 XBT2D-1, Port Wing Flap with Thermal Test Panels Installed, Outboard Portion - Shot 8

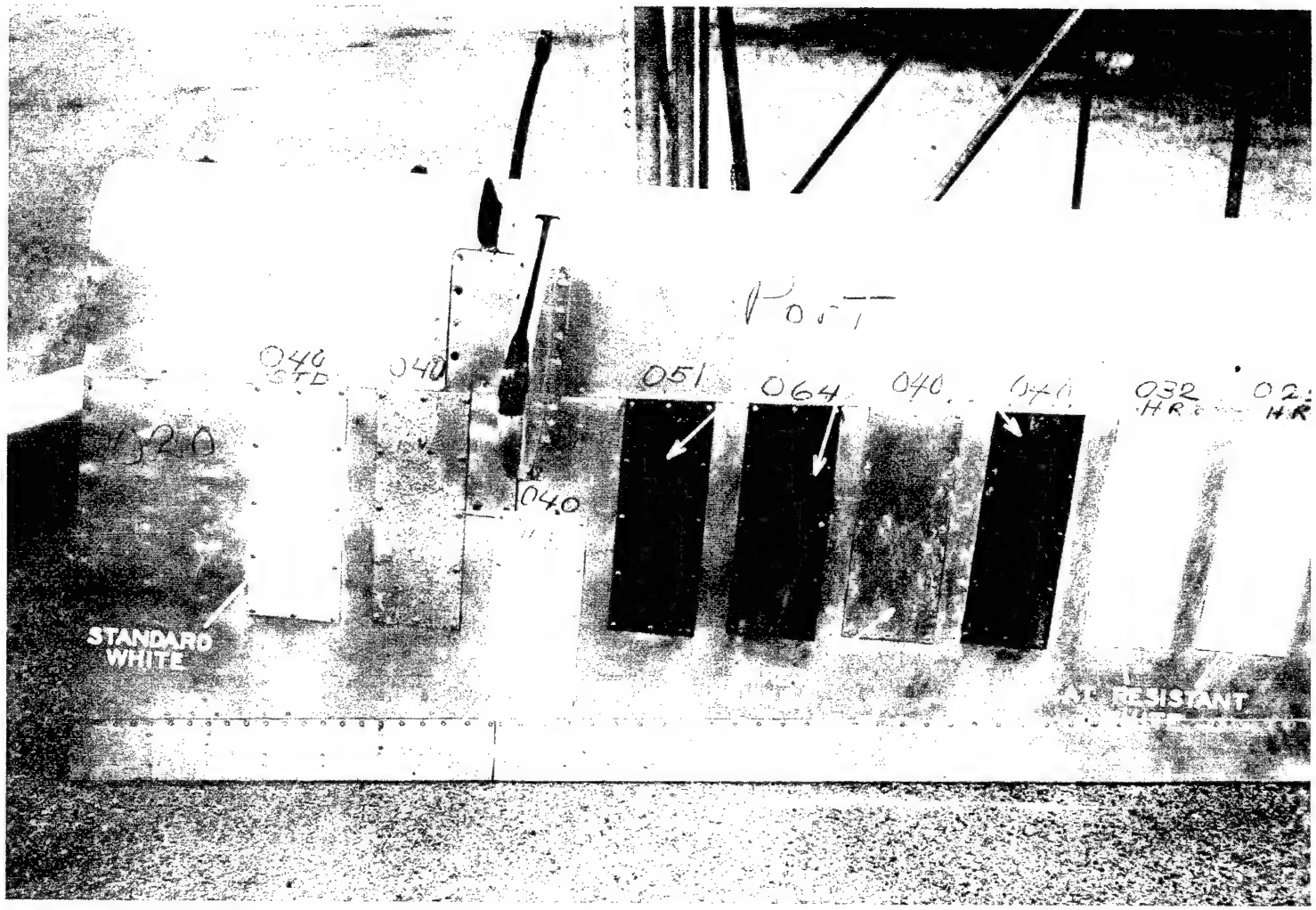

Fig. 2.27 XBT2D-1, Port Wing Flap with Thermal Test Panels Installed, Inboard Portion - Shot 8

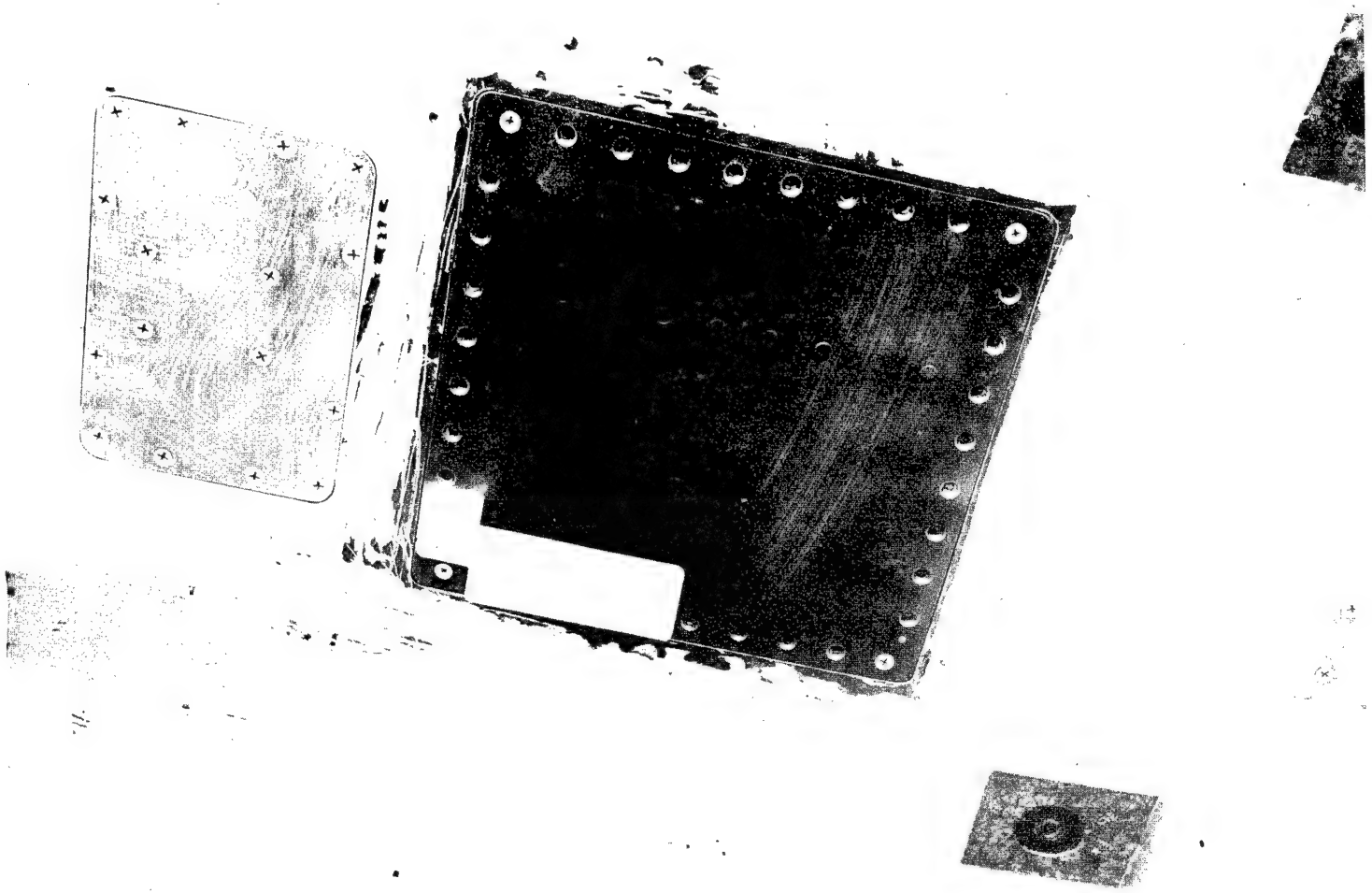

Fig. 2.28 XBT2D-1, Center of Wing Showing Scorched Blue Paint on 0.032 Skin - Shot 8

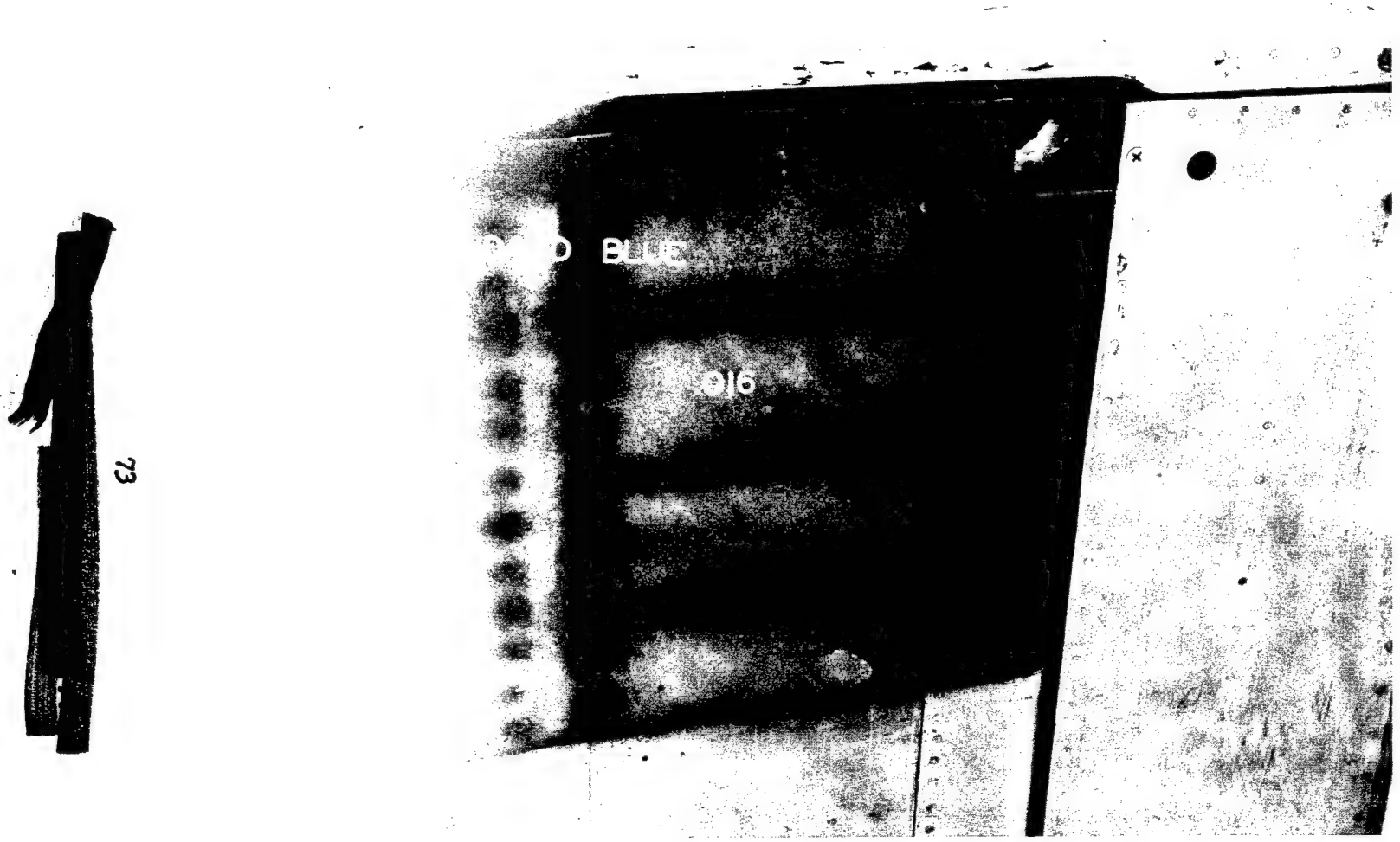

Fig. 2.29 XBT2D-1, Starboard Aileron Wing Tip Showing Scorched Standard Blue Paint on 0.016 and 0.040 skin. Note ripples on standard blue painted 0.016 skin. - Shot 8

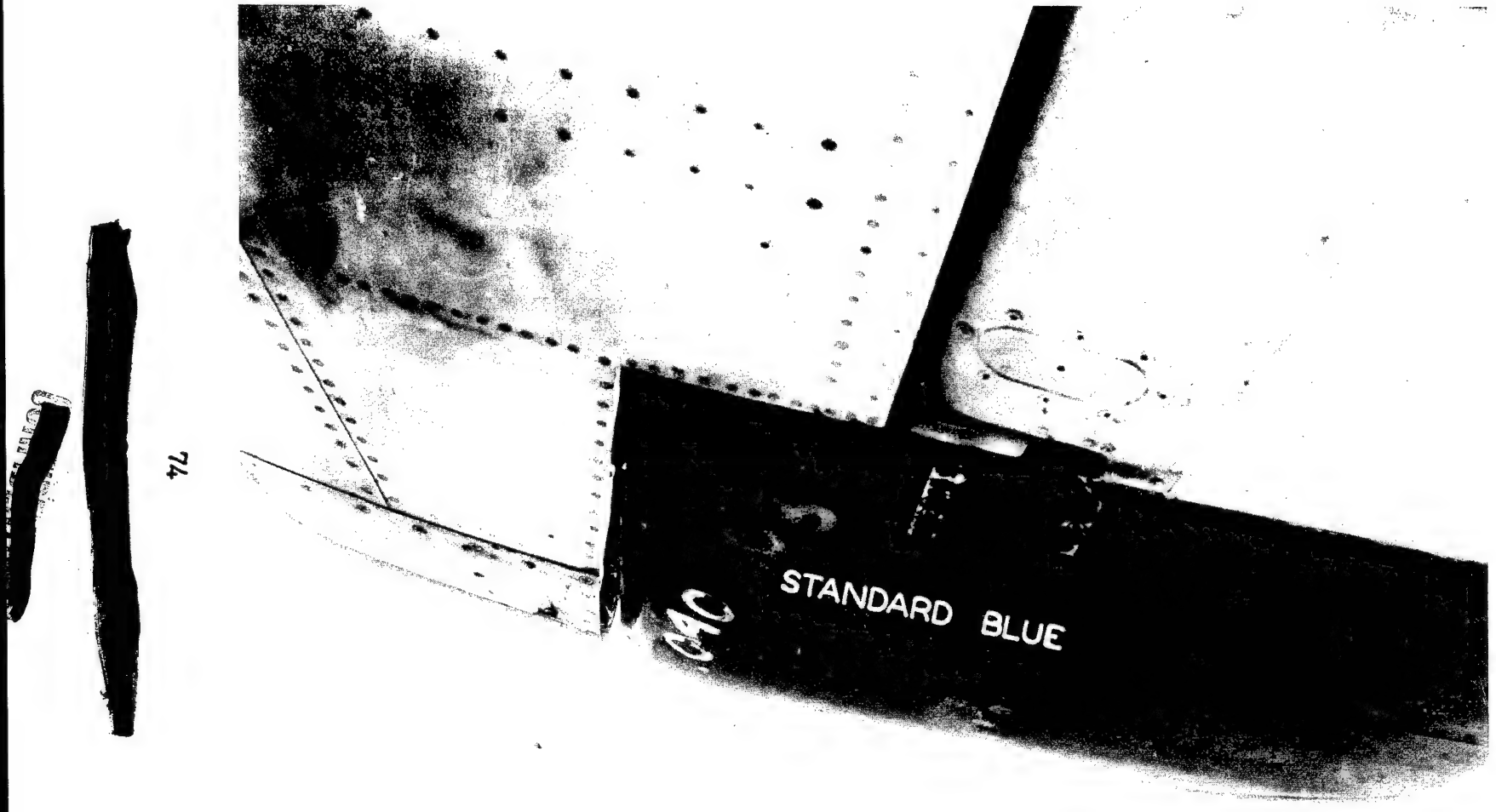

Fig. 2.30 XBT2D-1, Starboard Stabilizer and Elevator Showing Scorched Blue Paint on 0.032 and 0.040 Skin - Shot 8

CHAPTER 3

DISCUSSION

3.1 GENERAL

The data in this report permit the determination of a relatively complete picture of weapons effects on AD type aircraft for a representative escape position following the delivery of an atomic weapon. In the presentation of these data, certain relationships are indicated by means of curves superimposed on the basic data. Limited theoretical analyses were employed in arriving at these curves and it is conceivable that some changes may result when more detailed analytical methods are applied. In all cases, however, the recorded data presented herein are considered accurate to within ± 5 percent of the maximum readings obtained.

3.2 THERMAL EFFECTS

3.2.1 General

Although the flight test thermal radiation and temperature data as measured on the inside face of the aircraft skin show reasonable consistency and agreement with thermal damage and with expected values, initial results of metallographic studies of the internal structure of skin specimens from these flights (Appendix A) indicate effects normally associated with temperatures far in excess of the temperatures measured. This condition is believed to be a result of microscopic thermal concentrations in the grain structure of the material. These concentrations are associated with the extremely rapid rate of thermal radiation. Structural tests on these specimens indicate no loss in strength corresponding to the indicated metallographic damage. Accordingly the thermal data presented in this report are considered to adequately represent the thermal information necessary for aircraft structural considerations. The data presented in Appendix B should prove to be of assistance in further analysis. It is to be noted that although this phenomenon was not evidenced in the ground specimens, it is believed that local conditions, such as the dust layer, might have resulted in this discrepancy.

3.2.2 Thermal Radiation

The aircraft and calorimeter orientation relative to the burst point at t_o for all shots is given in Figure 3.1. Aircraft positions with respect to Ground Zero at t_o were determined from automatically plotted radar tracking data. Calorimeter orientations with respect to the burst points and their fields of view were obtained from motion picture films taken from GSAP cameras which were essentially mounted on the axes of the calorimeters. Figure 3.2 gives the value of thermal radiation as measured by the various calorimeters. These two figures indicate certain facts with respect to ground reflection. In Shot 8 two calorimeters were used. The port wing calorimeter was pointed back toward the burst point but aimed above it by approximately 30°. The starboard wing calorimeter was mounted to measure thermal radiation normal to the wing and was aimed approximately 15° below the burst point. The direct readings of these two calorimeters were 17.8 and 24.9 cal/cm^2 respectively. These values, increased to 19.2 and 26.9 when corrected by + 8 per cent for the quartz filter on the calorimeter; were verified by corresponding readings of 17 and 27 on identically oriented cloth thermal indicators. The calculated direct radiation received by these calorimeters is 12.3 and 13.6. Using ground reflectivity calculations with a least squares value of albedo of 0.55 based on data from Shots 1, 2 and 8, the calculated total thermal radiation for these two installations is 20.8 and 25.7. These values are seen to correspond closely to the true calorimeter readings. The fact that the starboard wing calorimeter would have been exposed to maximum effects of ground reflection in addition to direct radiation from the fireball appears to justify its reading. The effect of reduced ground reflection on the port calorimeter similarly explains its lower reading. In Shot 9 the position of the fireball is approaching the ± 45° field of view limit of the calorimeter and as such it is expected that a large portion of the direct thermal radiation from the burst would be missed. This is more strongly evidenced in Shot 7 where the fireball is partially outside of the calorimeter field of view. Almost the entire thermal reading for this condition would be due to reflected thermal radiation. Considering all such factors, estimates for thermal radiation received normal to the wing can be made for the shots in which it was not directly measured. Figures 3.3 and 3.4, based on ref (9), present the reflectivity information used for this work. A comparison of calculated and measured calorimeter readings is given in Figures 3.5 and 3.6. The results appear to verify the ground reflection effect indicated in ref (7), where reflection from the ground was estimated to be 50 per cent of the direct radiation.

3.2.3 Aircraft Skin Temperature Rise

Temperature rise in aircraft skin, was initially assumed to be directly proportional to the heat received and to the reciprocal of skin thickness. The time histories of temperature rise shown on Figure 3.7 indicate that the cooling rate is an important factor in this problem. Figure 3.8 shows the general agreement between measured cooling

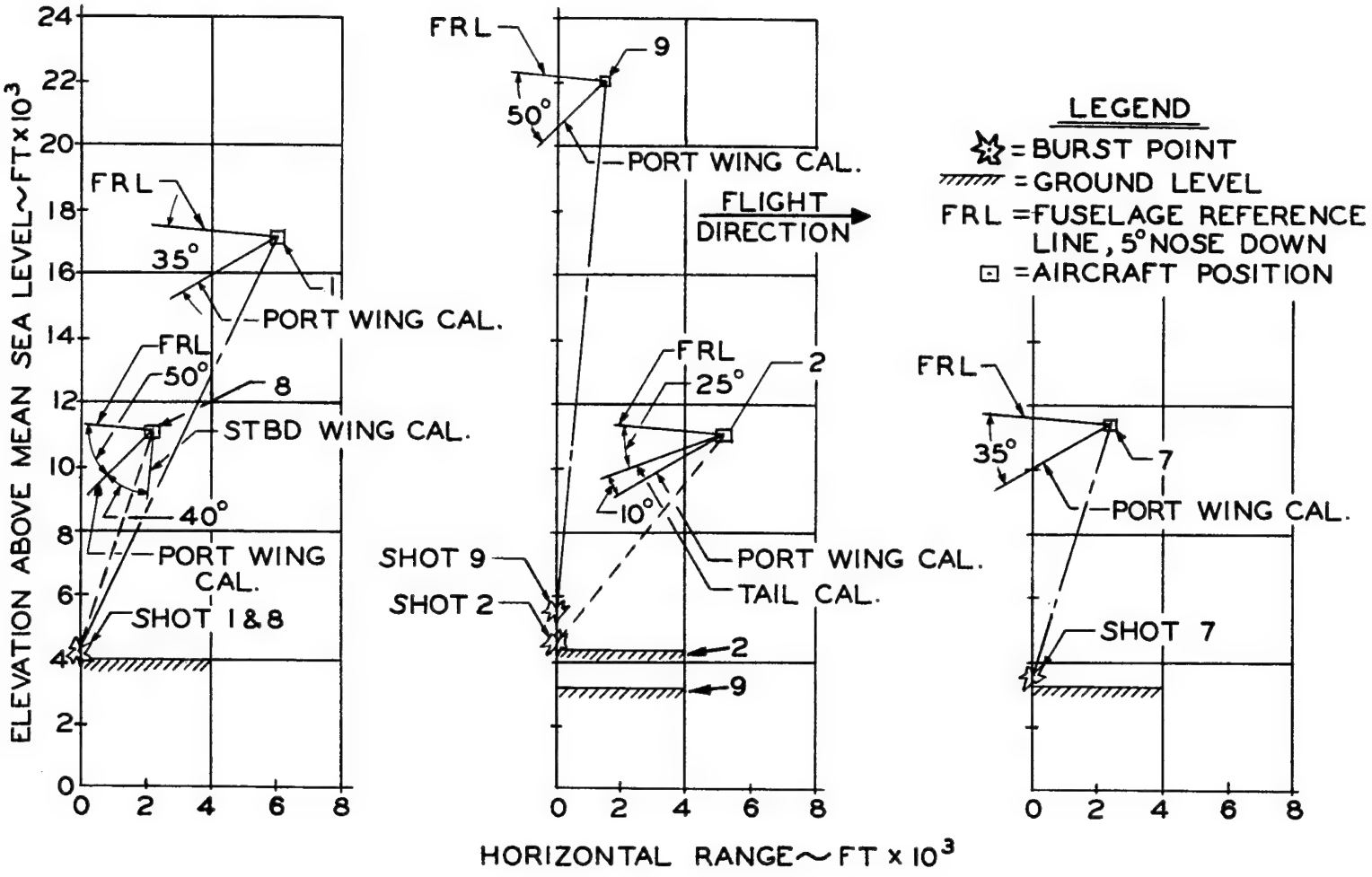

Fig. 3.1 Aircraft and Calorimeter Orientation Relative to Burst.

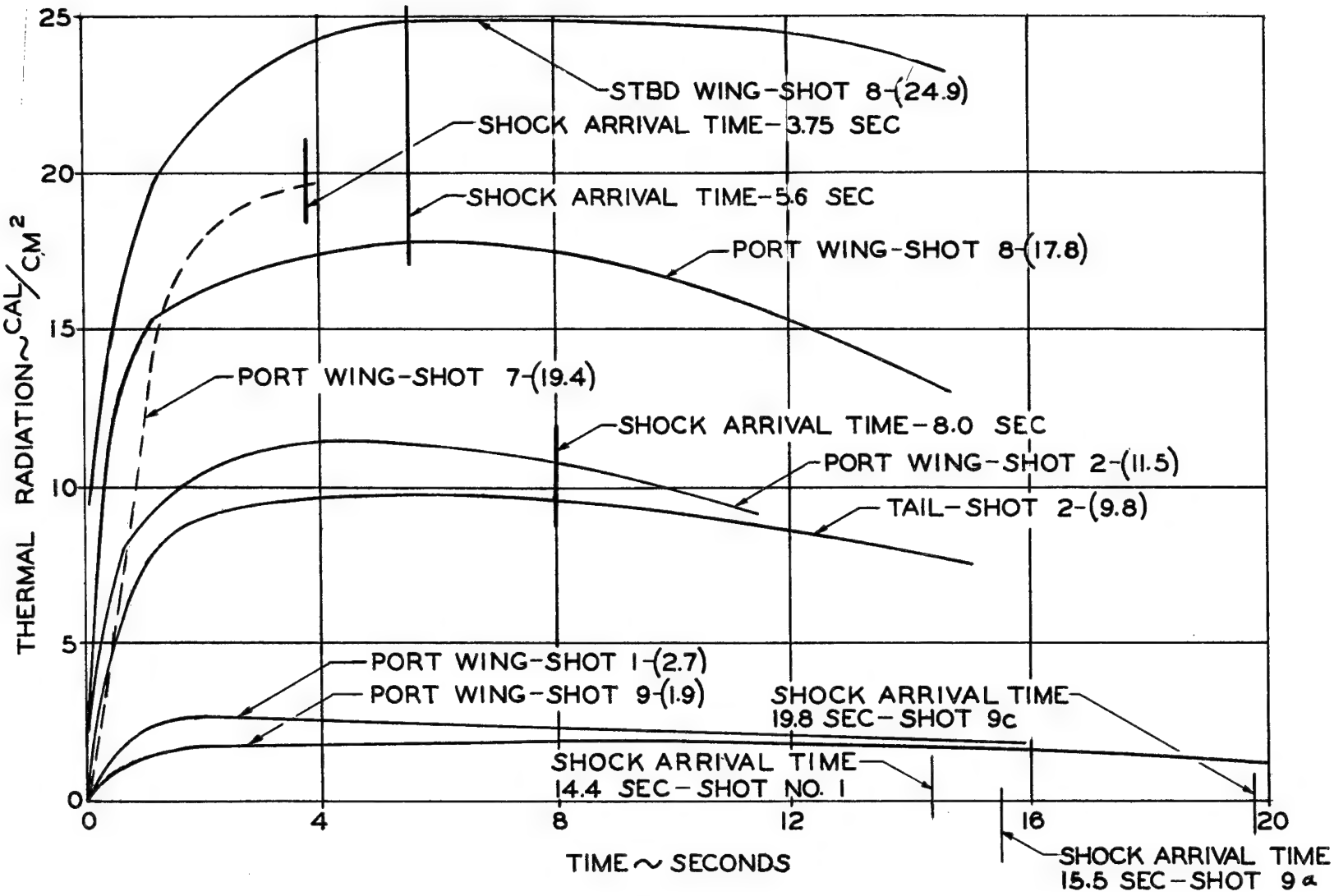

Fig. 3.2 Time History of Measured Thermal Radiation

rates and those calculated following the methods of ref (14), if the proper assumption of turbulent or laminar flow is made.

A lowering of effective absorptivity values for thinner skin independently of surface finish is shown in Figures 3.9 through 3.13 for Shot 8 specimens. The curves through the test points were drawn with an attempt to minimize this effect. Figure 3.14 summarizes these data in the form of a family of curves based on readings from temperature sensitive papers. Two temperature sensitive gage readings are included as an indication of the general agreement of data measured by two different devices. Figure 3.15 is a summary of temperature rise data from Shot 2. Although the data were limited, it can be seen that curves of the same characteristic shape fit the points. An indication of the range of equivalent absorptivities for different surface finish and skin thickness for Shot 8 and Shot 2 is given in Figure 3.16. The effect of aerodynamic cooling does not appear to fully explain the lowering of the effective absorptivity values for thinner skins. This can be seen in Table 3.1 which compares the equivalent absorptivity values for representative cases of surface finish and skin thickness in Shot 8 with absorptivities considering the methods of ref (14). The same general trend of lower absorptivity for thinner skin is indicated here. In a discussion of an equivalent absorptivity value it is important to remember that it is dependent on the amount of heat assumed to be received by the material. Any amount of heat added or lost as a result of thermal damage to surface coatings will have a tendency to influence this value. Using average values for these absorptivities and the assumed normal thermal radiation of 55 cal/cm^2, the temperature rise in 0.016 and 0.064 in. skin for Shot 7 was estimated. The two estimated values for skin with an aluminized lacquer finish appear to substantiate the 450°F temperature rise in the 0.040 in. skin. The predicted temperature rise appears consistent with the observed damage for the aircraft skin in this shot. References (15) and (16) present the results of preliminary metallurgical studies conducted in an attempt to determine the approximate temperature attained by the aircraft skin in Shot 7. The data in Appendix A are the results of additional work of a similar nature.

The extreme importance of aircraft skin surface finish is readily seen in the results from Shot 7. Heat resistant white painted panels remained intact where similar panels with standard blue paint, subjected to identical thermal radiation, were completely destroyed. Bare aluminum held up almost as well as heat resistant white but in all cases experienced higher temperatures. It is to be noted here that heat resistant white and standard white paint afford roughly the same protection as long as the finish is not charred. At thermal levels high enough to seriously affect the standard white surface, it proves to be no better than aluminized lacquer. Field analysis of the structural failures which caused loss of the drone in Shot 7 were conducted by project personnel and representatives of the Structures Department, Douglas Aircraft Co. Indications are that the aircraft might have survived had the under skin been bare aluminum or painted heat resistant white instead of standard blue.

TABLE 3.1 - Calculated Absorptivity Values - Shot 8
(Turbulent Flow Assumed)

SPECIMEN		ABSORPTIVITY	
Color	Skin Thickness (in.)	Reference (11)	Figure 3.13
Standard Blue	0.016	0.232 - 0.398	0.262
	0.025	0.415 - 0.505	--
	0.040	0.436 - 0.710	--
	0.064	0.483	0.464
Bare Aluminum	0.016	0.159 - 0.232	0.172
	0.025	0.245	--
	0.040	0.274	--
	0.064	--	0.256
Heat Resistant White	0.016	0.103 - 0.141	0.146
	0.025	0.178 - 0.280	--
	0.040	0.215	--
	0.064	--	0.244

The coating of other thermally vulnerable items, such as fabric seals and rubber tires, with heat resistant white paint permitted them to withstand approximately four times the thermal radiation that they could in their natural state.

3.3 NUCLEAR RADIATION

3.3.1 Gamma Radiation

Gamma radiation was considered to be the most important of the nuclear radiations. Gamma measurements were made at several locations on the aircraft. These measurements are presented in Figure 3.17 as compared to calculated gamma radiation where aircraft motion, density at point of burst, and aircraft clock position were considered. The reading underneath the wing, where there was no protection from direct radiation, was the highest reading. The lower readings, inside the rear fuselage, inside the wing folds and inside the cockpit for both Shot 8 and Shot 2, were roughly proportional to the amount of structural shielding associated with these locations. The materials provid-

ing shielding are listed under Results for these two shots. The data from Shot 1 and Shot 9 were too low to be of significance, being less than 0.1r. All pertinent gamma information is summarized on the basis of a 1 KT yield in Figure 3.18.

3.3.2 Neutron Radiation

The effects of neutron radiation were assumed to be negligible for all test positions.

3.4 OVERPRESSURE AND GUST EFFECTS

3.4.1 Overpressure

Shots 1, 2, 7 and 8 had 300 ft burst heights while Shot 9 had a burst height of 2400 ft. On the basis of the triple point trajectory curves in Figure 3.19 it can be seen that the aircraft position for Shot 9 was in the free air region. For all other shots the aircraft was in the region of reflection and the calculated pressures were considered to be produced by a weapon with a yield of 1.8 times the given radio-chemical yield.

For these conditions, measured overpressures were found to be in close agreement with calculated when the method of ref (17) was employed in reducing the data. This consisted of taking the best straight line through that portion of the overpressure record which exhibited conventional smooth behavior, and extending it back to time of shock arrival.

Time of shock arrival for ground burst data was found to be in close agreement with shock arrival times in the region of reflection. Converting the free air yield of Shot 9 to an equivalent ground burst yield using the 1.8 reflection factor, brings this point exactly on the (Figure 3.20) shock arrival curve. A comparison of measured and calculated overpressure is given in Figure 3.21. Figure 3.22 presents the measured overpressures in terms of a standard 1 KT free air burst. The range of pressure and density ratios investigated is indicated in Figure 3.23. The associated gust velocities are given in Figure 3.24. The curves included here are good only for standard atmospheric conditions. Since temperature is the factor governing the relationship between gust velocity and altitude, an equivalent temperature altitude based on measured temperature must be used for non-standard atmospheric conditions.

No overpressure damage was noted up to approximately 2 psi. In no case was any adverse overpressure effect on the structure noted except when it occurred in conjunction with extremely high skin temperatures.

3.4.2 Gust Effects

Gust effects were recorded in terms of accelerations and structural loads resulting from measured overpressures. These records are reproduced in Figures 3.25 through 3.33. In all cases wing gust

effects were noted approximately 0.01 sec after the tail as indicated in Figures 3.25 and 3.26.

On the basis of a peak c.g. acceleration reading at a time associated with peak wing loads, and an average of two peak tail accelerations occurring in the time interval between peak tail and peak wing loads, excellent correlation was obtained between wing and tail acceleration. A comparison between these measured accelerations and corresponding calculated accelerations is given in Figure 3.34. The measured accelerations are seen to be almost twice the calculated values for all tests. How much of this is due to elastic structural

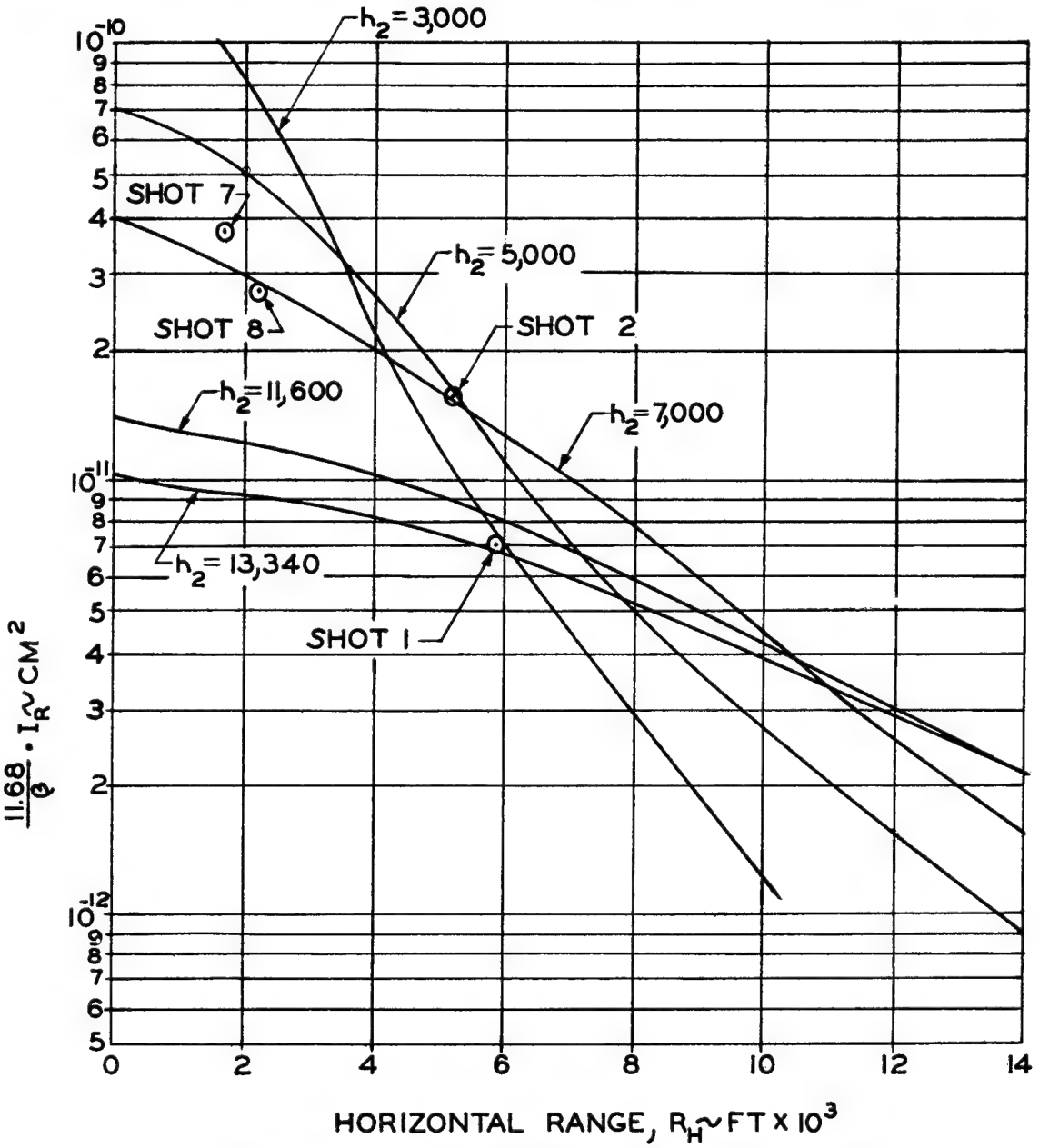

Fig. 3.3 Reflected Thermal Intensity from a Unit Source--Tower, h_1 = 300 ft.

[redacted]

accelerations affecting the overall acceleration picture and how much is due to limitations in the theoretical approach to the prediction of these accelerations must be evaluated by future laboratory tests and theoretical study. The fact that measured acceleration can be predicted consistently, however, is of great importance in view of the general agreement between measured and calculated structural loads and the relationship between load and acceleration (see Equation 1.10). The comparison between measured and calculated loads is made in Figures 3.35 through 3.39. Although in this particular airplane the dynamic overstress appears to approximately compensate for the gust alleviation, the fact that the recorded loads exhibit frequencies corresponding to first symmetrical bending illustrates the importance of

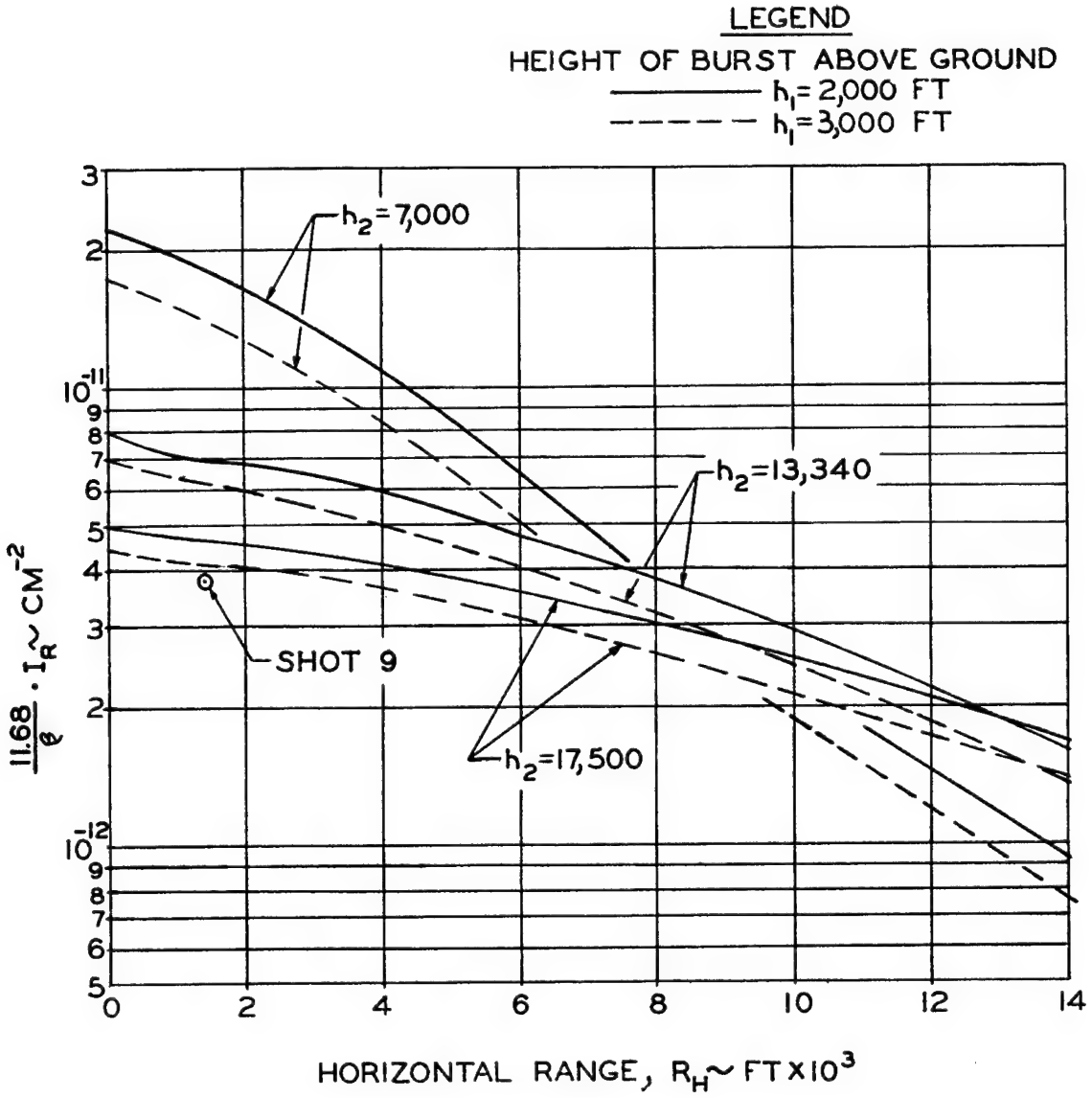

Fig. 3.4 Reflected Thermal Intensity from a Unit Source--Air Drop h_1 = 2432 feet

considering aeroelastic effects even on rigid aircraft. Figure 3.35 shows the time-history of the pitching motion of the drone aircraft during the period of shock arrival for Shots 2 and 8, indicating that pitching motion had a negligible effect on aircraft loading during the first 0.1 sec after shock arrival.

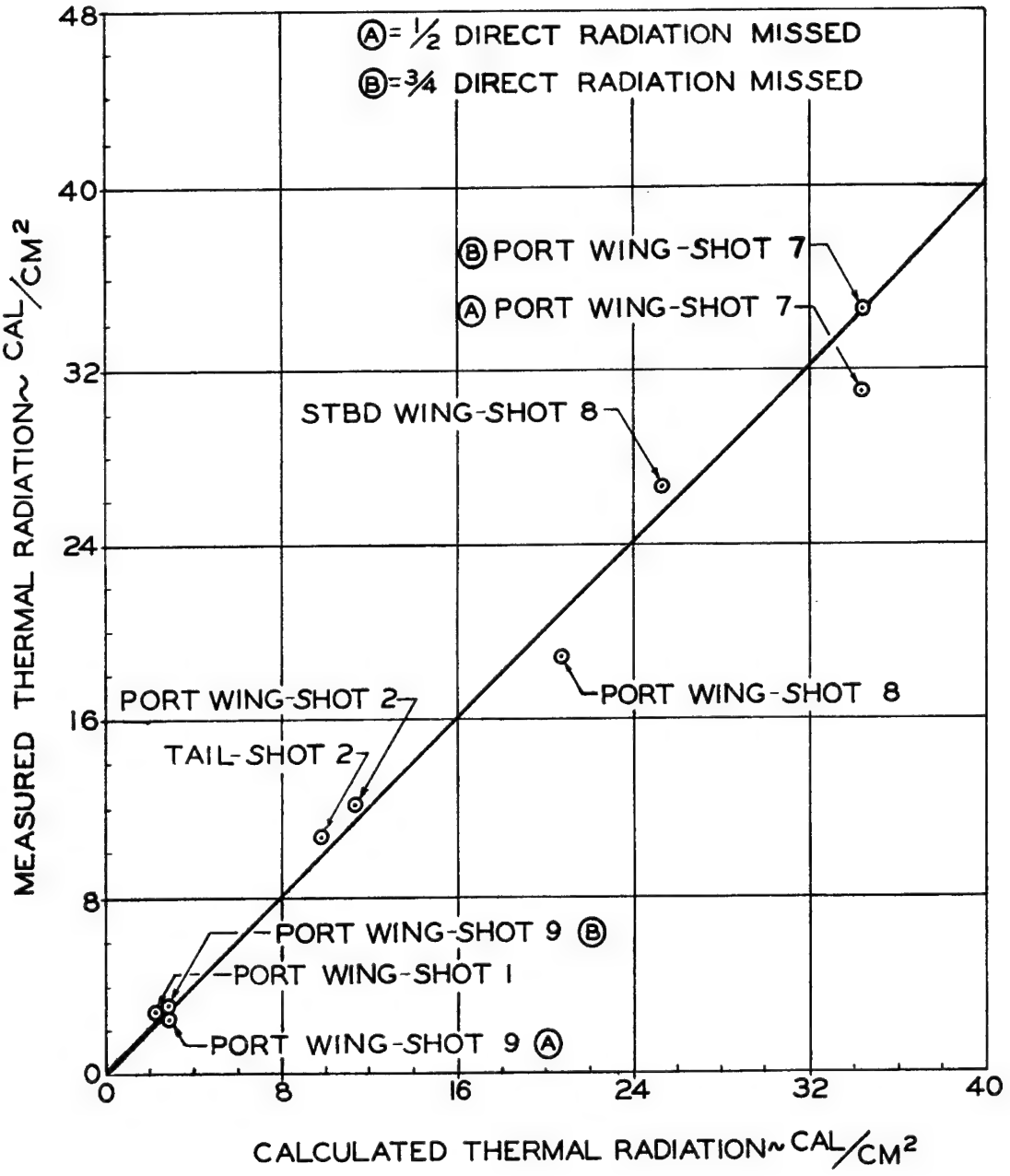

Fig. 3.5 Comparison of Measured and Calculated Thermal Radiation. Albedo = 0.55

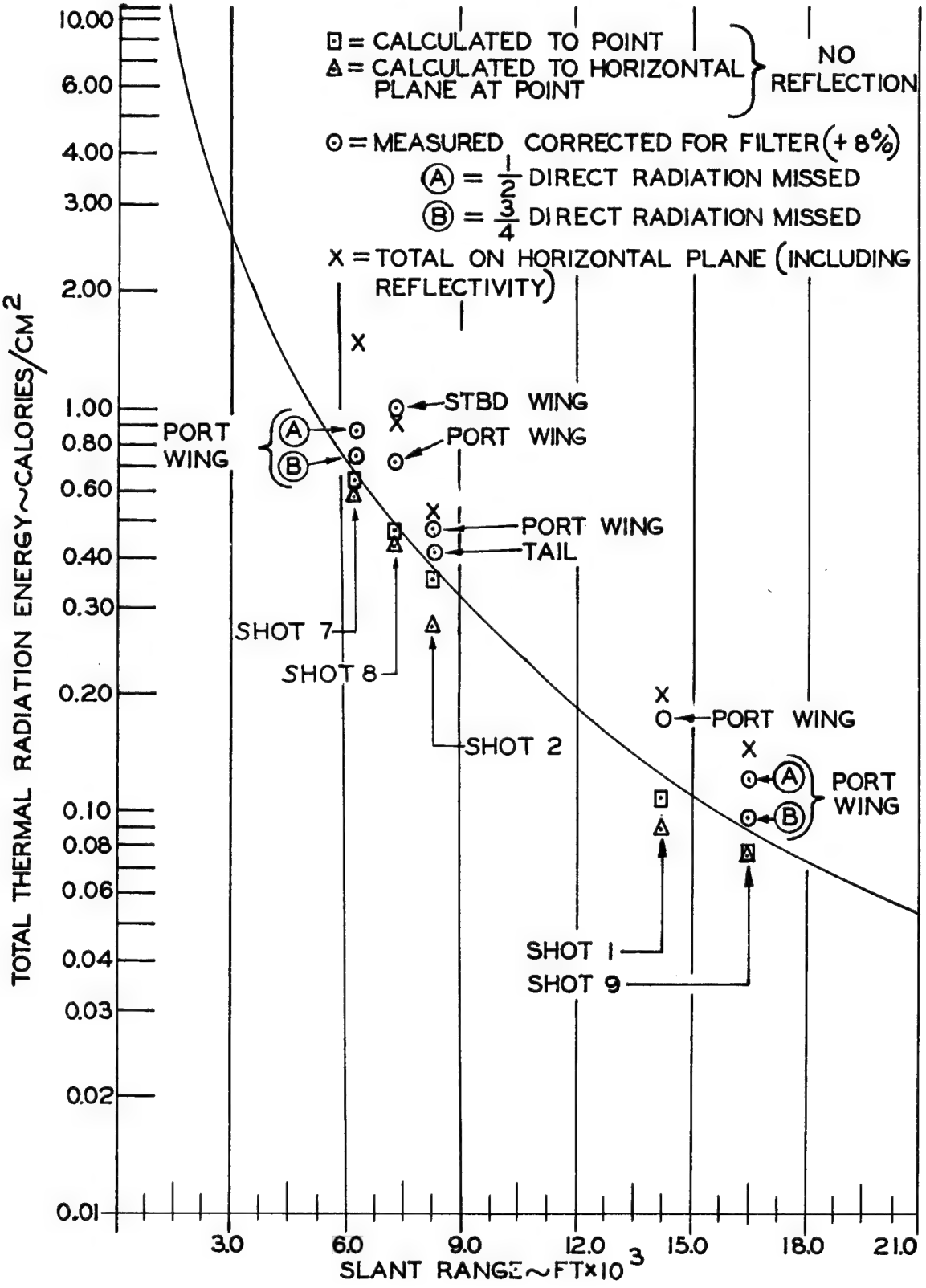

Fig. 3.6 Measured and Calculated Thermal Radiation Reduced to 1 KT

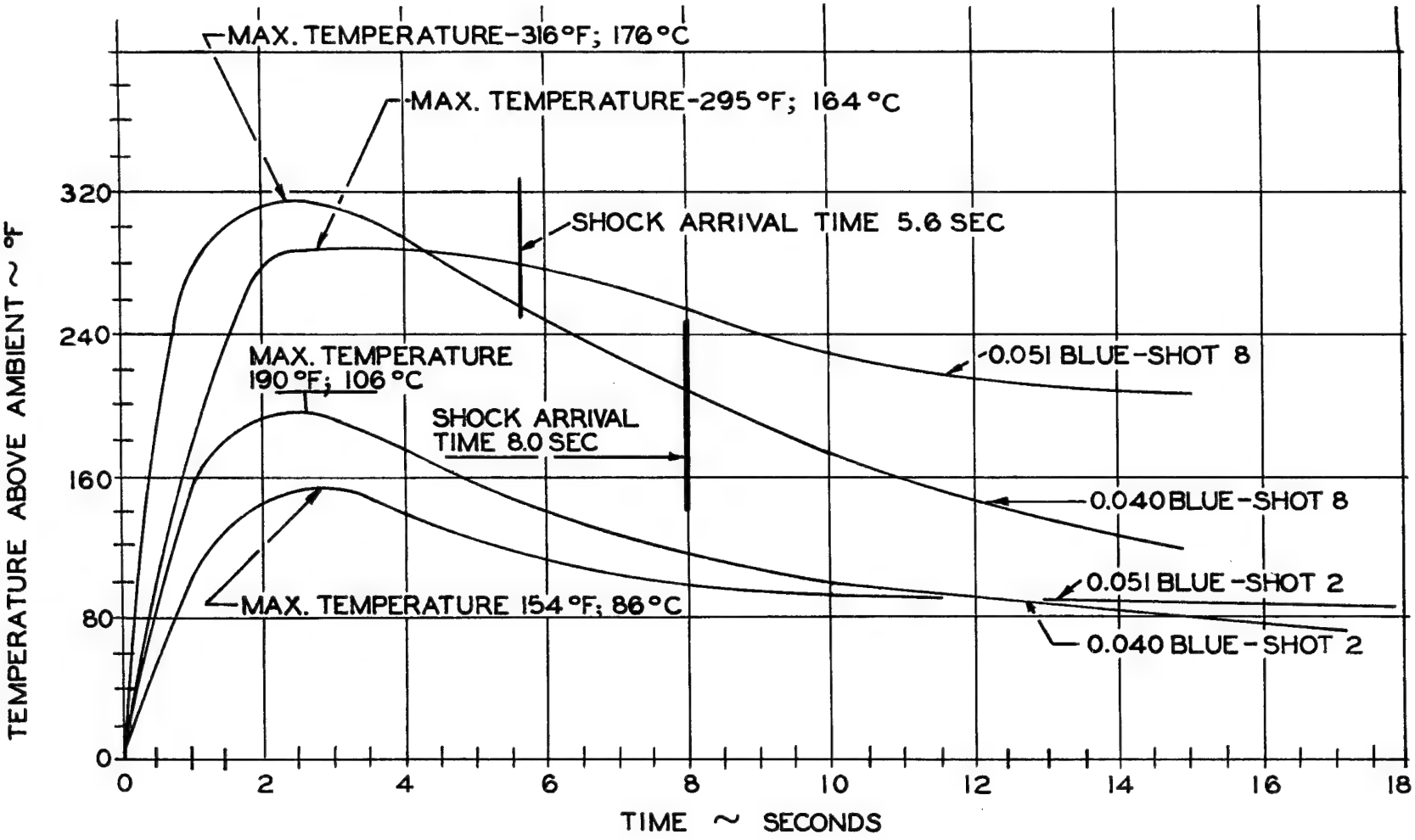

Fig. 3.7 Time History of Measured Aircraft Skin Temperature Rise

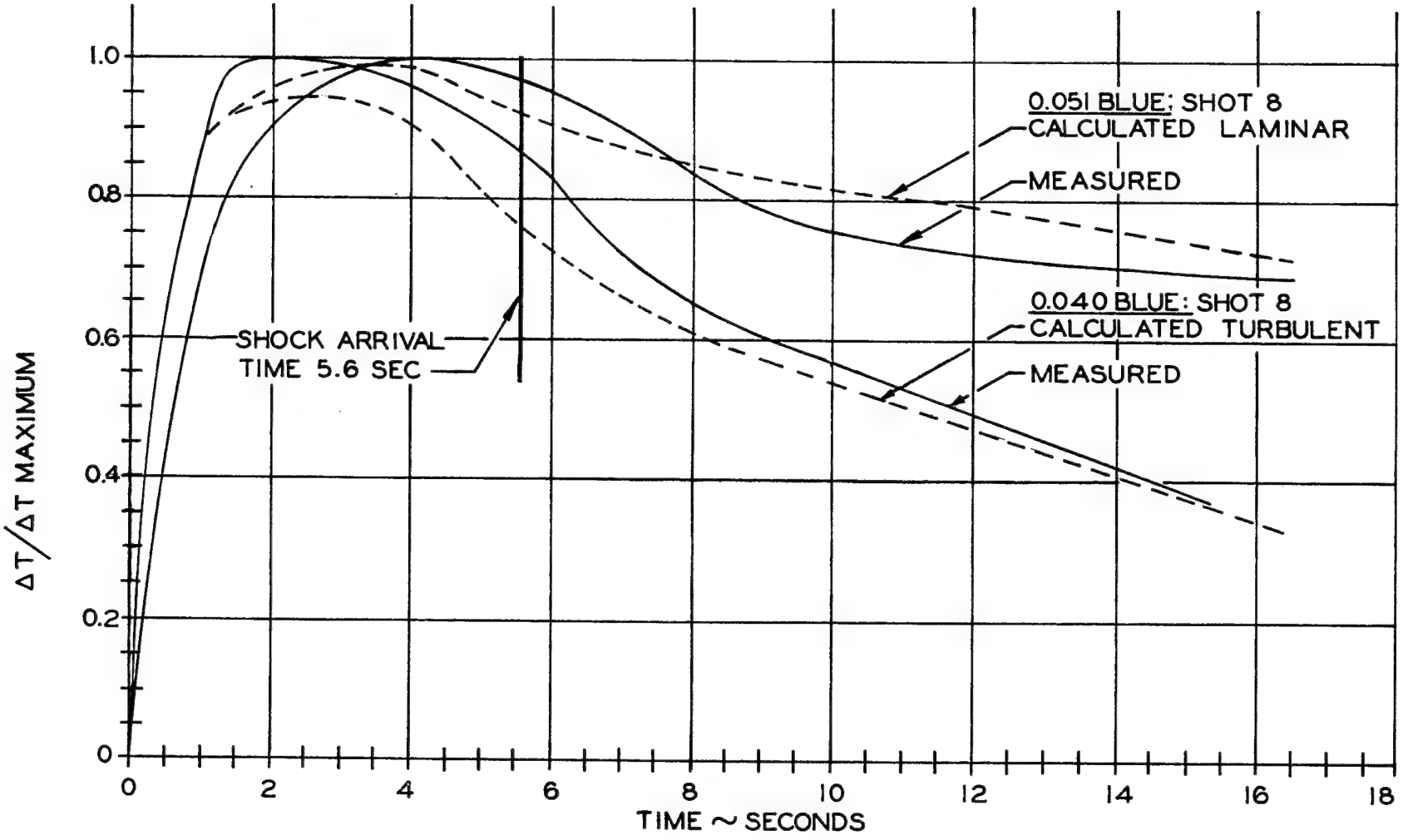

Fig. 3.8 Aircraft Skin Temperature, Time History for Measured and Calculated Cooling Rates

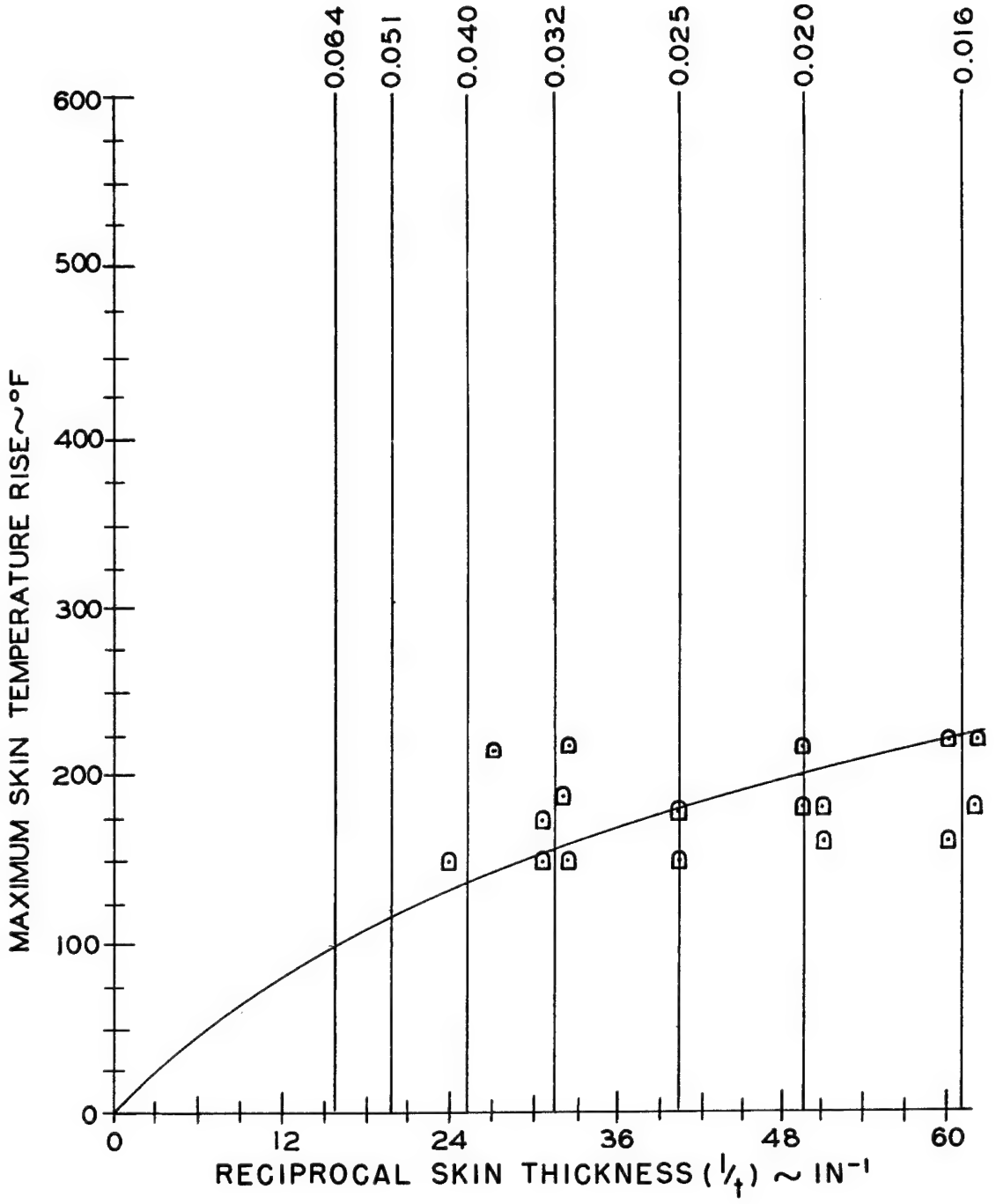

Fig. 3.9 Incremental Temperatures Measured in Aircraft Skin with a Heat Resistant White Paint Finish - Shot 8

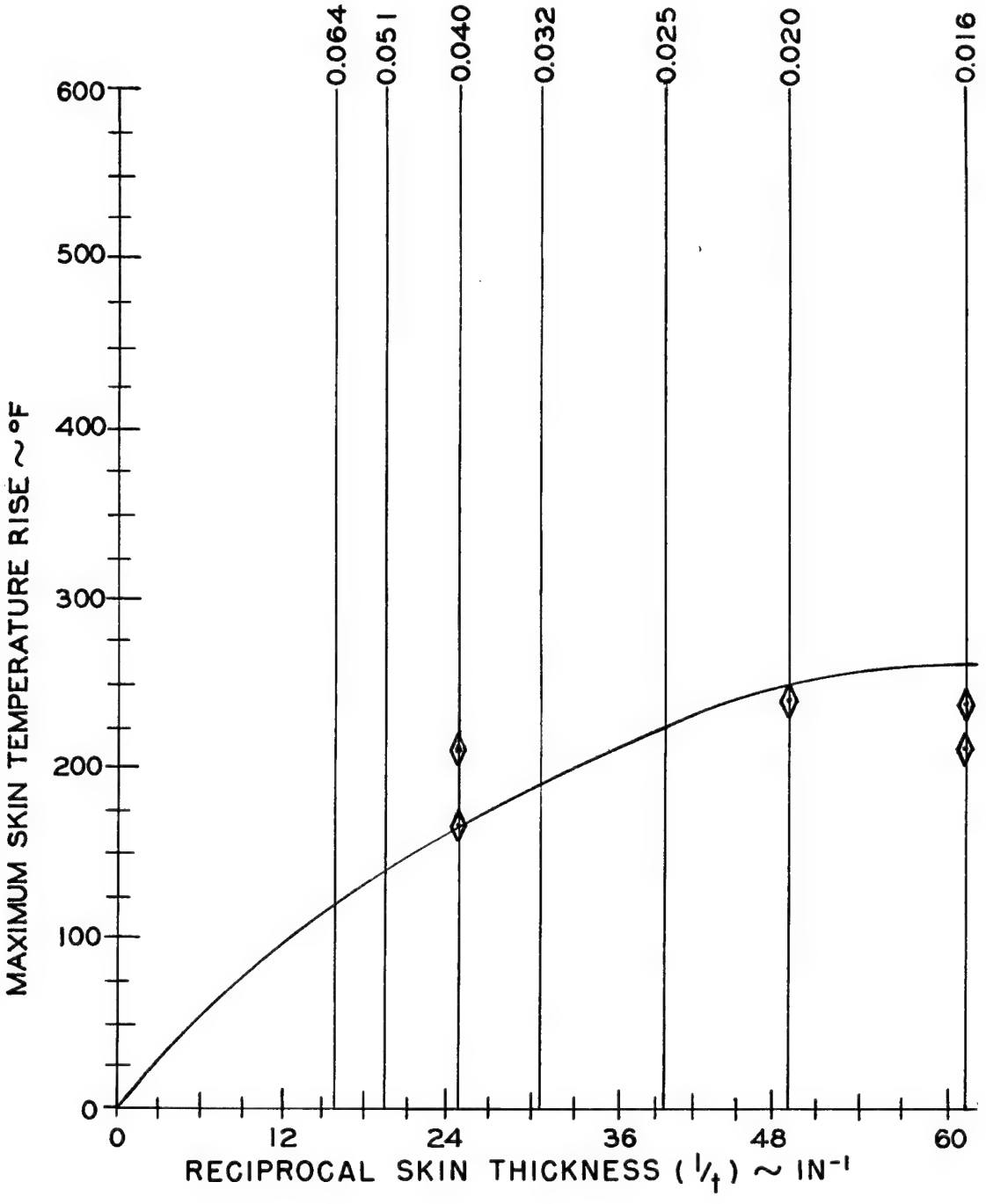

Fig. 3.10 Incremental Temperatures Measured in Standard White Painted Aircraft Skin - Shot 8

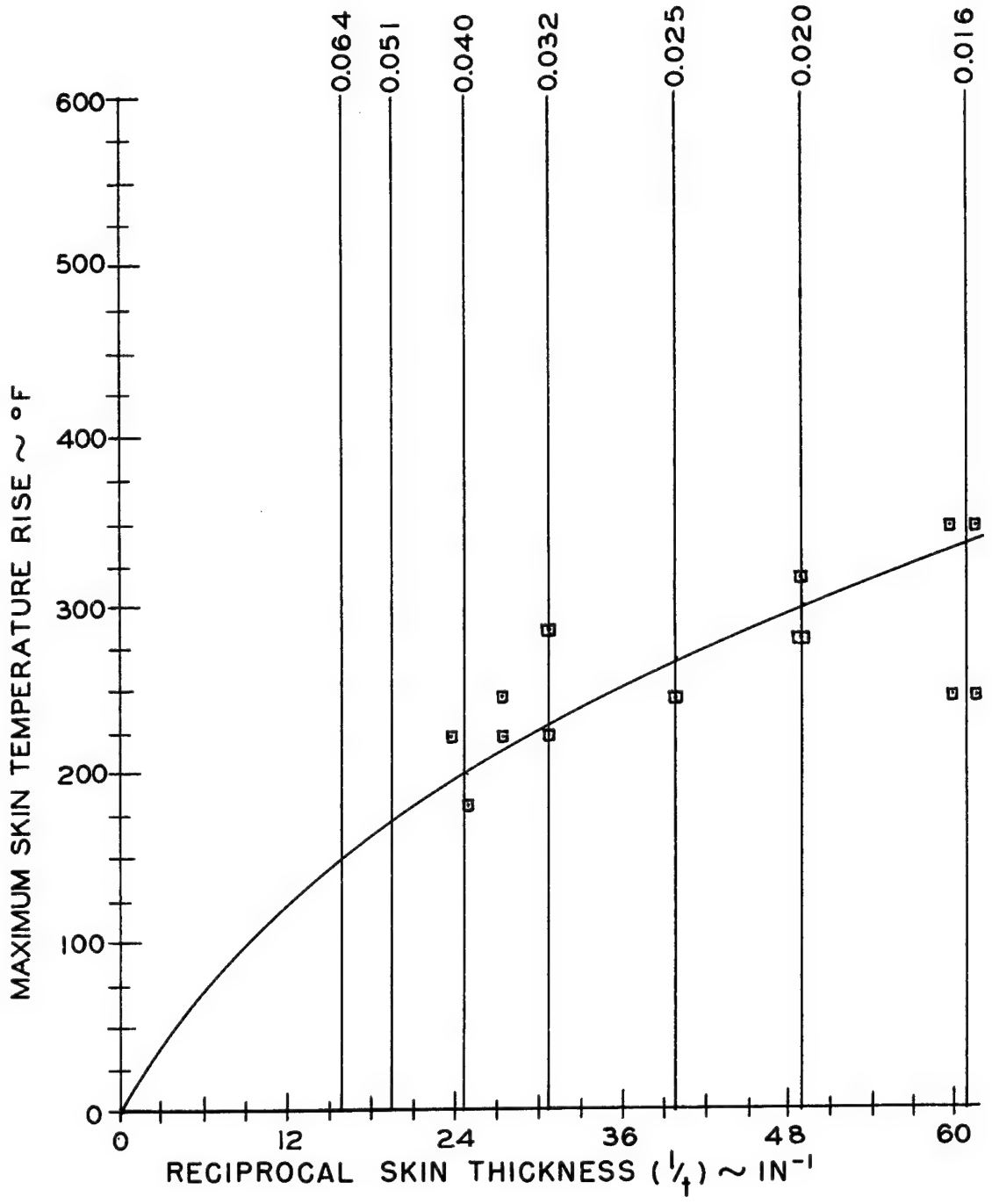

Fig. 3.11 Incremental Temperatures Measured in Unpainted Aircraft Skin - Shot 8

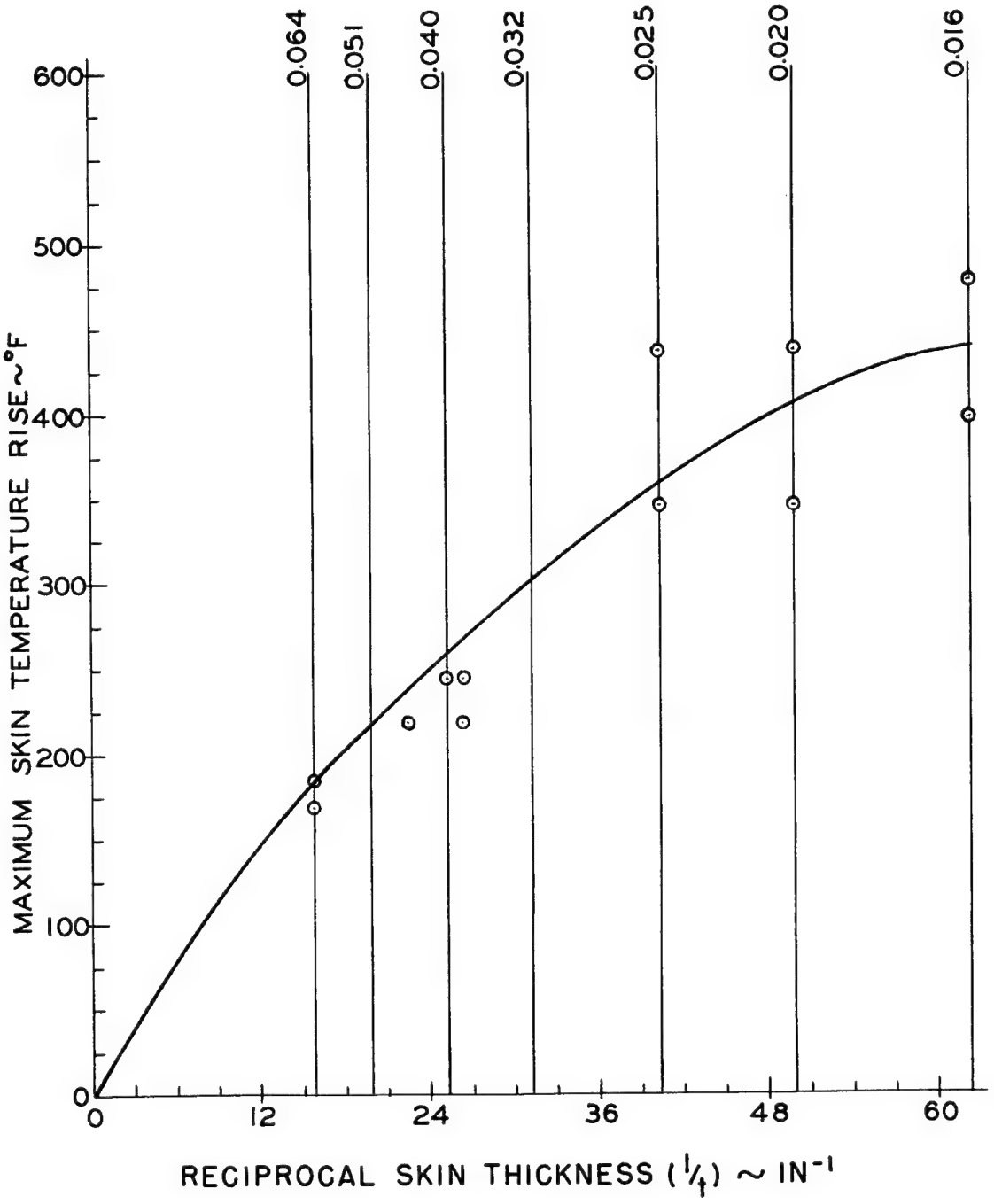

Fig. 3.12 Incremental Temperatures Measured in Aircraft Skin with an Aluminized Lacquer Finish - Shot 8

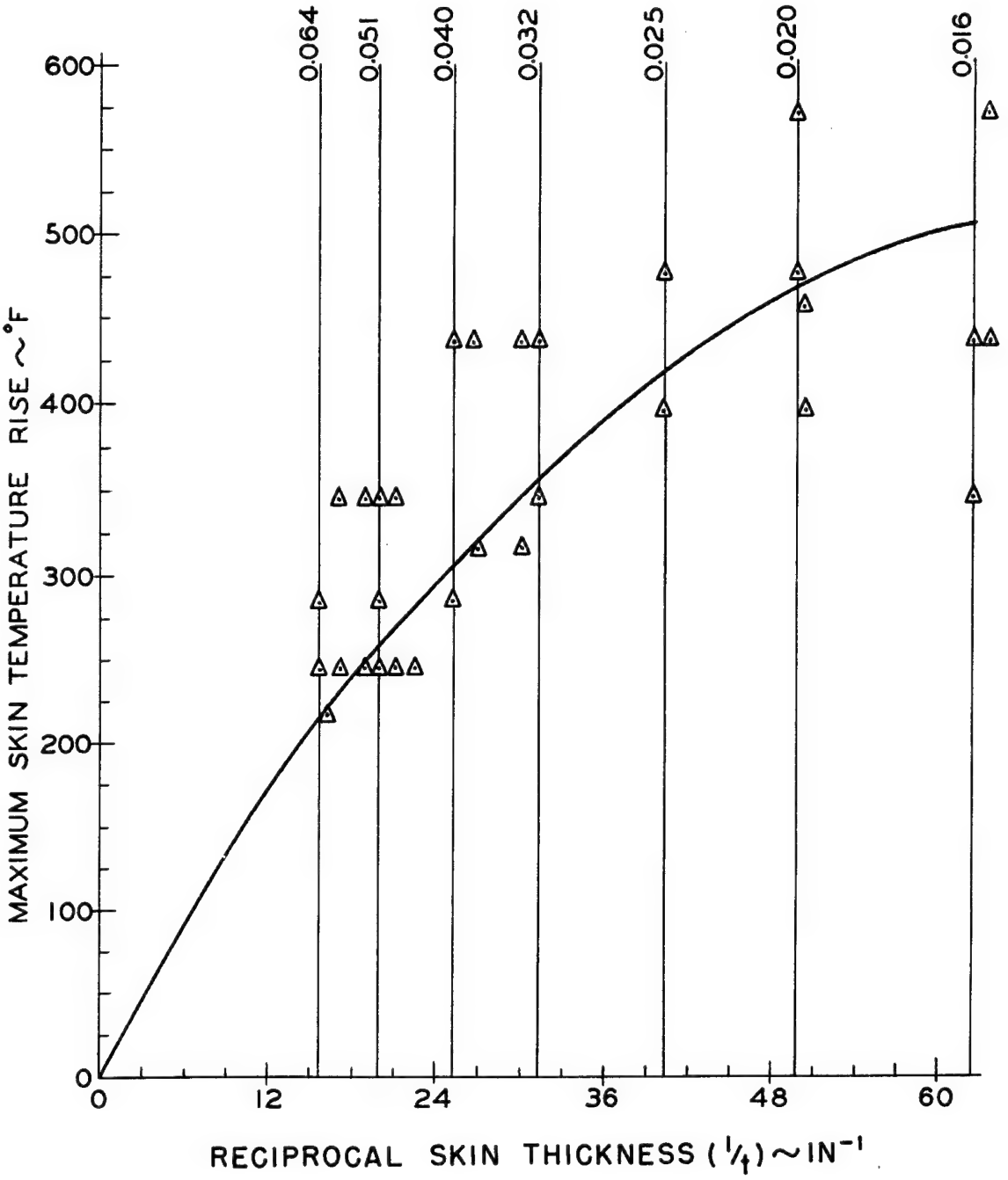

Fig. 3.13 Incremental Temperatures Measured in Standard Blue Painted Aircraft Skin - Shot 8

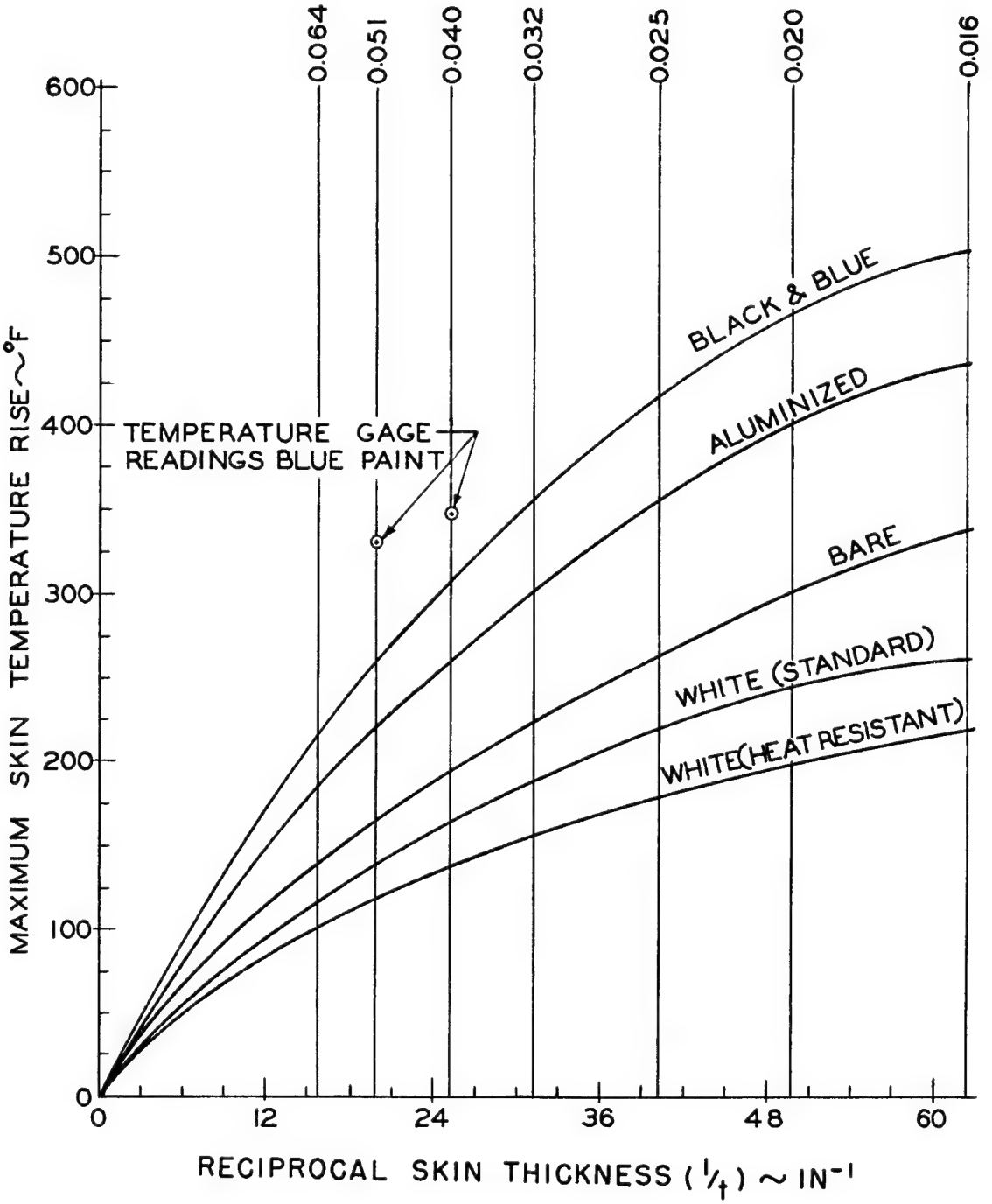

Fig. 3.14 Temperature Rise in Aircraft Skin vs the Reciprocal of Skin Thickness for Different Surface Finish - Shot 8

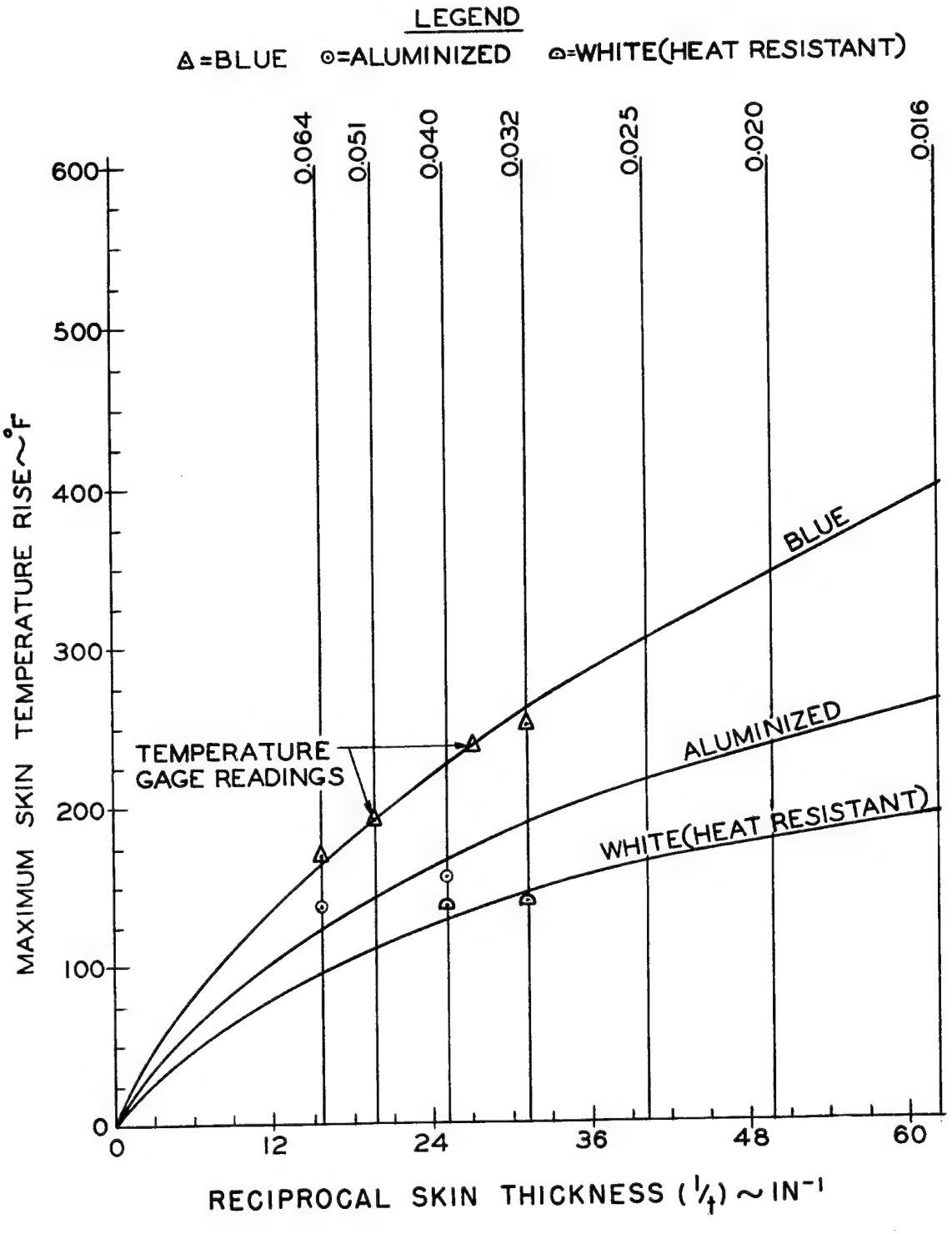

Fig. 3.15 Temperature Rise in Aircraft Skin vs the Reciprocal of Skin Thickness for Different Surface Finish - Shot 2

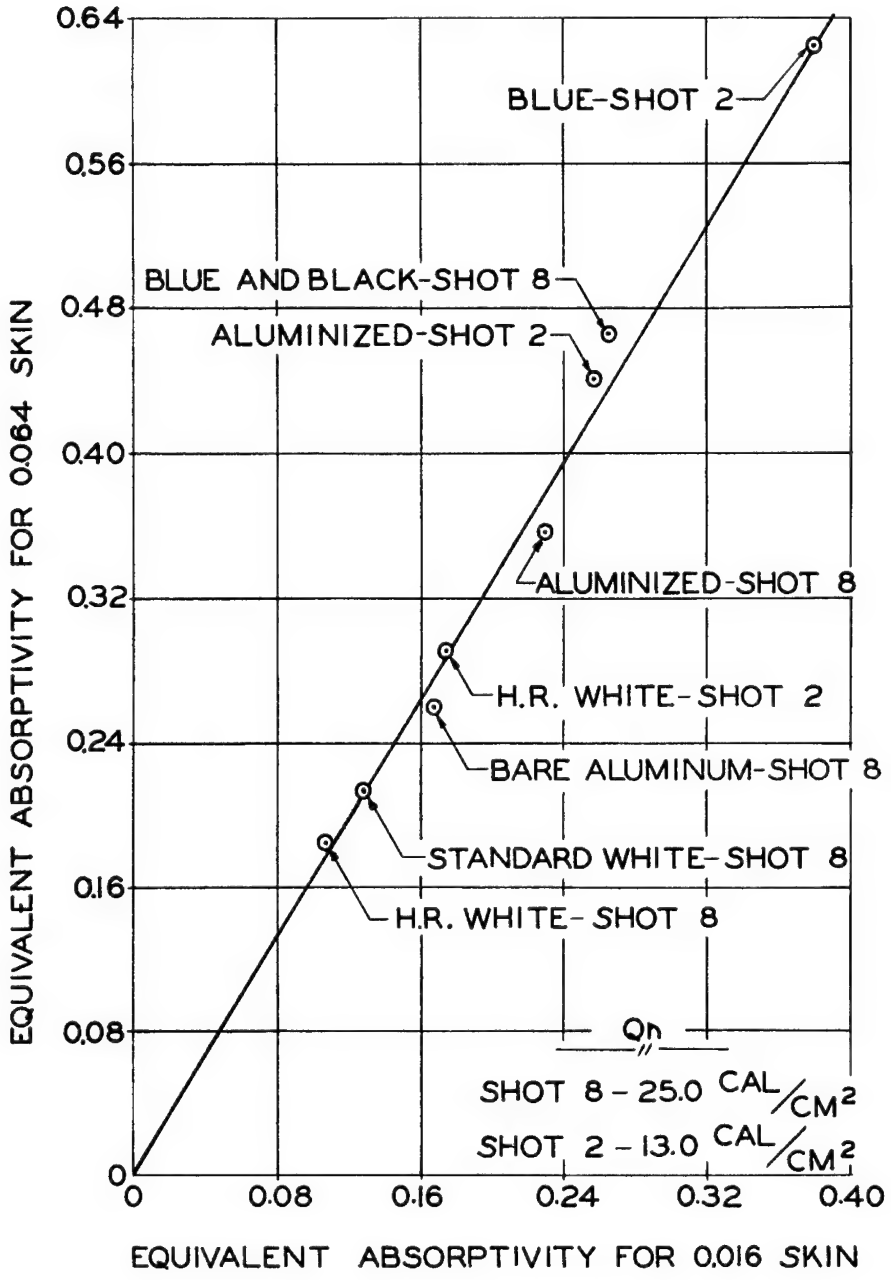

Fig. 3.16 Comparison of Equivalent Absorptivity for 0.016 and 0.064 Aircraft Skin with Different Surface Finish

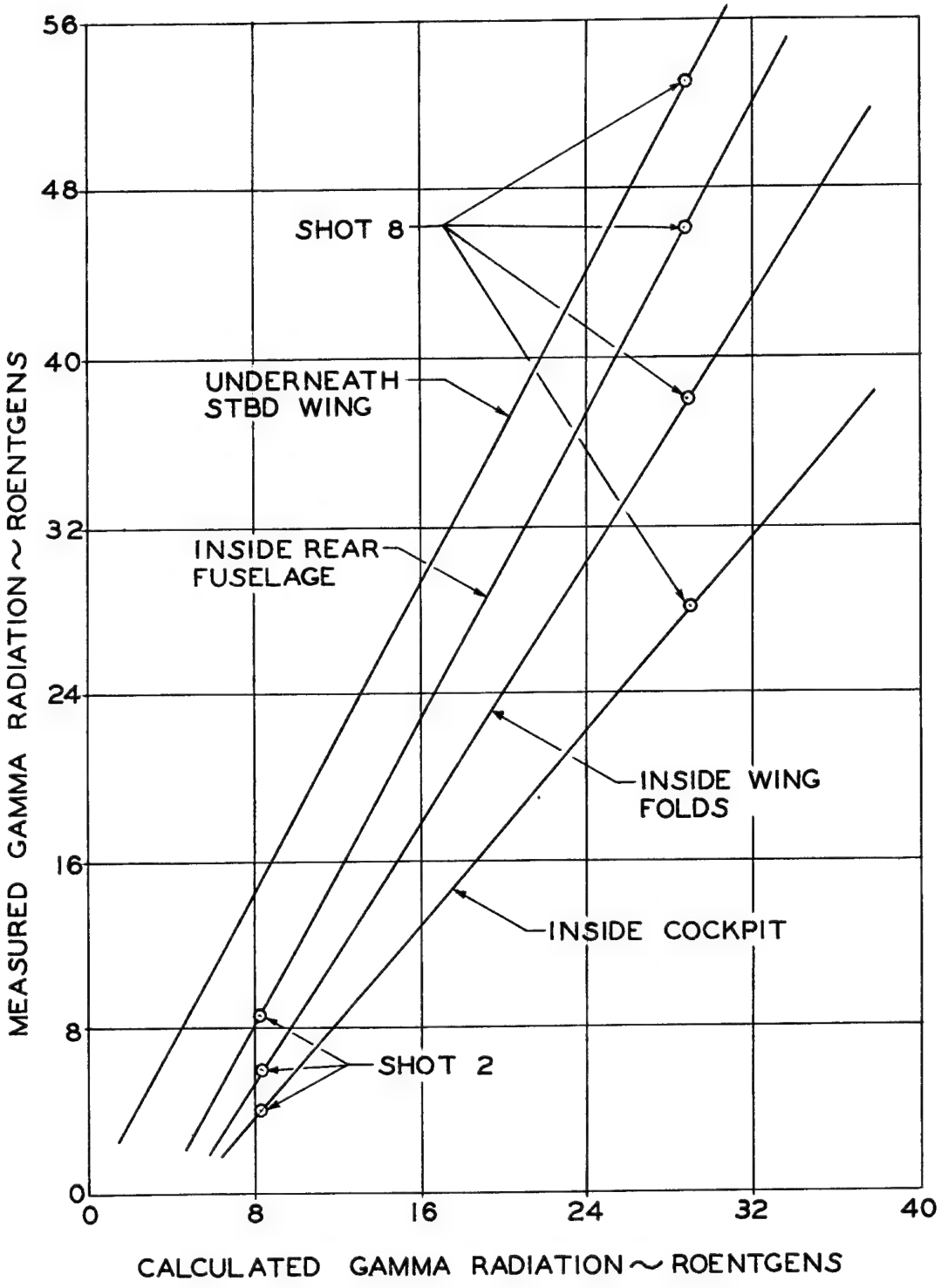

Fig. 3.17 Comparison of Measured and Calculated Gamma Radiation Indicating Structural Shielding Effects

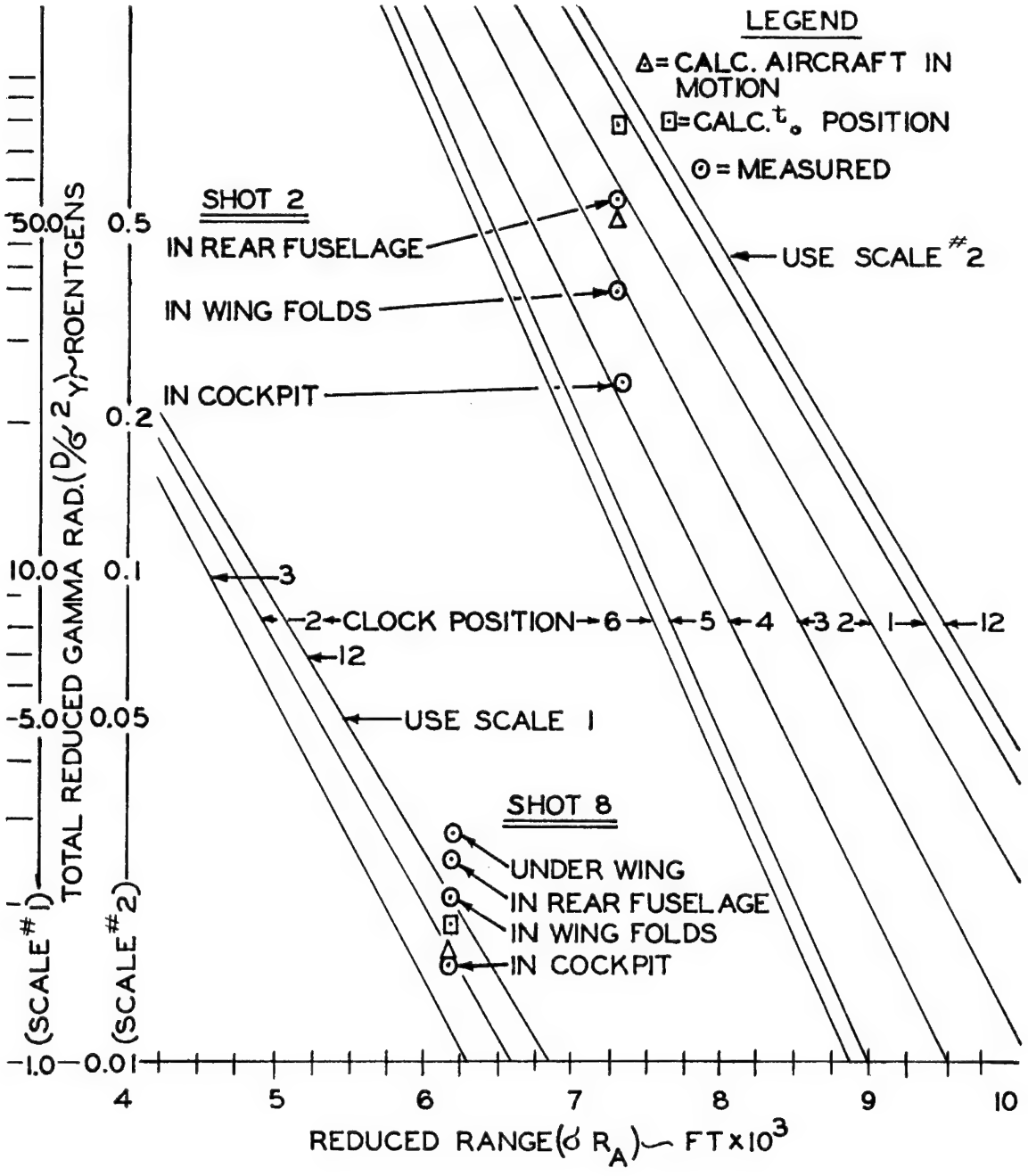

Fig. 3.18 Measured and Calculated Gamma Radiation Reduced to 1 KT in Sea Level Homogeneous Atmosphere

[redacted]

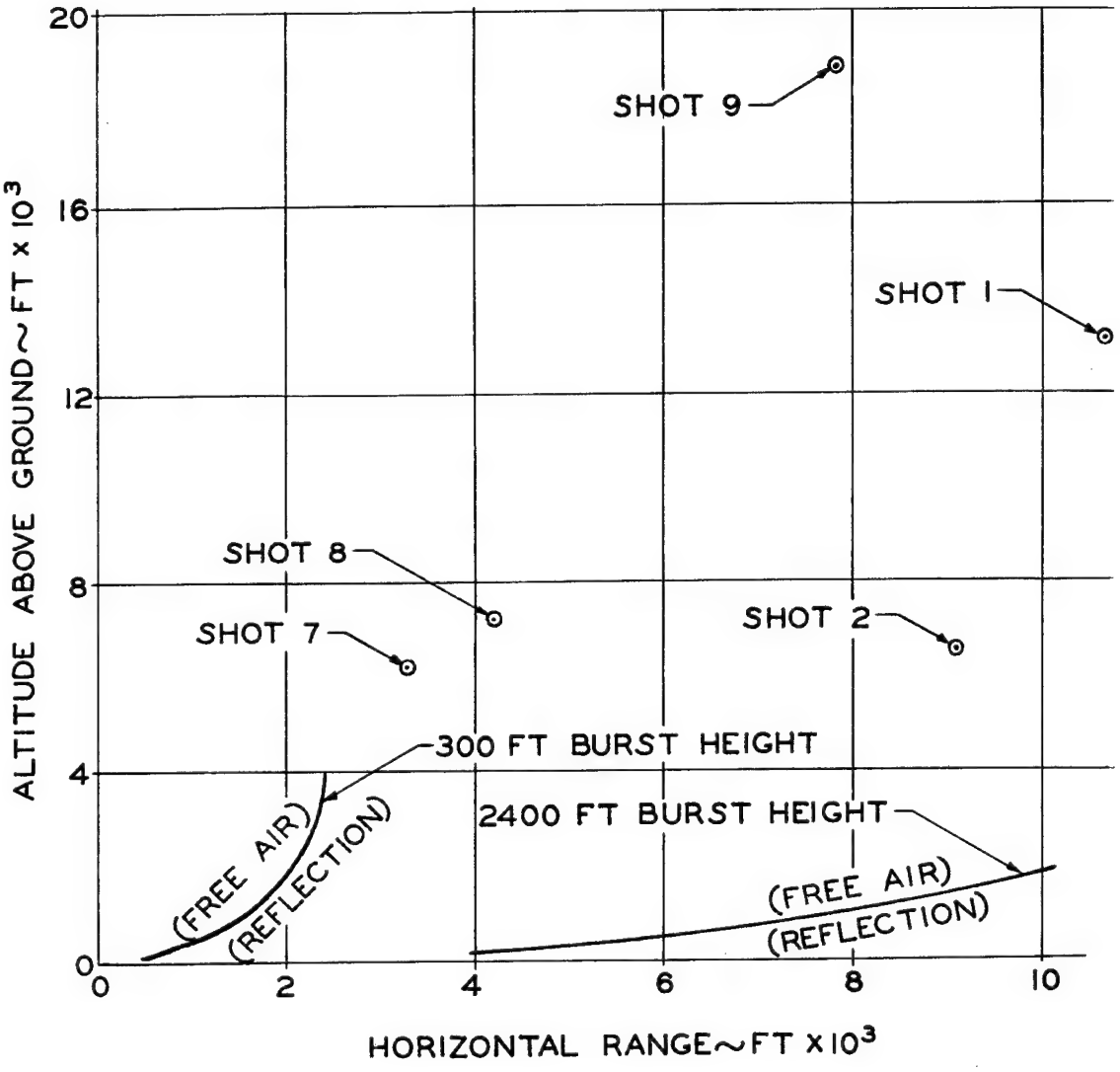

Fig. 3.19 Triple Point Trajectory Curves Indicating Aircraft Position at Shock Arrival

EQUIVALENT GROUND BURST YIELDS

SHOT	YIELD
1	16.2
2	24.5
7	43.4
8	27.0
9_a	14.5 ; $\left(\frac{26.0}{1.8}\right)^*$

* FREE AIR BURST CONVERTED TO EQUIVALENT GROUND BURST USING 1.8 REFLECTION FACTOR

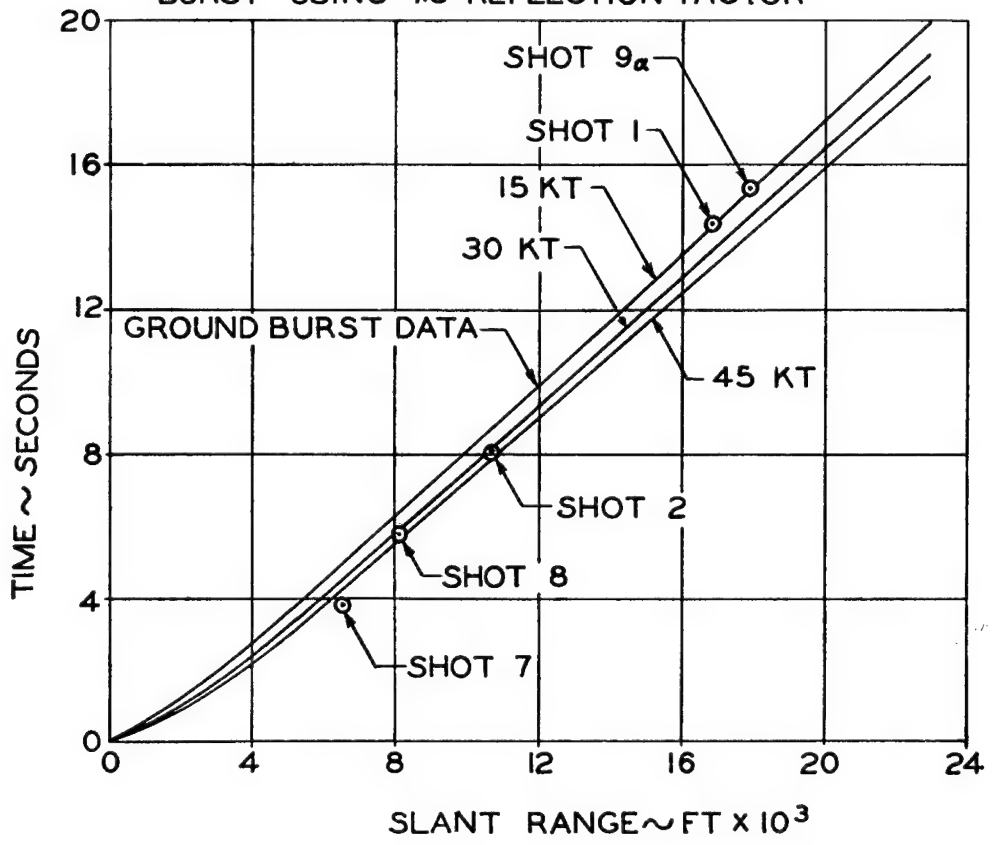

Fig. 3.20 Measured and Calculated Shock Arrival Times vs Slant Range

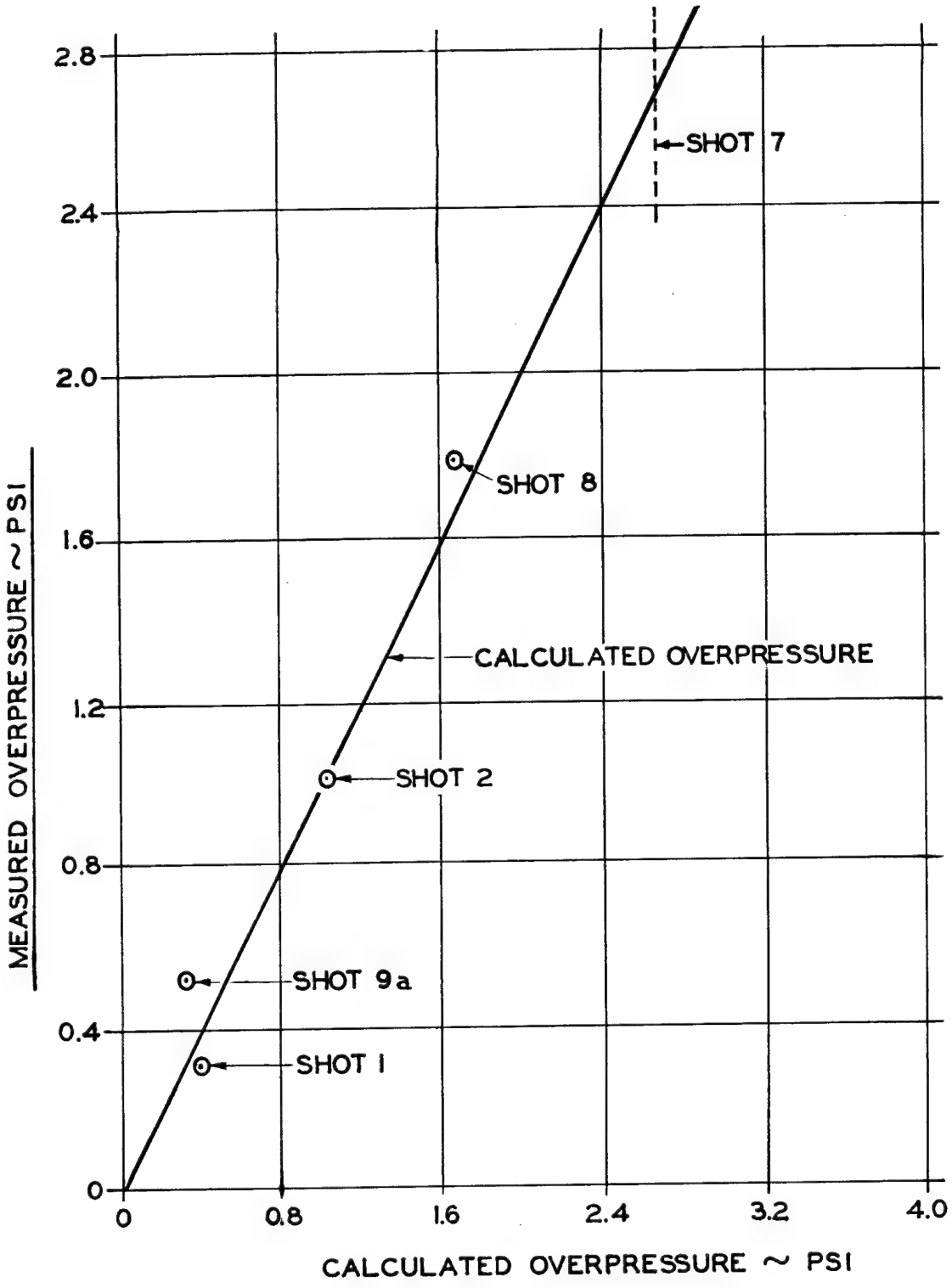

Fig. 3.21 Comparison of Measured and Calculated Overpressure

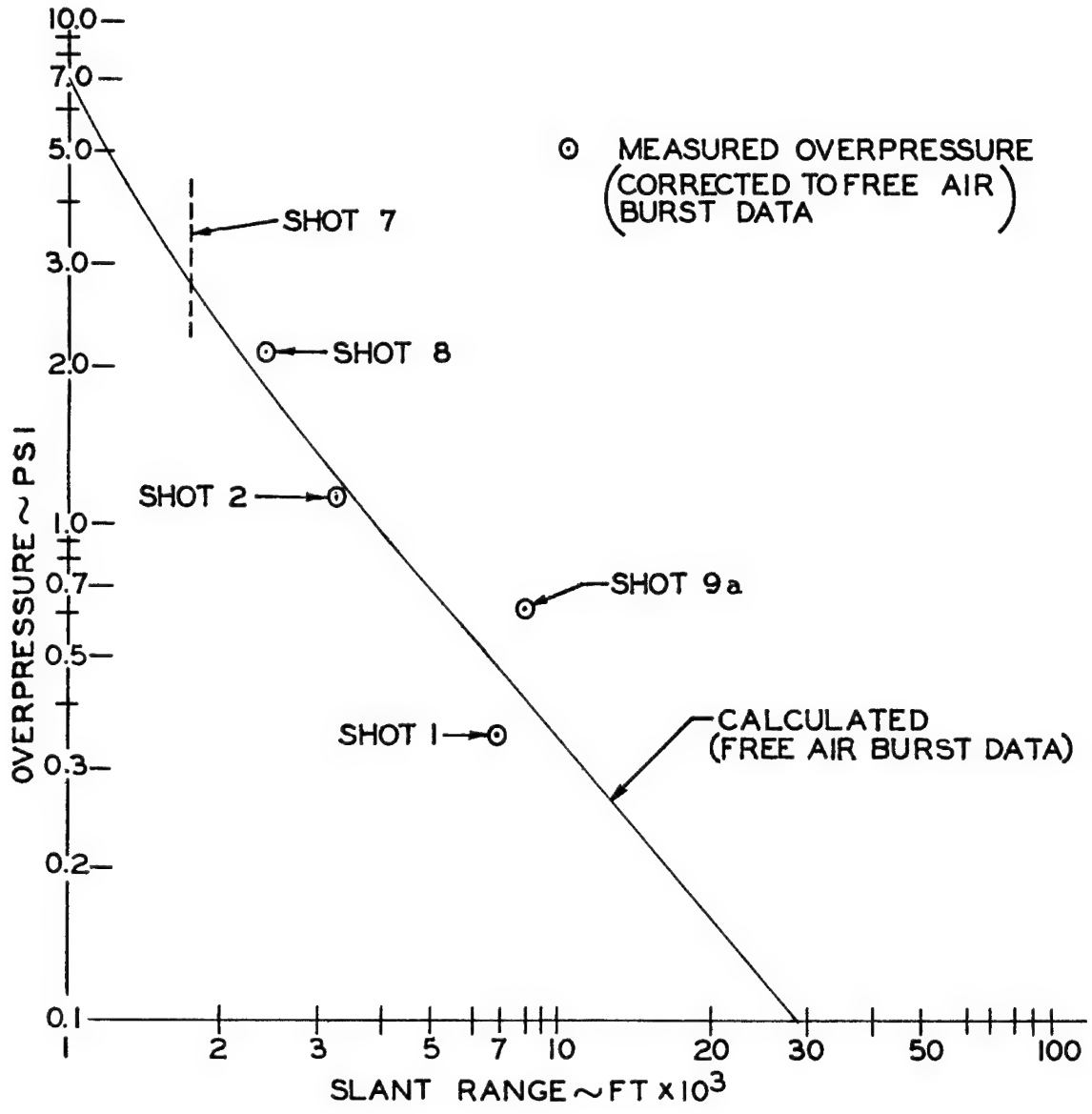

Fig. 3.22 Measured and Calculated Overpressure Reduced to 1 KT in a Sea Level Homogeneous Atmosphere

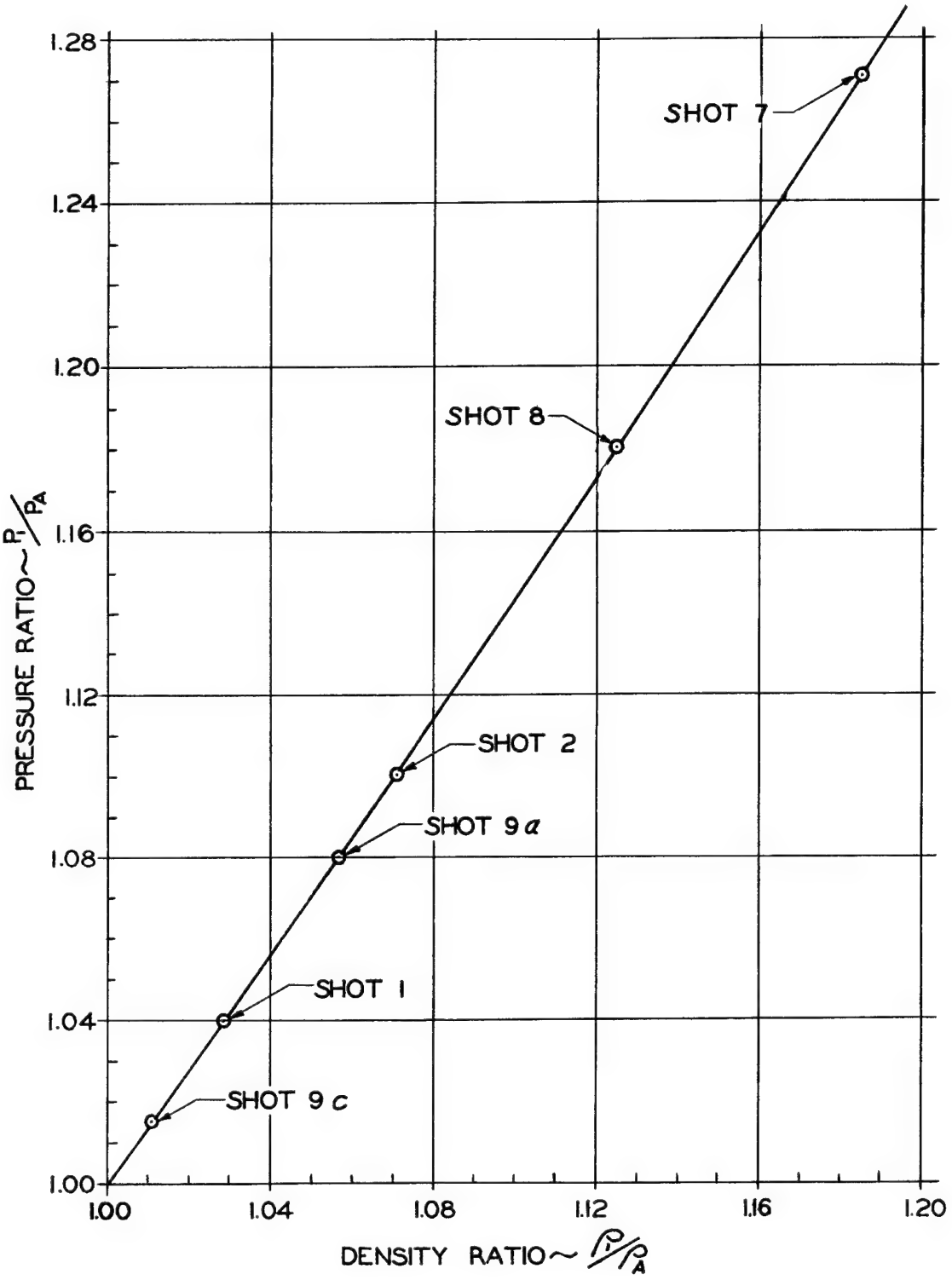

Fig. 3.23 Pressure Ratio vs Density Ratio

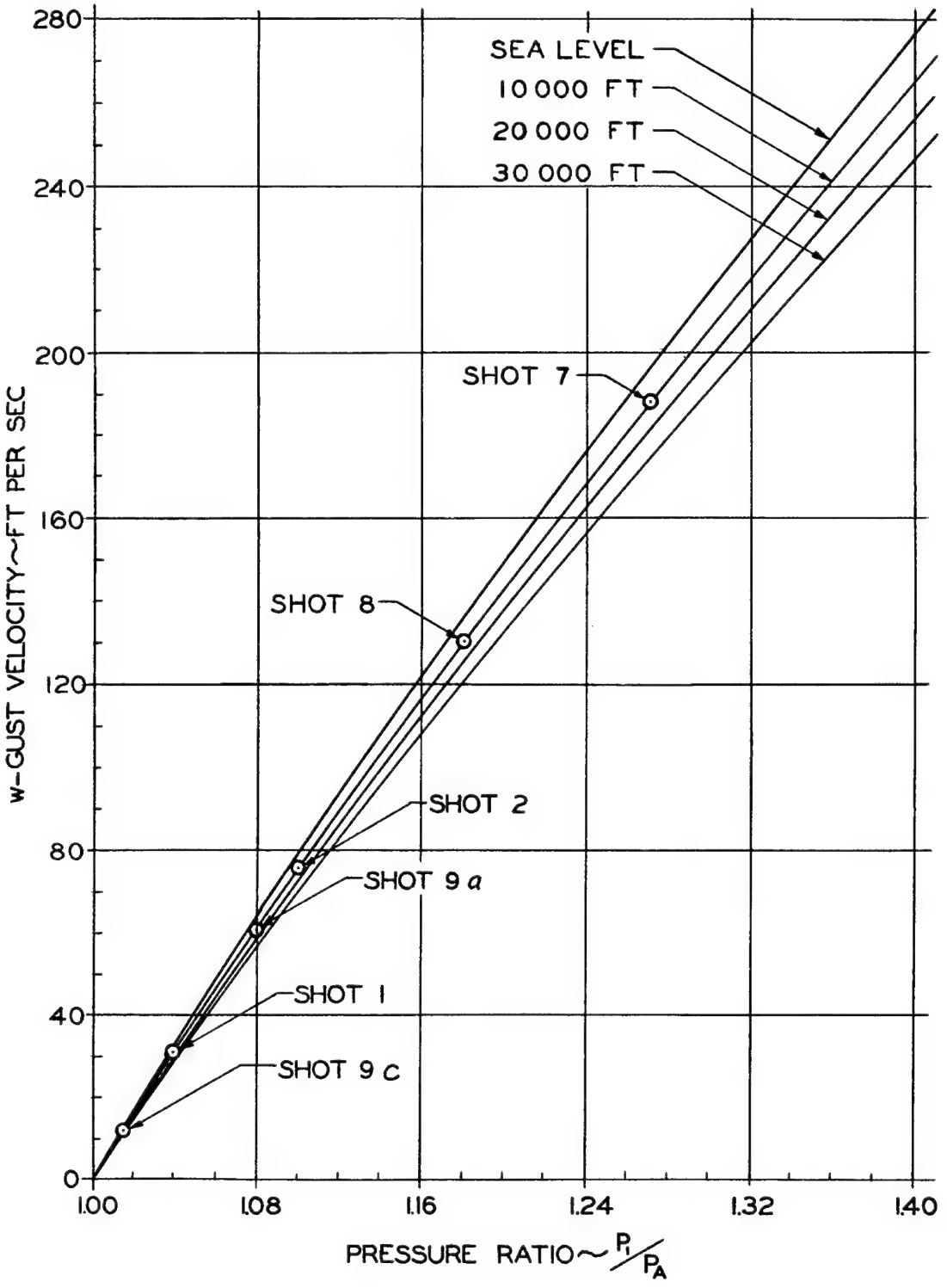

Fig. 3.24 Gust Velocity as a Function of Pressure Ratio and Altitude

[redacted]

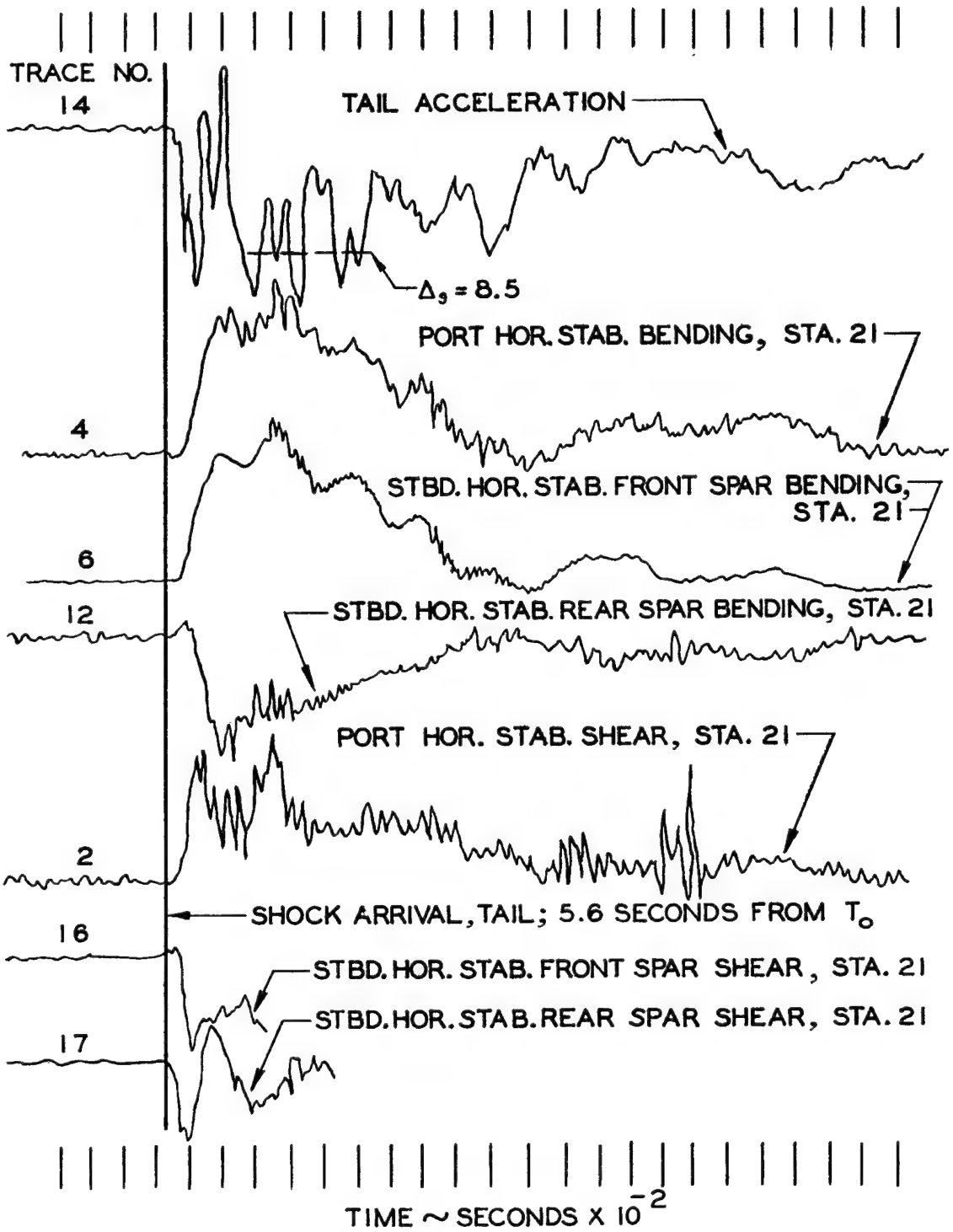

Fig. 3.25 Time History of Tail Acceleration and Tail Loads - Shot 8

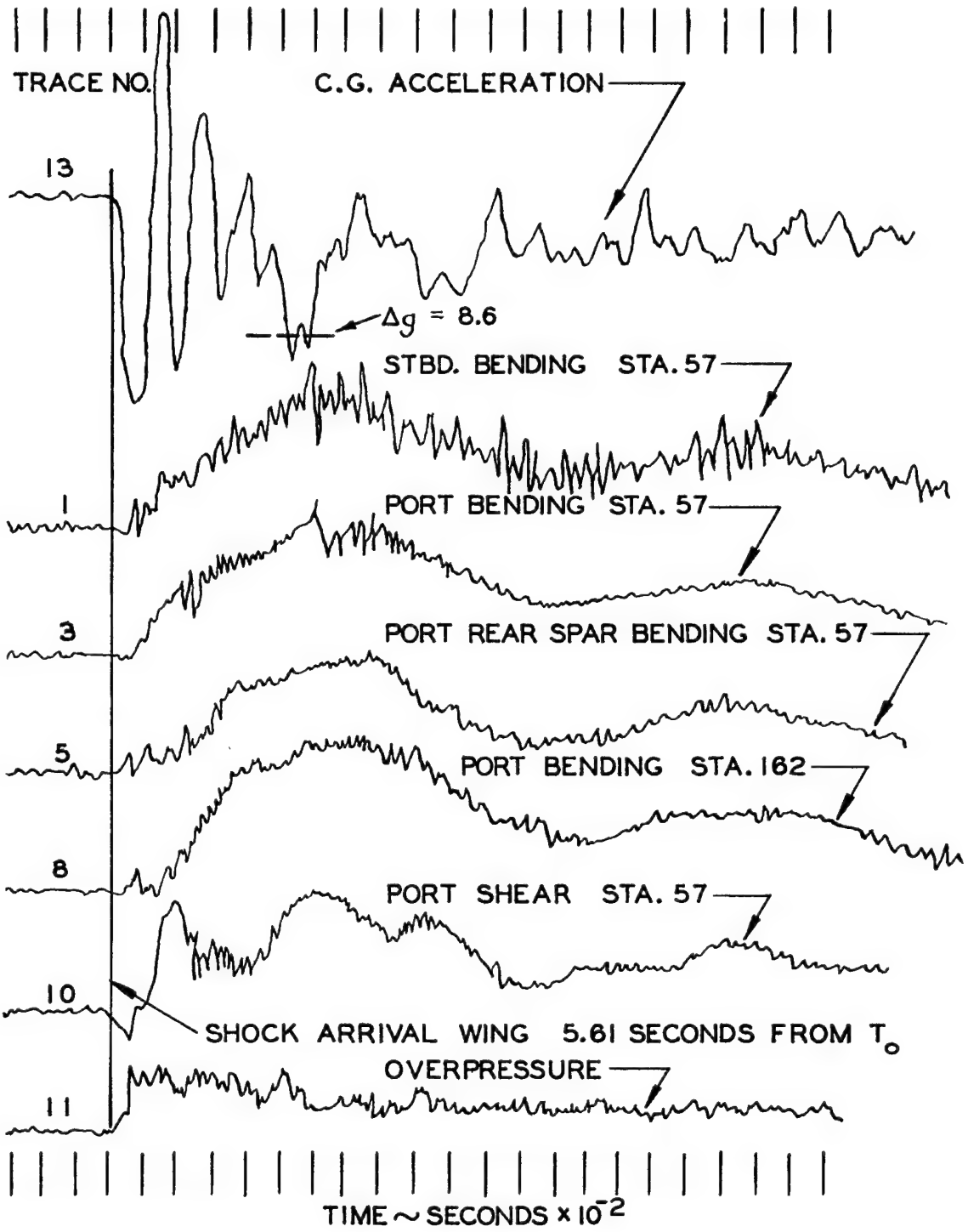

Fig. 3.26 Time History of c.g. Acceleration, Wing Loads and Overpressure - Shot 8

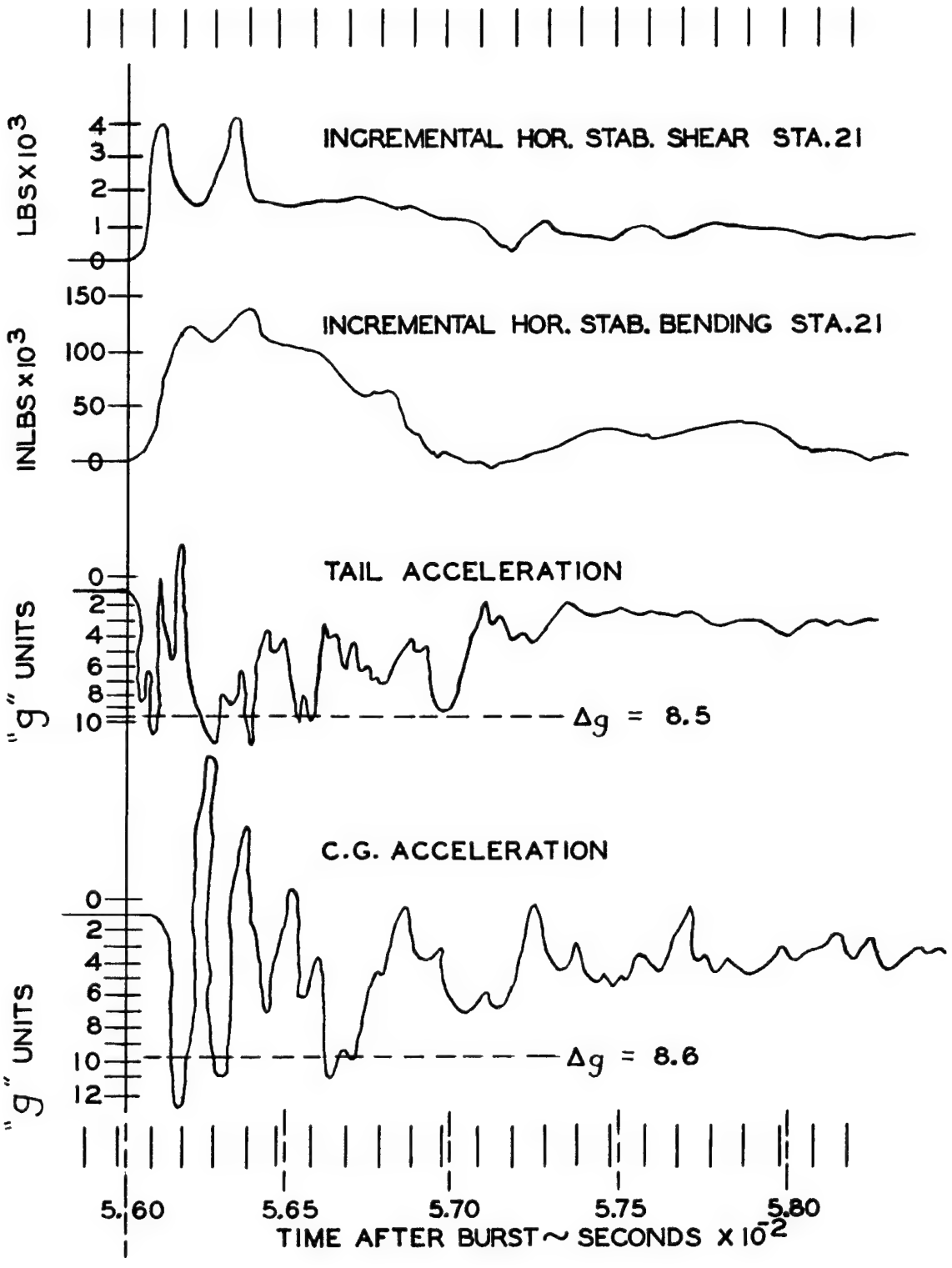

Fig. 3.27 Measured Aircraft Acceleration and Tail Loads - Shot 8

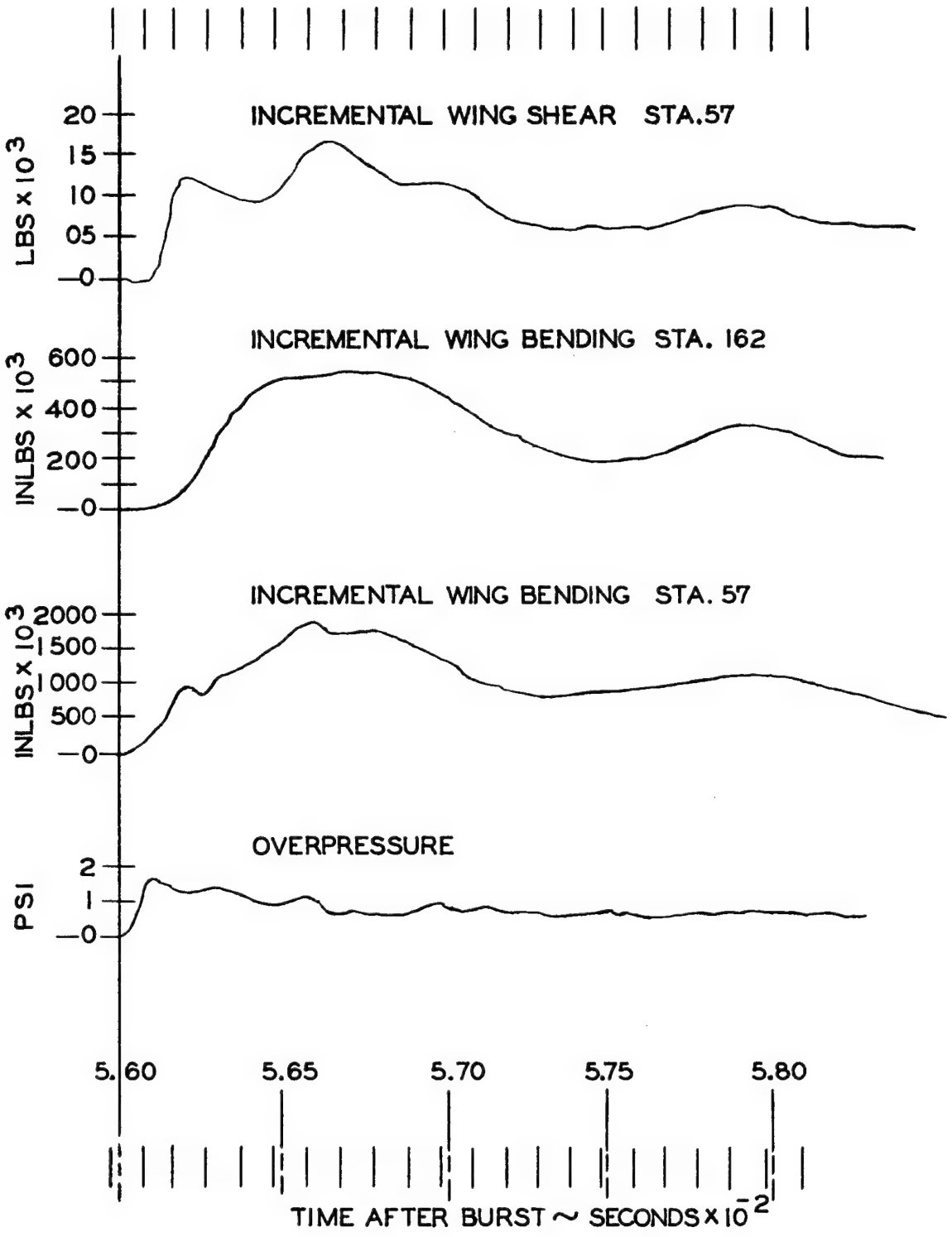

Fig. 3.28 Measured Overpressure and Aircraft Wing Load - Shot 8

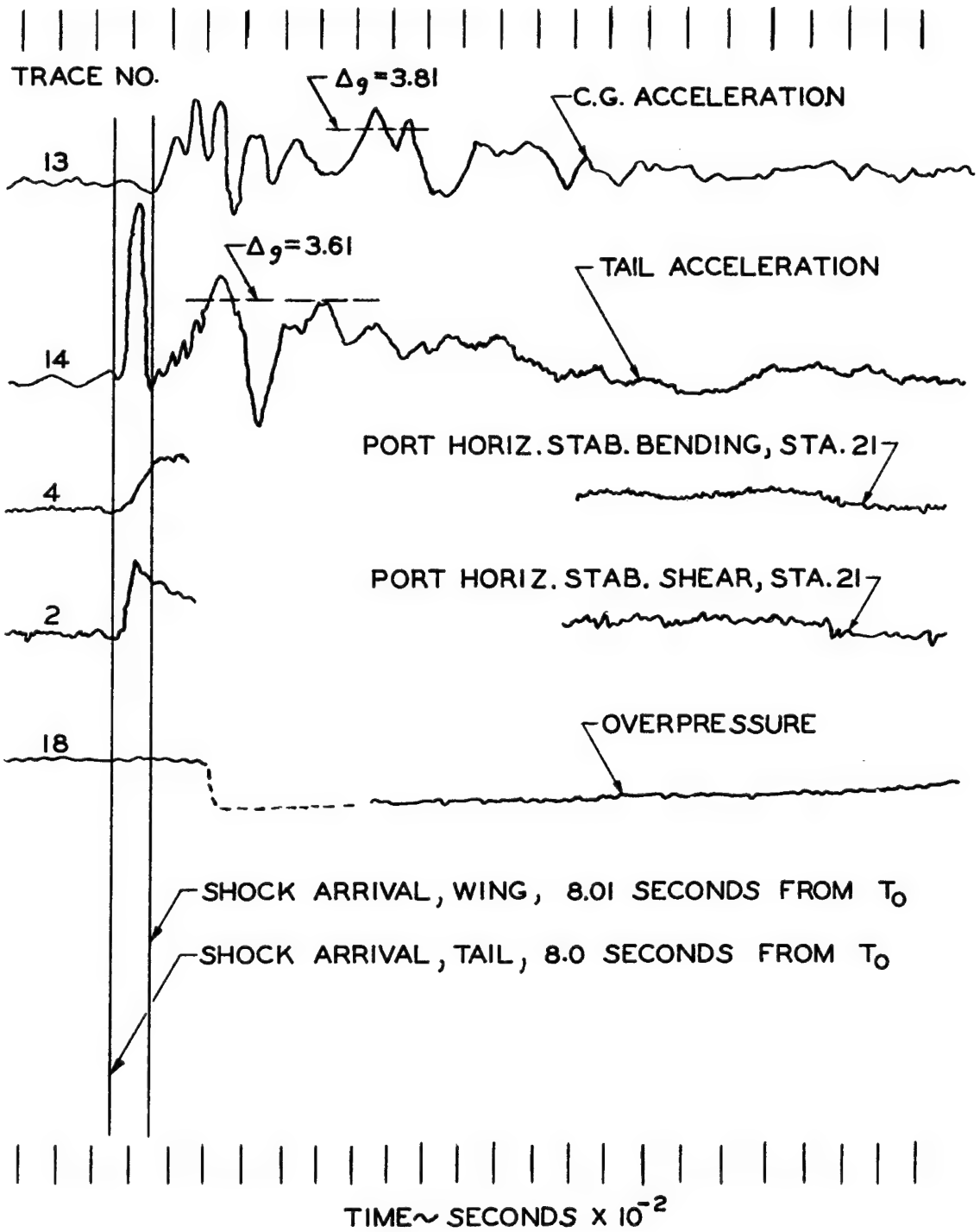

Fig. 3.29 Time History of c.g. Acceleration, Tail Acceleration, Tail Loads and Overpressure - Shot 2

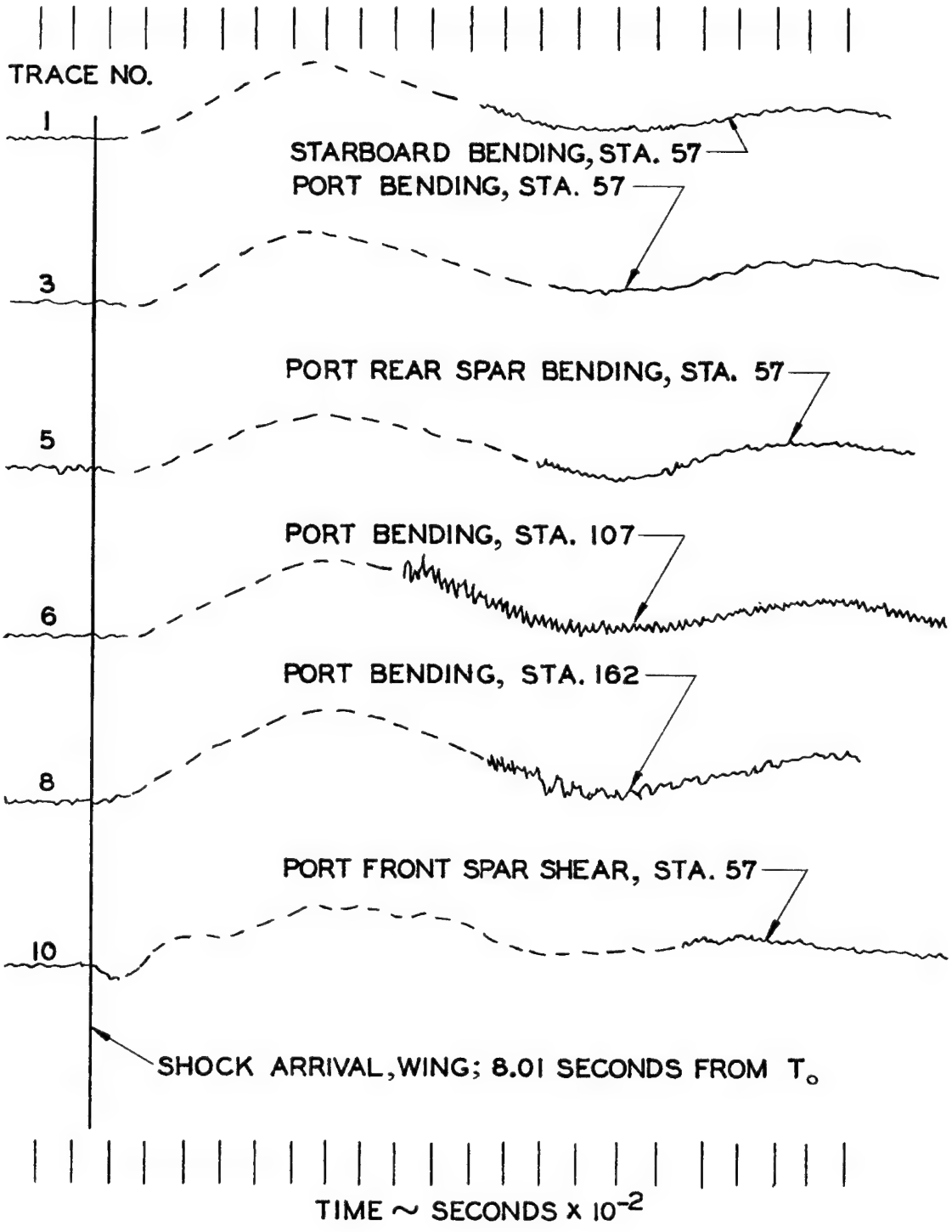

Fig. 3.30 Time History of Wing Loads Indicating Shot 2 Estimated Peaks Based on Wing Dynamic Response

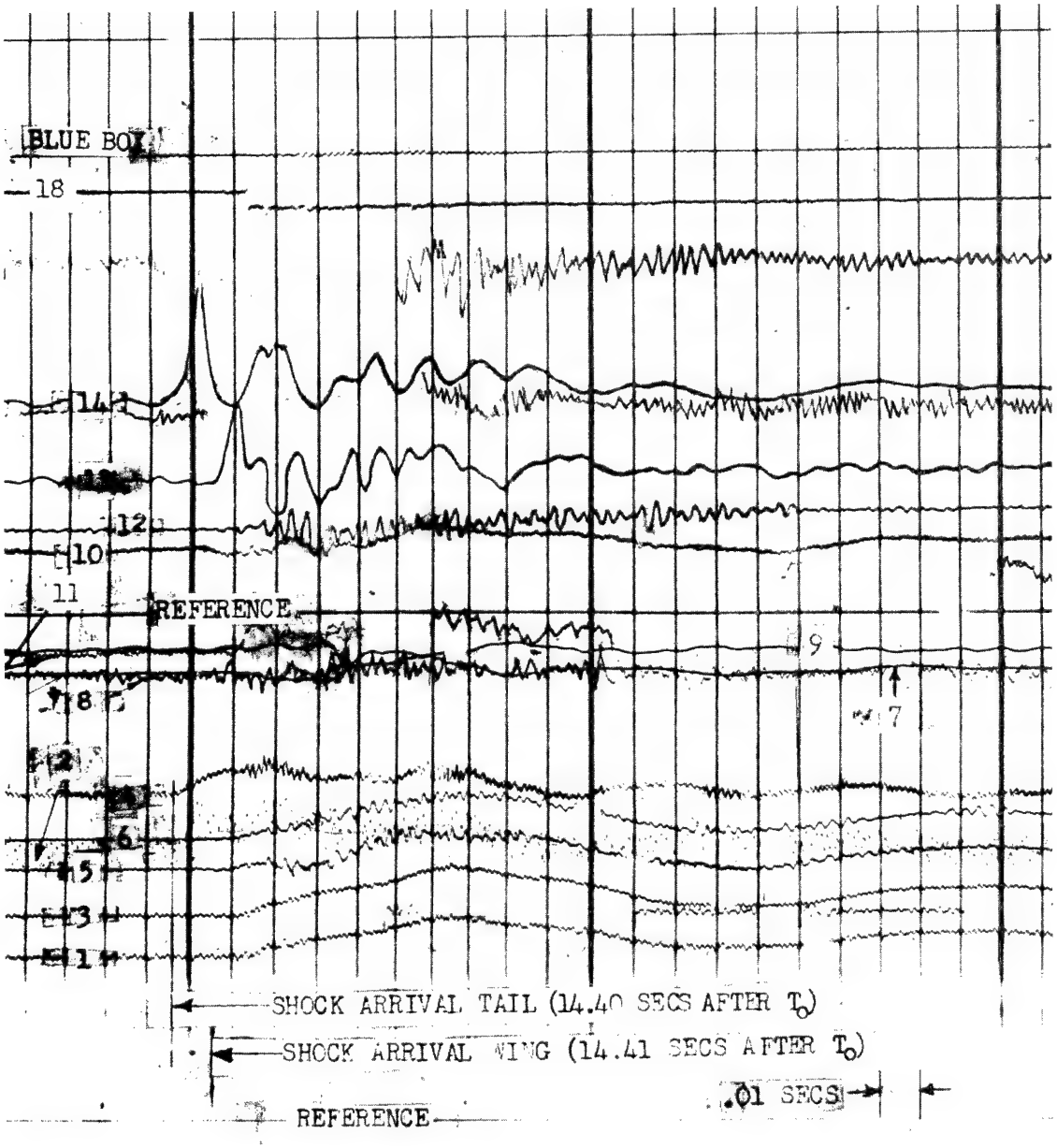

1. Stbd. Wing Bending, Sta. 57
2. Port Horiz. Stab. Shear, Sta. 21
3. Port Wing Bending, Sta. 57
4. Port Horiz. Stab. Bending, Sta. 21
5. Port Wing Rear Spar Bending, Sta. 57
6. Port Wing Bending, Sta. 107
7. Thermal Radiation
8. Port Wing Bending, Sta. 162
9. Thermal Radiation
10. Port Wing Shear, Sta. 57
11. Over Pressure
12. Indicated Airspeed
13. C.G. Acceleration
14. Tail Acceleration
18. Over Pressure

Fig. 3.31 Time History of Blast Data - Shot 1

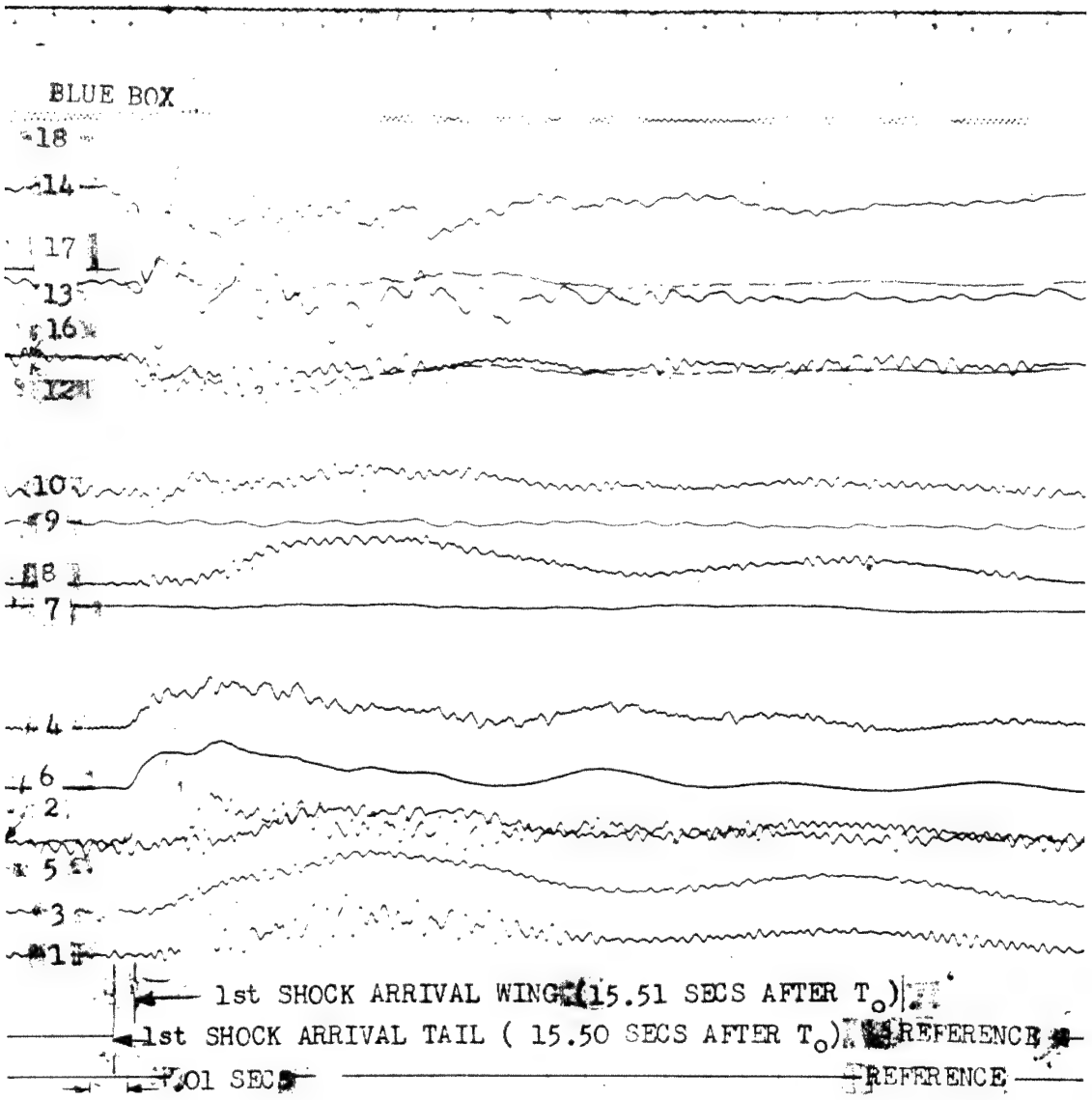

1. Stbd. Wing Bending, Sta. 57.5
2. Port Horiz. Stab. Shear, Sta. 21
3. Port Wing Bending, Sta. 57.5
4. Port Horiz. Stab. Bending, Sta.21
5. Port Wing Rear Spar Bending Sta.575
6. Stbd. Horiz. Stab. Front Spar Bending, Sta. 21
7. Thermal Radiation
8. Port Wing Bending, Sta. 164
9. Thermal Radiation
10. Port Wing Shear, Sta. 57.5
11. Over Pressure
12. Stbd. Horiz. Stab.Rear Spar Bending, Sta. 21
13. C. G. Acceleration
14. Tail Acceleration
16. Stbd. Horiz.Stab.Front Spar Shear, Sta. 21
17. Stbd. Horiz.Stab.Rear Spar Shear, Sta. 21
18. Over Pressure

Fig. 3.32 Time History of Blast Data - Shot 9a (First Shock, Shot 9)

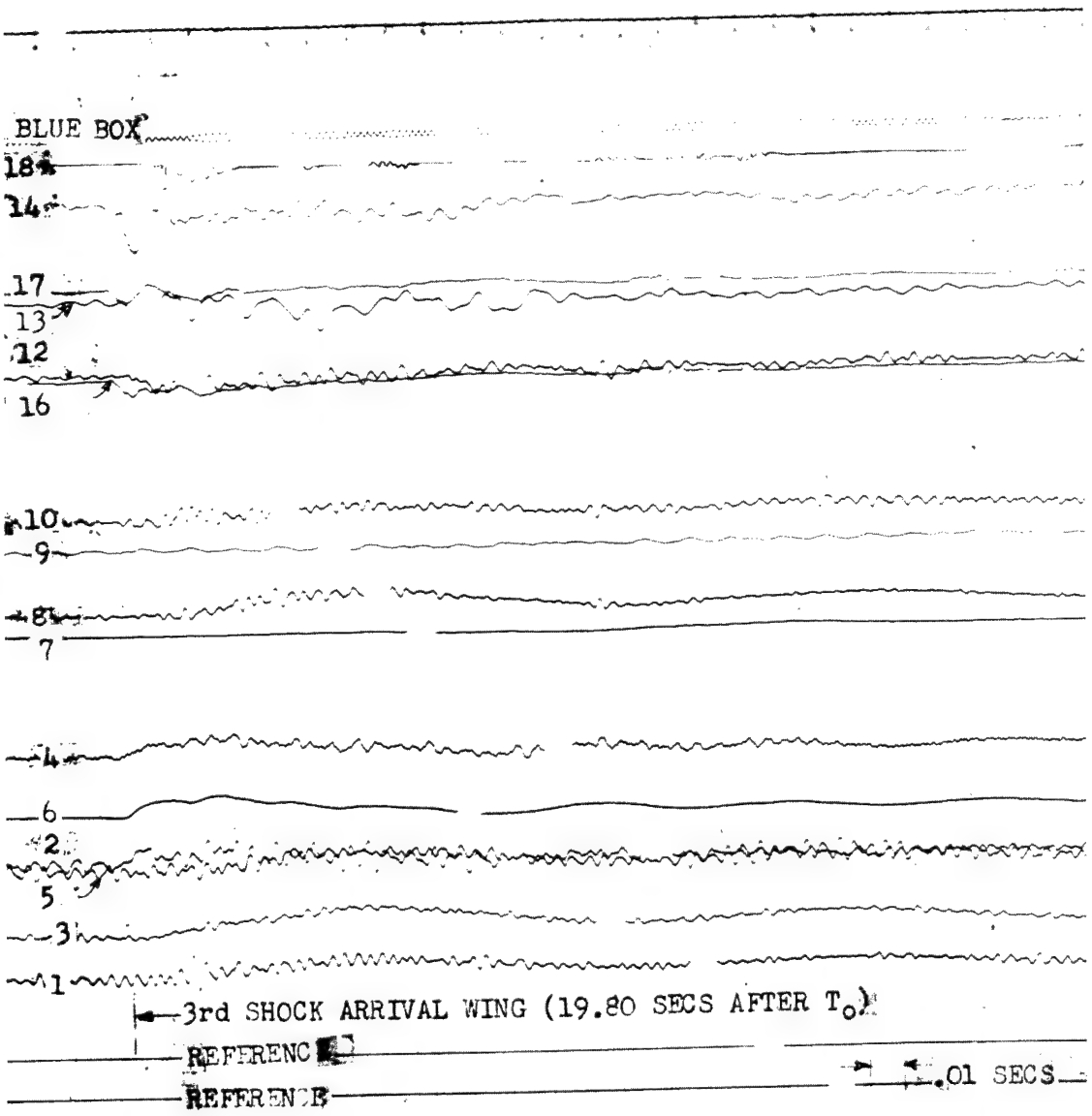

1. Stbd. Wing Bending, Sta. 57.5
2. Port Horiz. Stab. Shear, Sta. 21
3. Port Wing Bending, Sta. 57.5
4. Port Horiz. Stab. Bending, Sta. 21
5. Port Wing Rear Spar Bending Sta.57.5
6. Stbd. Horiz. Stab. Front Spar Bending, Sta. 21
7. Thermal Radiation
8. Port Wing Bending, Sta. 164
9. Thermal Radiation
10. Port Wing Shear, Sta. 57.5
11. Over Pressure
12. Stbd. Horiz. Stab. Rear Spar Bending, Sta. 21
13. C. G. Acceleration
14. Tail Acceleration
16. Stbd. Horiz.Stab.Front Spar Shear, Sta. 21
17. Stbd. Horiz.Stab.Rear Spar Shear, Sta. 21
18. Over Pressure

Fig. 3.33 Time History of Blast Data - Shot 9c (Third Shock, Shot 9)

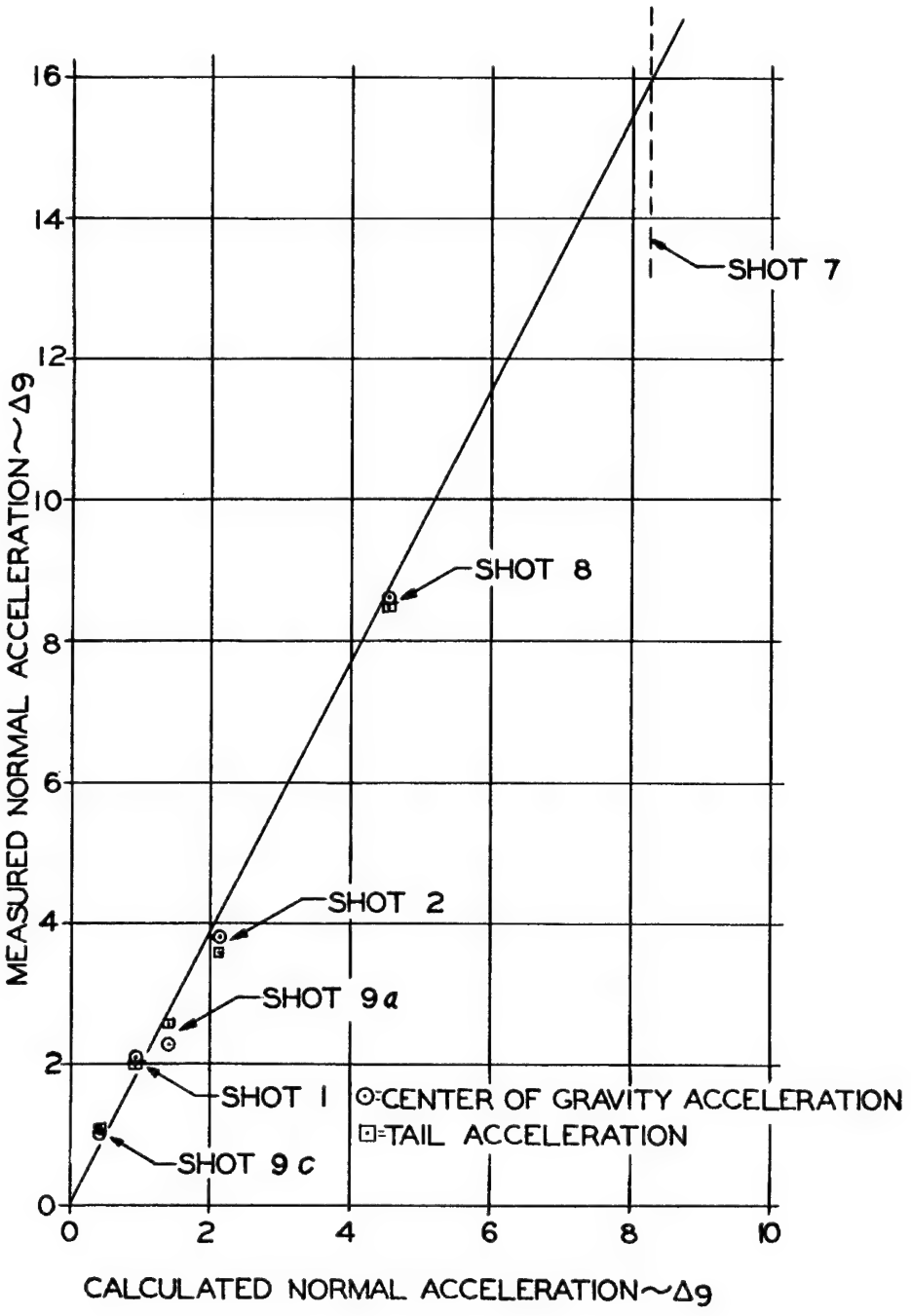

Fig. 3.34 Comparison of Measured and Calculated Aircraft Normal Acceleration

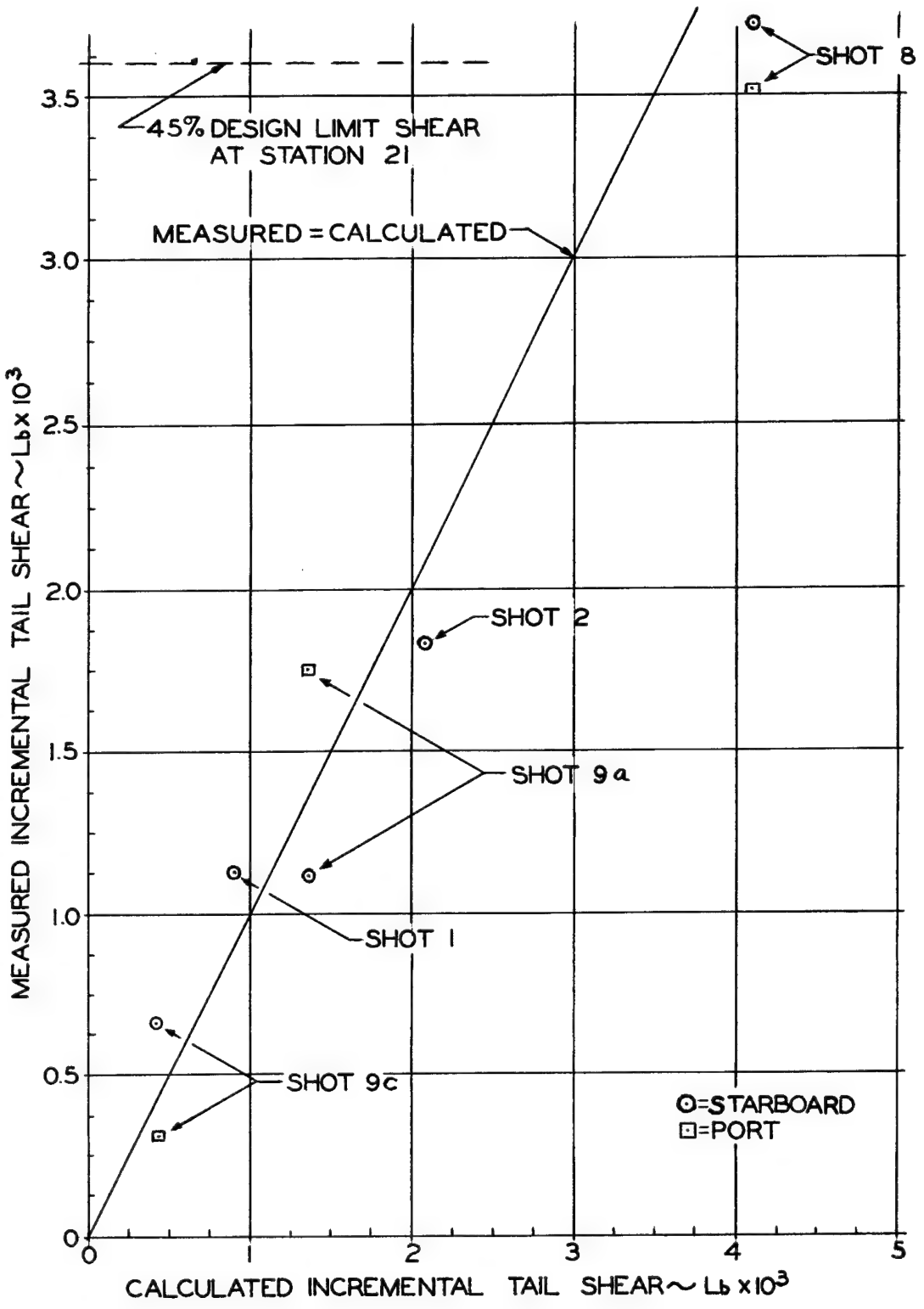

Fig. 3.35 Comparison of Measured and Calculated Horizontal Stabilizer Shear

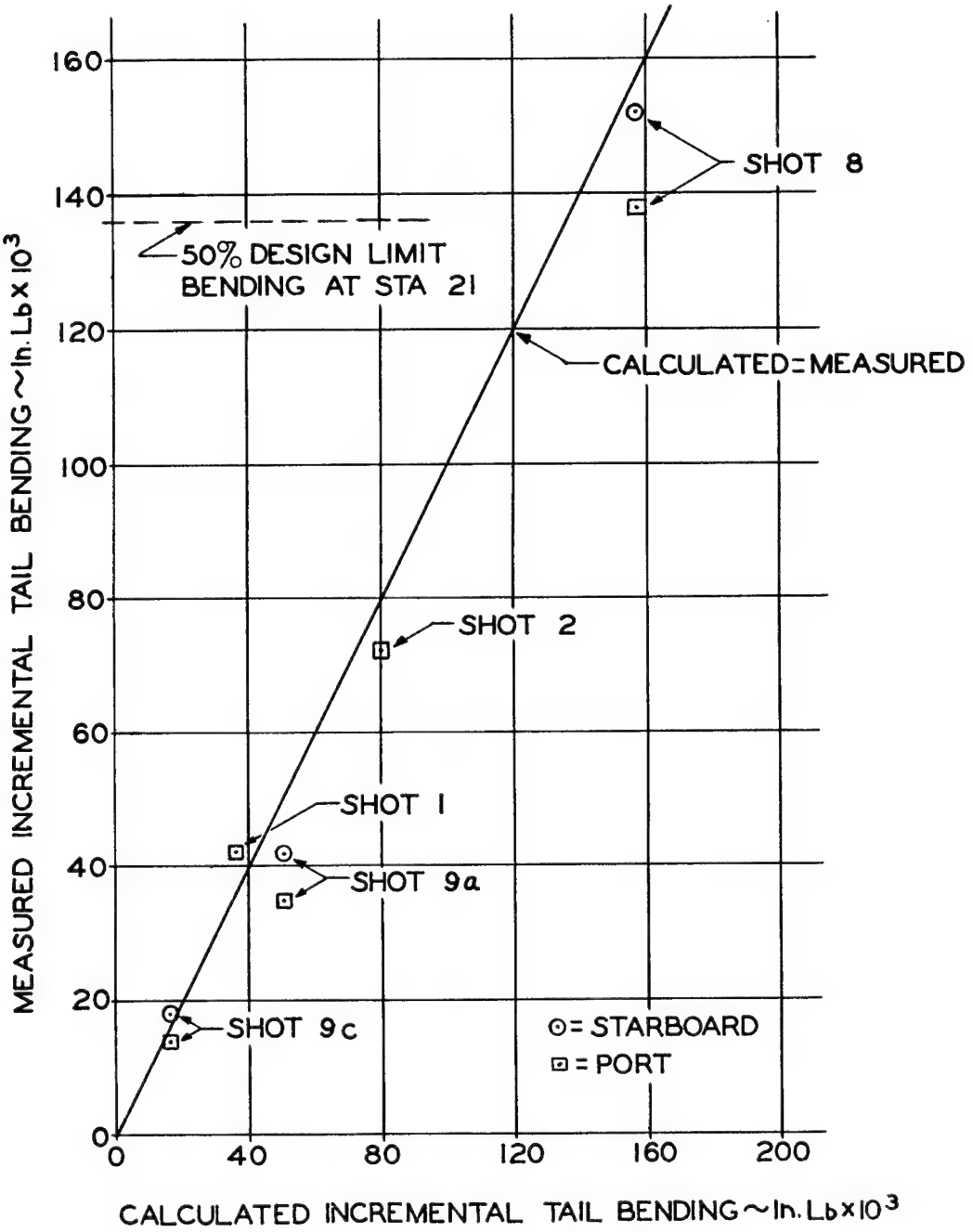

Fig. 3.36 Comparison of Measured and Calculated Horizontal Stabilizer Bending

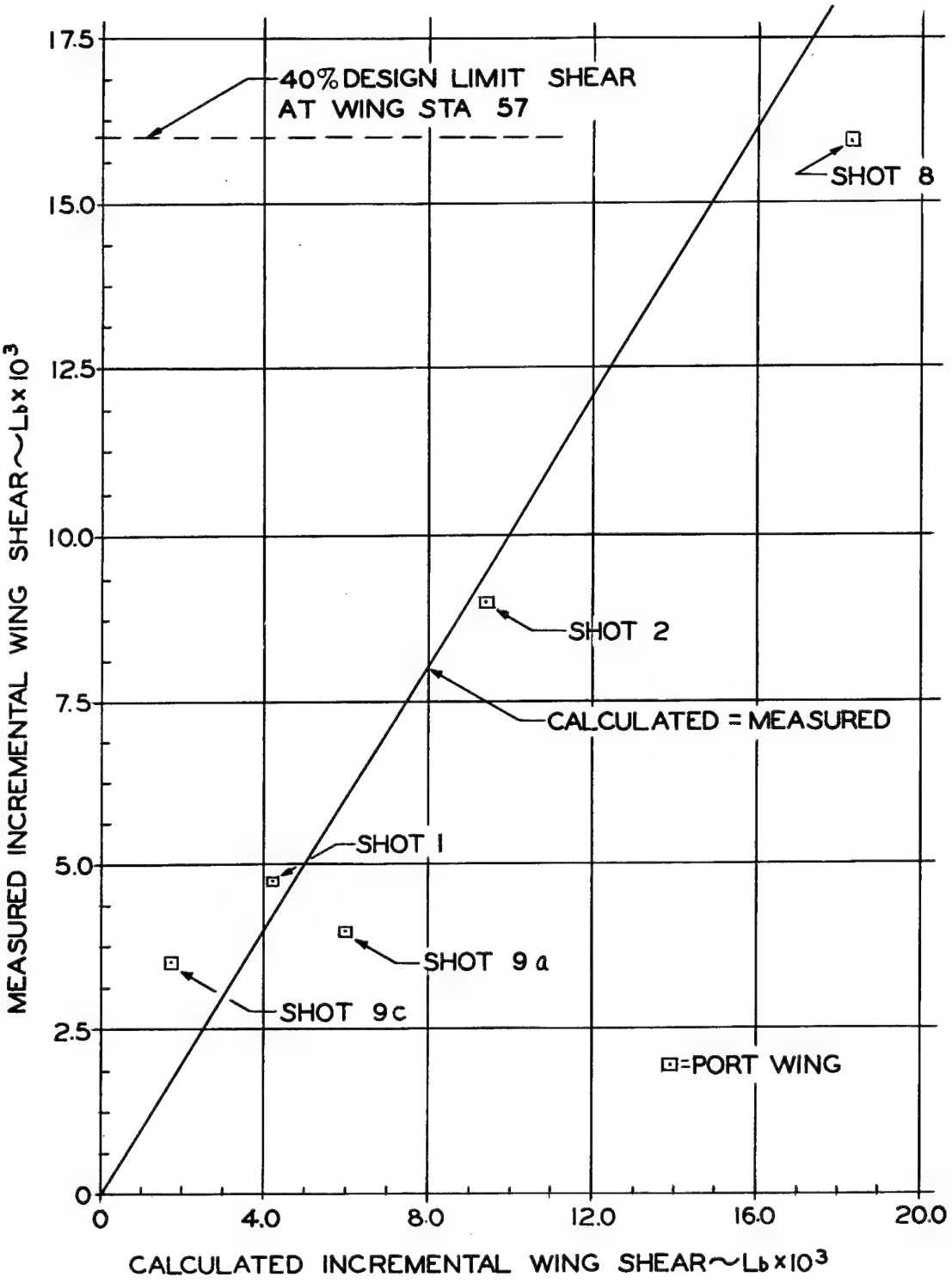

Fig. 3.37 Comparison of Measured and Calculated Wing Shear - W. S. 57

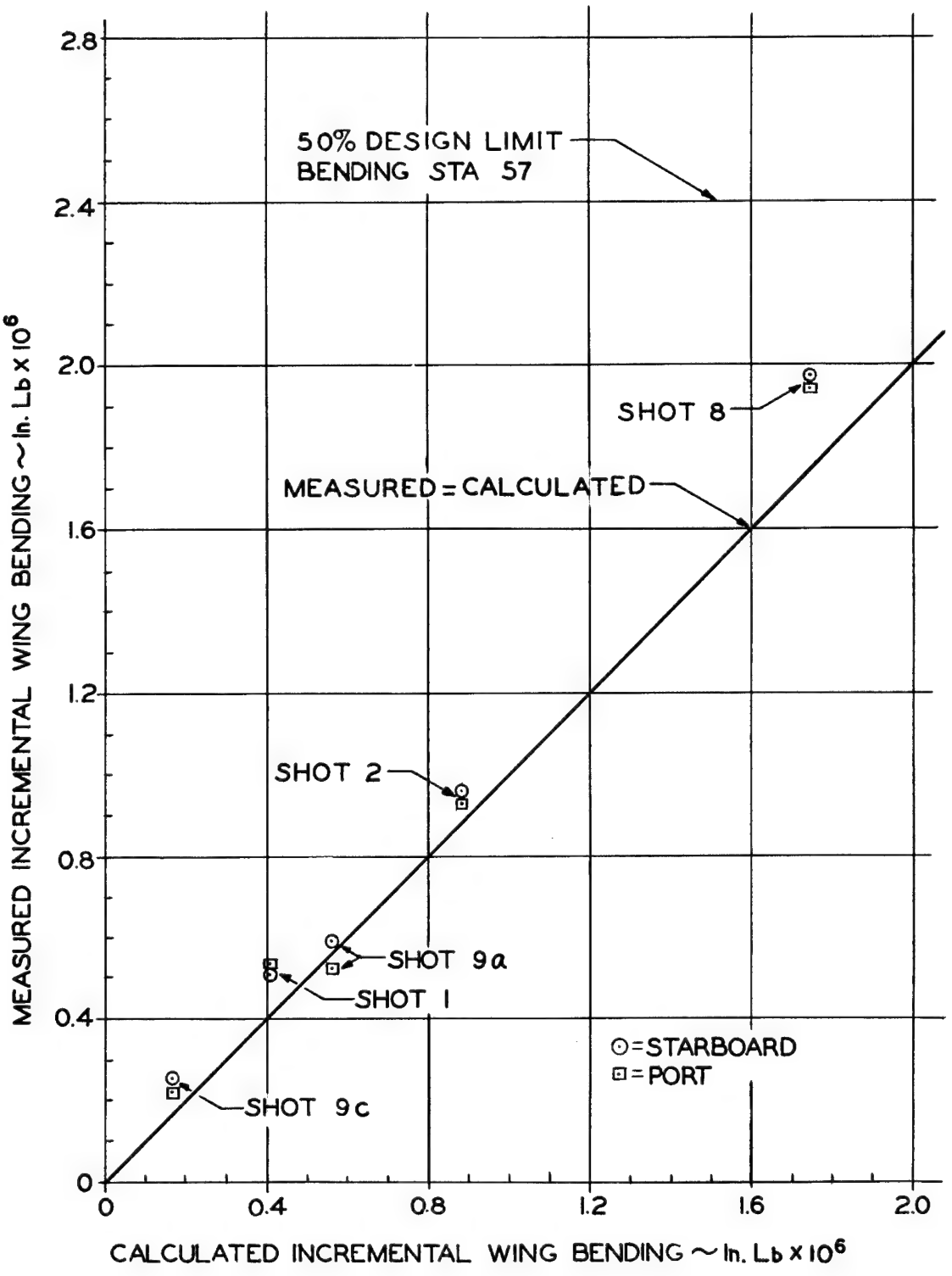

Fig. 3.38 Comparison of Measured and Calculated Wing Bending - W. S. 57

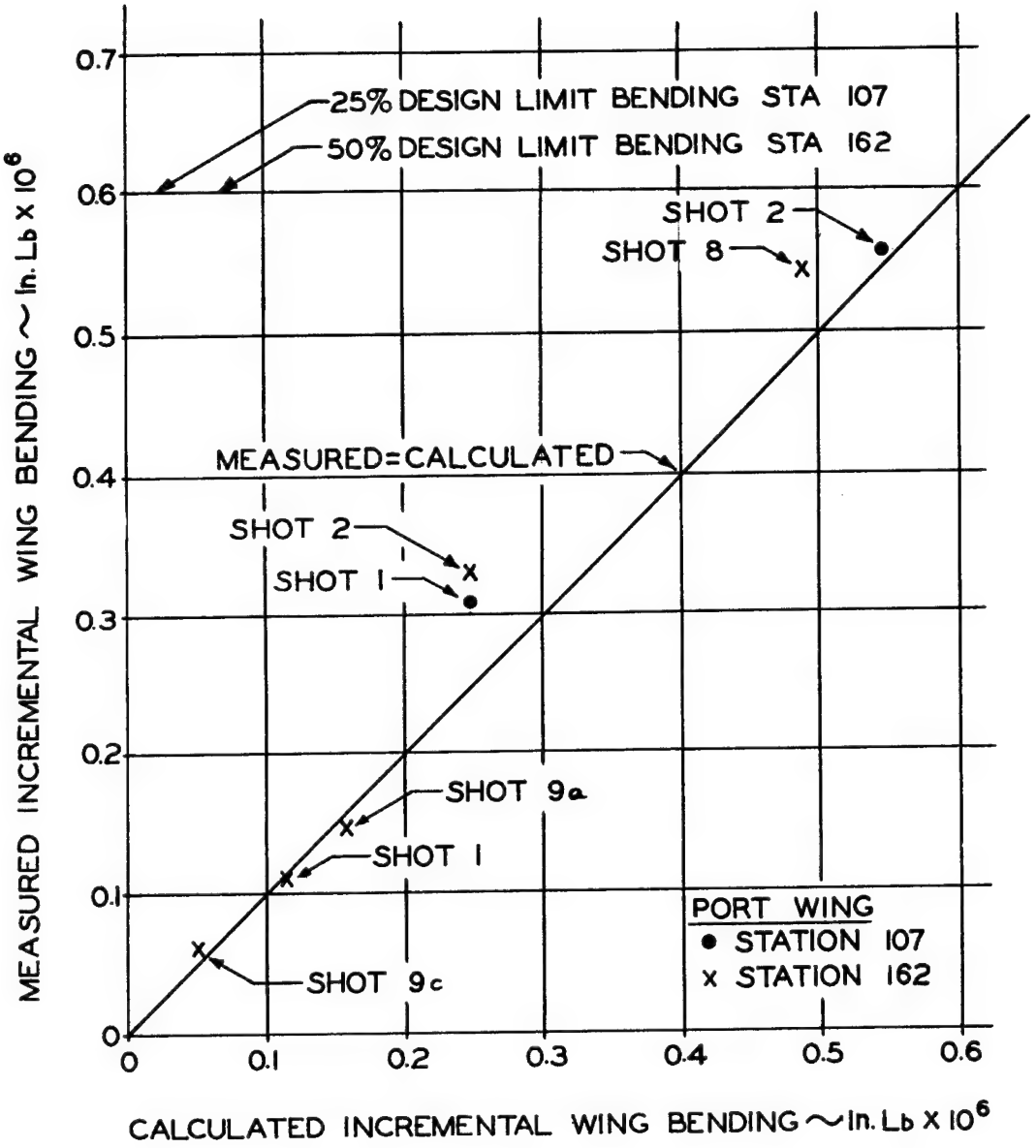

Fig. 3.39 Comparison of Measured and Calculated Wing Bending - W. S. 107 and W. S. 162

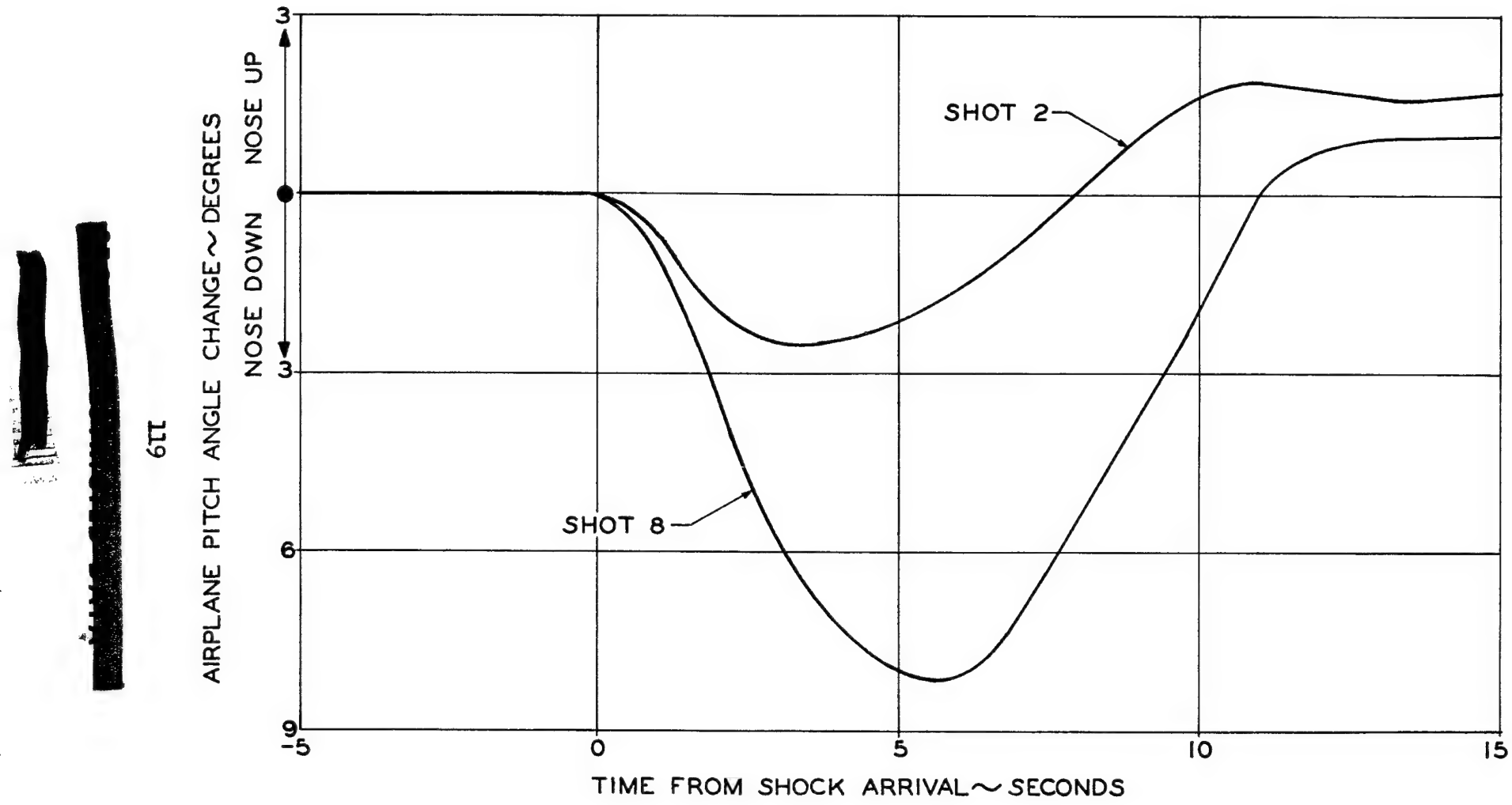

Fig. 3.40 Time History of Airplane Pitching Motion

CHAPTER 4

CONCLUSIONS AND RECOMMENDATIONS

4.1 CONCLUSIONS

4.1.1 Thermal Effects

a. Thermal radiation on aircraft in flight in clear air is a result of ground reflection as well as direct radiation from the fireball. Additional thermal radiation may also be received from clouds through reflection, depending upon cloud location with respect to both aircraft and burst point. As such, refs (1) and (8) appear to be inadequate for predicting thermal effects on aircraft in flight unless reflectivity calculations, such as are outlined in ref (9), are included.

b. Heat resistant white paint provides aircraft skin with a greater degree of protection from thermal radiation than any other surface finish tested. Next to heat resistant white, bare aluminum appears to offer the best protection against thermal damage. Aircraft skin painted standard blue is extremely vulnerable to thermal damage, being able to stand less than one-third of the thermal radiation withstood by skin painted with heat resistant white. Use of white or light colored paint on tires, aerodynamic seals and other dark colored materials provides similar protection against thermal radiation.

c. Microscopic thermal damage as indicated by metallographic tests on aircraft skin specimens does not appear to be an important factor where structural considerations associated with thermal radiation are involved. Temperature rise measured by temperature sensitive papers and strain gages on the back of these specimens appear consistent with structural thermal damage and as such are believed to be applicable to the investigation of aircraft thermal limitations as treated in this report.

d. Thermal damage to paint finishes, such as standard white, may modify its absorptivity characteristics. Equivalent absorptivity for a given finish appears to be affected by skin thickness and aerodynamic cooling. Reference (14) provides a satisfactory means of calculating the cooling rate if the aerodynamic flow conditions are known.

4.1.2 Overpressure and Gust Effects

a. When the yield of the weapon and the position of the airplane are known, the time of shock arrival may be predicted with negligible error.

b. The methods of predicting overpressures encountered by aircraft in flight in the vicinity of an atomic blast produce results which are in agreement with measured values to within ± 0.1 psi.

c. Overpressure up to at least 2 psi has no adverse effect on the structure of AD type aircraft. Overpressure effects in Shot 7, for approximately 3 psi, were masked by the associated thermal damage.

d. The methods of ref (1) used in predicting the acceleration introduced to AD type aircraft in flight by blast, appear to provide agreement with a sustained or effective acceleration rather than with the peak acceleration measured in flight. This is seen as a result of the close correlation between measured loads and those calculated using the accelerations determined by these methods.

4.1.3 General

a. Orientation of aircraft in flight with the longitudinal axis pointed directly away from the burst should result in reduced thermal and gust effects when compared with the positions investigated in this report.

b. The installations for the measurement of blast effects, as well as those used for the measurement of thermal effects, had certain limitations in that the effects as measured may have been modified by dynamic response characteristics associated with the airplane. Additional information concerning thermal and shock inputs might be obtained were comprehensive laboratory tests to be conducted to establish the dynamic characteristics of the complete measuring systems as installed in the test aircraft.

4.2 RECOMMENDATIONS

The following recommendations are made, based on data presented in this report.

4.2.1 Thermal Effects

It is recommended that:

a. Additional thermal radiation measurements in flight be made when opportunity permits, in order to further evaluate the effect of ground reflectivity. Time histories of aircraft skin temperature rise for various thicknesses and surface finishes should be included. Metallographical studies should be made on all specimens to provide additional data on measured temperatures and thermal damage.

b. Theoretical methods for predicting temperature rise and thermal effects on aircraft skin be further investigated in order to provide closer correlation with thermal phenomena as measured and observed.

c. In those atomic weapon delivery problems where critical thermal conditions exist, consideration be given to the use of a skin finish of naval aircraft with better thermal characteristics than that of the standard blue paint. Tires, aerodynamic seals, and other exposed materials should be similarly protected.

4.2.2 Overpressure and Gust Effects

It is recommended that:

a. Dynamic analysis methods for predicting wing and tail loads on AD type aircraft be investigated in an attempt to provide additional correlation with flight test data.

SYMBOLS AND DEFINITIONS

a_A	Speed of sound at aircraft altitude, feet per second.
a_H	Speed of sound at burst height, feet per second.
cps	Instrument operational frequency, cycles per second.
$C_{L\alpha}$	Slope of lift curve, per radian.
D	Gamma dosage, roentgens.
g	Normal accelerometer indication, non-dimensional.
Δg	Incremental normal accelerometer indication, non-dimensional.
h_1	Burst height above ground, feet.
h_2	Aircraft height above ground, feet.
Δh	Aircraft height above burst, feet, $h_2 - h_1$.
I_R	Unit reflected thermal radiation from ground, per centimeter^2.
MSL	Mean sea level.
NOLO	No live occupant in drone aircraft.
P_A	Atmospheric pressure at aircraft altitude, pounds per square inch.
P_H	Atmospheric pressure at burst height, pounds per square inch.
P_1	Peak instantaneous pressure, pounds per square inch.
ΔP	Overpressure, pounds per square inch.
Q	Total thermal radiation, calories per square centimeter.
R	Range from point of burst to point in space, feet.
R_A	Range from point of burst to aircraft, feet.
R_H	Range from point of burst to point in space at burst altitude, feet

S	Aircraft wing area, square feet.
t	Aircraft skin thickness, inches.
t_o	Time of burst, time zero.
t_s	Time of shock arrival, seconds from t_o.
T_A	Absolute temperature of aircraft altitude, °R.
T_H	Absolute temperature at burst altitude, °R.
ΔT	Aircraft skin temperature rise, °F.
U_I	Peak instantaneous aircraft velocity, feet per second.
U_A	Initial aircraft velocity, feet per second.
w	Gust velocity, feet per second.
W	Weight of aircraft, pounds.
Y	Weapon yield, kilotons.
θ	Angle between horizontal and line joining burst point with aircraft, degrees.
β	Albedo, percent of thermal radiation reflected by a point, non-dimensional.
λ	Fuchs factor, non-dimensional; $\lambda \approx e^{-\frac{1}{4}\left(2\frac{P_A}{P_H}+3\frac{T_A}{T_H}-5\right)}$
μ_e	Equivalent thermal absorptivity factor, incorporating all heat loss considerations, non-dimensional.
ρ_A	Initial ambient density at aircraft altitude, slugs per cubic foot.
ρ_H	Ambient density at burst altitude, slugs per cubic foot.
ρ_I	Peak air density, slugs per cubic foot.
σ	Altitude density ratio at burst altitude; ρ_H/ρ_{SL}

APPENDIX A

METALLURGICAL TESTS OF SKIN SPECIMENS TAKEN FROM MODEL AD TYPE AIRCRAFT EXPOSED IN FLIGHT TO THERMAL RADIATION FROM AN ATOMIC EXPLOSION

by

RICHARD SCHMIDT

JOHN ERTHAL

NAVAL AIR MATERIAL CENTER

PHILADELPHIA 12, PENNSYLVANIA

[redacted]

APPENDIX A

METALLURGICAL TESTS OF SKIN SPECIMENS TAKEN FROM MODEL AD TYPE AIRCRAFT EXPOSED IN FLIGHT TO THERMAL RADIATION FROM AN ATOMIC EXPLOSION

A.1 OBJECTIVES

The primary objectives of these metallurgical tests were:

a. to determine the strength properties of the various aircraft skin specimens after exposure in flight to the thermal radiation from an atomic explosion.

b. to determine the approximate magnitude of the maximum temperature rise in the various aircraft skin specimens by ascertaining whether or not melting of the clad and/or base metal occurred.

A.2 METHOD

A.2.1 Strength Tests

Specimens for tensile tests were manufactured from samples of the aluminum alloy skin cut from various portions of the underside of the test aircraft which participated in Shots 2, 7, and 8. Skin samples were obtained having different thicknesses and surface finishes. Due to the restricted size and/or condition (thermal damage, etc.) of the various skin panels from which samples were cut, substandard size tensile specimens had to be manufactured.

SR-4 type strain gages were mounted on the various test specimens and tensile tests conducted to determine ultimate strength, yield strength, and per cent elongation. Where practical, at least three tensile specimens were obtained and tested from the same skin sample.

A.2.2 Metallographic Examinations

Small specimens cut from each of the various skin samples were mounted, polished, and subjected to microscopic examination.

By comparing the data obtained from the metallographic examination of these specimens with existing data on the solidus and liquidus

temperature of the alloys, an estimate of the maximum temperature reached by each specimen could be obtained. For example, the solidus temperature for 24S aluminum alloy is 935°F and the solidus of the cladding is 1190°F. If melting has occurred in the base metal and not in the cladding, the temperature reached was between these values.

A.3 RESULTS

A.3.1 Strength Tests

The physical properties of ultimate strength, yield strength, and per cent elongation of the specimens tested are listed in Table A.1 for Shot 8 and in Table A.2 for Shots 2 and 7. No attempt has been made to compare these results with "standard" values due to the fact that sub-standard size test specimens were used (elongation data not comparable) and no test specimen material in its original condition was available for establishing realistic reference standards. However, the following handbook values as obtained from ref (18) are listed for the different types of aluminum alloy specimens tested:

Material	Ultimate Strength psi	Yield Strength, psi	% Elongation/2 in.
24S T3 Alclad	64,000	44,000	18.0
24SO	27,000	11,000	19.0
61S T6	45,000	40,000	12.0
75S T6 Alclad	76,000	67,000	11.0
AL3SO	16,000	6,000	30.0
52SH34	37,000	31,000	10.0
52SO	27,000	12,000	25.0

A.3.2 Metallographic Tests

Results of the metallographic examinations indicating the maximum temperatures reached by the test specimens and their microstructural characteristics are listed in Table A.1 for Shot 8 and in Table A.2 for Shots 2 and 7. For purposes of comparison, the maximum temperatures attained by the different test specimens as measured during Shot 8 are also listed in Table A.1. These measurements were made by means of maximum indicating temperature sensitive papers covering the range from 130°F to 580°F in specified increments. The temperature papers were mounted on the interior surface of the aircraft skin. Similar data are not available for comparison with the metallographic test results listed in Table A.2.

TABLE A.1 - Summary of Metallurgical Test Results on Skin Specimens from Model XBT2D-1 Airplane

NOMINAL THICKNESS AND COLOR	MATERIAL	SHOT NO. AND SPECIMEN LOCATION ON TEST A/C	STRENGTH TEST RESULTS*			ΔT °F.# TEMP. TAPE & GAGE DATA	METALLOGRAPHIC TEST RESULTS	
			ULTIMATE STRESS —PSI—	YIELD STRESS —PSI—	% ELONGATION —PER IN.—		ΔT$_1$ °F. PROBABLE	REMARKS
0.016 Standard Blue	24ST	8-Flaps	63,840[3]	45,230[2]	11.5[2]	>228 <304	1000	Eutectic Melting
0.020 Standard Blue	24S0	" "	Specimen Lost			>250 <304	1000	Eutectic Melting
0.020 Standard Blue	24S0	" "	29,720[3]	15,300[1]	12.0[2]	>205 <239	1200	Severe Eutectic Melting
0.025 Standard Blue	24ST	" "	69,030[3]	49,000[1]	18.0[2]	>205 <250	Below 900	No Eutectic Melting
0.032 Standard Blue	24ST	Inspection Plate	67,660[3]	49,800[1]	18.5[2]	>177 <228	1000	Eutectic Melting
0.032 Standard Blue	52SH34	Flaps	36,160[3]	29,500[1]	11.0[2]	>166 <228	1150	Melting within grains
0.040 Standard Blue	24ST	"	66,380[3]	44,600[1]	21.0[2]	>166 <228	Below 900	No Eutectic Melting

TABLE A.1 (Continued)

NOMINAL THICKNESS AND COLOR	MATERIAL	SHOT NO. AND SPECIMEN LOCATION ON TEST A/C	STRENGTH TEST RESULTS*			#	METALLOGRAPHIC TEST RESULTS	
			ULTIMATE STRESS —PSI—	YIELD STRESS —PSI—	% ELONGATION —PER IN.—	ΔT °F. TEMP. TAPE & GAGE DATA	ΔT_1 °F. PROBABLE	REMARKS
0.051 Standard Blue	24ST	Flaps	69,260[3]	47,800[1]	21.5[2]	>121 <177	Below 900	No Eutectic Melting
0.051 Black	24ST	Inspection Plate	65,450[3]	42,000[1]	23.0[2]	>121 <177	1100	Dendritic Melting
0.016 Alumi-nized Lac.	24ST	Flaps	69,626[3]	55,165[3]	[illegible].5[2]	>205 <250	1000	Slight Eutectic Melting
0.020 Alumi-nized Lac.	24S0	Flaps	28,046[3]	15,395[2]	17.5[2]	>177 <228	1300	Clad melted on both sides
0.025 Alumi-nized Lac.	24ST	"	68,775[3]	47,500[1]	19.0[2]	>177 <228	975	Slight Eutectic Melting
0.040 Alumi-nized Lac.	24ST	"	68,590[3]	47,400[1]	20.0[2]	<121	Below 900	No Eutectic Melting
0.040 Alumi-nized Lac.	25ST	Inspection Plate	78,540[3]	72,400[1]	13.0[2]	<107	Below 890	No Eutectic Melting

TABLE A.1 (Continued)

NOMINAL THICKNESS AND COLOR	MATERIAL	SHOT NO. AND SPECIMEN LOCATION ON TEST A/C	STRENGTH TEST RESULTS*			ΔT °F.# TEMP TAPE & GAGE DATA	METALLOGRAPHIC TEST RESULTS	
			ULTIMATE STRESS —PSI—	YIELD STRESS —PSI—	% ELONGATION —PER IN.—		ΔT_1 °F. PROBABLE	REMARKS
0.016 Standard White	24ST	Flaps	73,276[3]	59,276[3]	15.5[2]	>107 <102	Below 900	No Eutectic Melting
0.020 Standard White	24SO	"	32,126[3]	16,863[3]	19.0[1]	<121	1300	Surface Clad Melted Interior Melted
Heat Resist. 0.016 White	24ST	"	68,730[3]	51,500[1]	16.5[2]	> 77 <107	1000	Eutectic Melting
Heat Resist. 0.020 White	24SO	"	31,793[3]	16,901[3]	19.5[2]	> 77 <108	1250	Clad Melting
Bare 0.016 Aluminum	24ST	"	70,640[3]	55,500[1]	18.0[2]	>121 <177	Probably below 900	Possible Eutectic Melting
Bare 0.020 Aluminum	24SO	"	32,130[3]	16,746[3]	17.0[1]	>142 <161	1300	Melting of Clad and Interior

* Number in upper right-hand corner of each block indicates number of tests conducted to obtain average value tabulated.

Max. temp. rise in skin specimen as measured during Blast Test using temp. sensitive papers.

TABLE A.2 Summary of Metallurgical Test Results on Skin Specimens from Model AD-2 Drone

NOMINAL THICKNESS AND COLOR	MATERIAL	SHOT NO. AND SPECIMEN LOCATION ON TEST A/C	STRENGTH TEST RESULTS *			METALLOGRAPHIC TEST RESULTS	
			ULTIMATE STRESS — PSI —	YIELD STRESS — PSI —	% ELONGATION — PER IN. —	ΔT_1 °F. PROBABLE	REMARKS
0.016 Standard Blue	24ST	2-Aileron	64,220 [3]	46,900 [1]	18.0 [1]	Below 900	No Eutectic Melting
0.025 Standard Blue	24ST	2-Aileron	65,800 [3]	44,200 [1]	19.5 [1]	Below 900	No Eutectic Melting
0.016 Standard Blue	24ST	7-Aileron	No tensile specimen			1300	Cladding surface melted and re-solidified
0.025 Standard Blue	24ST	7-Wing Panel	No tensile specimen			1300	Cladding surface melted and re-solidified
0.032 Standard Blue	75ST	7-Wing Panel	No tensile specimen			Surface over 890 Interior below 890	Evidence of Eutectic surface melting
0.032 Standard Blue	75ST	7-Aileron	No tensile specimen			900	Eutectic Melting
0.040 Standard Blue	24ST	7-Aileron	60,590 [2]	36,400 [1]	18.0 [1]	1000	Eutectic Melting

TABLE A.2 (Continued)

NOMINAL THICKNESS AND COLOR	MATERIAL	SHOT NO. AND SPECIMEN LOCATION ON TEST A/C	STRENGTH TEST RESULTS*			METALLOGRAPHIC TEST RESULTS	
			ULTIMATE STRESS —PSI—	YIELD STRESS —PSI—	% ELONGATION —PER IN.—	ΔT_1 °F. PROBABLE	REMARKS
0.051 Standard Blue	AL3S0	7-Tip of Wing	16,820 [3]	10,083 [3]	40.0 [2]	Below 1190	No Eutectic Melting
0.032 Standard Blue	61ST	7-Wing Tip	30,600	20,000 [1]	--	1150	Intergranular and Eutectic Melting
0.040 Standard Blue	75ST	7-Wing Panel	No tensile specimen			1100	Eutectic Melting
0.025 Standard Blue	52S0	7-Elevator Tip	62,020 [3]	42,300 [3]	24.0 [2]	1150	Intergranular and Eutectic Melting
0.075 Aluminized Lac.	24ST	7-Aileron	62,300 [1]	43,300 [1]	14.0 [1]	1000	Eutectic Melting
0.025 Standard White	24ST	7-Aileron	No tensile specimen			Surface 1200 Interior 1100	Eutectic Melting and Slight Clad Melting
0.016 Standard White	24ST	7-Aileron	No tensile specimen			1000	Eutectic Melting

TABLE A.2 (Continued)

NOMINAL THICKNESS AND COLOR	MATERIAL	SHOT NO. AND SPECIMEN LOCATION ON TEST A/C	STRENGTH TEST RESULTS*			METALLOGRAPHIC TEST RESULTS	
			ULTIMATE STRESS —PSI—	YIELD STRESS —PSI—	% ELONGATION —PER IN.—	ΔT_i °F. PROBABLE	REMARKS
0.032 Standard White	24ST	7-Elevator	63,710 [2]	47,800 [1]	14.0 [1]	Surface 1200 Interior 1000	Melting of Clad and Eutectic Melting
0.016 Heat Resist.White	24ST	7-Aileron	69,600 [1]	53,100 [1]	23.1 [1]	Surface 1200 Interior 1000	Melting of Clad and Eutectic Melting
0.025 Heat Resist.White	24ST	7-Aileron	64,310 [3]	44,600 [1]	20.0 [1]	Surface 1200 Interior 1000	Melting of Clad and Eutectic Melting
0.016 Bare Aluminum	24ST	7-Aileron	No tensile specimen			1250	Intergranular and Eutectic Melting
0.025 Bare Aluminum	24ST	7-Aileron	59,055 [2]	41,300 [1]	14.0 [1]	1000	Eutectic Melting
0.032 Stand. White on Stand. Blue	75ST	7-Wing Panel	73,900 [1]	46,250 [1]	25.7 [1]	Below 890	No Eutectic Melting
0.040 Stand. White on Stand, Blue	75ST	7-Wing Panel	69,050 [2]	53,750 [1]	9.0 [1]	Below 890	No Eutectic Melting

* Number in upper right-hand corner of each block indicates number of tests conducted to obtain average value tabulated.

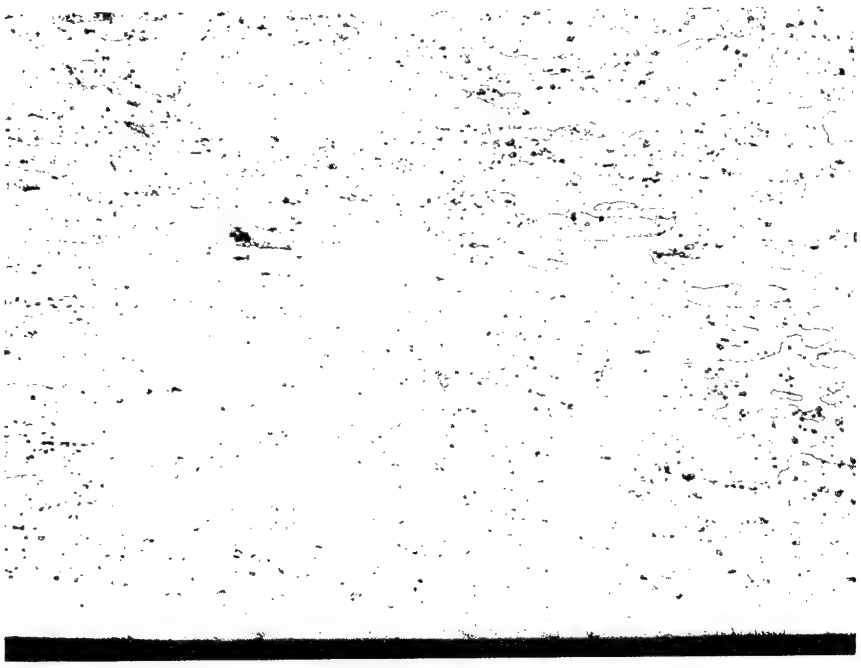

(a) Magnification: 150X

Description: Etched microstructure of sample heated below 900°F.

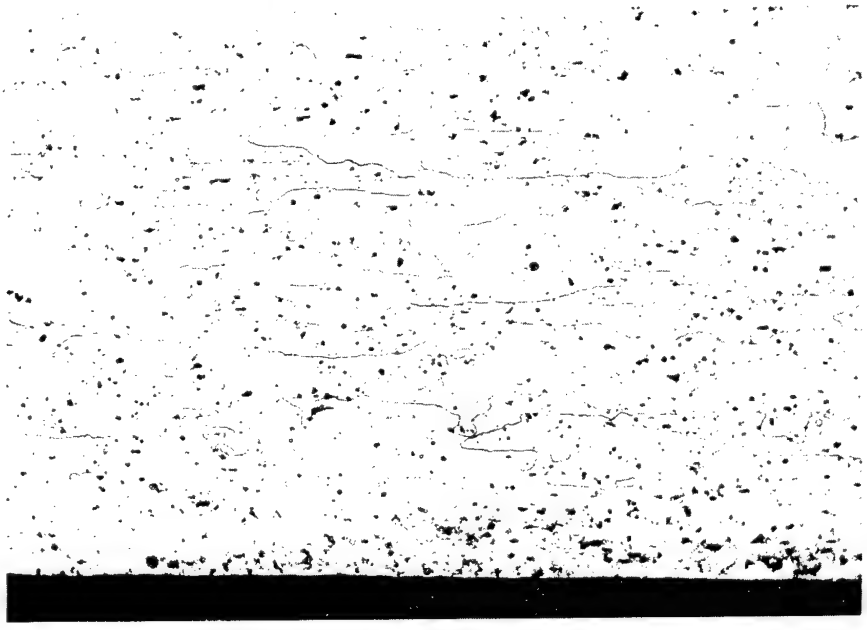

(b) Magnification: 150X

Description: Etched microstructure of submitted sample showing evidence of surface melting.

Fig. A.1 - Photomicrographs Showing Unaffected and Slightly Overheated Aluminum Alloy Sheets

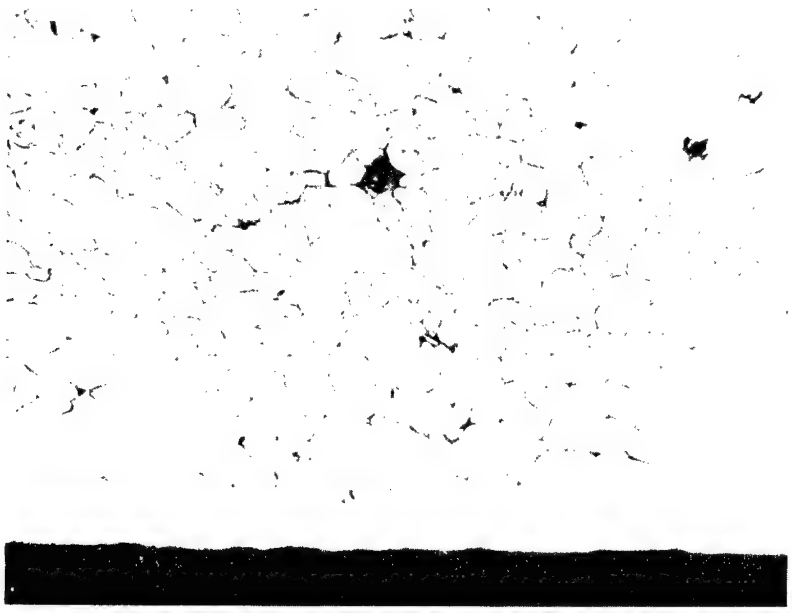

(a) Magnification: 250

Description: Etched microstructure showing the effect of melting of base metal and unmelted cladding.

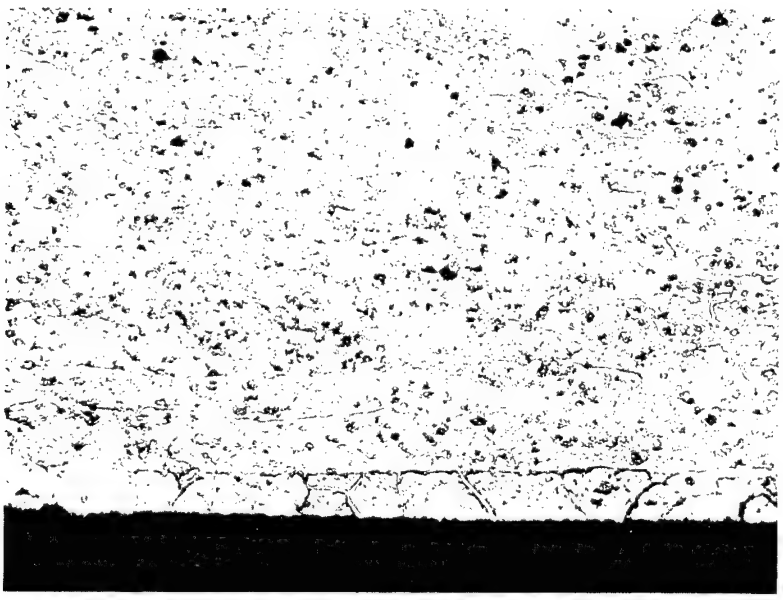

(b) Magnification: 250X

Description: Etched microstructure showing the effect of melting of both the cladding and base metal.

Fig. A.2 - Photomicrographs Showing the Effect of Overheating 24S Aluminum Alloy Sheet

APPENDIX B

EFFECTS OF THERMAL RADIATION ON THIN ALUMINUM ALLOY PANELS EXPOSED ON THE GROUND TO AN ATOMIC EXPLOSION

by

M. BENNON

NAVAL AIR MATERIAL CENTER

PHILADELPHIA 12, PENNSYLVANIA

APPENDIX B

EFFECTS OF THERMAL RADIATION ON THIN ALUMINUM ALLOY PANELS EXPOSED ON THE GROUND TO AN ATOMIC EXPLOSION

B.1 OBJECTIVE

The objectives of these tests were:

a. to determine the values of the equivalent thermal absorption coefficients for aluminum sheet metal panels of different thicknesses coated with various aircraft lacquers when exposed on the ground to thermal radiation from an atomic explosion.

b. to determine the magnitude of structural strength changes in sheet metal panels prepared to simulate aircraft skins after exposure to radiation from an atomic weapon.

B.2 BACKGROUND

The tests from which the reported data were obtained were made at the request and with the cooperation of the Bureau of Aeronautics to obtain data supplementary to that from the drone flight test program during UPSHOT-KNOTHOLE. The circumstances under which these supplementary data were to be obtained required that only passive types of thermal instrumentation be employed. All test material was exposed during Shot 9.

A significant variable for assessing the damage to aircraft skin structure resulting from exposure to radiation of an atomic explosion is the peak temperature reached by the exposed sheet metal. This peak temperature for a given level of exposure is a function of surface condition, material composition and skin thickness. For convenience in assessing the effect of surface condition on peak temperature attained a coefficient of equivalent thermal absorptivity has been defined as follows:

$$\mu_e = \frac{WC\Delta T\, t}{Q_A}$$

μ_e (equivalent thermal absorptivity coefficient) = fraction of Q_A absorbed by metal to produce temperature rise ΔT

W = density of material

C = specific heat of metal

ΔT = maximum temperature rise of metal during exposure

t = skin thickness

Q_A = total radiant energy normal to unit area of skin surface

B.3 TEST DESCRIPTION

Three frames to which were attached 35 24 ST aluminum alloy panels were placed at each of three stations at various slant ranges from and with the faces of the panels normal to the intended burst point of Shot 9. Each panel was hinged along its upper edge to permit free rotation except for the frictional restraint offered by a sheet metal clip bearing on the stiffener attached to the lower edge of the panel. This frictional restraint was intended to initially maintain the orientation of the panel with respect to the burst point but not offer appreciable restraint against the blast pressure wave. The panels were of various thicknesses and four types of surface preparation. The surfaces of one group of panels were in the bare "as received" condition. The other three groups received a conventional wash primer coating followed by a 2 mil coat of Military Specification MIL-L-7178 cellulose nitrate lacquer on the surface to be exposed. One of these groups received a glossy sea blue (color #623) coat. A second group received a white (color #511 with omission of the blue tint) coat. A third group received an aluminized coat. On the back close to the center of each panel was attached a Temp Tape temperature indicator. Each of the three frames carried along its upper edge a set of passive type thermal energy indicators. Figures B.1 and B.2 show the details of the panel and frame construction. Figures B.5, B.7, B.8, B.9 and B.10 show the thermal energy indicators on their mounting strip, a frame with mounted panels and thermal energy indicators, an illustration of a Temp Tape installation, a frame with the temporary protective covering (removed before the test exposure), and a frame set up at the test site with its supporting braces.

In addition to the three frames, four AD airplane elevator sections were exposed at each of two of the three frame stations. The orientations of the elevator sections are shown in Figure B.50. Each elevator section carried either two or three Temp Tapes on the inside skin surface of the exposed side.

Each panel carried an identifying number. The arrangement of panels in the frames is given in Figure B.3.

The actual burst point differed somewhat from the intended; however, the cosine of the angle between the lines from intended burst point and actual burst point to a frame in all cases exceeded 0.97. Slant ranges from actual burst point to the frames were as follows:

Station 1 (Frame 1) - 7150 ft
Station 2 (Frame 2) - 5330 ft
Station 3 (Frame 3) - 3800 ft

The AD airplane elevator sections were located at Stations 1 and 2.

After exposure tensile test specimens (Figure B.4) were cut from the panels and elevator sections and yield and ultimate strength data measured.

Locations and numbering of the elevator tensile specimens and Temp Tapes are given on Figure B.51. Specimens were taken in pairs from directly opposite sides of the section, one from the exposed and one from the unexposed side. An "E" is added to the identifying number for the specimen taken from the exposed side.

B.4 INSTRUMENTATION

B.4.1 Temperature Indicators

Peak temperatures reached by the sheet metal surfaces of the test specimens were recorded by Temp Tapes. These devices were developed by the University of Dayton under contract with the Wright Air Development Center. They consist of a fiberglas fabric coated on one side with a pressure sensitive adhesive to which are attached an array of 24 temperature sensitive discs each approximately 1/8 in. in diameter. The discs are of two types, the four to indicate the highest temperatures are thin low-melting-point metals, the melting of which indicates that certain temperatures have been exceeded. The other sensitive discs are of the material developed by the Quartermaster Research Laboratories (see ref(19)). They consist of a black absorbent paper base coated with white organic compounds of suitable melting points. When the coated surface of the paper reaches the melting point of the coating, the coating melts and is absorbed by the paper making the surface appear darker. Figure B.11 shows the adhesive coated side of a Temp Tape and the temperature indicating discs. The Temp Tapes are fastened by means of the pressure sensitive adhesive to the desired surface. Calibrations made by the Naval Materials Laboratory were employed in interpreting the Temp Tape data. The highest temperature indicated on the Temp Tape is 640°F. Peak temperature indicated was generally taken as the average between the highest positive melting temperature indicated and the lowest positive non-melting temperature indicated. Several of the indicator discs which were found to be unreliable were neglected in reading the data.

B.4.2 Thermal Energy Indicators

The thermal energy indicators consisted of mounted cotton and

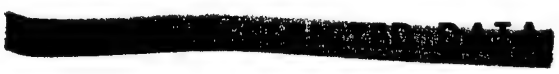

wool fabrics and maple-wood blocks. The degree of destruction or charring of the material when compared to the degree of charring under known conditions of irradiation provided an indication of the amount of radiant energy to which the indicators were exposed. The materials were provided by the Naval Materials Laboratory which also evaluated the resulting data.

B.5 RESULTS

Test data on the panels are presented in Tables B.1, B.2 and B.3. Ultimate and yield strength of unexposed test specimens taken from the same 24ST aluminum alloy sheets from which the exposed panels were fabricated are presented in Table B.4. Photographs of the panels in the three frames after the test exposure are shown in Figures B.12, B.13 and B.14. Individual photographs of the 35 panels after the test exposure are shown in Figures B.15 to B.49, inclusive. As shown in the photographs, some of the specimens were distorted or damaged as a result of their striking the back of the mounting cage at time of shock arrival.

Test results on the type AD airplane elevator sections are presented in Tables B.5 and B.6. Photographs of both the exposed and unexposed sides of the individual elevator sections are shown in Figures B.52 to B.67, inclusive. Data for the equivalent absorptivity coefficient against peak temperature attained for each type of surface are presented in Figures B.68 to B.71. Data for the equivalent thermal absorptivity coefficient vs panel thickness for sea blue lacquered surfaces are plotted in Figure B.72.

Radiant energy at the three stations are presented in Table B.7. Values are given as indicated by the passive indicators mounted on the frames. In addition values extrapolated from measurements made by the Naval Materials Laboratory along the line of test frames utilizing metal foils are presented. The Naval Materials Laboratory data were used for the computations in this report as they were considered to represent more accurately the conditions at the various panel stations. In the case of Station 3 no value was available from the frame indicators.

The scatter in the thermal data obtained (Figures B.68, B.69, B.70, B.71, and B.72) obscures many of the trends which would probably otherwise be more distinct. Two such relationships are the expected increase in equivalent absorptivity coefficient with increasing sheet metal thickness and with declining total thermal energy. For the sea blue lacquered panels sufficient data exist to permit plotting the data by stations to demonstrate the trend (Figure B.72). A larger number of panels and temperature indicators having a more closely spaced set of temperature indications would have afforded more satisfactory data. Some uncertainty exists as to the rapidity of response of the temperature indicators, any lags in response would tend to make the peak temperature readings somewhat lower than the true peak for short temperature pulses.

In frame 1, panels 8 and 10, although of the same gage metal and having similar coatings, experienced markedly different peak temperatures, the plate closer to ground reaching the higher temperature. An explanation for this behavior is not presently available.

B.6 CONCLUSIONS

Based on test results, the following conclusions are made:

a. As indicated in Figures B.68 through B.71, the limited data obtained show considerable scatter and accurate determination of the values of equivalent thermal absorptivity coefficients cannot be made. Since deterioration of the lacquer surface has occurred in some of the panels due to charring or flaming or the presence of a dust film prior to thermal exposure, the coefficients obtained in these cases may not be representative of the original type surface.

b. The expected increase of equivalent thermal absorptivity coefficient with increasing panel thickness and decreasing thermal irradiation is indicated by the set of data plotted on Figure B.72.

c. As indicated in Tables B.1 through B.4, tests conducted on exposed and unexposed specimens of the 24ST panel material show, in general, only a slight reduction in strength properties due to the heating cycle. In a few cases melting of the panels has occurred as shown in Figures B.39 and B.42.

B.7 RECOMMENDATIONS

It is recommended that:

a. Further measurements and associated analytic studies be made to obtain a detailed quantitative picture of the factors influencing the peak temperature rise in coated thin metal panels.

b. Where practicable in future field test programs, attempts be madeto obtain temperature-time histories on similar test panels.

c. Attempts be made to improve the existing Temp Tape type of device to provide more reliable indicators in place of those which have proven unsatisfactory, with a possible increase in both temperature range and number of temperature indications, such instrumentation to be used where a large number of points are to be instrumented with minimum effort or where time-history recording equipment cannot be employed.

d. That data be obtained to permit the dynamic error in peak temperature data obtained from Temp Tapes to be evaluated.

[redacted]

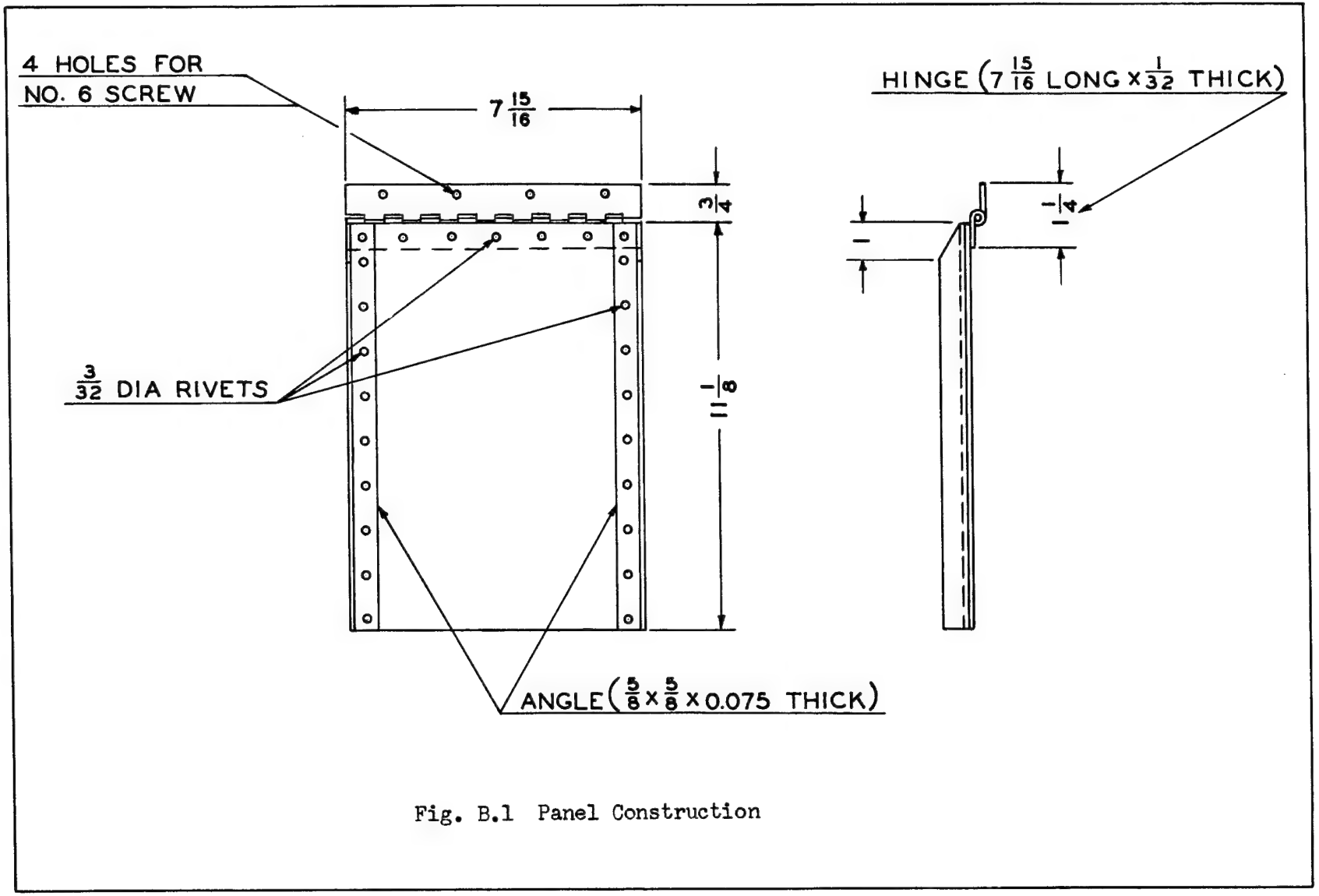

Fig. B.1 Panel Construction

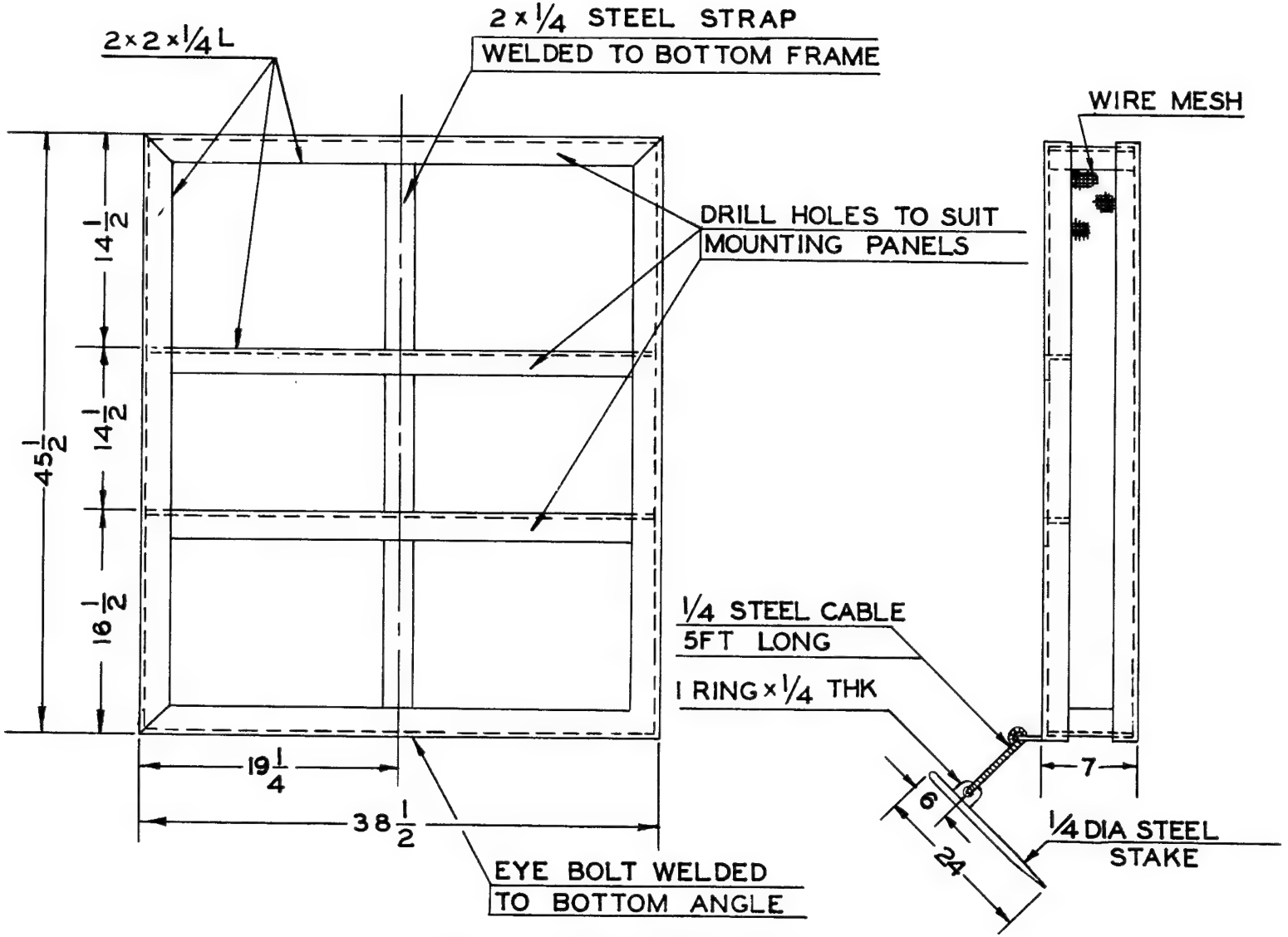

Fig. B.2 Frame Construction

PANEL-10 SEA BLUE LACQUER 0.016 IN.	PANEL-3 WHITE LACQUER 0.012 IN.	PANEL-2 ALUMINIZED LACQUER 0.012 IN.	PANEL-1 BARE METAL 0.012 IN.
PANEL-17 SEA BLUE 0.020 IN.	PANEL-15 WHITE 0.020 IN.	PANEL-13 ALUMINIZED 0.020 IN.	PANEL-11 BARE 0.020 IN.
PANEL-23 SEA BLUE 0.025 IN.	PANEL-26 SEA BLUE 0.032 IN.	PANEL-34 SEA BLUE 0.051 IN.	PANEL-8 SEA BLUE 0.016 IN.

FRAME NO.1

PANEL-9 SEA BLUE 0.016 IN.	PANEL-7 WHITE 0.016 IN.	PANEL-6 ALUMINIZED 0.016 IN.	PANEL-5 BARE 0.016 IN.
PANEL-24 SEA BLUE 0.025 IN.	PANEL-22 WHITE 0.025 IN.	PANEL-21 ALUMINIZED 0.025 IN.	PANEL-20 BARE 0.025 IN.
PANEL-18 SEA BLUE 0.020 IN.	PANEL-27 SEA BLUE 0.032 IN.	PANEL-29 SEA BLUE 0.040 IN.	PANEL-35 SEA BLUE 0.051 IN.

FRAME NO.2

PANEL-19 SEA BLUE 0.020 IN.	PANEL-16 WHITE 0.020 IN.	PANEL-14 ALUMINIZED 0.020 IN.	PANEL-12 BARE 0.020 IN.
PANEL-36 SEA BLUE 0.051 IN.	PANEL-33 WHITE 0.051 IN.	PANEL-32 ALUMINIZED 0.051 IN.	PANEL-31 BARE 0.051 IN.
———	PANEL-25 SEA BLUE 0.025 IN.	PANEL-28 SEA BLUE 0.032 IN.	PANEL-30 SEA BLUE 0.040 IN.

FRAME NO.3

Fig. B.3 Arrangement of Panels in Frames

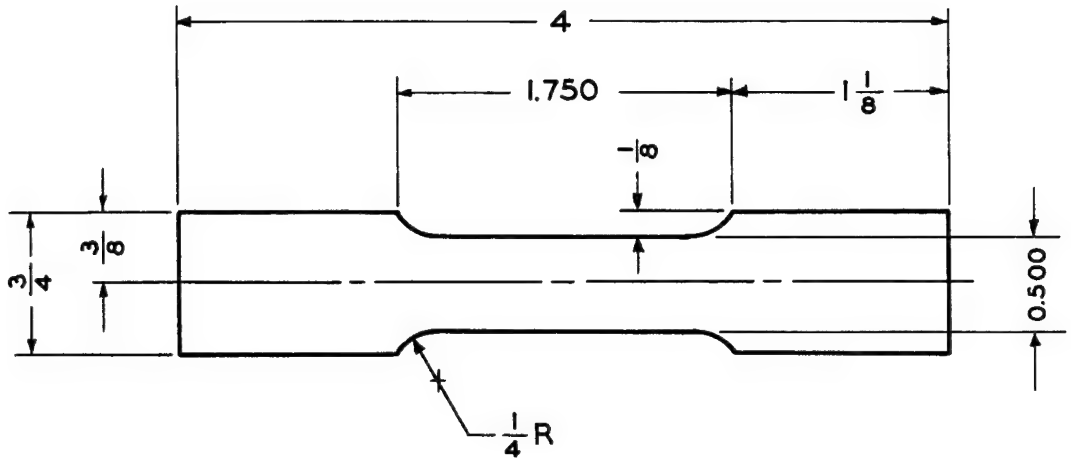

Fig. B.4 Tensile Test Specimen

Fig. B.5 Thermal Energy Indicator Strip before Exposure

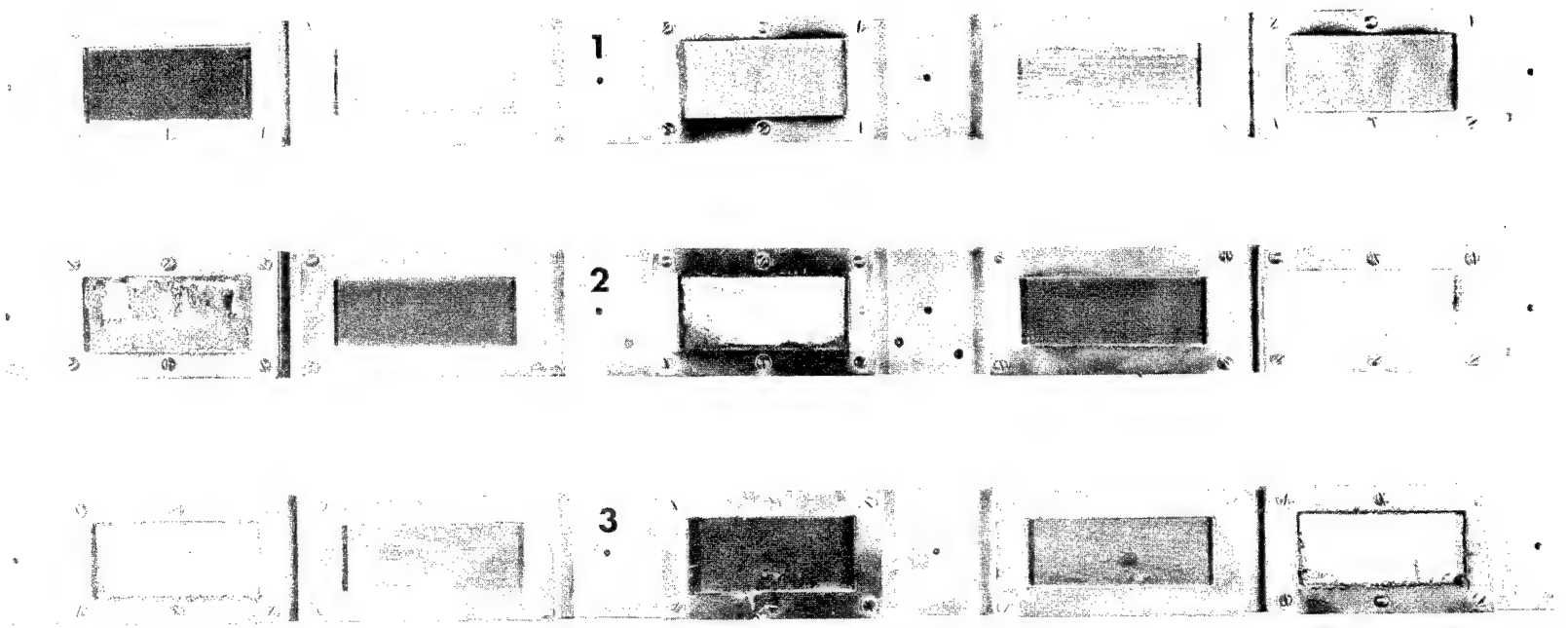

Fig. B.6 Thermal Energy Indicators after Exposure

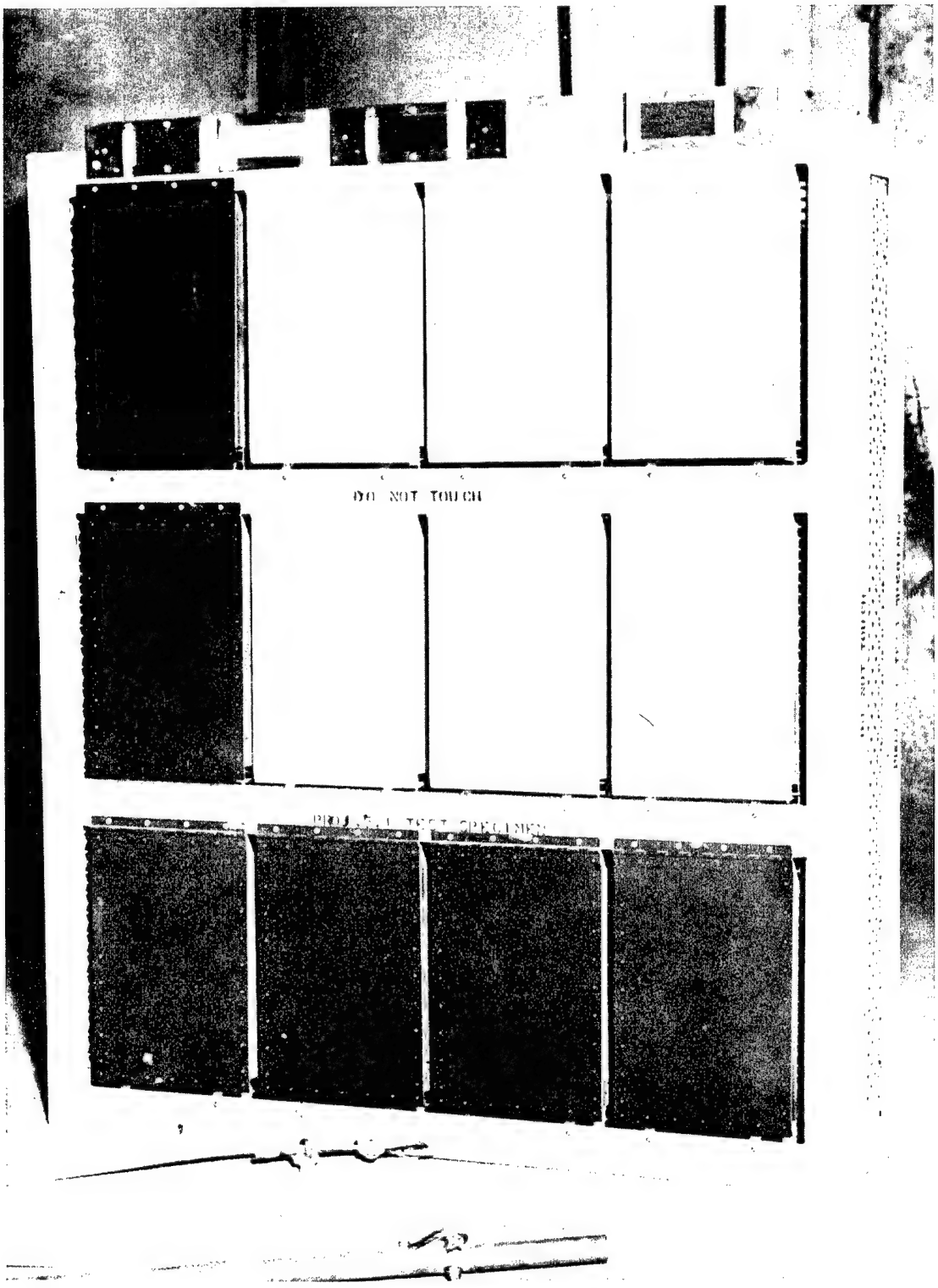

Fig. B.7 Frame with Mounted Panels and Thermal Energy Indicators

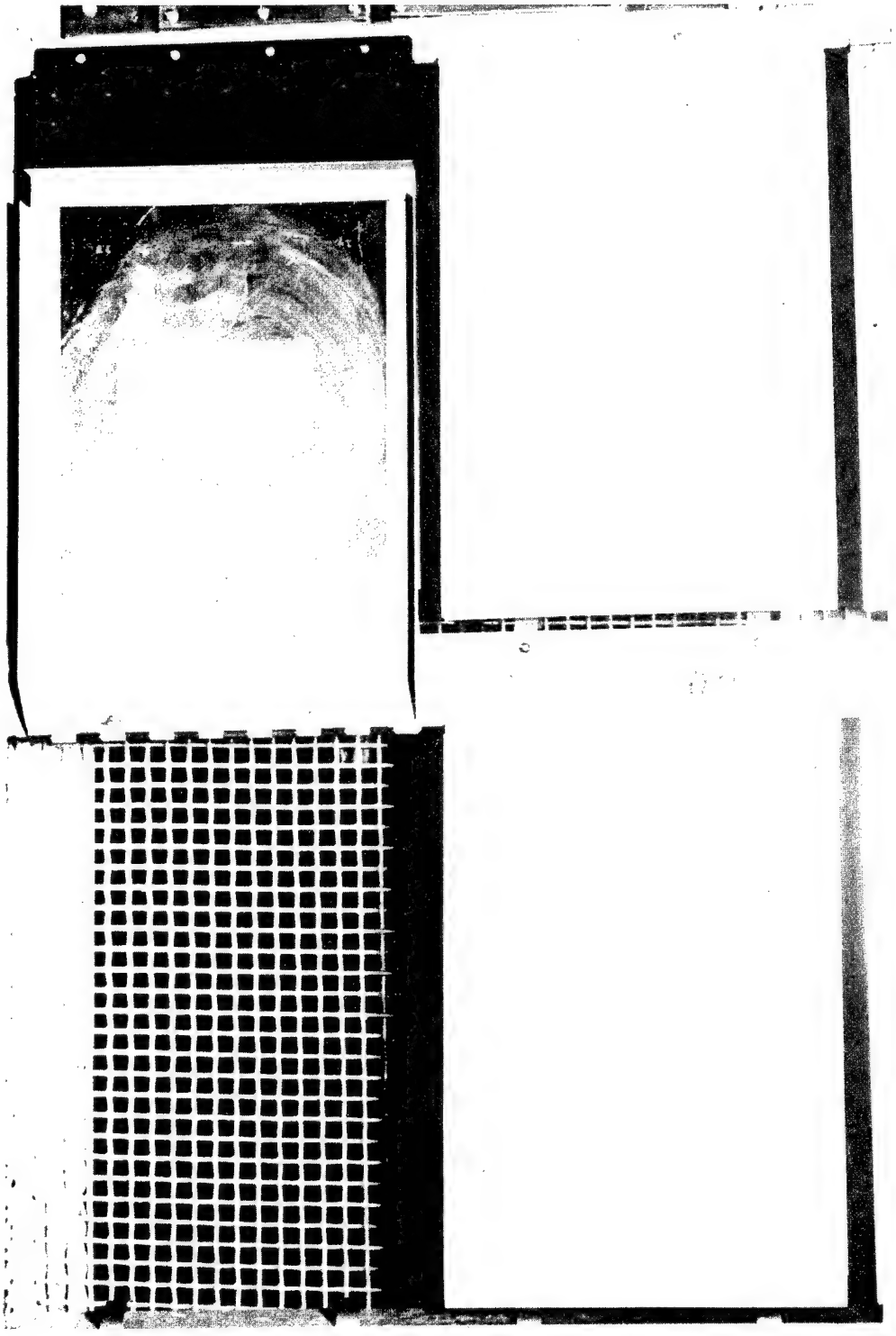

Fig. B.8 Mounted Panel Showing Temp Tape Installation

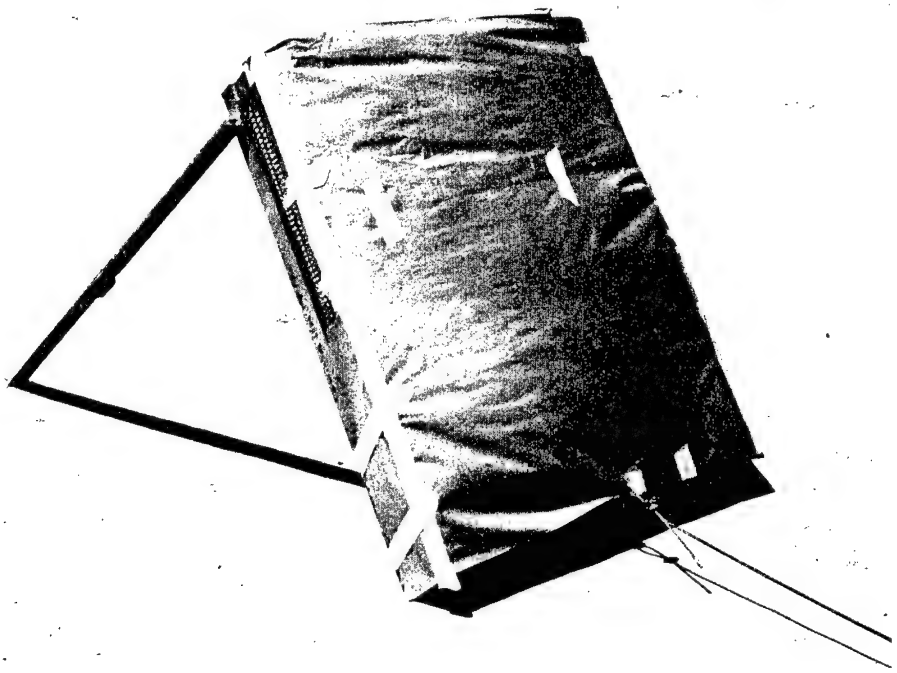

Fig. B.9 Frame with Temporary Protective Covering

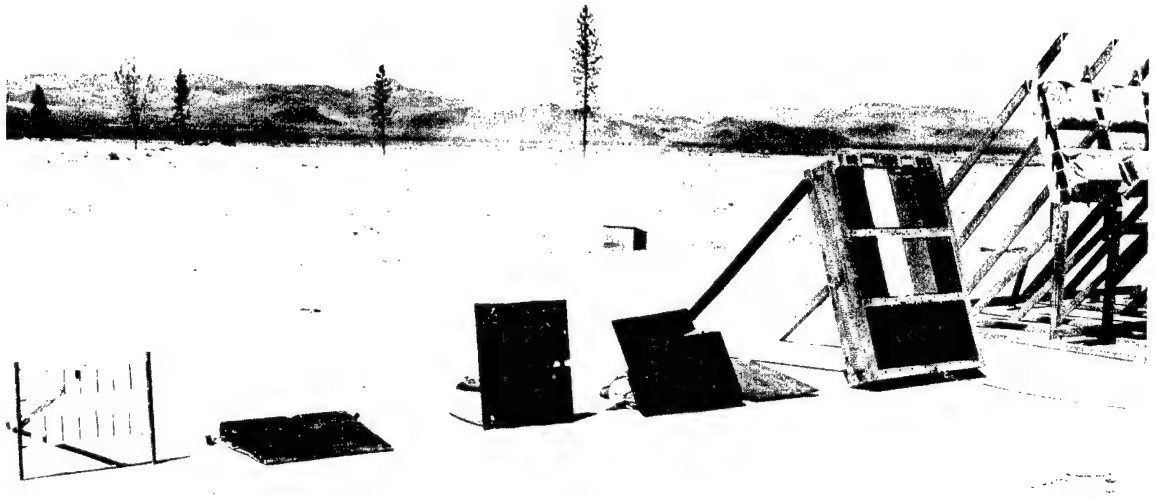

Fig. B.10 Frame at Test Site before Exposure

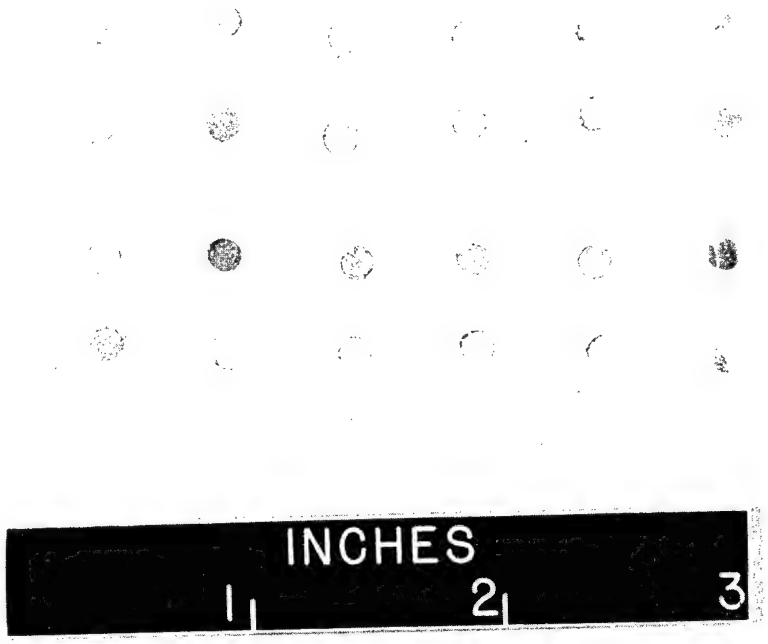

Fig. B.11 Temp Tape

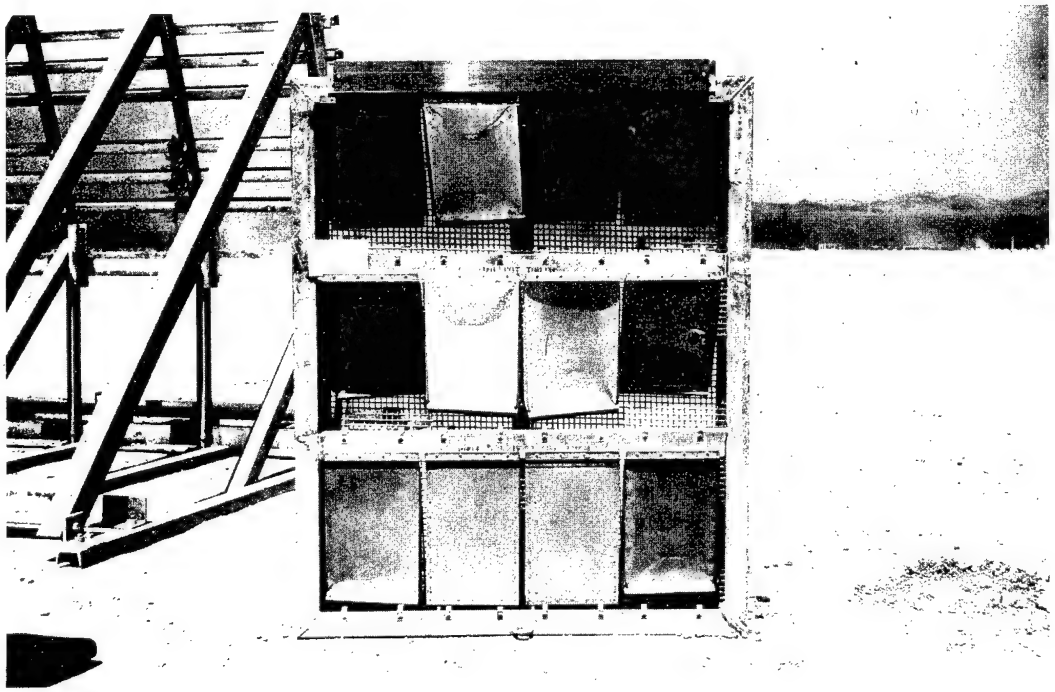

Fig. B.12 Frame No. 1 after Exposure - Slant Range 7150 ft, Thermal Energy 18.3 cal/cm^2

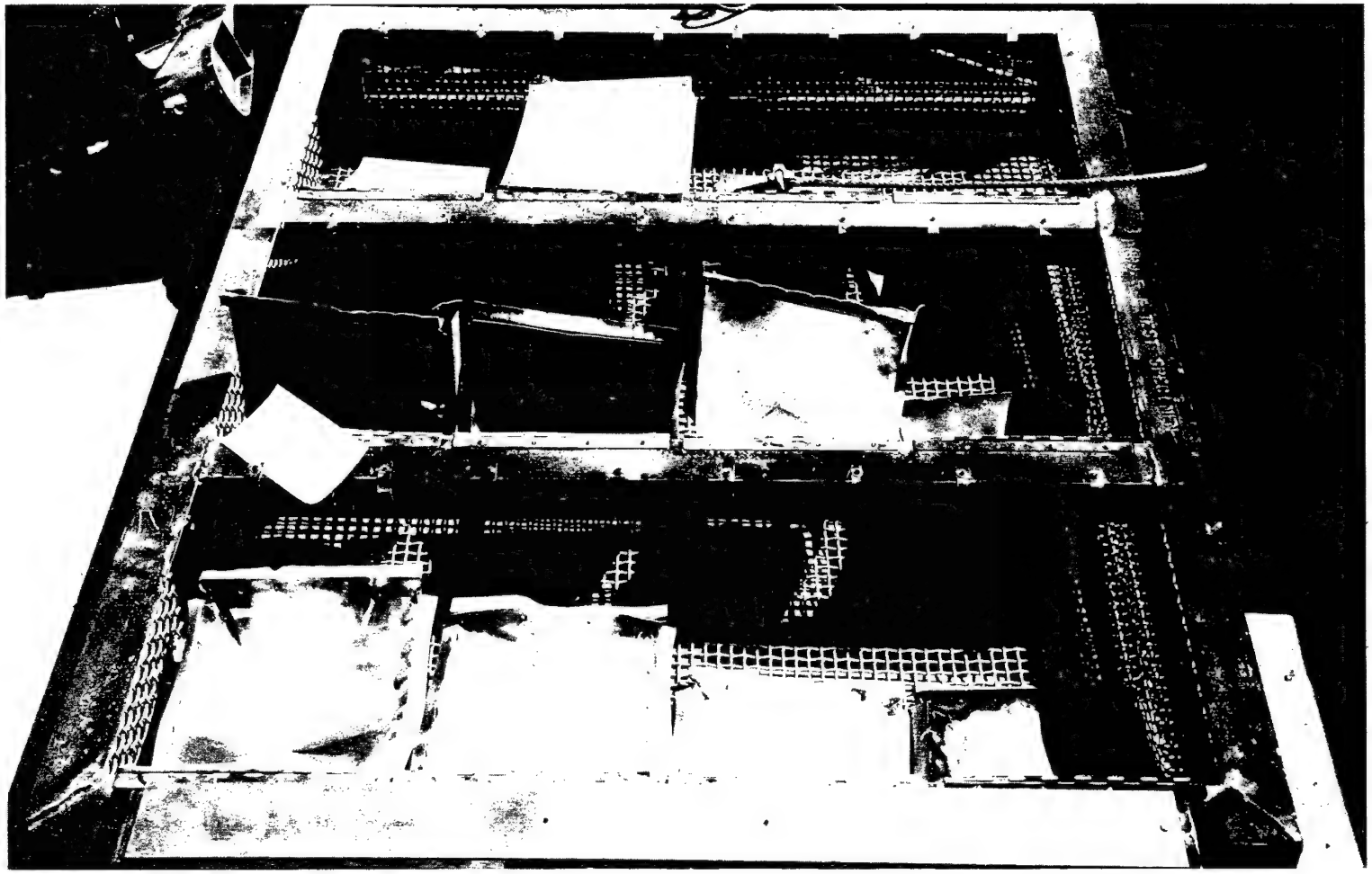

Fig. B.13 Frame Number 2 after Exposure - Slant Range 5330 Ft, Thermal Energy 30 cal/cm^2

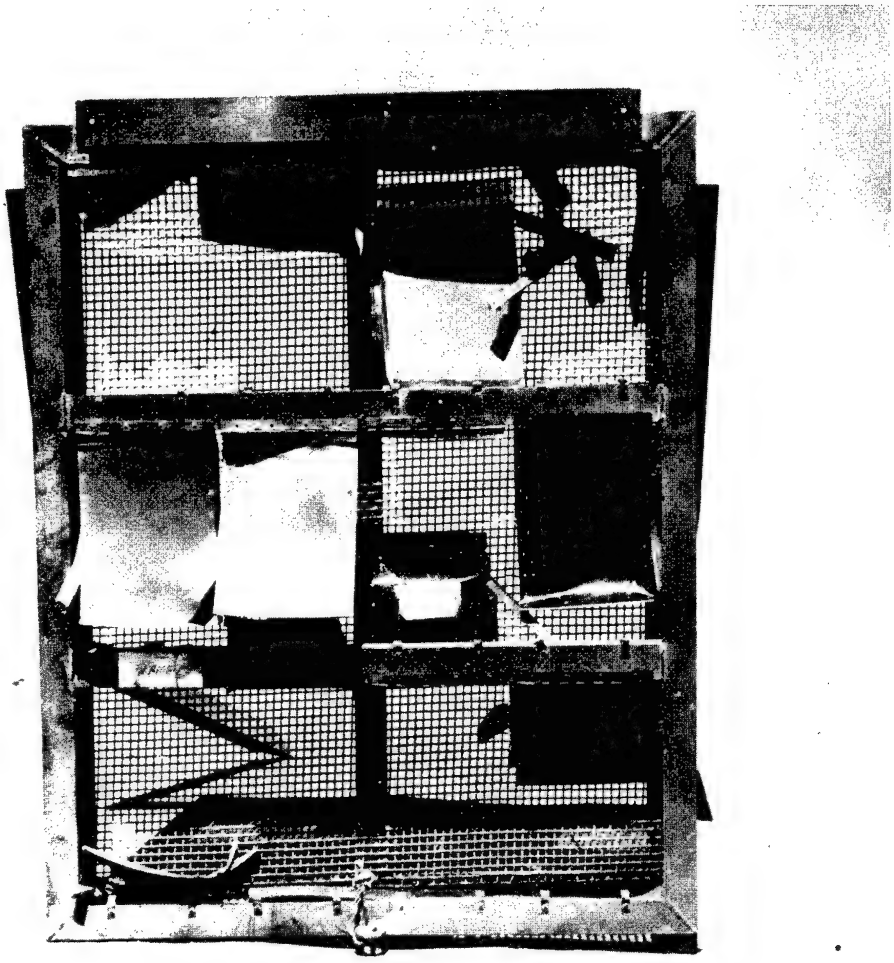

Fig. B.14 Frame Number 3 after Exposure - Slant Range 3800 Ft, Thermal Energy 43 cal/cm^2

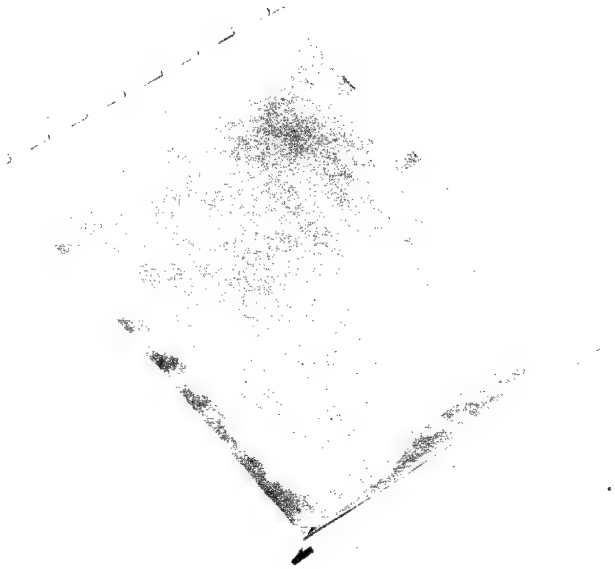

Fig. B.15 Panel 1 after Exposure - 0.012 In. Thick - Bare Metal - Station 1

Fig. B.16 Panel 2 after Exposure - 0.012 In. Thick - Aluminized Lacquer - Station 1

Fig. B.17 Panel 3 after Exposure - 0.012 In. Thick - White Lacquer - Station 1

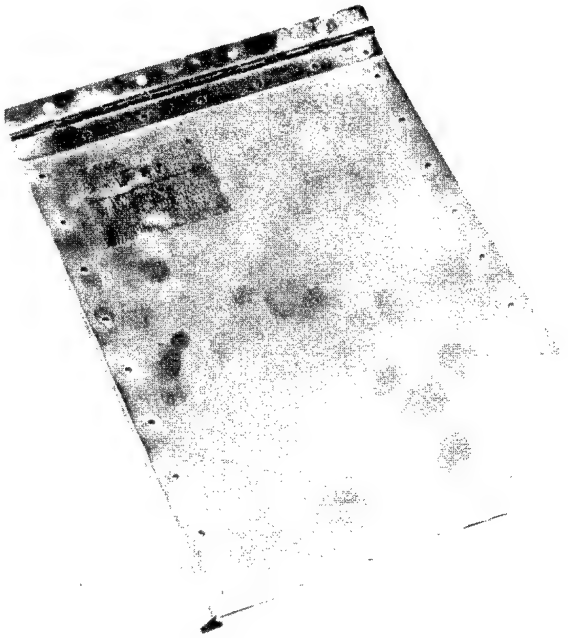

Fig. B.18 Panel 8 after Exposure - 0.016 In. Thick - Sea Blue Lacquer - Station 1

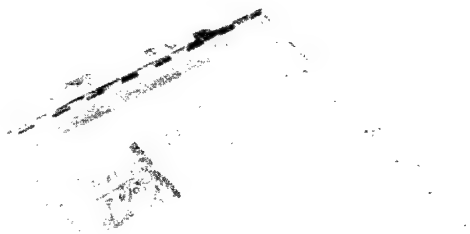

Fig. B.19 Panel 10 after Exposure - 0.016 In. Thick - Sea Blue Lacquer - Station 1

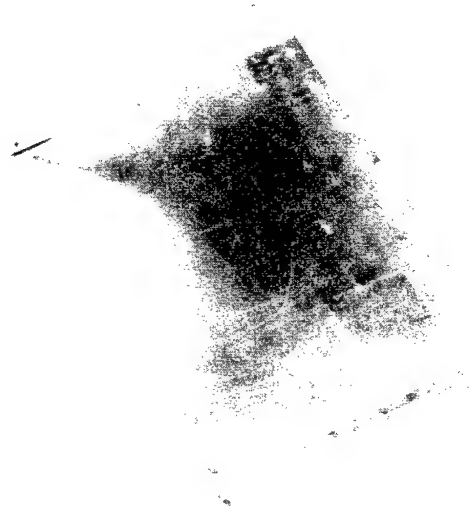

Fig. B.20 Panel 11 after Exposure - 0.020 In. Thick - Bare Metal - Station 1

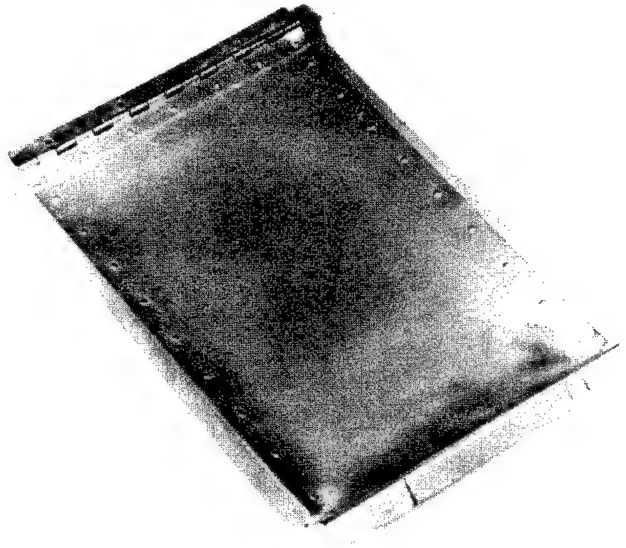

Fig. B.21 Panel 13 after Exposure - 0.020 In. Thick - Aluminized Lacquer - Station 1

Fig. B.22 Panel 15 after Exposure - 0.020 In. Thick - White Lacquer - Station 1

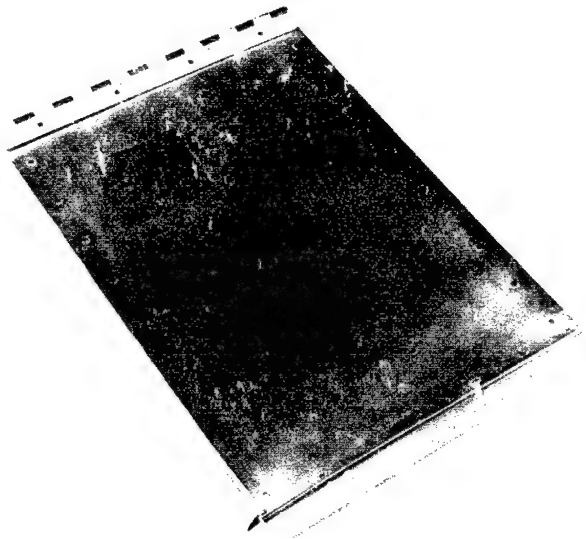

Fig. B.23 Panel 17 after Exposure - 0.020 In. Thick - Sea Blue Lacquer - Station 1

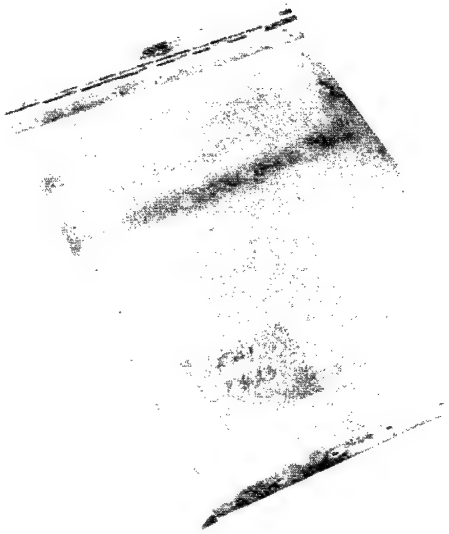

Fig. B.24 Panel 23 after Exposure - 0.025 In. Thick - Sea Blue Lacquer - Station 1

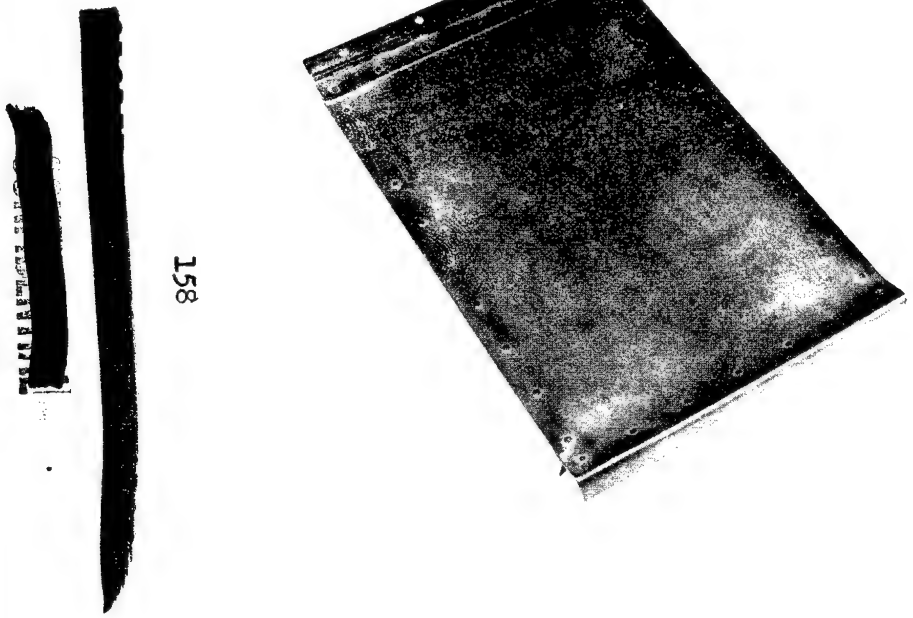

Fig. B.25 Panel 26 after Exposure - 0.032 In. Thick - Sea Blue Lacquer - Station 1

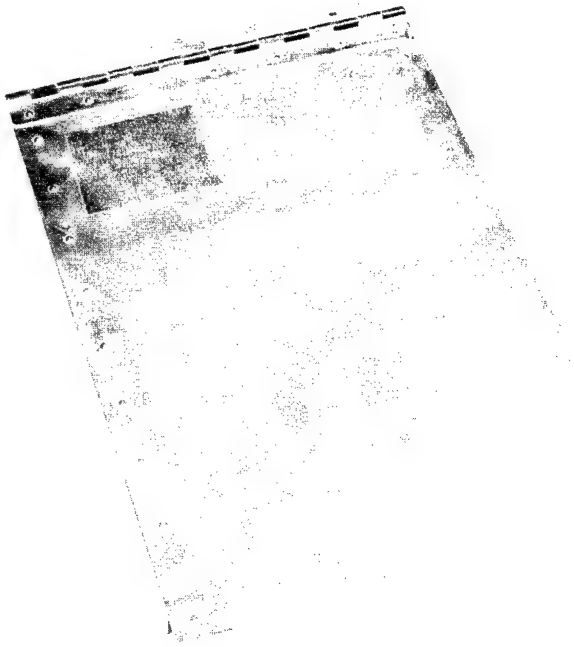

Fig. B.26 Panel 34 after Exposure - 0.051 In. Thick - Sea Blue Lacquer - Station 1

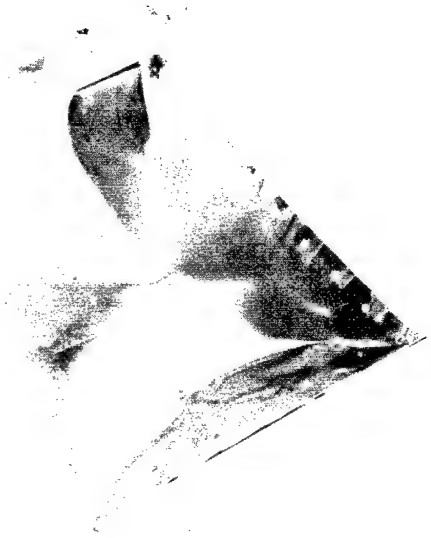

Fig. B.27 Panel 5 after Exposure - 0.016 In. Thick - Bare Metal - Station 2

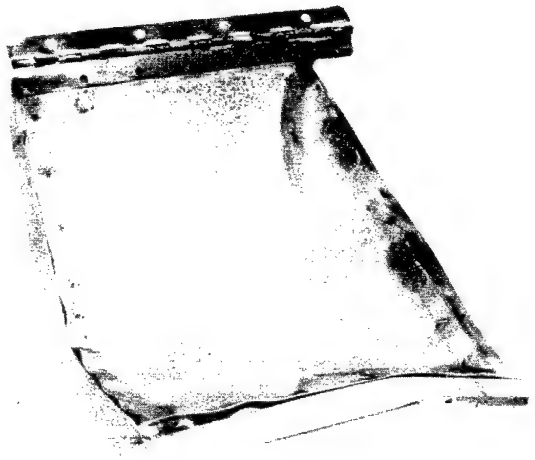

Fig. B.28 Panel 6 after Exposure - 0.016 In. Thick - Aluminized Lacquer - Station2

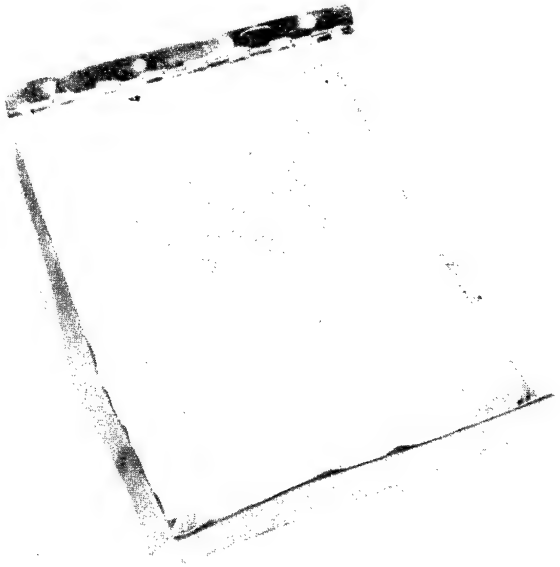

Fig. B.29 Panel 7 after Exposure - 0.016 In. Thick - White Lacquer - Station 2

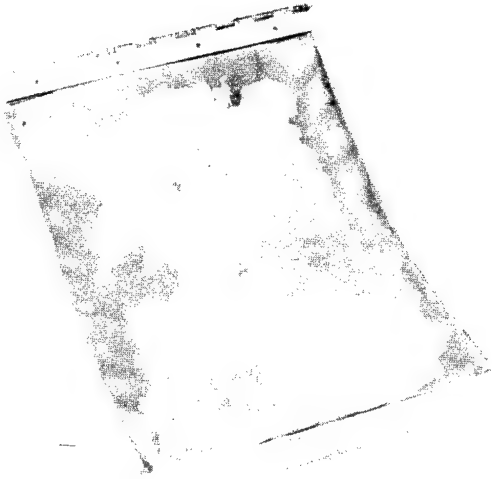

Fig. B.30 Panel 9 after Exposure - 0.016 In. Thick - Sea Blue Lacquer - Station 2

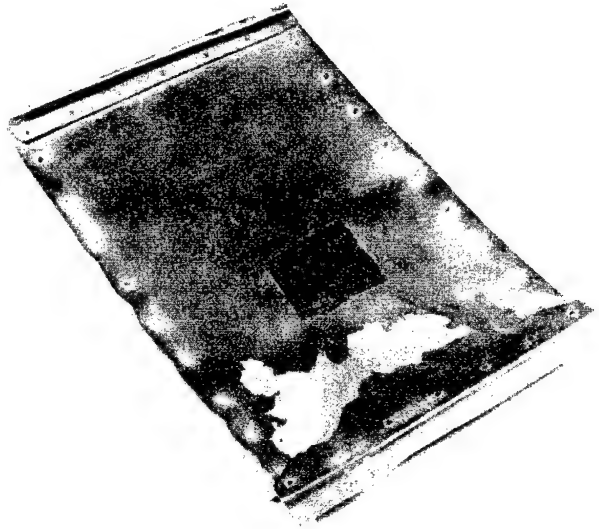

Fig. B.31 Panel 18 after Exposure - 0.020 In. Thick - Sea Blue Lacquer - Station 2

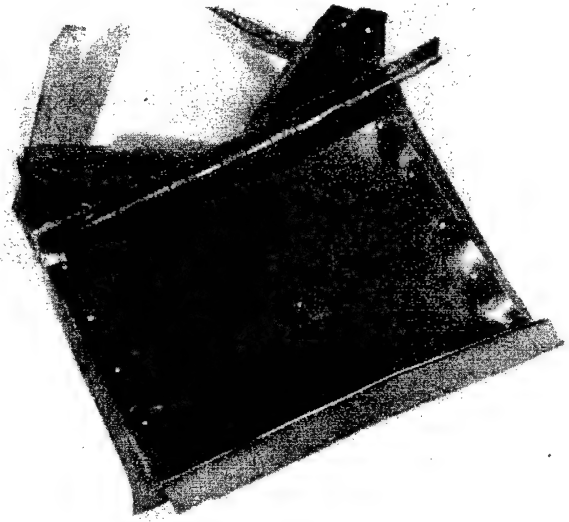

Fig. B.32 Panel 20 after Exposure - 0.025 In. Thick - Bare Metal - Station 2

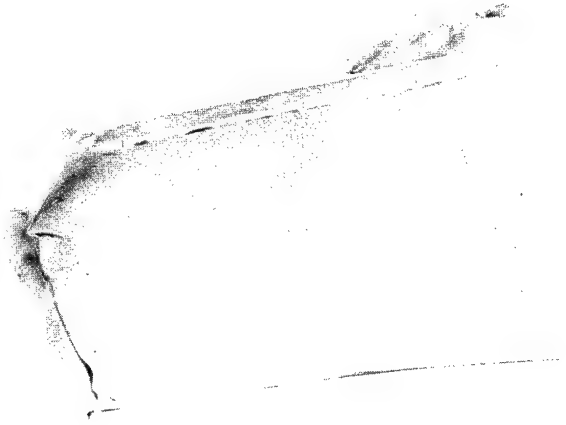

Fig. B.33 Panel 21 after Exposure - 0.025 In. Thick - Aluminized Lacquer - Station 2

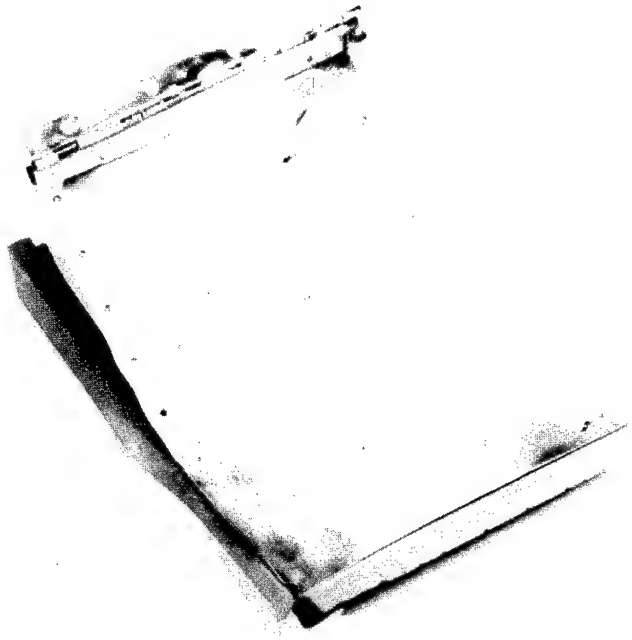

Fig. B.34 Panel 22 after Exposure - 0.025 In. Thick - White Lacquer - Station 2

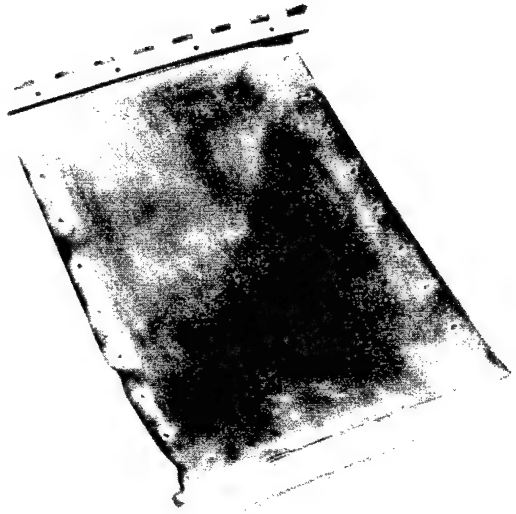

Fig. B.35 Panel 24 after Exposure - 0.025 In. Thick - Sea Blue Lacquer - Station 2

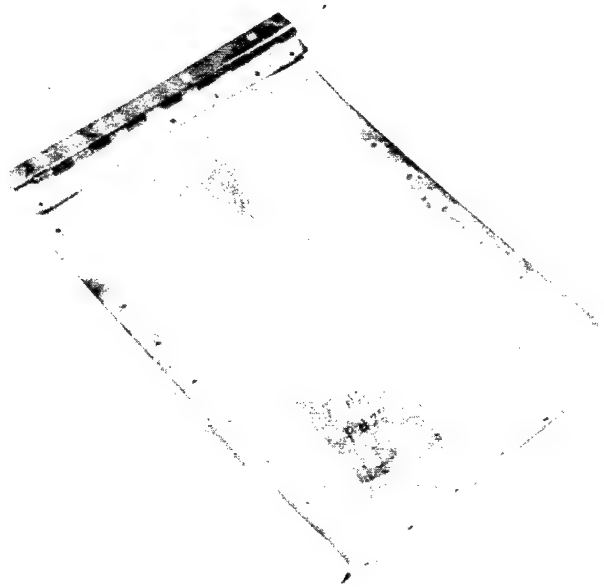

Fig. B.36 Panel 27 after Exposure - 0.032 In. Thick - Sea Blue Lacquer - Station 2

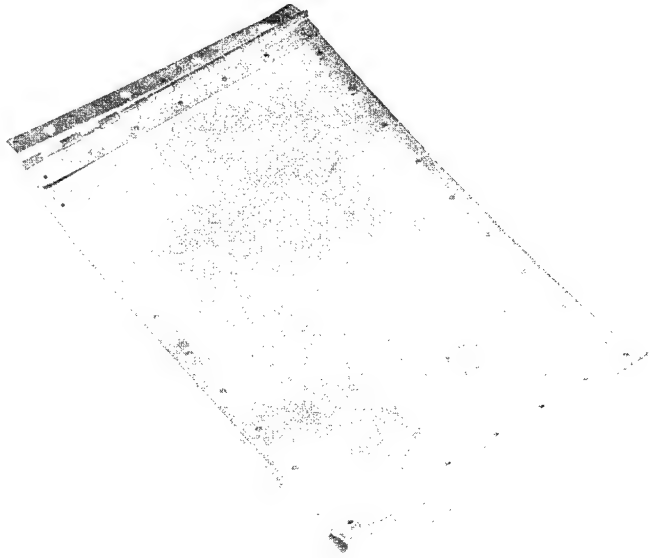

Fig. B.37 Panel 29 after Exposure - 0.040 In. Thick - Sea Blue Lacquer - Station 2

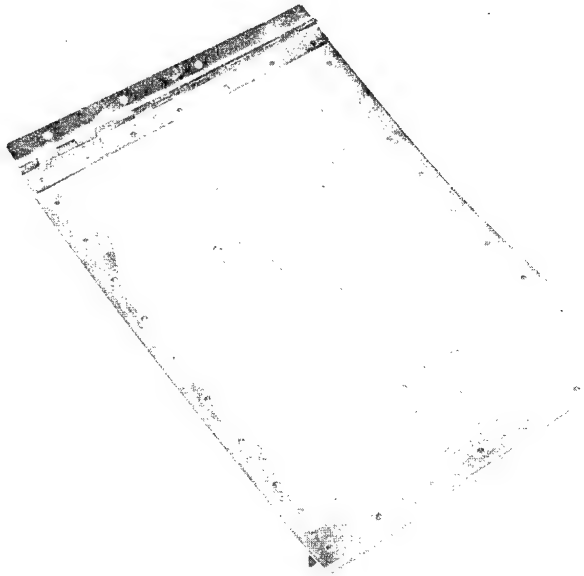

Fig. B.38 Panel 35 after Exposure - 0.051 In. Thick - Sea Blue Lacquer - Station 2

Fig. B.39 Panel 12 after Exposure - 0.020 In. Thick - Bare Metal - Station 3

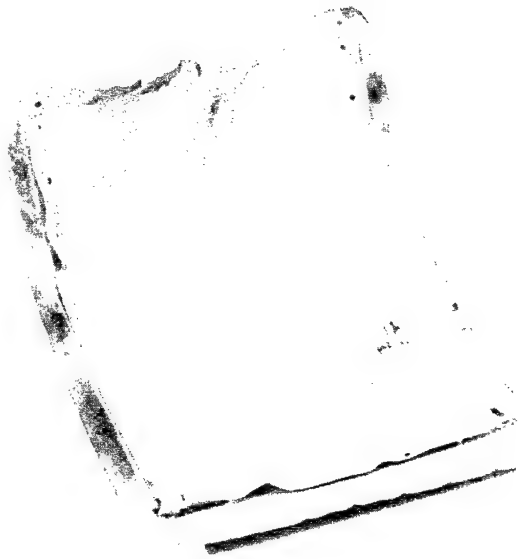

Fig. B.40 Panel 14 after Exposure - 0.020 In. Thick - Aluminized Lacquer - Station 3

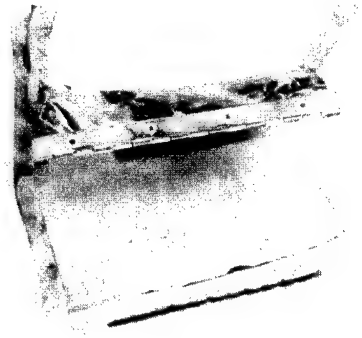

Fig. B.41 Panel 16 after Exposure - 0.020 In. Thick - White Lacquer - Station 3

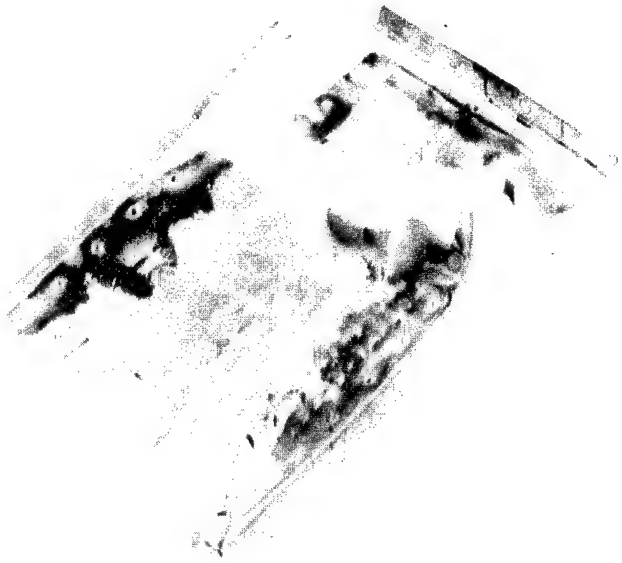

Fig. B.42 Panel 19 after Exposure - 0.020 In. Thick - Sea Blue Lacquer - Station 3

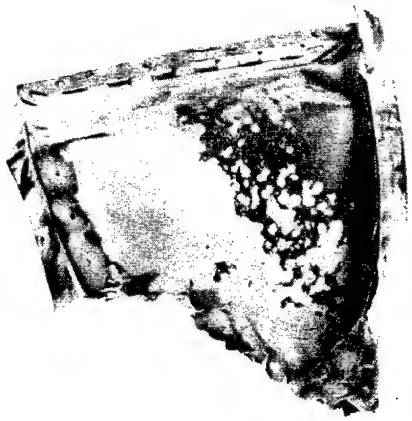

Fig. B.43 Panel 25 after Exposure - 0.025 In. Thick - Sea Blue Lacquer - Station 3

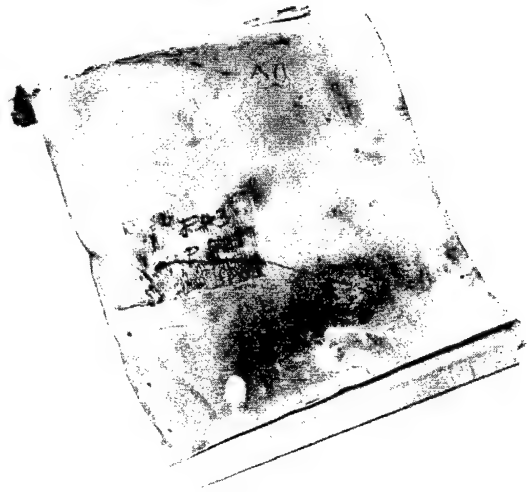

Fig. B.44 Panel 28 after Exposure - 0.032 In. Thick - Sea Blue Lacquer - Station 3

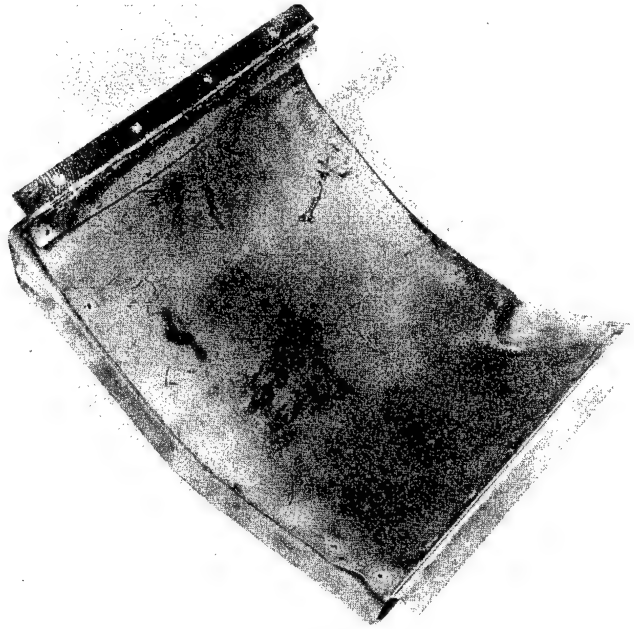

Fig. B.45 Panel 30 after Exposure - 0.040 In. Thick - Sea Blue Lacquer - Station 3

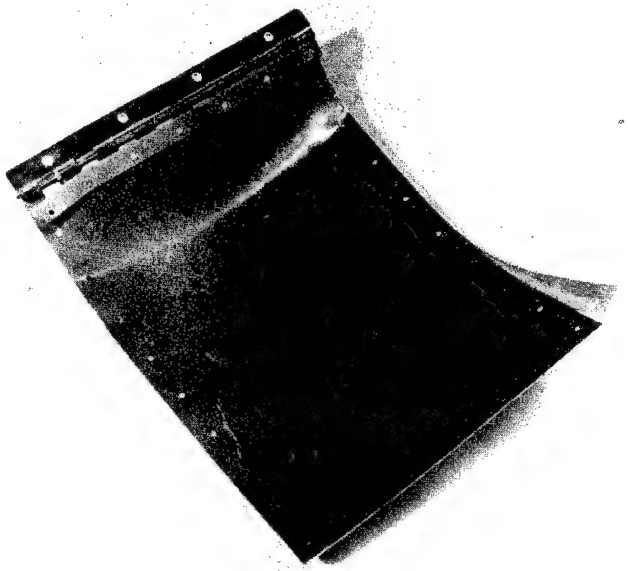

Fig. B.46 Panel 31 after Exposure - 0.051 In. Thick - Bare Metal - Station 3

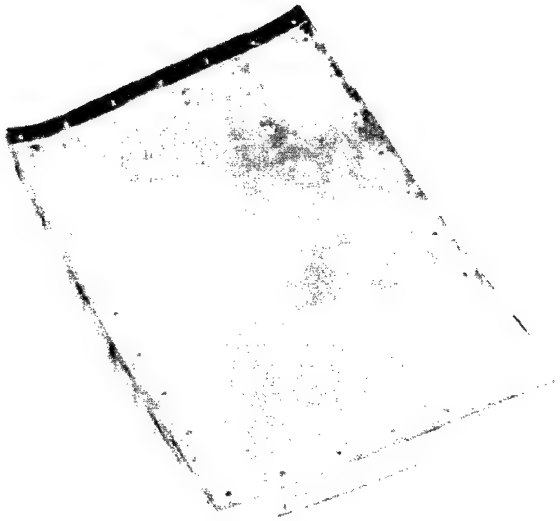

Fig. B.47 Panel 32 after Exposure - 0.051 In. Thick - Aluminized Lacquer - Station 3

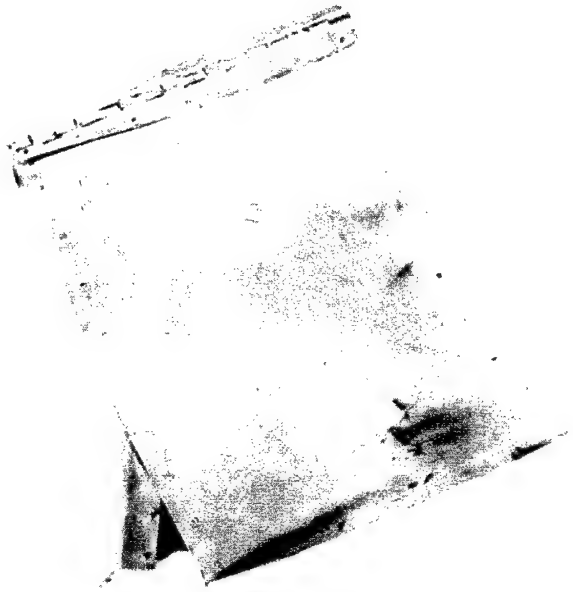

Fig. B.48 Panel 33 after Exposure - 0.051 In. Thick - White Lacquer - Station 3

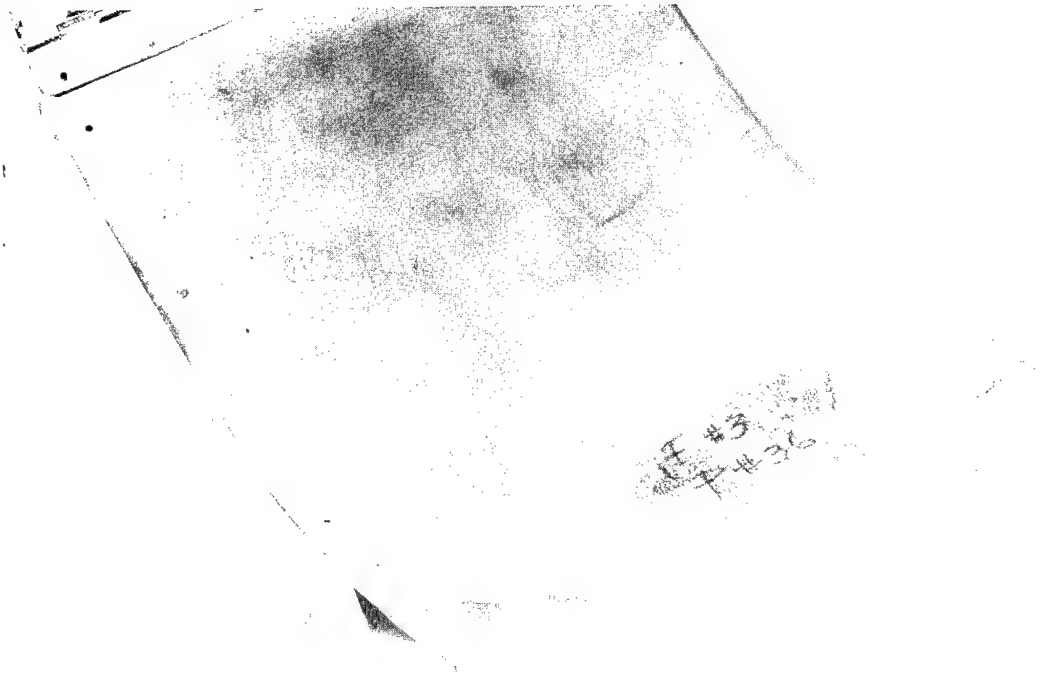

Fig. B.49 Panel 36 after Exposure - 0.051 In. Thick - Sea Blue Lacquer - Station 3

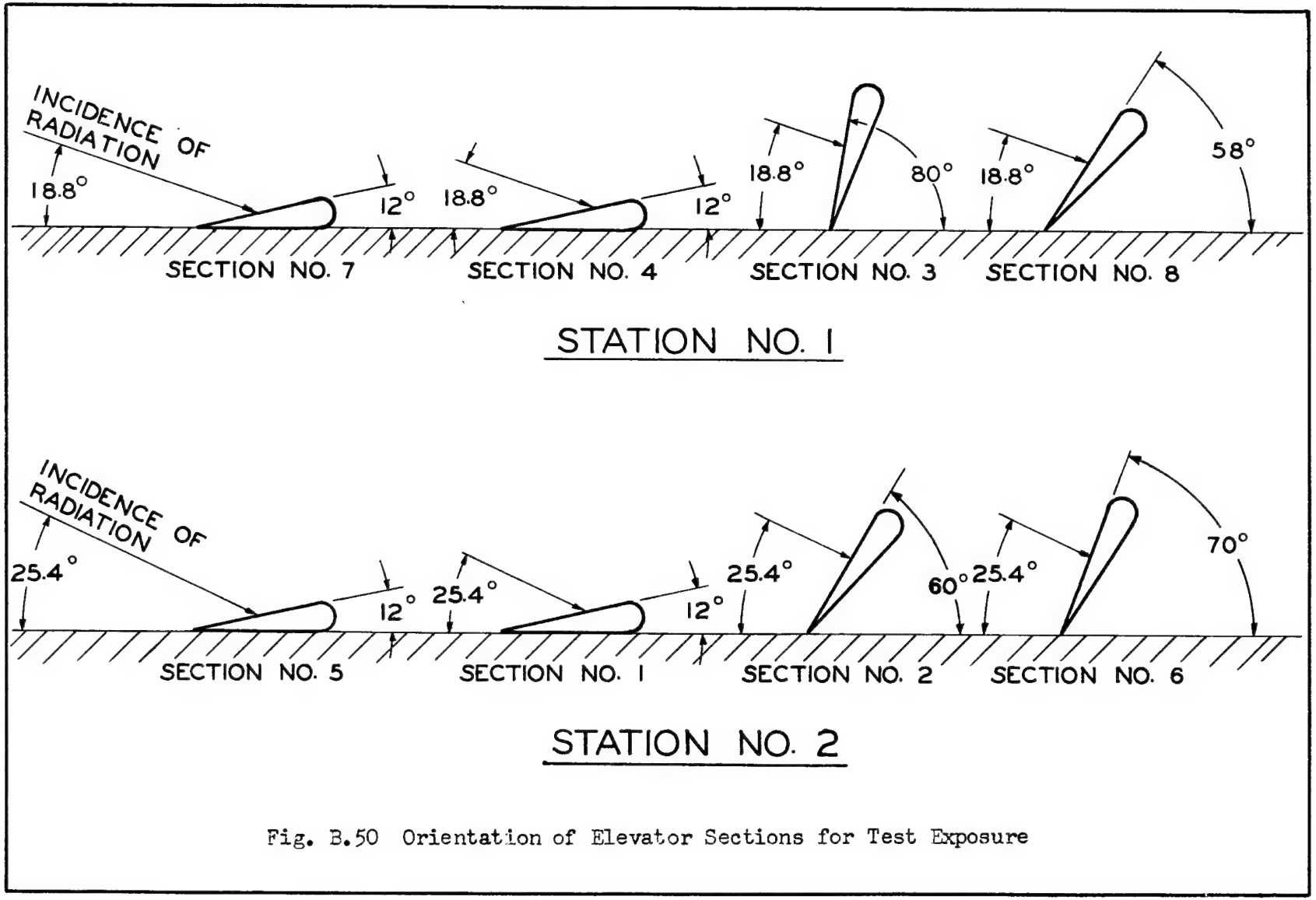

Fig. B.50 Orientation of Elevator Sections for Test Exposure

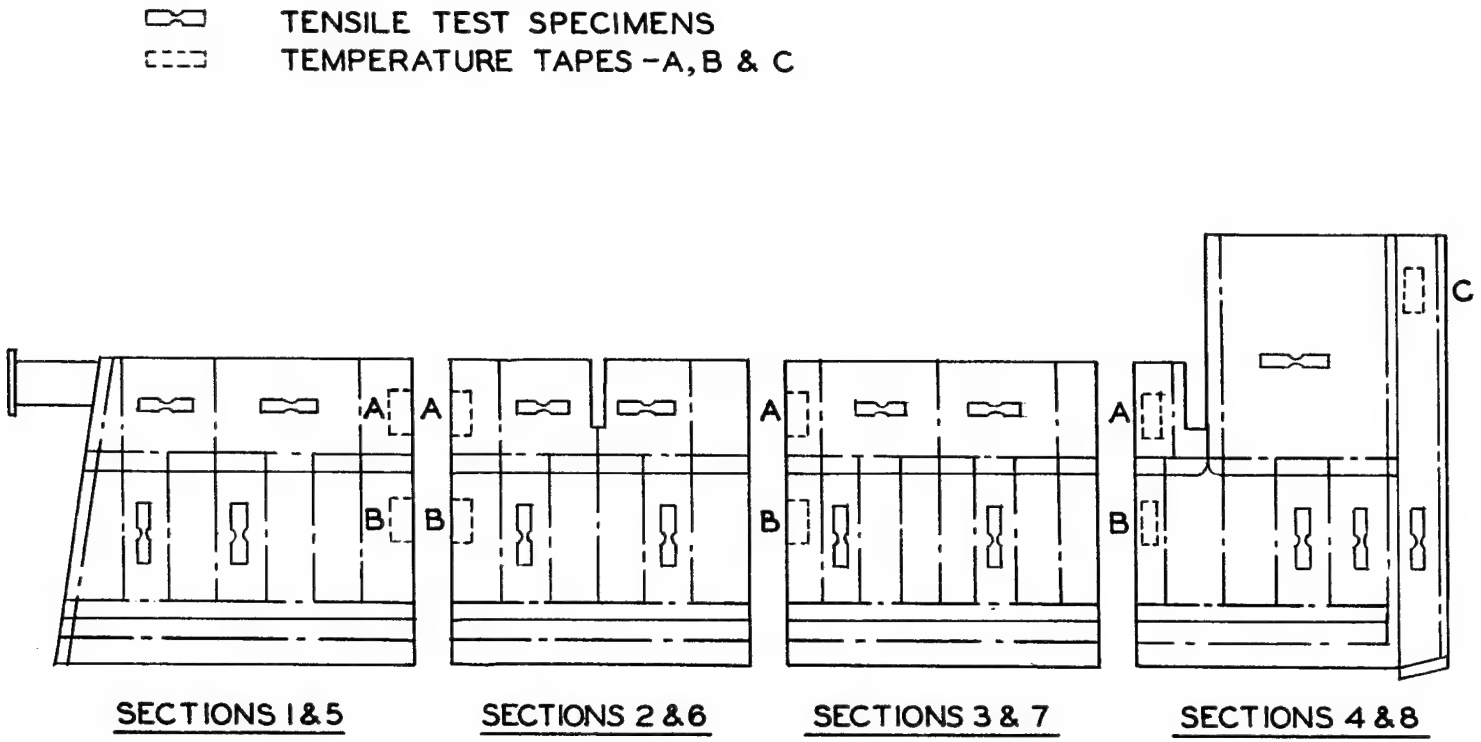

Fig. B.51 Elevator Sections Showing Locations of Test Specimens and Temp Tapes

Fig. B.52 Elevator Section 1 - Exposed Side - Station 2

Fig. B.53 Elevator Section 1 - Unexposed Side - Station 2

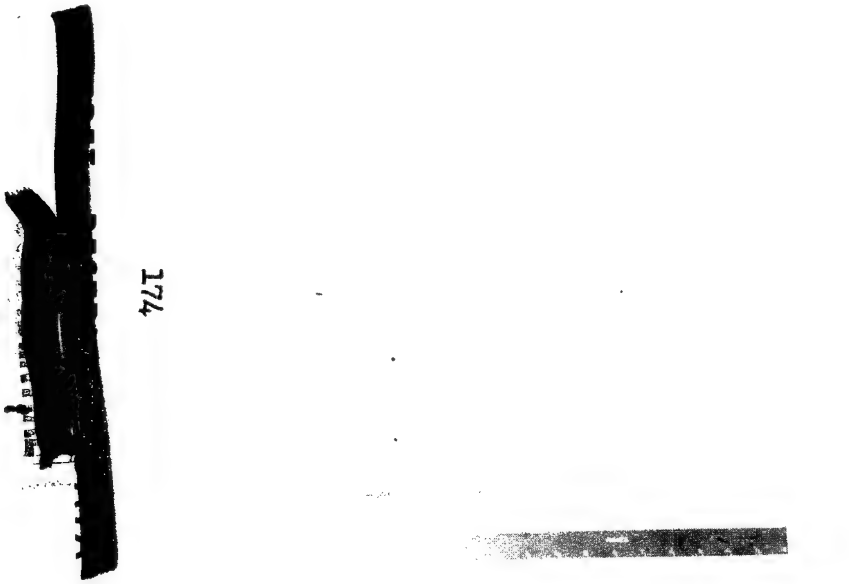

Fig. B.54 Elevator Section 2 - Exposed Side - Station 2

Fig. B.55 Elevator Section 2 - Unexposed Side - Station 2

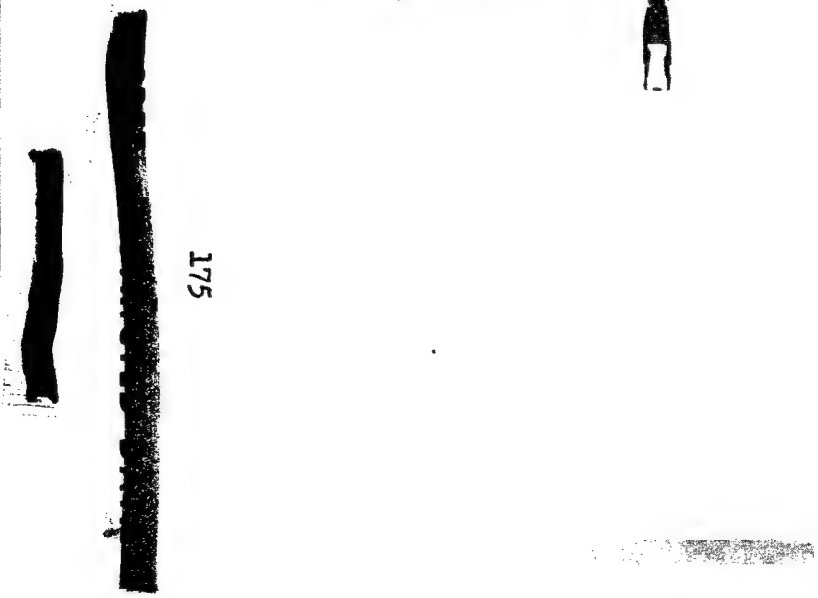

Fig. B.56 Elevator Section 3 - Exposed Side - Station 1

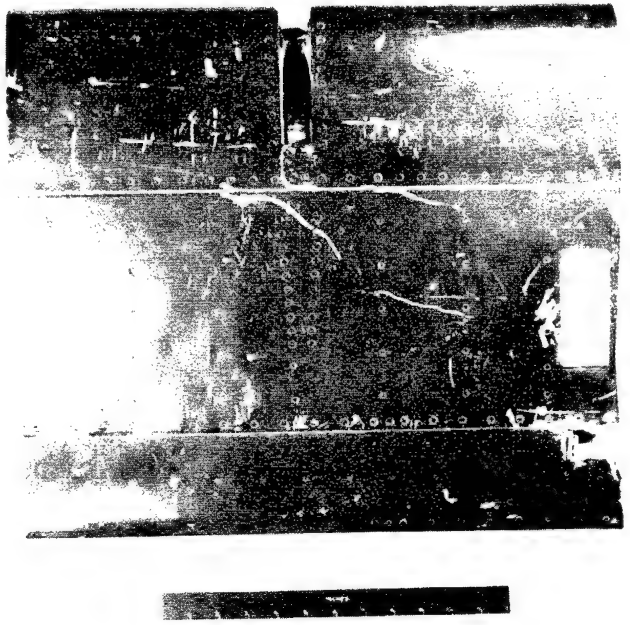

Fig. B.57 Elevator Section 3 - Unexposed Side - Station 1

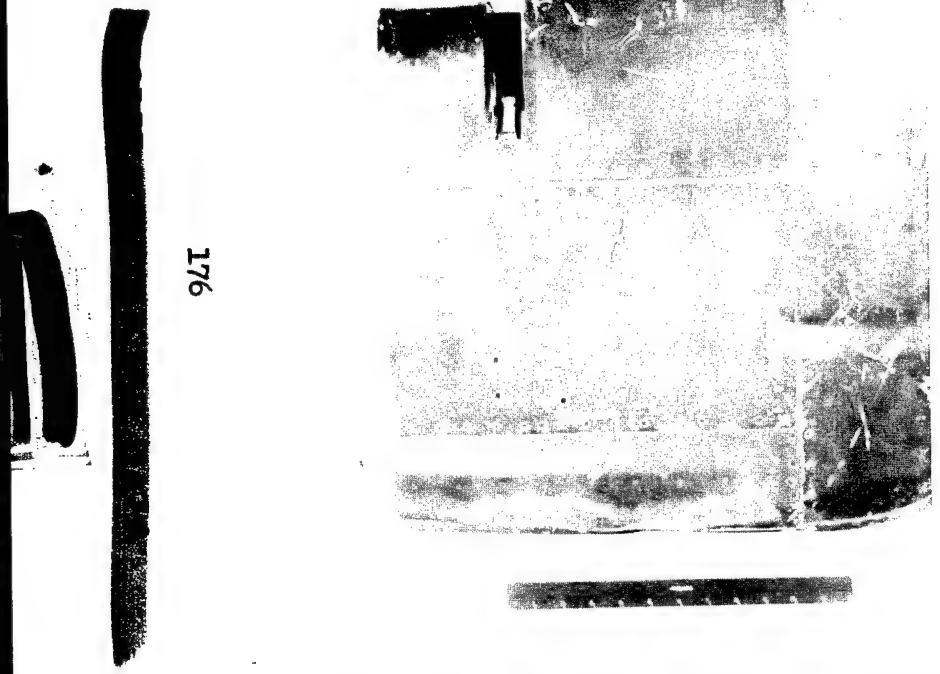

Fig. B.58 Elevator Section 4 - Exposed Side - Station 1

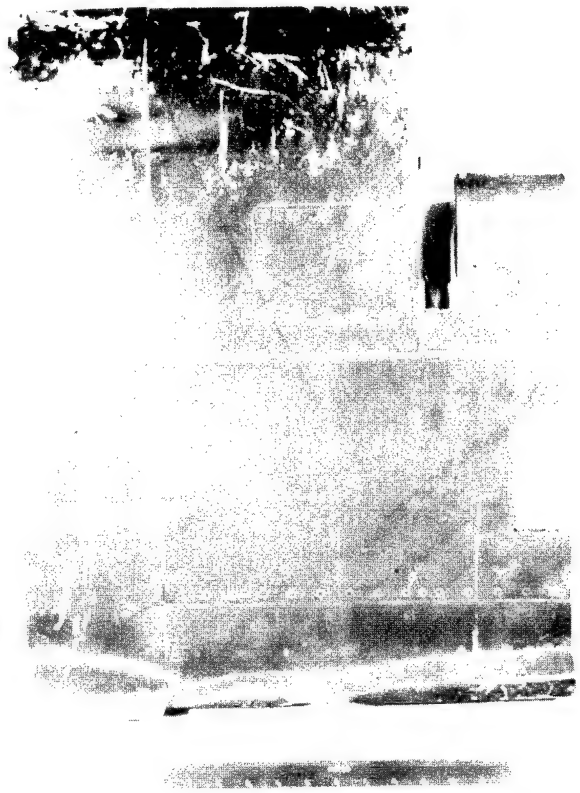

Fig. B.59 Elevator Section 4 - Unexposed Side - Station 1

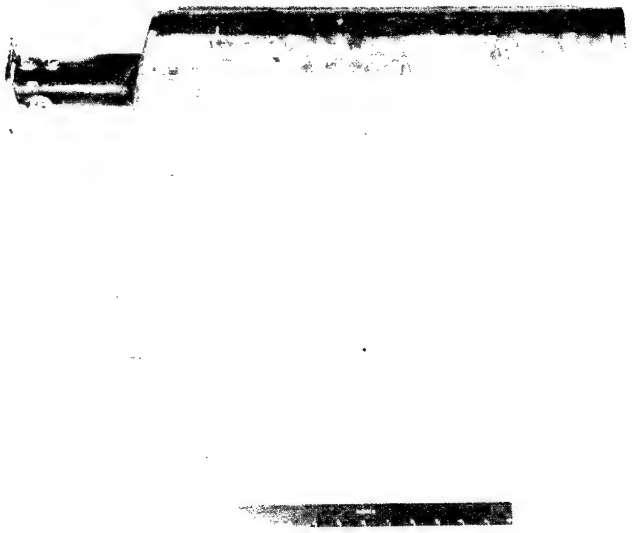

Fig. B.60 Elevator Section 5 - Exposed Side - Station 2

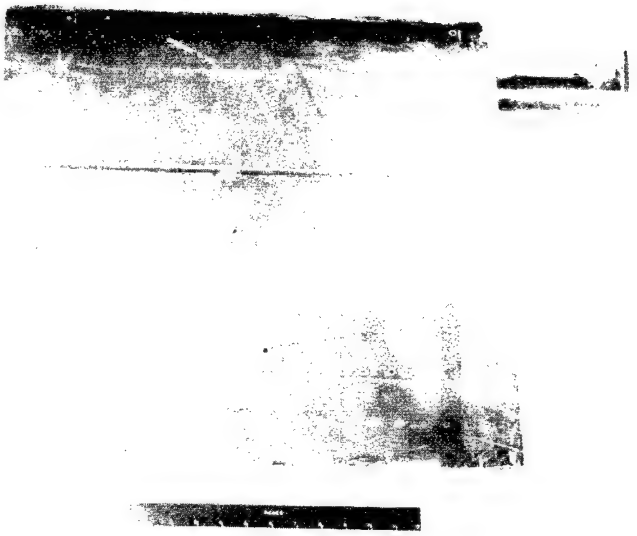

Fig. B.61 Elevator Section 5 - Unexposed Side - Station 2

Fig. B.62 Elevator Section 6 - Exposed Side - Station 2

Fig. B.63 Elevator Section 6 - Unexposed Side - Station 2

Fig. B.64 Elevator Section 7 - Exposed Side - Station 1

Fig. B.65 Elevator Section 7 - Unexposed Side - Station 1

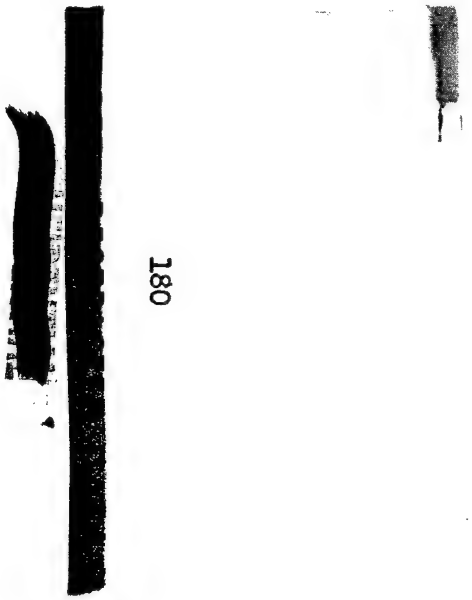

Fig. B.66 Elevator Section 8 - Exposed Side - Station 1

Fig. B.67 Elevator Section 8 - Unexposed Side - Station 1

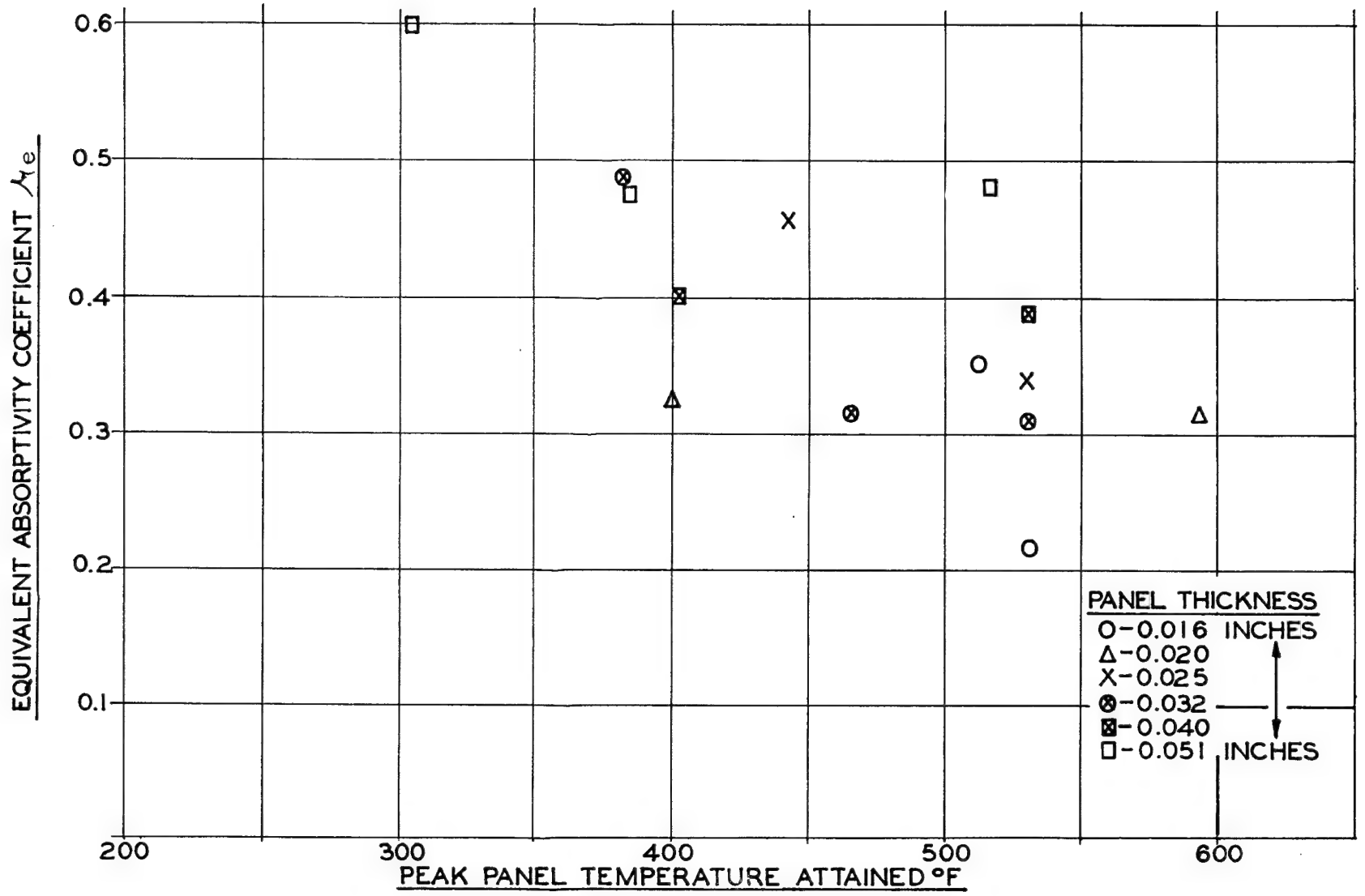

Fig. B.68 Equivalent Thermal Absorptivity Coefficient vs Peak Temperature Attained - Sea Blue Lacquer

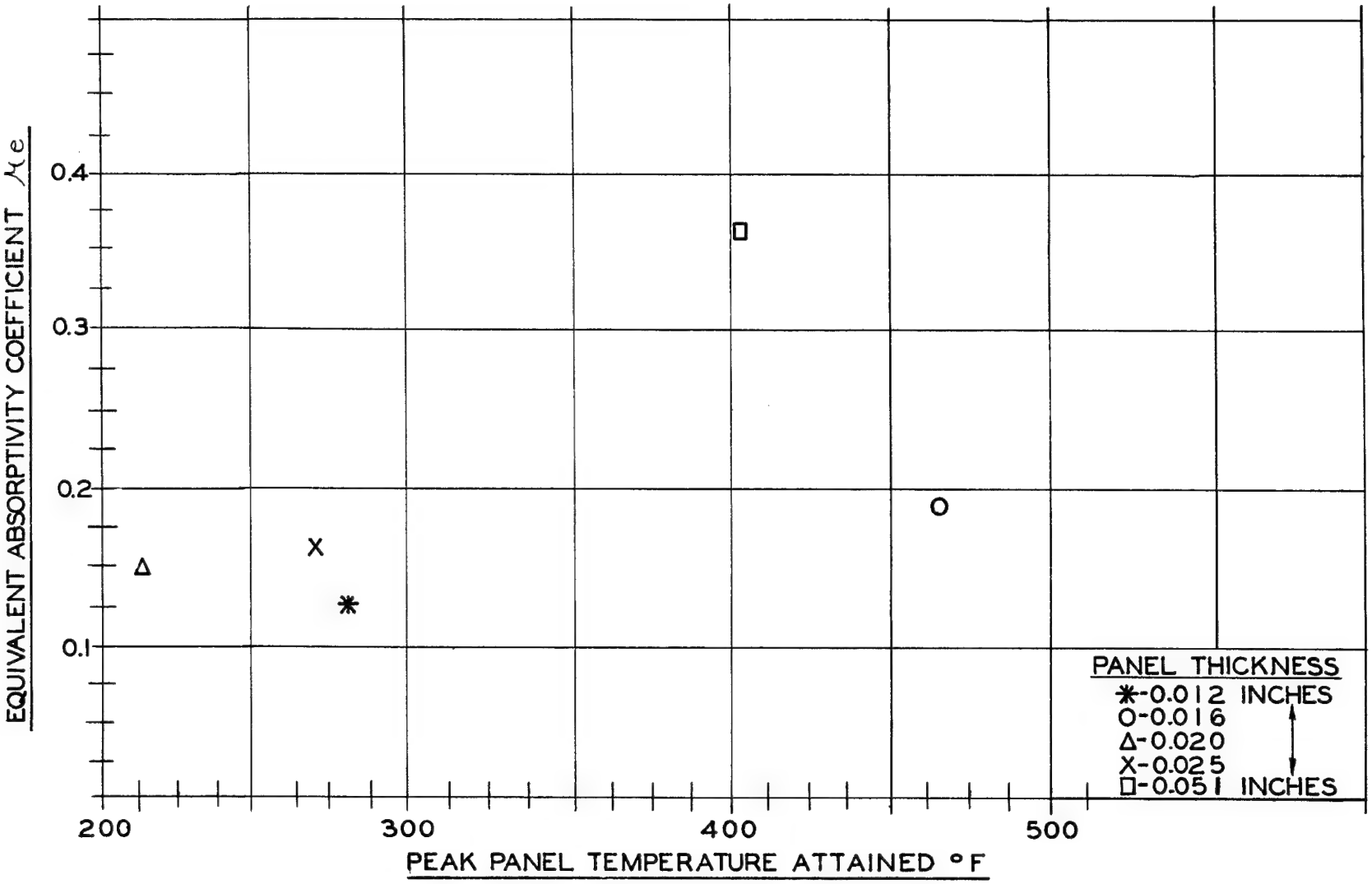

Fig. B.69 Equivalent Thermal Absorptivity Coefficient vs Peak Temperature Attained - White Lacquer

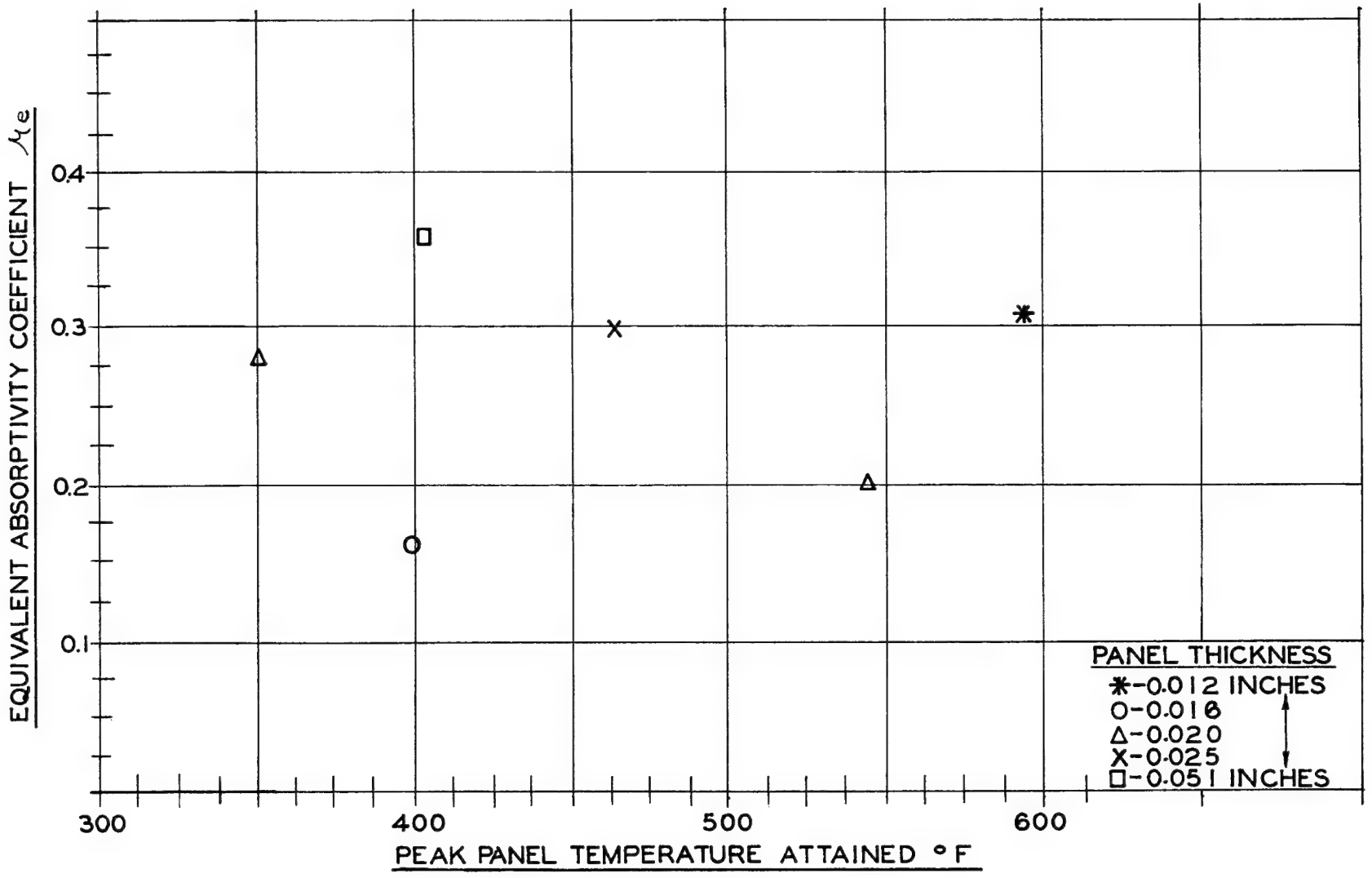

Fig. B.70 Equivalent Thermal Absorptivity Coefficient vs Peak Temperature Attained - Aluminized Lacquer

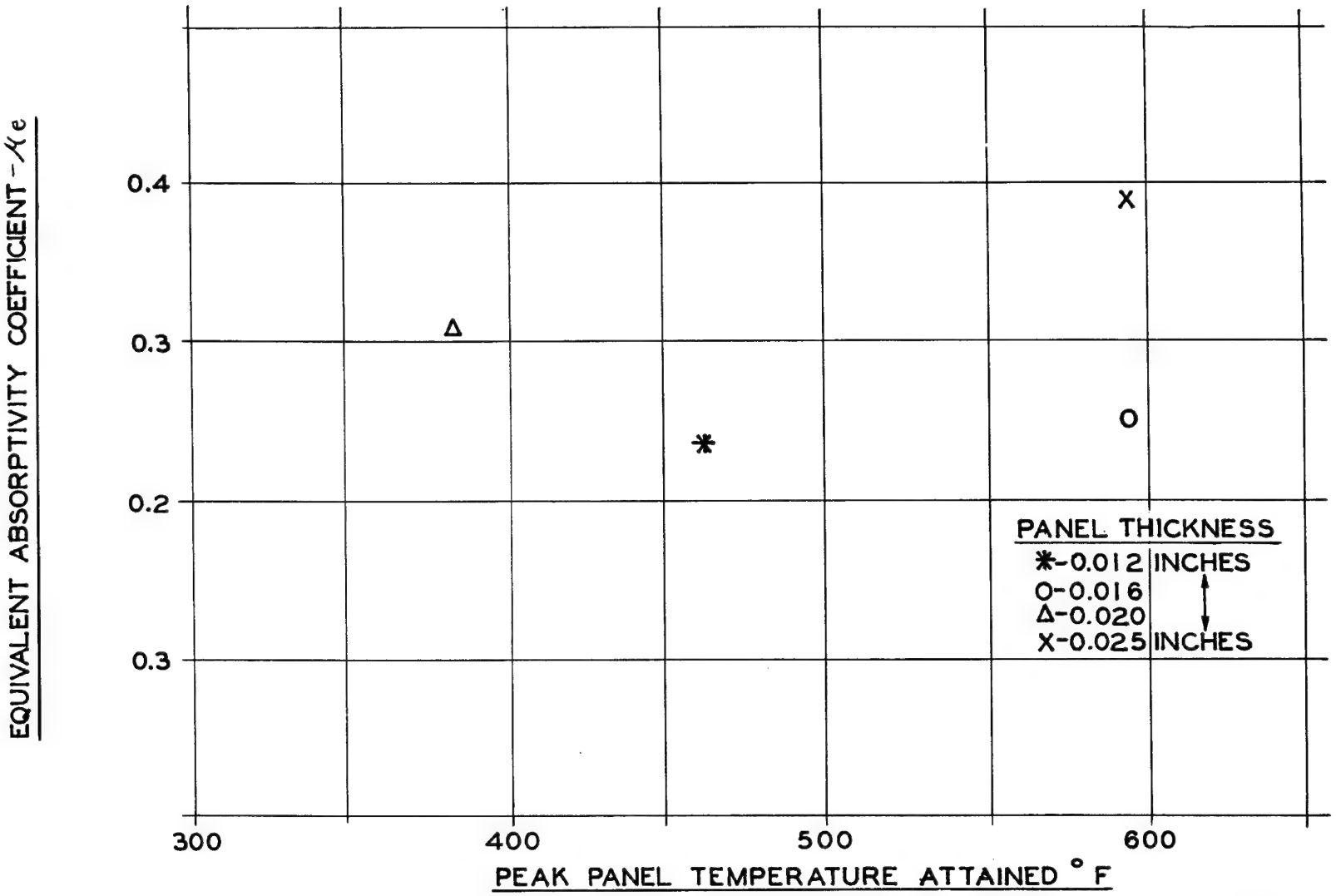

Fig. B.71 - Equivalent Thermal Absorptivity Coefficient vs Peak Temperature Attained - Bare Metal

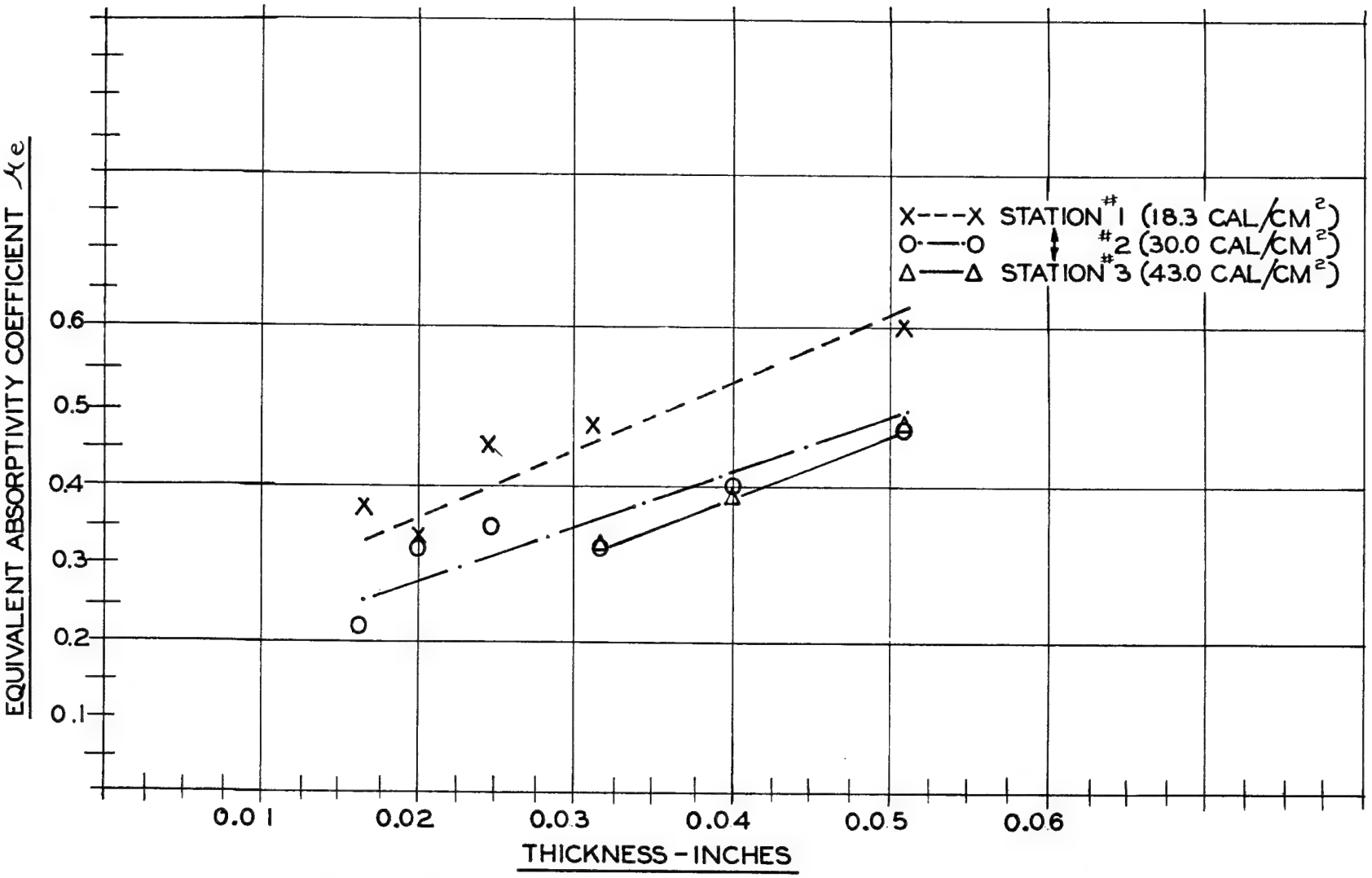

Fig. B.72 Equivalent Thermal Absorptivity Coefficient vs Panel Thickness - Sea Blue Lacquer

TABLE B.I

FRAME NO. 1 — PANEL TEST DATA
THERMAL ENERGY — 18.3 CALORIES PER CM^2

PANEL NUMBER	METAL THICKNESS INCHES	SURFACE	PEAK TEMP. RISE ^{o}F ABOVE 62° F AMBIENT	EQUIVALENT ABSORPTIVITY COEFFICIENT/μ_e	ULTIMATE STRENGTH —PSI—	YIELD STRENGTH —PSI—
1	0.012	BARE METAL	406	0.235	64,900	47,300
2	0.012	ALUMINIZED LACQUER	530	0.306	65,700	48,700
3	0.012	WHITE LACQUER	217	0.125	68,200	50,400
8	0.016	SEA BLUE LACQUER	>578	——	65,100	52,900
10	0.016	SEA BLUE LACQUER	456	0.352	66,200	48,700
11	0.020	BARE METAL	317	0.306	67,500	45,200
13	0.020	ALUMINIZED LACQUER	288	0.278	66,900	43,900
15	0.020	WHITE LACQUER	154	0.148	67,500	45,100
17	0.020	SEA BLUE LACQUER	337	0.325	67,100	46,700
23	0.025	SEA BLUE LACQUER	381	0.459	66,800	45,500
26	0.032	SEA BLUE LACQUER	315	0.485	66,400	43,400
34	0.051	SEA BLUE LACQUER	244	0.600	70,200	47,400

TABLE B. 2

FRAME NO. 2 PANEL TEST DATA
THERMAL ENERGY — 30 CALORIES PER CM^2

PANEL NUMBER	METAL THICKNESS INCHES	SURFACE	PEAK TEMP RISE ^{o}F ABOVE 62°F AMBIENT	EQUIVALENT ABSORPTIVITY COEFFICIENT —M_e—	ULTIMATE STRENGTH —PSI—	YIELD STRENGTH —PSI—
5	0.016	BARE METAL	530	0.249	64,500	51,300
6	0.016	ALUMINIZED LACQUER	337	0.158	67,600	51,800
7	0.016	WHITE LACQUER	406	0.191	63,400	45,500
9	0.016	SEA BLUE LACQUER	469	0.220	59,700	37,000
18	0.020	SEA BLUE LACQUER	530	0.312	66,500	49,600
20	0.025	BARE METAL	530	0.389	66,600	50,400
21	0.025	ALUMINIZED LACQUER	406	0.298	64,600	44,900
22	0.025	WHITE LACQUER	211	0.155	67,900	47,000
24	0.025	SEA BLUE LACQUER	469	0.344	69,300	47,500
27	0.032	SEA BLUE LACQUER	406	0.312	65,300	44,300
29	0.040	SEA BLUE LACQUER	340	0.400	65,500	42,400
35	0.051	SEA BLUE LACQUER	317	0.475	68,800	45,400

TABLE B. 3

FRAME NO. 3–PANEL TEST DATA
THERMAL ENERGY–43 CALORIES PER CM^2

PANEL NUMBER	METAL THICKNESS INCHES	SURFACE	PEAK TEMP RISE ^{o}F ABOVE 62°F AMBIENT	EQUIVALENT ABSORPTIVITY COEFFICIENT $-M_e-$	ULTIMATE STRENGTH —PSI—	YIELD STRENGTH —PSI—
12	0.020	BARE METAL	TEMP TAPE MISSING	——	——	——
14	0.020	ALUMINIZED LACQUER	481	0.197	64,400	44,800
16	0.020	WHITE LACQUER	TEMP TAPE ILLEGIBLE	——	65,500	47,600
19	0.020	SEA BLUE LACQUER	TEMP TAPE MISSING	——	57,800	36,400
25	0.025	SEA BLUE LACQUER	>578	——	59,700	39,700
28	0.032	SEA BLUE LACQUER	469	0.308	57,500	38,600
30	0.040	SEA BLUE LACQUER	469	0.384	62,700	48,600
31	0051	BARE METAL	>578	——	66,300	53,400
32	0.051	ALUMINIZED LACQUER	340	0.356	68,400	45,200
33	0.051	WHITE LACQUER	340	0.356	69,700	46,700
36	0.051	SEA BLUE LACQUER	456	0.478	70,500	50,000

[redacted]

TABLE B.4

ULTIMATE STRENGTH AND YIELD STRENGTH OF UNEXPOSED 24 ST ALUMINUM ALLOY PANEL MATERIAL

METAL THICKNESS INCHES	ULTIMATE STRENGTH P.S.I.	YIELD STRENGTH P.S.I.
0.012	67,500	49,800
0.016	66,400	49,100
0.020	65,200	44,200
0.025	69,300	47,200
0.032	69,200	47,800
0.040	68,800	49,000
0.051	70,400	49,700

TABLE B 5

ELEVATOR SECTION DATA - STATION 1
24ST ALCLAD - SLANT RANGE - 7150FT AMBIENT TEMP 62°F

ELEVATOR SECTION #3
"A" TEMP TAPE - 403°F "B" TEMP TAPE - 592°F

TEST SPECIMEN NO	SECTION SIDE	METAL THK IN	ULTIMATE STRENGTH PSI	YIELD STRENGTH PSI
1	UNEXPOSED	0.016	61,500	44,700
1E	EXPOSED	0.016	61,000	46,500
2	UNEXPOSED	0.016	61,300	45,600
2E	EXPOSED	0.016	58,800	44,000
3	UNEXPOSED	0.032	67,900	52,500
3E	EXPOSED	0.032	64,000	46,000
4	UNEXPOSED	0.032	64,600	NO DATA
4E	EXPOSED	0.032	66,700	NO DATA

ELEVATOR SECTION #4
"A" TEMP TAPE - 180°F "B" TEMP TAPE - 351°F "C" TEMP TAPE - 235°F

TEST SPECIMEN NO	SECTION SIDE	METAL THK IN	ULTIMATE STRENGTH PSI	YIELD STRENGTH PSI
1	UNEXPOSED	0.016	62,300	47,000
1E	EXPOSED	0.016	62,700	46,200
2	UNEXPOSED	0.016	61,700	45,900
2E	EXPOSED	0.016	63,100	47,300
3 *	UNEXPOSED	0.040	28,000	15,900
3E *	EXPOSED	0.040	33,500	16,700
4	UNEXPOSED	0.032	66,200	48,300
4E	EXPOSED	0.032	67,500	49,700

* 52-SO ALUMINUM ALLOY

TABLE B 5
(CONTINUED)

ELEVATOR SECTION #7 "A" TEMP TAPE-226° F "B" TEMP TAPE-351° F				
TEST SPECIMEN NO	SECTION SIDE	METAL THK IN	ULTIMATE STRENGTH PSI	YIELD STRENGTH PSI
1	UNEXPOSED	0.016	62,600	44,700
1 E	EXPOSED	0.016	58,300	41,800
2	UNEXPOSED	0.016	62,400	45,300
2 E	EXPOSED	0.016	58,400	43,100
3	UNEXPOSED	0.032	70,200	56,300
3 E	EXPOSED	0.033	67,600	52,300
4	UNEXPOSED	0.032	63,300	37,700
4 E	EXPOSED	0.032	64,200	49,800
ELEVATOR SECTION #8 "A" TEMP TAPE-306° F "B" TEMP TAPE-NO DATA "C" TEMP TAPE-279° F				
TEST SPECIMEN NO	SECTION SIDE	METAL THK IN	ULTIMATE STRENGTH PSI	YIELD STRENGTH PSI
1	UNEXPOSED	0.016	62,500	44,200
1 E	EXPOSED	0.016	NO DATA	45,600
2	UNEXPOSED	0.016	62,800	47,000
2E	EXPOSED	0.016	62,300	45,600
3 *	UNEXPOSED	0.040	28,800	NO DATA
3 E *	EXPOSED	0.040	28,900	NO DATA
4	UNEXPOSED	0.032	65,300	46,500
4 E	EXPOSED	0.032	66,000	47,000

* 52-SO ALUMINUM ALLOY

TABLE B 6

ELEVATOR SECTION DATA STATION 2
24ST ALCLAD - SLANT RANGE-5330FT AMBIENT TEMP 62° F

ELEVATOR SECTION #1
"A" TEMP TAPE- NO DATA "B" TEMP TAPE- >640° F

TEST SPECIMEN NO	SECTION SIDE	METAL THK IN	ULTIMATE STRENGTH PSI	YIELD STRENGTH PSI
1	UNEXPOSED	0.016	60,500	49,900
1E	EXPOSED	0.018	51,600	32,300
2	UNEXPOSED	0.016	61,300	45,600
2E	EXPOSED	0.017	51,700	34,800
3	UNEXPOSED	0.032	66,300	52,300
3E	EXPOSED	0.033	65,000	48,000
4	UNEXPOSED	0.032	67,000	55,000
4E	EXPOSED	0.032	66,700	50,600

ELEVATOR SECTION #2
"A" TEMP TAPE-NO DATA "B" TEMP TAPE- NO DATA

TEST SPECIMEN NO	SECTION SIDE	METAL THK IN	ULTIMATE STRENGTH PSI	YIELD STRENGTH PSI
1	UNEXPOSED	0.016	62,300	47,100
1E	EXPOSED	0.016	57,300	41,000
2	UNEXPOSED	0.016	62,500	47,700
2E	EXPOSED	0.016	59,300	37,700
3	UNEXPOSED	0.032	65,900	51,100
3E	EXPOSED	0.032	66,800	48,800
4	UNEXPOSED	0.032	66,700	54,200
4E	EXPOSED	0.032	65,700	50,500

TABLE B 6
(CONTINUED)

ELEVATOR SECTION # 5 "A" TEMP TAPE- 468° F "B" TEMP TAPE ->640° F				
TEST SPECIMEN NO	SECTION SIDE	METAL THK IN	ULTIMATE STRENGTH PSI	YIELD STRENGTH PSI
1	UNEXPOSED	0.016	63,900	46,300
1E	EXPOSED	0.016	63,300	50,000
2	UNEXPOSED	0.016	64,600	44,800
2E	EXPOSED	0.016	62,500	47,000
3	UNEXPOSED	0.032	68,700	54,900
3E	EXPOSED	0.032	68,000	53,800
4	UNEXPOSED	0.032	70,300	56,600
4E	EXPOSED	0.032	68,200	55,300
ELEVATOR SECTION # 6 "A" TEMP TAPE-408° F "B" TEMP TAPE-NO DATA				
TEST SPECIMEN NO	SECTION SIDE	METAL THK IN	ULTIMATE STRENGTH PSI	YIELD STRENGTH PSI
1	UNEXPOSED	0.016	67,300	41,800
1E	EXPOSED	0.016	62,000	48,100
2	UNEXPOSED	0.016	64,300	45,700
2E	EXPOSED	0.016	59,900	45,600
3	UNEXPOSED	0.032	64,900	52,300
3E	EXPOSED	0.032	64,000	49,200
4	UNEXPOSED	0.032	60,800	50,300
4E	EXPOSED	0.032	57,800	45,700

TABLE B.7

RADIANT ENERGY MEASUREMENTS

STATION	SLANT RANGE FT.	ENERGY FROM PASSIVE INDICATORS ON FRAMES CALORIES PER CM^2	ENERGY VALUES EXTRAPOLATED FROM NML DATA CALORIES PER CM^2
1	7150	15	18.3
2	5330	32	30.0
3	3800	>44	43.0

BIBLIOGRAPHY

(1) Bureau of Aeronautics Structures Memorandum No. 33 of April 1952, Effects of Airburst Atomic Weapons on Naval Aircraft, Secret Restricted Data.

(2) Naval Air Material Center Report No. ASL NAM DE-260, Part I of April 1952, Instrumentation of Model AD-2 Airplane, BUNO 122363 for Blast Tests, Calibration of the AD-2 Airplane Wing for Flight Load Measurement.

(3) Naval Air Material Center Report No. ASL NAM DE-260, Part II of January 1953, Instrumentation of Model AD Airplanes for Blast Tests; Load Calibration of the Horizontal Stabilizer of the AD-2 Airplane BUNO 122363, and Load Calibration of the Wing and Horizontal Stabilizer of the XBT2D-1 Airplane, BUNO 09103.

(4) Naval Air Material Center Report No. ASL NAM AD-276 of 17 August 1953, Modernization of/and Use of NAXSTA Radar Tracking Equipment for Structural Flight Test Programs.

(5) Naval Air Material Center Project No. TED NAM AD-260, Reports to be issued, Instrumentation of Model AD Airplane for Atomic Blast Test.

(6) Naval Air Material Center Report No. ASL NAM DE-260.2, Part I of February 1953, The Positioning of Model AD Drone Aircraft for the Investigation of Critical Atomic Weapons Effects, Secret Restricted Data.

(7) Armed Forces Special Weapons Project, Operation Tumbler-Snapper, Project 8.3 Report WT-543 of March 1953, Thermal Radiation from a Nuclear Detonation, Secret Restricted Data.

(8) Armed Forces Special Weapons Project Report, Department of the Army Technical Manual TM 23-200, Department of the Navy OPNAV Instruction 003400.1, Department of the Air Force AFOAT 385.2 of October 1952, Capabilities of Atomic Weapons, Secret.

[redacted]

(9) Bureau of Aeronautics Report DR-1434, Part I of June 1953 and Part II of November 1953, Reflection of Radiation from an Indefinite Plane.

(10) Bureau of Aeronautics Report DR-1485 of April 1953, Atomic Weapon Effects from Standpoint of Air Delivery Vehicles, Secret Restricted Data.

(11) Massachusetts Institute of Technology, Department of Aeronautical Engineering Report of January 1950, Handbook of Normal Shock Relationships.

(12) Douglas Aircraft Company Report No. ES 6613 Vol. 1 of December 1944, Wing Loads, Model XBT2D-1.

(13) Douglas Aircraft Company Report No. ES 6705 of March 1945, Empennage Loads, Model XBT2D-1.

(14) Bureau of Aeronautics Structures Project Report No. 42 of August 1953, Analytical Determination of the Effect of Aerodynamic Cooling on the Temperature of a Metal Plate Heated by an Atomic Bomb Thermal Pulse, Confidential Restricted Data.

(15) Douglas Aircraft Co. Report No. ES 17329 of May 1953, Skin Samples Tension Tests, Confidential

(16) Douglas Aircraft Co. Laboratory Report No. ES-3 134 of May 1953, Short Time High Temperature Radiant Head Studies, Secret.

(17) Armed Forces Special Weapons Project, Operation Tumbler Project 1.2 Report WT 512 of February 1953, Air Pressure vs Time, Secret.

(18) Aluminum Co. of America Handbook, ALCOA Aluminum and Its Alloys, pgs. 113-114.

(19) Quartermaster Research and Development Laboratories, Pioneering Research Laboratories Research Service Test Report No. QC-30 of October 1951, Temperature Indicator Papers.

(20) Armed Forces Special Weapons Project, Report No. 903 of November 1953

DISTRIBUTION

Military Distribution Categories 5-21, 5-30, and 5-60

Copy

ARMY ACTIVITIES

1 Asst. Chief of Staff, G-3, D/A; Washington 25, D.C. ATTN: Dep. CofS, G-3 (RR&SW)
2 Deputy Chief of Staff for Logistics, D/A Washington 25, D.C. ATTN: Director of Research & Development
3 Chief of Ordnance, D/A, Washington 25, D.C. ATTN: ORDTX-AR
4- 6 Chief Signal Officer, D/A, P&O Division, Washington 25, D.C. ATTN: SIGOP
7 The Surgeon General, D/A, Washington 25, D.C. ATTN: Chief, R&D Division
8- 9 Chief Chemical Officer, D/A, Washington 25, D.C.
10- 13 The Quartermaster General, CBR, Liaison Officer, Research and Development Div., D/A, Washington 25, D.C.
14- 18 Chief of Engineers, D/A, Washington 25, D.C. ATTN: ENGNB
19 Chief of Transportation, Military Planning and Intelligence Div., Washington 25, D.C.
20- 22 Chief, Army Field Forces, Ft. Monroe, Va.
23 President, Board #1, OCAFF, Ft. Bragg, N.C.
24 President, Board #2, OCAFF, Ft. Knox, Ky.
25 President, Board #3, OCAFF, Ft. Benning, Ga.
26 President, Board #4, OCAFF, Ft. Bliss, Tex.
27 Commanding General, U.S. Army Caribbean, Ft. Amador, C.Z. ATTN: Cml. Off.
28 Commander-in-Chief, European Command, APO 128, c/o PM, New York, N.Y.
29- 30 Commander-in-Chief, Far East Command, APO 500, c/o PM,
31- 32 Commanding General, U.S. Army Europe, APO 403, c/o PM, New York, N.Y. ATTN: OPOT Div., Combat Dev. Br.
33- 34 Commanding General, U.S. Army Pacific, APO 958, c/o PM, San Francisco, Calif. ATTN: Cml. Off.
35- 36 Commandant, Command and General Staff College, Ft. Leavenworth, Kan. ATTN: ALLLS(AS)
37 Commandant, The Artillery School, Ft. Sill, Okla.
38 Secretary, The AA&GM Branch, The Artillery School, Ft. Bliss, Tex. ATTN: Lt. Col. Albert D. Epley, Dept. of Tactics and Combined Arms
39 Commanding General, Medical Field Service School, Brooke Army Medical Center, Ft. Sam Houston, Tex.
40 Director, Special Weapons Development Office, Ft. Bliss, Tex. ATTN: Lt. Arthur Jaskierny
41 Commandant, Army Medical Service Graduate School, Walter Reed Army Medical Center, Washington 25, D.C.
42 Superintendent, U.S. Military Academy, West Point, N.Y. ATTN: Prof. of Ordnance
43 Commandant, Chemical Corps School, Chemical Corps Training Command, Ft. McClellan, Ala.
44- 45 Commanding General, Research and Engineering Command, Army Chemical Center, Md. ATTN: Deputy for RW and Non-Toxic Material
46- 47 Commanding General, Aberdeen Proving Grounds, Md. (inner envelope) ATTN: RD Control Officer (for Director, Ballistics Research Laboratory)
48- 50 Commanding General, The Engineer Center, Ft. Belvoir, Va. ATTN: Asst. Commandant, Engineer School
51 Commanding Officer, Engineer Research and Development Laboratory, Ft. Belvoir, Va. ATTN: Chief, Technical Intelligence Branch
52 Commanding Officer, Picatinny Arsenal, Dover, N.J. ATTN: ORDBB-TK
53 Commanding Officer, Frankford Arsenal, Philadelphia 37, Pa. ATTN: Mr. C. C. Fawcett
54 Commanding Officer, Army Medical Research Laboratory, Ft. Knox, Ky.
55- 56 Commanding Officer, Chemical Corps Chemical and Radiological Laboratory, Army Chemical Center, Md. ATTN: Tech. Library
57 Commanding Officer, Transportation R&D Station, Ft. Eustis, Va.

Copy

58 Director, Technical Documents Center, Evans Signal Laboratory, Belmar, N.J.
59 Director, Waterways Experiment Station, PO Box 631, Vicksburg, Miss. ATTN: Library
60 Director, Armed Forces Institute of Pathology, 7th and Independence Avenue, S.W., Washington 25, D.C.
61 Director, Operations Research Office, Johns Hopkins University, 7100 Connecticut Ave., Chevy Chase, Md. ATTN: Library
62- 68 Technical Information Service, Oak Ridge, Tenn. (Surplus)

NAVY ACTIVITIES

69- 70 Chief of Naval Operations, D/N, Washington 25, D.C. ATTN: OP-36
71 Chief of Naval Operations, D/N, Washington 25, D.C. ATTN: OP-374(OEG)
72 Director of Naval Intelligence, D/N, Washington 25, D.C. ATTN: OP-922V
73 Chief, Bureau of Medicine and Surgery, D/N, Washington 25, D.C. ATTN: Special Weapons Defense Div.
74 Chief, Bureau of Ordnance, D/N, Washington 25, D.C.
75- 76 Chief, Bureau of Ships, D/N, Washington 25, D.C. ATTN: Code 348
77 Chief, Bureau of Yards and Docks, D/N, Washington 25, D.C. ATTN: D-440
78 Chief, Bureau of Supplies and Accounts, D/N, Washington 25, D.C.
79- 80 Chief, Bureau of Aeronautics, D/N, Washington 25, D.C.
81 Chief of Naval Research, Department of the Navy Washington 25, D.C. ATTN: LT(jg) F. McKee, USN
82 Commander-in-Chief, U.S. Pacific Fleet, Fleet Post Office, San Francisco, Calif.
83 Commander-in-Chief, U.S. Atlantic Fleet, U.S. Naval Base, Norfolk 11, Va.
84- 87 Commandant, U.S. Marine Corps, Washington 25, D.C. ATTN: Code A03H
88 President, U.S. Naval War College, Newport, R.I.
89 Superintendent, U.S. Naval Postgraduate School, Monterey, Calif.
90 Commanding Officer, U.S. Naval Schools Command, U.S. Naval Station, Treasure Island, San Francisco, Calif.
91 Commanding Officer, U.S. Fleet Training Center, Naval Base, Norfolk 11, Va. ATTN: Special Weapons School
92- 93 Commanding Officer, U.S. Fleet Training Center, Naval Station, San Diego 36, Calif. ATTN: (SPWP School)
94 Commanding Officer, Air Development Squadron 5, VX-5, U.S. Naval Air Station, Moffett Field, Calif.
95 Commanding Officer, U.S. Naval Damage Control Training Center, Naval Base, Philadelphia 12, Pa. ATTN: ABC Defense Course
96 Commanding Officer, U.S. Naval Unit, Chemical Corps School, Army Chemical Training Center, Ft. McClellan, Ala.
97 Joint Landing Force Board, Marine Barracks, Camp Lejeune, N.C.
98 Commander, U.S. Naval Ordnance Laboratory, Silver Spring 19, Md. ATTN: EE
99 Commander, U.S. Naval Ordnance Laboratory, Silver Spring 19, Md. ATTN: EH
100 Commander, U.S. Naval Ordnance Laboratory, Silver Spring 19, Md. ATTN: R
101 Commander, U.S. Naval Ordnance Test Station, Inyokern, China Lake, Calif.
102 Officer-in-Charge, U.S. Naval Civil Engineering Res. and Evaluation Lab., U.S. Naval Construction Battalion Center, Port Hueneme, Calif. ATTN: Code 753
103 Commanding Officer, U.S. Naval Medical Research Inst., National Naval Medical Center, Bethesda 14, Md.

[redacted]

54WO 81009

[redacted]

Copy

104 Director, U.S. Naval Research Laboratory, Washington 25, D.C. ATTN: Code 2029
105 Director, The Material Laboratory, New York Naval Shipyard, Brooklyn, N.Y.
106 Commanding Officer and Director, U.S. Navy Electronics Laboratory, San Diego 52, Calif. ATTN: Code 4223
107-110 Commanding Officer, U.S. Naval Radiological Defense Laboratory, San Francisco 24, Calif. ATTN: Technical Information Division
111-112 Commanding Officer and Director, David W. Taylor Model Basin, Washington 7, D.C. ATTN: Library
113 Commander, U.S. Naval Air Development Center, Johnsville, Pa.
114 Director, Office of Naval Research Branch Office, 1000 Geary St., San Francisco, Calif.
115 Officer-in-Charge, U.S. Naval Clothing Factory, U.S. Naval Supply Activities, New York, 3rd Avenue and 29th Street, Brooklyn, N.Y. ATTN: R&D Division
116-122 Technical Information Service, Oak Ridge, Tenn. (Surplus)

AIR FORCE ACTIVITIES

123 Asst. for Atomic Energy, Headquarters, USAF, Washington 25, D.C. ATTN: DCS/O
124 Director of Operations, Headquarters, USAF, Washington 25, D.C. ATTN: Operations Analysis
125 Director of Plans, Headquarters, USAF, Washington 25, D.C. ATTN: War Plans Div.
126 Director of Research and Development, Headquarters, USAF, Washington 25, D.C. ATTN: Combat Components Div.
127-128 Director of Intelligence, Headquarters, USAF, Washington 25, D.C. ATTN: AFOIN-1B2
129 The Surgeon General, Headquarters, USAF, Washington 25, D.C. ATTN: Bio. Def. Br., Pre. Med. Div.
130 Deputy Chief of Staff, Intelligence, Headquarters, U.S. Air Forces Europe, APO 633, c/o PM, New York, N.Y. ATTN: Directorate of Air Targets
131 Commander, 497th Reconnaissance Technical Squadron (Augmented), APO 633, c/o PM, New York, N.Y.
132 Commander, Far East Air Forces, APO 925, c/o PM, San Francisco, Calif.
133 Commander, Strategic Air Command, Offutt Air Force Base, Omaha, Nebraska. ATTN: Special Weapons Branch, Inspection Div., Inspector General
134 Commander, Tactical Air Command, Langley AFB, Va. ATTN: Documents Security Branch
135 Commander, Air Defense Command, Ent AFB, Colo.
136-137 Commander, Air Materiel Command, Wright-Patterson AFB, Dayton, O. ATTN: MCAIDS
138 Commander, Air Training Command, Scott AFB, Belleville, Ill. ATTN: DCS/O GTP
139 Commander, Air Research and Development Command, PO Box 1395, Baltimore, Md. ATTN: RDDN
140 Commander, Air Proving Ground Command, Eglin AFB, Fla. ATTN: AG/TRB
141-142 Commander, Air University, Maxwell AFB, Ala.
143-150 Commander, Flying Training Air Force, Waco, Tex. ATTN: Director of Observer Training
151 Commander, Crew Training Air Force, Randolph Field, Tex. ATTN: 2GTS, DCS/O

Copy

152 Commander, Headquarters, Technical Training Air Force, Gulfport, Miss. ATTN: TA&D
153-154 Commandant, Air Force School of Aviation Medicine, Randolph AFB, Tex.
155-160 Commander, Wright Air Development Center, Wright-Patterson AFB, Dayton, O. ATTN: WCOESP
161-162 Commander, Air Force Cambridge Research Center, 230 Albany Street, Cambridge 39, Mass. ATTN: CRQST-2
163-165 Commander, Air Force Special Weapons Center, Kirtland AFB, N. Mex. ATTN: Library
166 Commandant, USAF Institute of Technology, Wright-Patterson AFB, Dayton, O. ATTN: Resident College
167 Commander, Lowry AFB, Denver, Colo. ATTN: Department of Armament Training
168 Commander, 1009th Special Weapons Squadron, Headquarters, USAF, Washington 25, D.C.
169-170 The RAND Corporation, 1700 Main Street, Santa Monica, Calif. ATTN: Nuclear Energy Division
171-177 Technical Information Service, Oak Ridge, Tenn. (Surplus)

OTHER DEPARTMENT OF DEFENSE ACTIVITIES

178 Asst. Secretary of Defense, Research and Development, D/D, Washington 25, D.C.
179 U.S. National Military Representative, Headquarters, SHAPE, APO 55, c/o PM, New York, N.Y. ATTN: Col. J. P. Healy
180 Director, Weapons Systems Evaluation Group, OSD, Rm 2E1006, Pentagon, Washington 25, D.C.
181 Asst. for Civil Defense, OSD, Washington 25, D.C.
182 Armed Services Explosives Safety Board, D/D, Building T-7, Gravelly Point, Washington 25, D.C.
183 Commandant, Armed Forces Staff College, Norfolk 11, Va. ATTN: Secretary
184-189 Commanding General, Field Command, Armed Forces Special Weapons Project, PO Box 5100, Albuquerque, N. Mex.
190-191 Commanding General, Field Command, Armed Forces, Special Weapons Project, PO Box 5100, Albuquerque, N. Mex. ATTN: Technical Training Group
192-200 Chief, Armed Forces Special Weapons Project, Washington 25, D.C.
201-207 Technical Information Service, Oak Ridge, Tenn. (Surplus)

ATOMIC ENERGY COMMISSION ACTIVITIES

208-210 U.S. Atomic Energy Commission, Classified Technical Library, 1901 Constitution Ave., Washington 25, D.C. ATTN: Mrs. J. M. O'Leary (For DMA)
211-213 Los Alamos Scientific Laboratory, Report Library, PO Box 1663, Los Alamos, N. Mex. ATTN: Helen Redman
214-219 Sandia Corporation, Classified Document Division, Sandia Base, Albuquerque, N. Mex. ATTN: Martin Lucero
220-221 University of California Radiation Laboratory, PO Box 808, Livermore, Calif. ATTN: Margaret Edlund
222 Weapon Data Section, Technical Information Service, Oak Ridge, Tenn.
223-260 Technical Information Service, Oak Ridge, Tenn. (Surplus)

[redacted]

AEC, Oak Ridge, Tenn., A33448

[redacted]